Final Technical Report
Next Generation Solid Oxide Fuel Cell Module Development
DE-FE0031648
June 9, 2024

PI: Hossein Ghezel-Ayagh, PhD

Prepared by:
FuelCell Energy, Inc.
3 Great Pasture Road
Danbury, CT 06810

Prepared for:
National Energy Technology Laboratory (NETL)
U.S. Department of Energy

DISCLAIMER

This Final Technical Report was prepared with the support of the U.S. Department of Energy, under Award No. DE-FE0031648. However, any opinions, findings, conclusions, or recommendations expressed herein are those of the author(s) and do not necessarily reflect the views of the DOE.

TABLE OF CONTENTS

LIST OF FIGURES

LIST OF TABLES

EXECUTIVE SUMMARY

The overall objective of this project was to develop a transformative Solid Oxide Fuel Cell (SOFC) building block configuration comprised of multi-stack arrays that can be utilized in large-scale power plants. This transformative design signified the benefits of lower performance degradation coupled with improved reliability, low cost, smaller packaging for easier transport and installation, and improved maintenance and field serviceability characteristics.

The project goal was to design and fabricate a scalable hot module for housing an array of SOFC stacks and to demonstrate the characteristics of the module gas distribution, insulation and instrumentation, and DC power take-off. The approach was to validate the design of a stack prototype scalable to megawatt (MW) class systems using FuelCell Energy's Compact SOFC Architecture (CSA) stacks.

The scope of work was intended to design, build, and test a compact and low-cost multi-stack sub-module with flexibility to house CSA stacks and scalable to 350 kW which could ultimately be deployed in construction of MW-class systems. The project scope of work comprised of the following research thrusts:

- Research and development (R&D) focusing on performance, reliability, and reduction in cost of the state-of-the-art SOFC cell and stack technology through improvements in the areas of cell materials, stack design, and manufacturing quality control.
- Development of cathode materials using Atomic Layer Deposition surface modification with a promise to reduce cell degradation rate.
- Design for automation through miniaturization of parts and consolidation to fewer distinct parts.
- Optimization of the SOFC stack modules for Balance of Plant (BOP) integration including elimination of external compression and reducing the fuel pre-reforming and preheat requirements.
- Fabrication of a thermally self-sustaining module housing to accommodate an array of 6 CSA stacks serving as a test article to address multiple related areas of the module and balance of plant design.

Activities/Accomplishments (Results of Work by Tasks)

1 Project Management and Planning

Under Task 1, Project Management, the activities were conducted in accordance with the Statement of Project Objectives (SOPO) to accomplish the following Tasks:

- Task 2.0, Core Cell Technology, involved in advancing cell materials and manufacturing processes to improve endurance and stability of the cell performance.
- Task 3.0, SOFC Stack Development, involved in refining the CSA stack design and manufacturing quality control to improve long term reliability.
- Task 4.0, Stack Module Development, focused on design of a sub-MW modular building block that could be easily scaled up to larger configurations suitable for MW-scale applications. This Task included the analysis and process simulation centered on understanding the heat transfer and flow distribution mechanisms driving flow non-uniformities and temperatures as well as the materials and geometries required to accommodate the operational induced stresses.
- Task 5.0, Module Demonstration, centered on design and fabrication of a prototype multi-stack module scalable to larger modules of up to 48-60 stacks. The prototype multi-stack module had provisions to house up to six 350-cell CSA stacks and was planned for ≥50 hours of test duration using two CSA stacks near the end of this project.

The details of the project tasks are described in the following sections.

2 Core Technology

Objective:

The objective of this task was to advance cell materials and cell manufacturing processes to improve the long-term operational reliability of SOFC power systems. Novel gas stream impurity mitigation strategies and manufacturing quality control measures were developed. This work included the critical support of SOFC materials development and validation using button and single cell testing.

2.1 Cathode Improvement

Approach:

FCE developed cell cathode materials to mitigate the long-term cell voltage degradation effects of airborne impurities from the cathode gas stream – mainly Chrome (Cr). Cathode powders were altered with Hafnium Oxide using Atomic Layer Deposition (ALD). The process recipe and coating thickness was varied, characterized, and optimized through button cell experimentation. Bulk and modified cathode formulations, developed by ceramic processing and modified by ALD processes were studied in detail to understand bulk and surface structural, chemical and morphological characteristics. Characterization methods included transmission electron microscopy (TEM) to measure coating uniformity and Raman spectroscopy to characterize the crystal structure of the as-coated and sintered powders.

The role of exposure atmospheres (ambient air containing H_2O and CO_2) under electrochemical cell operating conditions (varying bias) was studied using symmetric cell configurations. Humidified air streams equilibrated with gaseous chromium vapor species (predominantly $CrO_2(OH)_2$) was used to study the role of Cr assisted poisoning of the cathode. Electrode

performance (power degradation and Electrochemical Impedance Spectroscopy) with time was studied and changes in ohmic and non-ohmic polarizations was analyzed. After completion of tests, electrodes were analyzed for bulk, surface and interface chemistry and structure. Surface studies were focused on A-site dopant exsolution and dopant interactions with ALD induced surface compound layer, and interface studies included cathode- electrolyte and ALD- electrolyte interactions. Cationic interdiffusion, particle growth, compound formation and related morphologies were studied using a variety of analytical and surface characterization techniques such as X-Ray Diffraction (XRD), X-Ray Photoelectron Spectroscopy (XPS), Scanning Electron Microscopy (SEM), Energy-Dispersive X-Ray Spectroscopy (EDS), Focused Ion Beam (FIB) and TEM/ STEM.

Results & Discussion:

The sub-contract with Sonata Scientific LLC was established and work on this task was initiated with initial runs of surface modification of perovskite cathode powders provided by FuelCell Energy using atomic layer deposition (ALD).

For the ALD coating process, approximately 9 grams of milled FCE cathode powder was loaded, as received, into a porous vessel (nominally 10-micron pore size). The vessel was loaded into a rotary ALD reactor preheated to 250°C with a base pressure of 0.1 torr and allowed to reach the reactor temperature over two hours. The vessel is rotated in the reactor to prevent particle agglomeration and create a gentle tumbling of the cathode powder, ideal for the ALD process. The ALD process consisted of alternating injections of Tetrakis (dimethylamino) hafnium (IV) (TDMAH) and water. TDMAH was liquid injected from a 0.1 M solution of TDMAH dissolved in toluene. In a TDMAH half cycle (precursor dose), 10 discrete injection periods were used to ensure enough precursor was used to saturate the cathode surface. Water was injected by vapor draw from a water reservoir. For each half cycle there was a hold period to allow the precursor to fully diffuse into the porous vessel. After the hold period, a pump/purge cycle was used to evacuate all the precursor from the vessel before the next half cycle. A total of 10, 20, or 30 cycles was used to create thickness variations in the ALD HfO_2 coating deposited on the cathode powder. During the ALD process, residual gas analysis (RGA) was continuously monitored on a fragment TDMAH precursor (m/z = 43) on three samples. Details of the RGA results are shown in Figure 2.1-1 and
Figure 2.1-2.

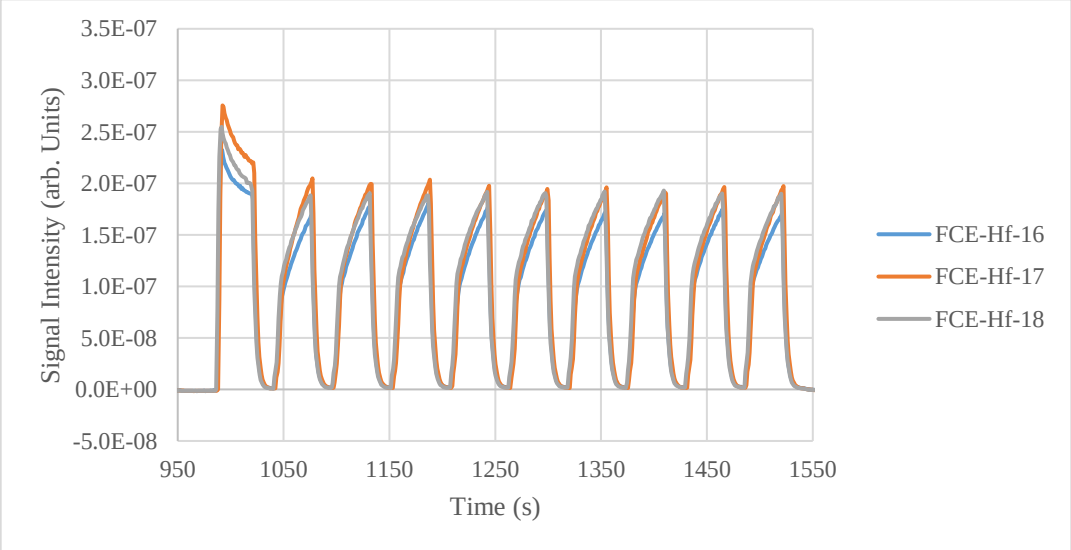

Figure 2.1-1 RGA Results: Precursor Injection Cycle, Multiple Samples

The precursor injection cycle, shown in Figure 2.1-1, includes 10 separate injection periods where a single injection period includes: TDMAH precursor injection (sharp rise), then a soak period (shallow rise) followed by a vacuum purge cycle (sharp decline) creating 10 discrete peaks. Deviations in the first peak are due to buildup of additional liquid behind the injector during the other stages of the ALD HfO_2 growth. Figure 2.1-1 shows strong injection to injection consistency over time and repeatability between all three sample runs. The stability of the injection-to-injection consistency is illustrated in Figure 2.1-2 on one continuous sample run. These results cover five complete ALD cycles during FCE-Hf-18 deposition (i.e. - 30 cycles total). Each cycle consists of 10 injection periods (ten peaks), a pump/purge cycle, 2 water injections (2 small peaks), and another pump/purge cycle. The consistency of these TDMAH peaks continued over the remaining 25 steps; indicating a stable, reproducible process.

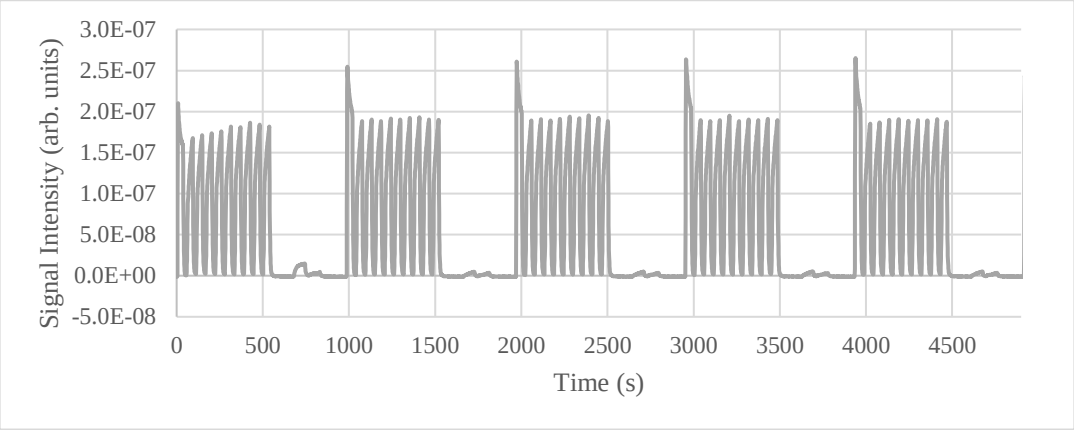

Figure 2.1-2 RGA Results: Multiple Injection Cycles, One Sample

Sonata Scientific has provided six HfO_2 ALD coated cathode powder samples to FCE for evaluation, summarized in Table 2.1-1. Here, the samples are divided into two groups based on the two different ALD system injectors used in the process. During the development of this coating process, Injector B was shown to have some non-uniformity issues. For sample numbers FCE-Hf-12, 13, and 14, that used Injector B, RGA results showed inconsistent injection profiles by RGA during the TDMAH injection step. This was initially thought to be an issue with the RGA but was found to be a malfunctioning injector. Injector B was then replaced by injector A. A second set of samples was prepared using injector A (samples FCE-Hf-16, 17, and 18). While coating with injector A, HfO_2 was observed on the sparger; an indicator that coating was actually taking place. RGA of these three processes showed the amount of precursor injected for each pulse was highly consistent, suggesting the cathode powder was exposed to the same quantity of TDMAH each cycle irrespective of sample number (shown in Figure 2.1-1 and Figure 2.1-2).

Table 2.1-1 Summary of cathode powders ALD coated by Sonata Scientific.

Sample Number	ALD Cycles	Comments
FCE-Hf-12	20	Injector B

FCE-Hf-13	10	
FCE-Hf-14	30	
FCE-Hf-16	10	Injector A
FCE-Hf-17	20	
FCE-Hf-18	30	

Six samples of coated cathode powder were processed into screen printable inks and button cell size half cells were tested (Figure 2.1-3). Figure 2.1-4 compares the Electrochemical Impedance Spectroscopy (EIS) data for sample FCE_Hf18 (a & c) compared to the baseline, uncoated powder (b & d). As compared to the coated sample, the baseline sample shows an increase over time in the polarization, observed at around 1000 Hz. This is thought to be due to Sr migration. Published literature shows that powder coating with Hf_2O has been shown to mitigate this problem (ECS Trans. 2017 volume 78, issue 1, 935-94).

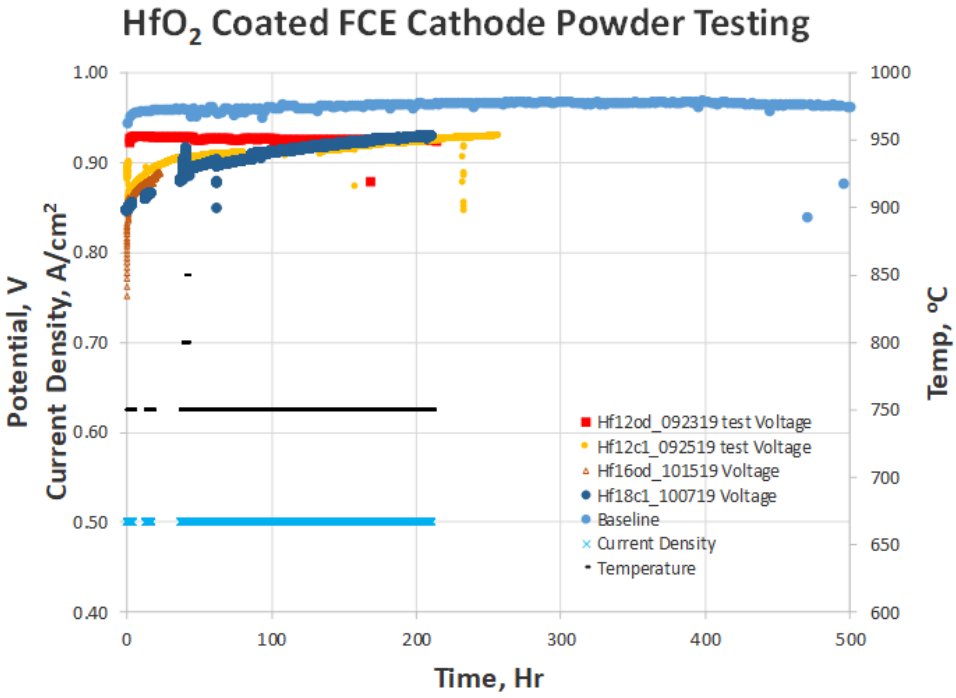

Figure 2.1-3 Button Cell testing of ALD modified cathode powder. Tested on 97% H_2, 3% H_2O fuel and air as oxidant.

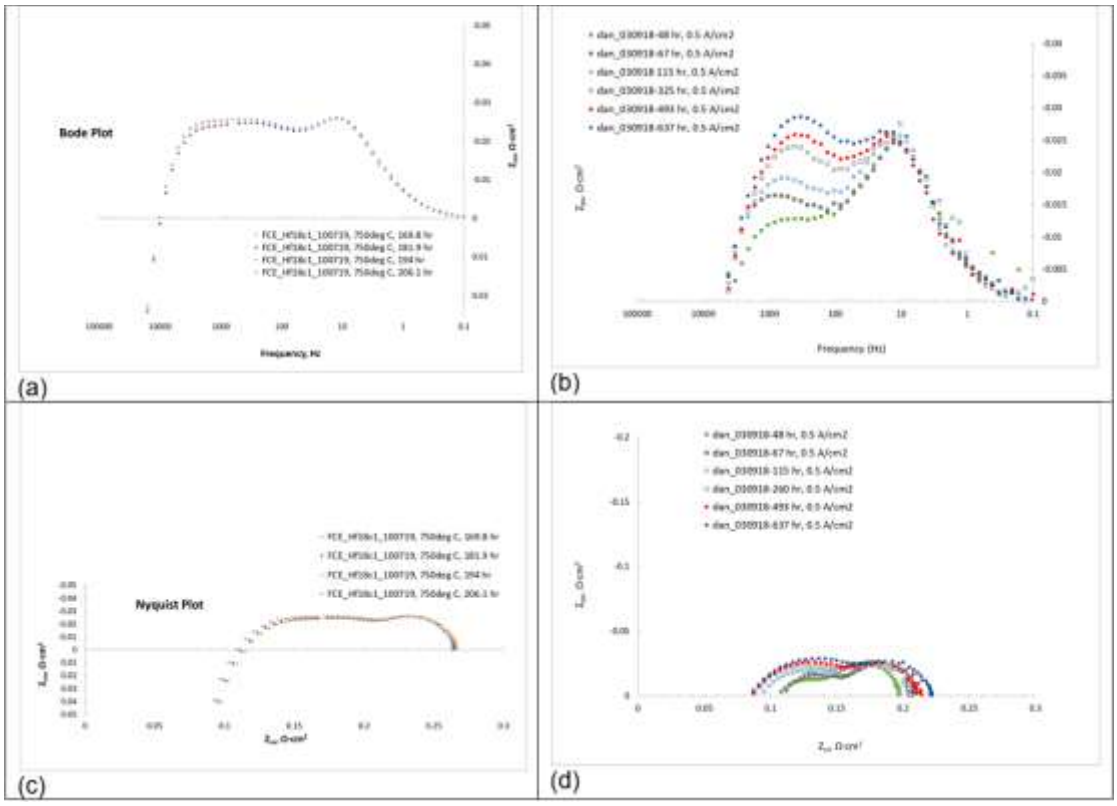

Figure 2.1-4 EIS results of sample FCE_Hf18 cell Bode plot (a) and Nyquist plot (c) compared to baseline, uncoated powder (b) and (d).

Figure 2.1-5 shows a large increase in the stability for the coated sample; noted by the lower slope of the high frequency peak curves shown.

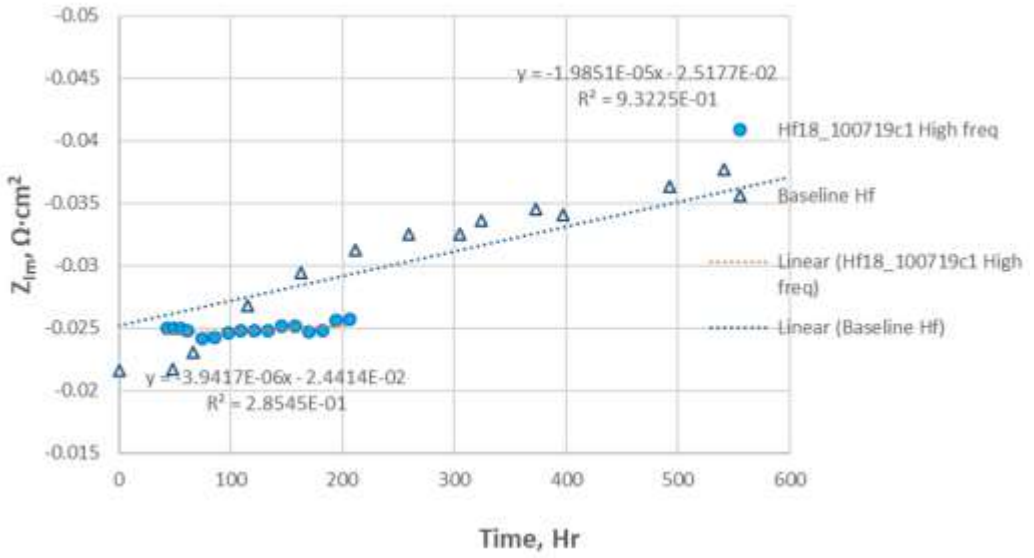

Figure 2.1-5 EIS results: Comparison of magnitude peaks vs time, 100-1000 Hz.

Results of continued testing of button cells with ALD modified cathode powder is given in Figure 2.1-6. The cell with 30-ALD cycles showed no degradation for over 1500 hours of testing and the

degradation seen at the end of the test is associated with sealing problems and the test was terminated. The other tests showed only short-term stability followed by steep degradation. This has been determined to be caused by the test fixture which has a large piece of stainless steel in the hot zone causing severe chromium poisoning.

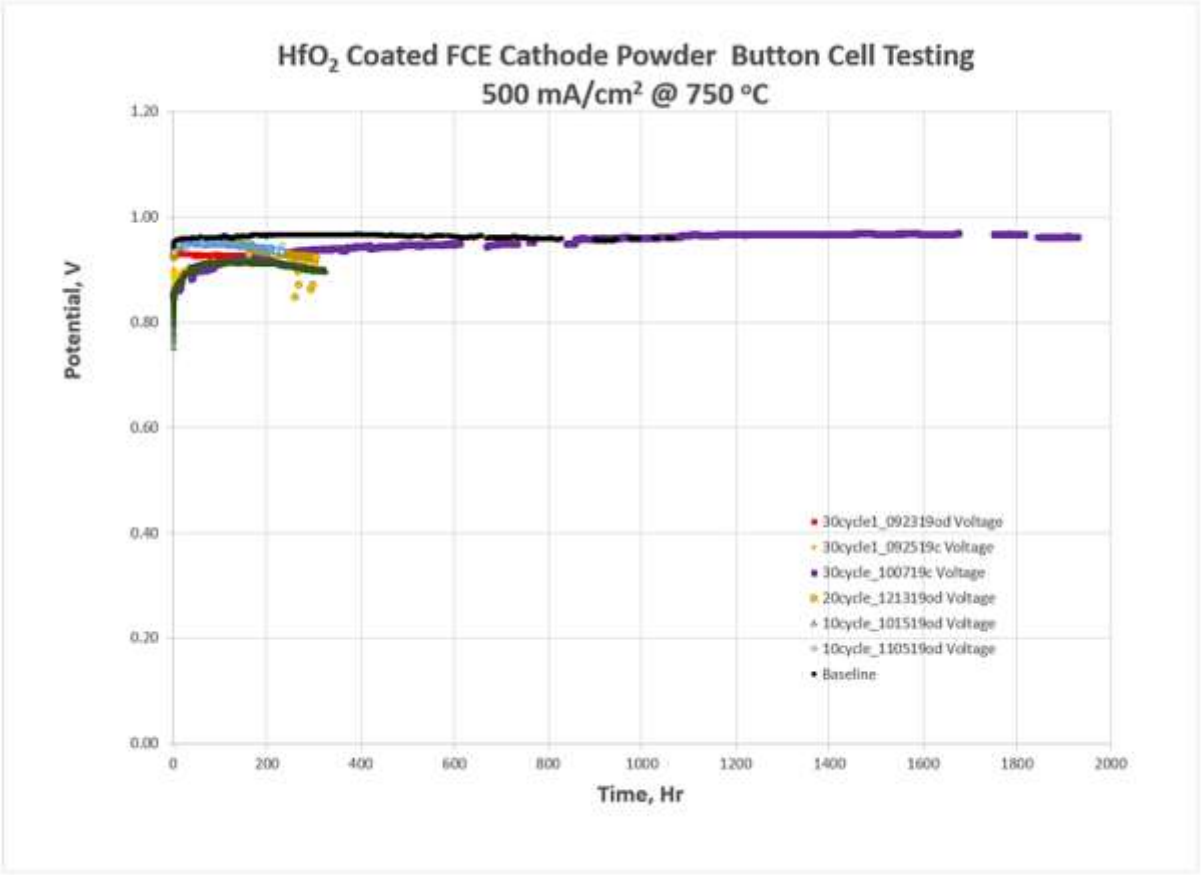

Figure 2.1-6 Button cell testing of ALD-modified Cathode powder.

Sonata provided another sample of powder coated with 5 cycles of HfO2, from which cathode paste has been prepared and a 5x5 cell was tested. Results are given in Figure 2.1-7. The degradation seen in the 30-cycle sample is thought to be due to insufficient MCO coating on the jig, and the 5-cycle test is with a freshly coated jig and is showing good stability.

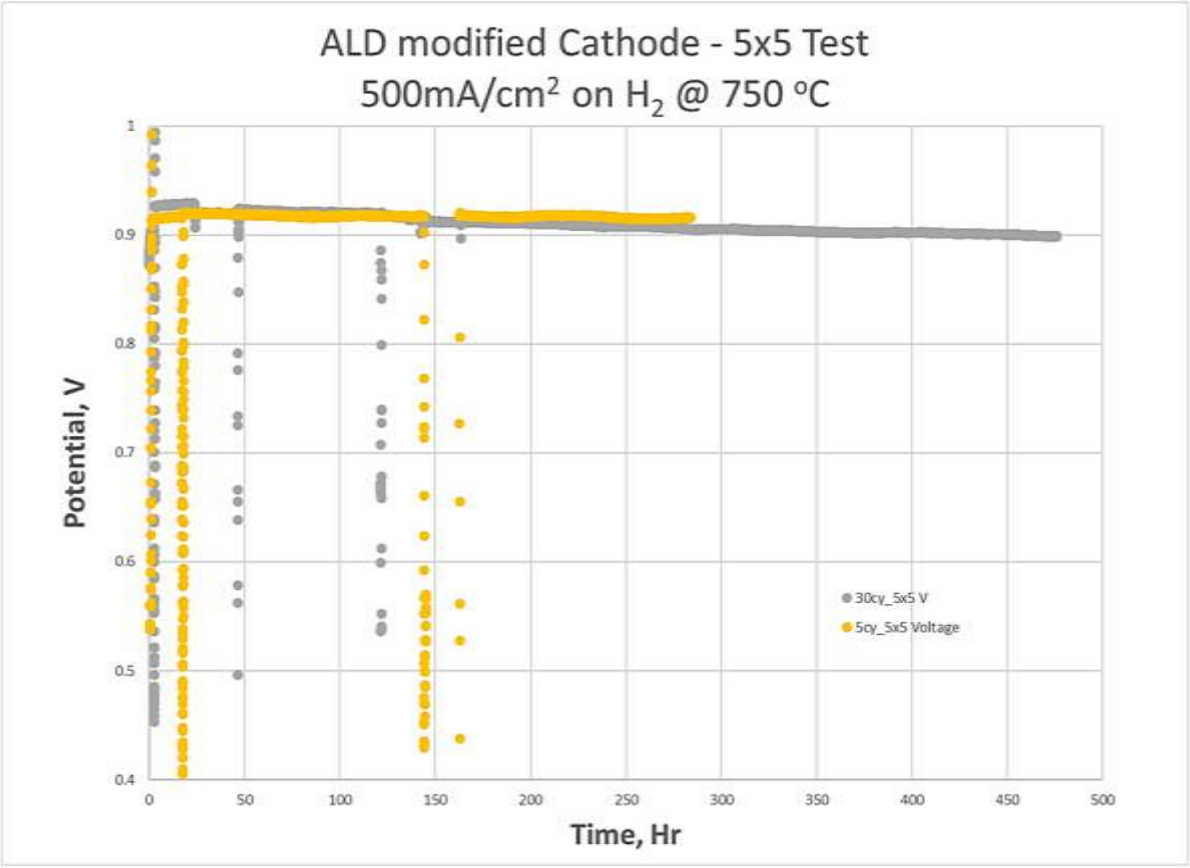

Figure 2.1-7 5cm x 5cm cell testing of ALD modified Cathode powder.

It has been previously observed that the peak power density decreased over time even when the voltage under galvanostatic load is stable, but the ALD modified cathode has demonstrated stable IV curve performance as seen in Figure 2.1-8 and Figure 2.1-9.

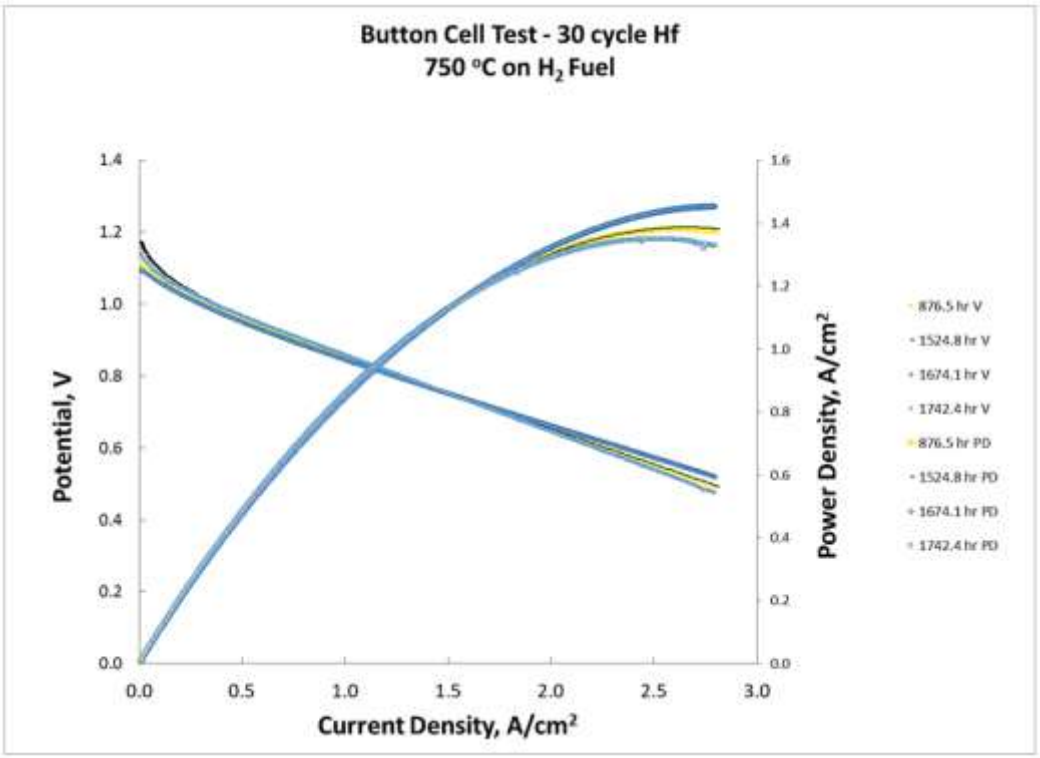

Figure 2.1-8 IV performance of 30 cycle ALD Hf button cell.

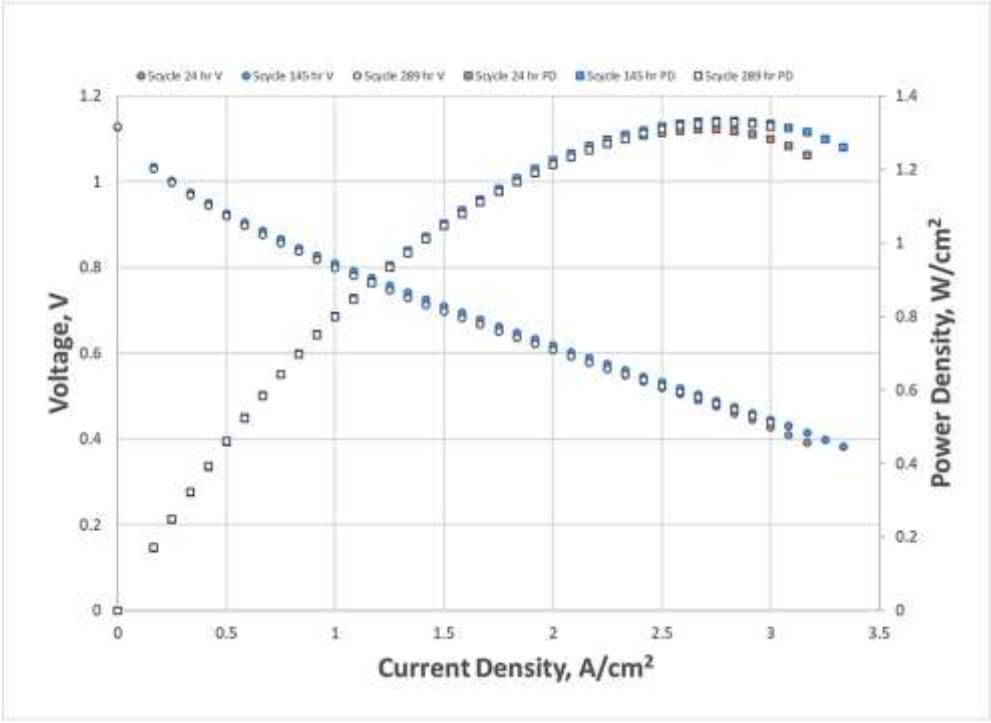

Figure 2.1-9 IV performance of 5 cycle ALD Hf 5x5 cm Cell.

A scaled-up version of the powder coating vessel was designed and fabricated. A solid model is shown in Figure 2.1-10. It consists of the porous vessel, a base and two pillow blocks with

bearings to allow rotation in the ALD reactor. The new vessel has 8x the internal volume of the previous vessel.

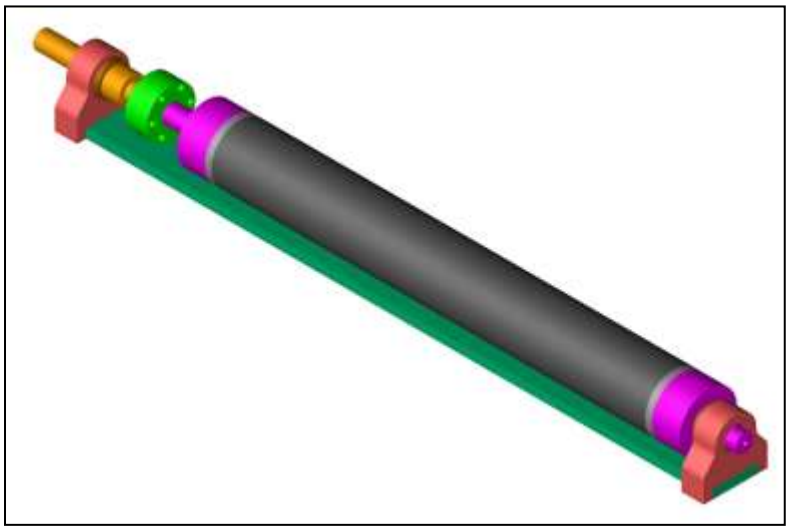

Figure 2.1-10 Solid Model of Scale Up Vessel

In addition to increased volume, which should accommodate approximately 50g of cathode powder, other improvements were made. The entire assembly is designed to sit inside a 75mm diameter ALD system. An external motor rotates the vessel at the desired speed (about 60-100 rpm). The motor is attached to the drive shaft though a vacuum feedthrough with a ferrofluidic seal (Figure 2.1-11). The new design incorporates high temperature graphite bushings to ensure continuous rotation and a Conflat sealed cap/drive assembly. This replaces a threaded assembly and should provide a tight seal so that the reactants are forced through the pores in the vessel to contact the powder contained within it.

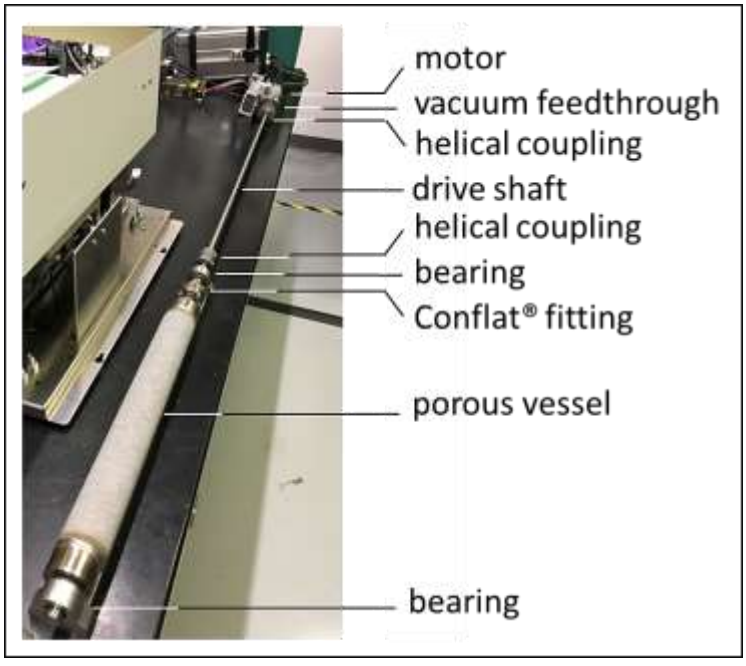

Figure 2.1-11 Scaled-up Porous Vessel Assembly on Benchtop showing Entire Apparatus

Scale-up of the ALD powder coating method was demonstrated and 60 g of coated cathode powder with 6 ALD cycles of Hf was delivered to FCE. Raman Spectroscopy was performed on 4 die pressed samples, 2 coated and 2 as received and then 1 of each was sintered @ 1000 ºC for 3 hours. Figure 2.1-12 shows the results and a difference is seen between the unsintered and sintered as the coating is amorphous and not Raman active prior to sintering. Figure 2.1-13 and Figure 2.1-14 are the reference spectra for Co3O4 and for Hafnium. The presence of Hf on the powder was verified by the spectra.

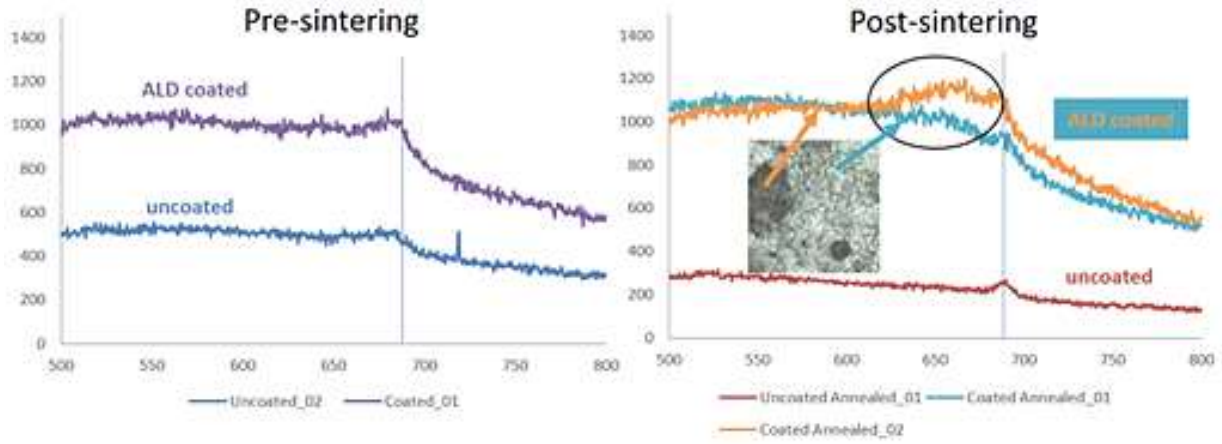

- Peak at 691 likely Co_3O_4 in cathode
- Additional Raman activity in 630-680 range after sintering appears related to ALD coating
  - HfO_2 and $SrHfO_3$ peaks are known to exist in this region
  - Light and dark regions observed optically on coated sintered cathode after sintering; further analysis needed to determine if this has any meaning

Figure 2.1-12 Raman Spectrum of Hf-coated Cathode Powder

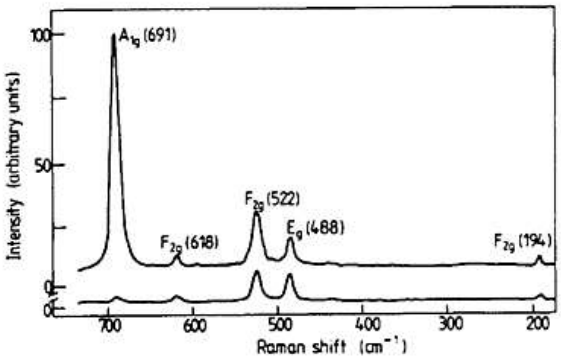

Hadjiev, VG, Iliev, MN, Vergilov, IV, "The Raman-spectra of Co_3O_4," J Phys C Solid State Phys 21 (1988) L199-201.

Figure 1. Polarised Raman spectra of Co_3O_4 at 312 K for parallel (top curve) and crossed (bottom curve) scattering polarisations. The λ_{ex} = 514.5 nm line of an Ar^+ laser was used for excitation.

- Line at 691 nm also observed in LSCF cathodes[1]
- Thin film peaks are often broad, this peak is sharper in the samples, suggesting that it may be from the cathode itself

Figure 2.1-13 Co3O4 Reference Raman Spectrum

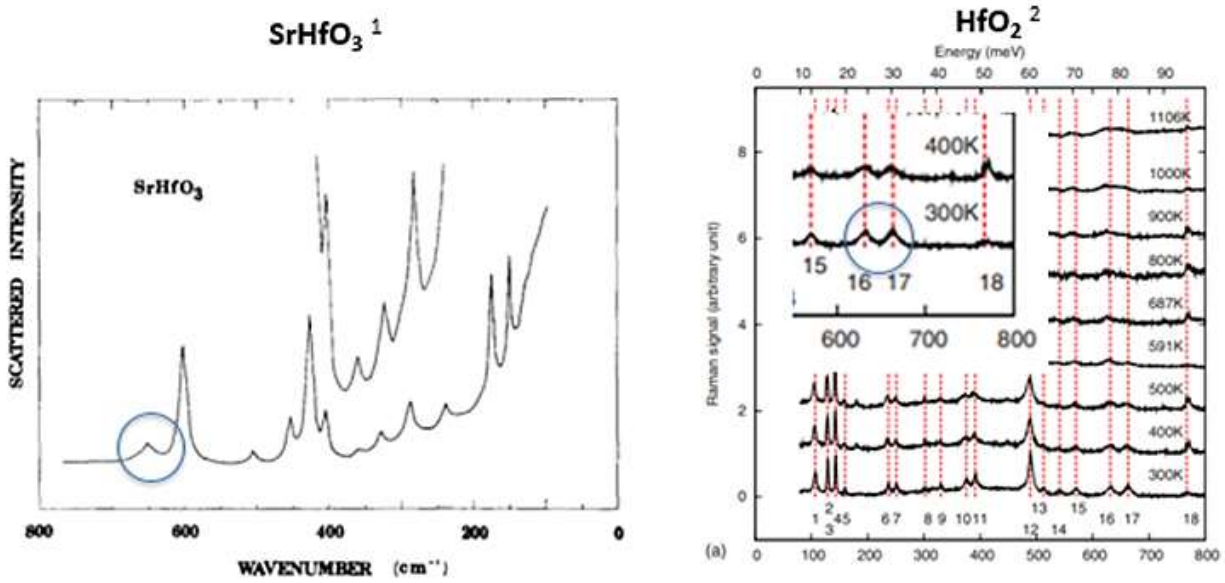

[1]C.I. Park, R.A. Condrate, Sr., and R.L. Snyder, "The Raman Spectra of Perovskite-Structured Alkaline Earth Hafnates," Appl. Spectroscopy 30 (1976) 352-353.
[2]C.W. Li, M.M. McKerns, and B. Fultz, "Raman Spectrometry study of phonon anharmonicity of hafnia at elevated temperatures," Phys. Rev. B 80 (2009) 054304.

Figure 2.1-14 Hafnia Reference Raman Spectra

2.2 Cell Manufacturing

Approach:

FCE implemented and demonstrated the efficacy of quality control inspection equipment and methods to fabricate cells and seals. The identification and implementation of appropriate equipment and methods was driven by the level of tolerance allowed of critical-to-quality (CTQ) measures required for these manufacturing steps. Current manufacturing steps were transitioned from semi-automated screen printing of the functional layers on the cell, and from dispensed seal application to fully automated vision guided screen and stencil printing, along with associated optical part inspection and measurement methods.

Technologies used to inspect critical cell measures, such as inner and outer diameter, was evaluated, and the most relevant technology was deployed. Once deployed, the resulting inspection and measurement methods were evaluated through repeatability and reproducibility studies (Gage R&R) and the quality control of the cell was maintained by continuous monitoring of measurement data and equipment inspections. The data captured from the initial lots of parts fabricated were reviewed.

Adjustments needed were implemented to the operating controls at upstream process steps, additional process steps required (such as waterjet or laser cut methods) or maintenance on equipment (inspection or other) was performed with the target of delivering 90% yield or better.

Results & Discussion:

The prior cell and stack technology, named the Large Area Stack (LAS), incorporated 254 mm x 254 mm square cells with 0.6 mm thickness. Manufacturing of this cell had successfully transitioned to automated screen printing of the functional layers. Automated screen printing proved successful in terms of throughput, quality, labour content, and operator satisfaction. With

the annular CSA cells, the transition to automated printing is somewhat more complicated with two factors complicating handling of the CSA cell relative to the LAS cell:

- The first is related to the shape of the cell. The automated screen-printing equipment is modified from the electronic printed circuit board industry. Machine vision tools are used to align the print with the part, and these vision tools while high speed and highly accurate, are designed around printed circuit board requirements, not ceramic cell printing requirements. The vision system uses a flying camera with a relatively small field of view and can identify corners or small printed features on the printed circuit board (fiducials). For the LAS cell the machine was able to identify and use the square cell corners for print alignment. For the annular CSA cells there is no usable reference geometry that the machine vision could use. By using vision tools there is no need for precise positioning of the parts (or the print screen), any offsets are corrected on the fly for every print.
- The second is related to size. With a useful print area roughly 40 cm x 40 cm it would be vastly underused relative to its potential if only one 81 cm^2 (12 cm diameter) annular cell was printed at a time. However, the machine vision alignment of the print applies to the full work area. It is not possible to have individual print cycles for an array of parts in the print area[1]. Even if it were, that would still reduce the throughput relative to the potential, as a significant portion of the operating cycle is the print. In other words, it was highly desirable to print many cells in one print cycle, and this requires that the cells be placed accurately with respect to a design position.

A consequence of the above constraints and the goal of printing many cells in a single cycle, is a need to locate all cells precisely within the print area. This needs to be done by tooling that operates in parallel with the overall automated printing line, while retaining all the benefits of automatic upstream and downstream feeding as well as the printing. As a first approach, tooling was manufactured that attempted to passively centre the cells as they were dropped from the feed position into the print position within the equipment. Without going into details this equipment used conical centering pins to guide the cell into a target position as it dropped into the print position.

The above approach failed to deliver the required placement accuracy. The problem was that the cells could not be guaranteed to be accurately circular so, for example, a cell that was slightly wider than tall might align properly front to back, but still have clearance side to side that allowed too much misplacement. A centering mechanism that independently centered in two directions was required, and this led to an active centring mechanism.

A new mechanism was built and incorporated into the semi-automated printing line. This line is run by an operator who loads and unloads the cell and triggers the screen-printing cycle which is carried out without any further machine alignment. There is no vision system on this printing line, and it only prints one cell per cycle, but it allowed iteration and debugging of a more complex active centering mechanism.

Figure 2.2-1 through Figure 2.2-3 shows the cell loading and centering sequence. In Figure 2.2-1 the cell has been dropped onto the print stage without much care as to position. In Figure 2.2-2 two independent sets of alignment pins have risen to centre the cell both front to back and side to side respectively. If the cell is slightly wider than it is tall, then the left/right pin pair would open slightly wider than the front/back pair. In Figure 2.2-3 the cell has been pulled against the print

[1] Some machines offer cycles that allow printing half the print area at a time (e.g.: front half then back half), but this does not address the overall desire to load many parts and print them simultaneously.

table with vacuum, and the pins have retracted, leaving the top surface fully clear for the screen printing cycle.

This jig has been deployed and successfully used. A large batch of cells were produced on this tooling, amounting to over 1000 cells. With these satisfying results, the intent was to move efforts back to the fully automated screen-printing line, building a 3x3 print layout using nine copies of this cell centering fixture on a common base plate.

Figure 2.2-1 Cell loaded roughly into position (offset left and up)

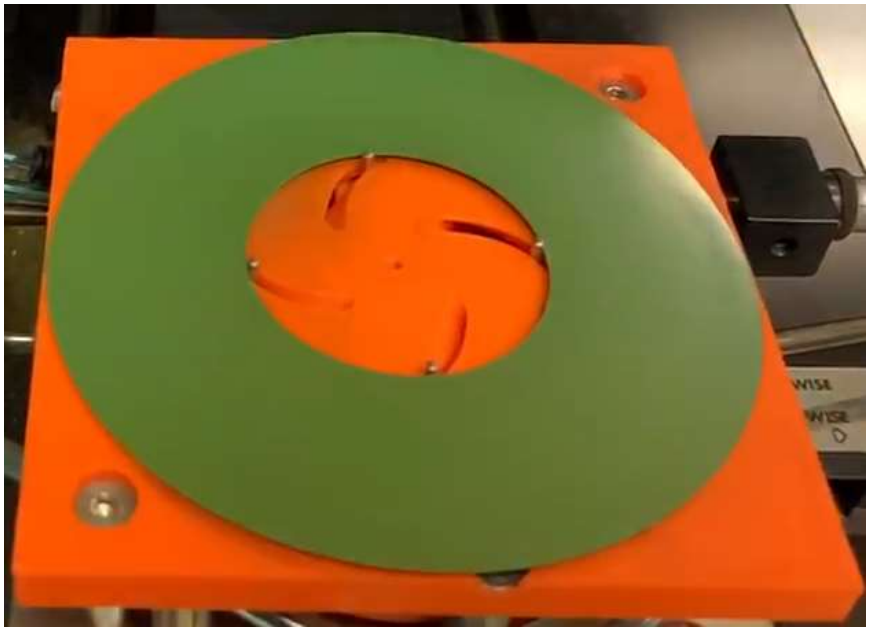

Figure 2.2-2 Cell centered vertically and horizontally.

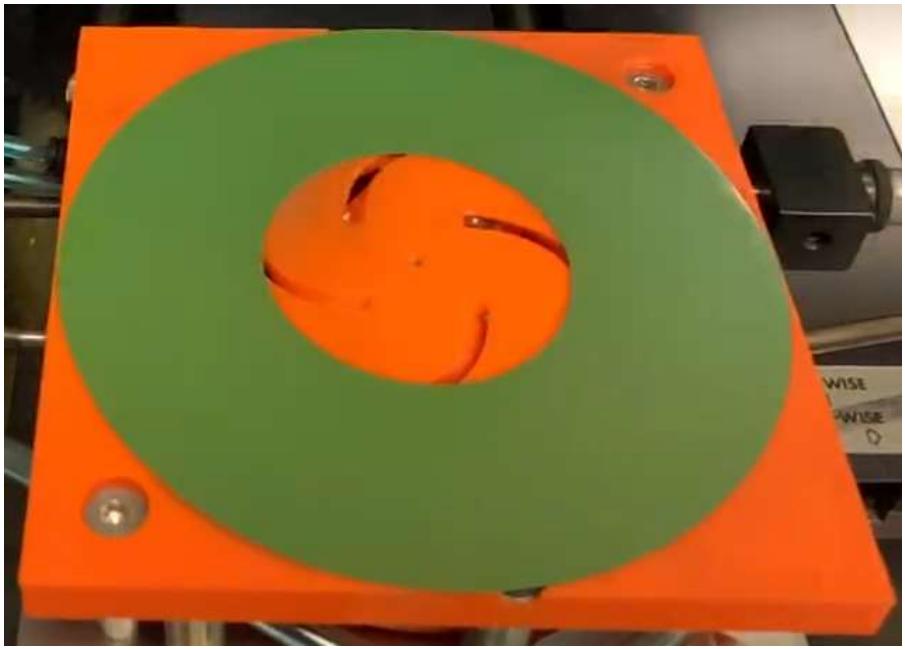

Figure 2.2-3 Cell vacuumed against print table and ready for the print cycle.

A cell sizing process to correct for dimensional variances in the OD and ID of the cells, through an automated cell grinding process was developed. The goal is to have sufficient control of manufacturing variables to meet the dell dimensional targets, with limited resultant warpage. This is a significant challenge with ceramics processing, but progress was made. Parallel waterjet cutting of cells (external supplier) has been demonstrated, and in-house wet grinding of cells is in development. Figure 2.2-4 shows a small robot (Denso VP-5243) with a custom end effector that can grip a cell while supporting the inside diameter and outside diameter for grinding. As process control has improved in cell manufacturing, the focus on these alternative sizing approaches has lessened.

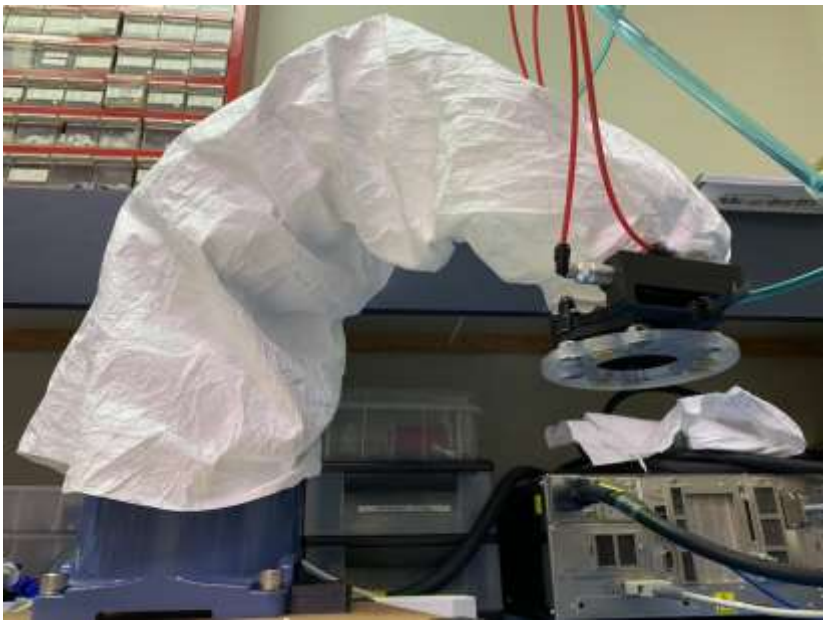

Figure 2.2-4 Cell Grinding Robot with Cell Gripper and Protective Cover

Cell production is manufacturing the 120 mm outer diameter CSA cell. This is an anode supported cell that is 300 µm thick. To meet cell requirements for the development stacks as well as the final 6 full size stack deliverables, CSA cell manufacturing process development and pilot production started. FCE addressed three major manufacturing challenges namely: (1) half-cells failing outer diameter specification, (2) half-cell visual defects, and (3) cell ironing failures.

For the first dimensional issue related to diameter, two solutions were pursued. As a preferred approach, cells are cut to a particular oval shape at the green state prior to cell sintering which adjusts for the anisotropic shrinkage of the sintering process. Continued Design of Experiment (DoE) and tracking of batch yields was actively and continually seeking to identify optimal green cutting size which would maximize dimensional yield after sintering. The second approach is related to outsourced waterjet cell cutting, which was qualified in the past, and development of in-house cell grinding.

The second issue that needed to be addressed was half-cell visual defects. Improvements in tape casting addressed in-cell / in-tape casting lines and resulted in higher half-cell visual yield.

In order to progress the automated screen-printing effort, discussions were held with Stone Mountain Tool, a specialist in designing tooling for the electronics industry. Among other things they design tooling to carry odd-shaped printed circuit boards through automated screen-printing equipment such as we operate at FuelCell Energy. These part pallets can range from simple carriers to complex auto-aligning fixtures. After several iterations, Stone Mountain recommended a relatively simple pallet design to mate with the automatic centering tooling installed into the screen printer.

In other efforts, general improvements to the cell production process have been rolled out, with the aim of increasing cell consistency to improve yield and lower net cost. Figure 2.2-5 illustrates upgrades to the continuous tape caster consisting of two main changes. In the original configuration the tape caster cast onto a polyester film (commonly known as Mylar) over a looped stainless-steel belt. The stainless-steel belt was guided by rollers and a conventional flooded casting box sat on top of the polyester film on the supported belt.

In the revised design a custom glass insert is placed between the stainless belt and the polyester film and anchored to the tape caster. The glass plate extends 6’ into the tape caster, providing a highly accurate and consistent surface below the casting box and into the initial drying section of the tape caster. Coupled with the glass plate is a new and novel casting box that has a very small fluid reservoir as compared to a conventional casting box but incorporates automatic height control in the slurry reservoir and a submerged inlet port. This casting box greatly reduces the influence of the free surface of the slurry on the resulting tape, making it largely insensitive to the inevitable solvent evaporation off the upper surface of the slurry.

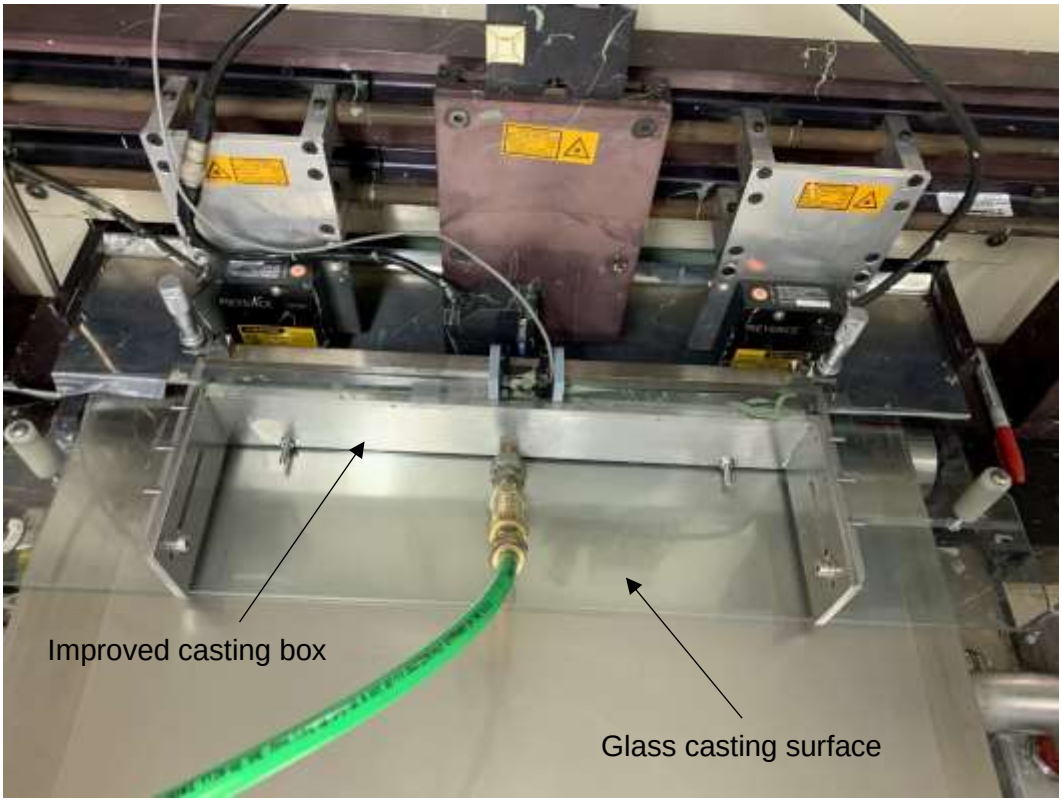

Figure 2.2-5 Glass Surface and Pressure-controlled Casting Box Modifications

Cell thickness consistency, measured as the reported cell thickness after firing, was improved dramatically with these changes. Figure 2.2-6 shows a run chart of cell thicknesses and the improvement from the glass casting surface is obvious.

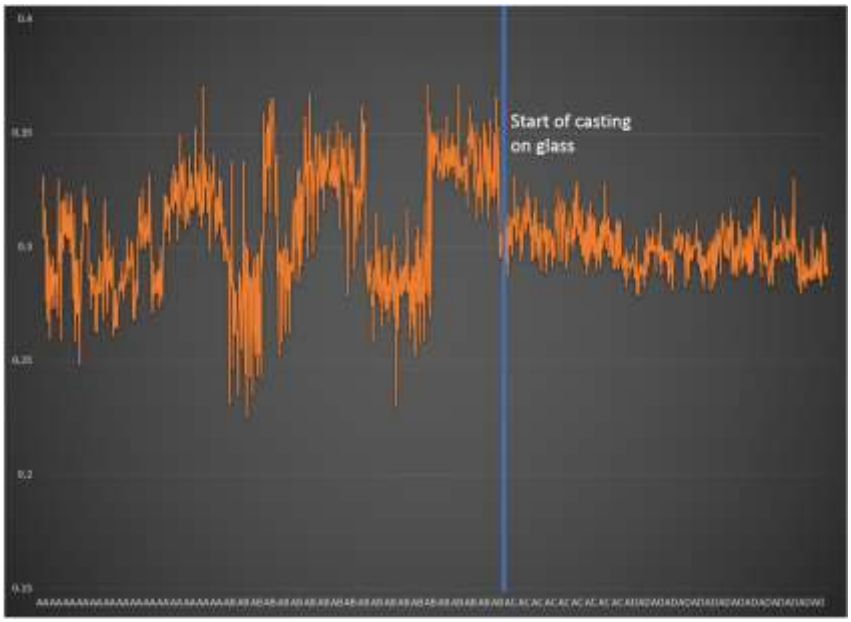

Figure 2.2-6 Run Chart of Cell Thickness, post-firing, after Glass Casting Surface Change

Another cell process improvement that was implemented was to move to localized printing of the cell functional layers (Figure 2.2-7). This consists of printing the anode functional layer and the electrolyte layers only where needed on the raw tape. The move to localized printing has required more accurate placement between prints and before cutting, and accounting for the slight shrinkage that occurs at each drying step. However, there are several benefits to this approach:

- Less material usage means lower intrinsic cost.
- Higher throughput in printing as refills are substantially reduced.
- Less distortion through drying and easier to handle tape.
- Better recyclability of the off-cut tape

Figure 2.2-7 Localized Functional Layer Printing

These pallets carry nine cells or interconnects and can be used for automatic feeding into an automated screen-printing line (for functional layer and contact layer printing) or an automated dispensing line (for seal application). Example pallets loaded with cells and with interconnects is shown in Figure 2.2-8.

Figure 2.2-8 Parts Pallet-loaded with cells (left) and interconnects (right)

Figure 2.2-9 Revised low-volume level-controlled casting box (right) installed at head of tape caster (right)

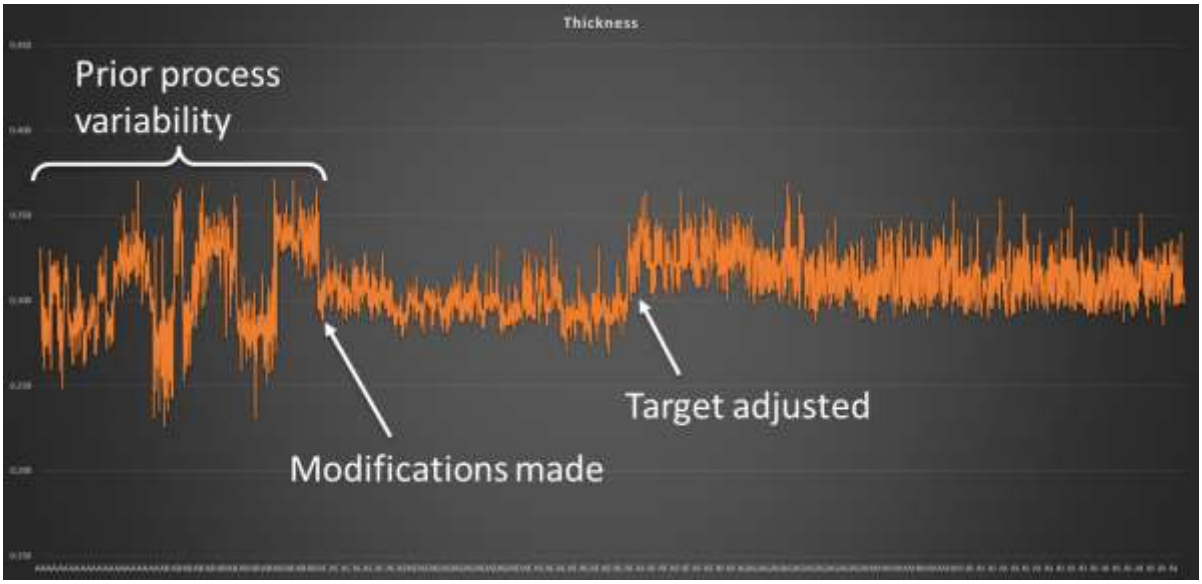

Figure 2.2-10 Run Chart – Final Cell Thickness

2.3 Cell Performance Testing

Approach:

FCE evaluated the next generation cells, based on the results obtained in Tasks 2.1 and 2.2, using conventional cell test procedures including, but not limited to, voltage current power curves and steady state degradation analysis. A number of 500-hour tests on cells, fabricated using the ALD coating solution developed during Task 2.1, verify both cell voltage degradation targets: 1) <0.5% per 1000 hours; and 2) <0.2% per 1000 hours. For success, the strategy here is that the component level performance needs to exceed and go beyond the targeted stack and modular level requirements in order to meet those upper-level performance targets. Electrochemical Impedance Spectroscopy analysis, and morphological and compositional analysis were

completed utilizing a variety of analytical and surface characterization on cells after completion of tests.

Results & Discussion:

Powder was received from Joseph Barton, FCE, Danbury labelled "ALD-Coated Cathode." Cathode paste was prepared using VPS standard cathode formulation and processing and substituting standard cathode powder with "ALD-Coated Cathode" powder on an equivalent weight basis. The cathode paste was printed onto a standard TSC-3 cell (10 cm x 10 cm with 81 cm2 active area). Paste viscosity was similar to standard cathode paste and so no modifications to processing were required. The test uses no coated jigs or Cr-getters. The cell was tested in station 18, first running power curves from 800 to 650 ˚C with 2 SLPM Air and 2 SLPM Hydrogen with 3% Water. Figure 2.3-1 shows the power curves run at 50 ˚C increments with performance comparable to standard TSC-3 cells. The cell was then set to run steady state at 750 C with Air (25% Uo) and Fuel (50% Uf) compositions as shown in Figure 2.3-2 and running at 40.5 A (0.5 A/cm2). The cell continues to operate at the time of writing after 1,120 hours uninterrupted operation with a degradation rate of 2 mV/khrs or 0.2 %/khrs.

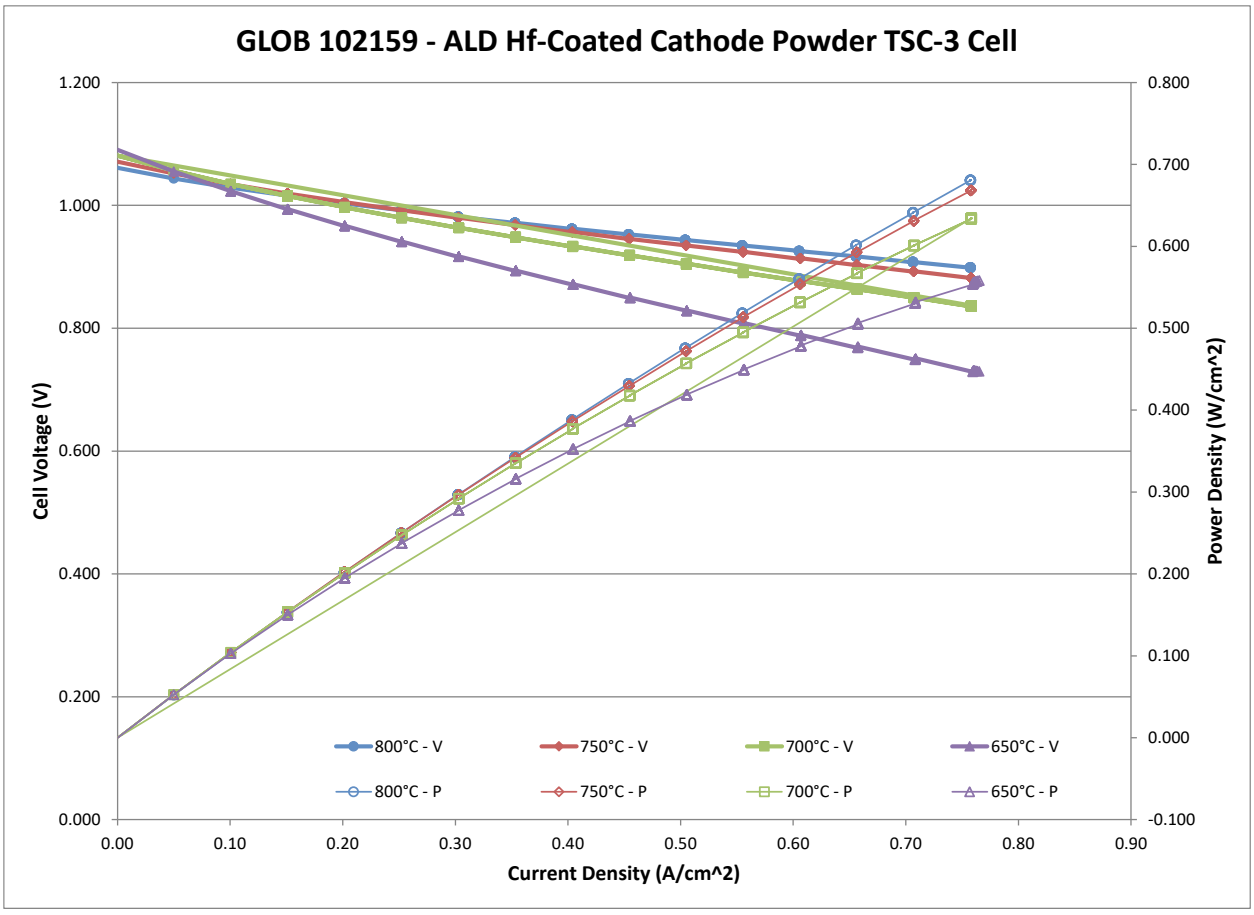

Figure 2.3-1 Power Curves 800 – 650°C for 102159, TSC-3 Cell with ALD Coated Cathode Powder

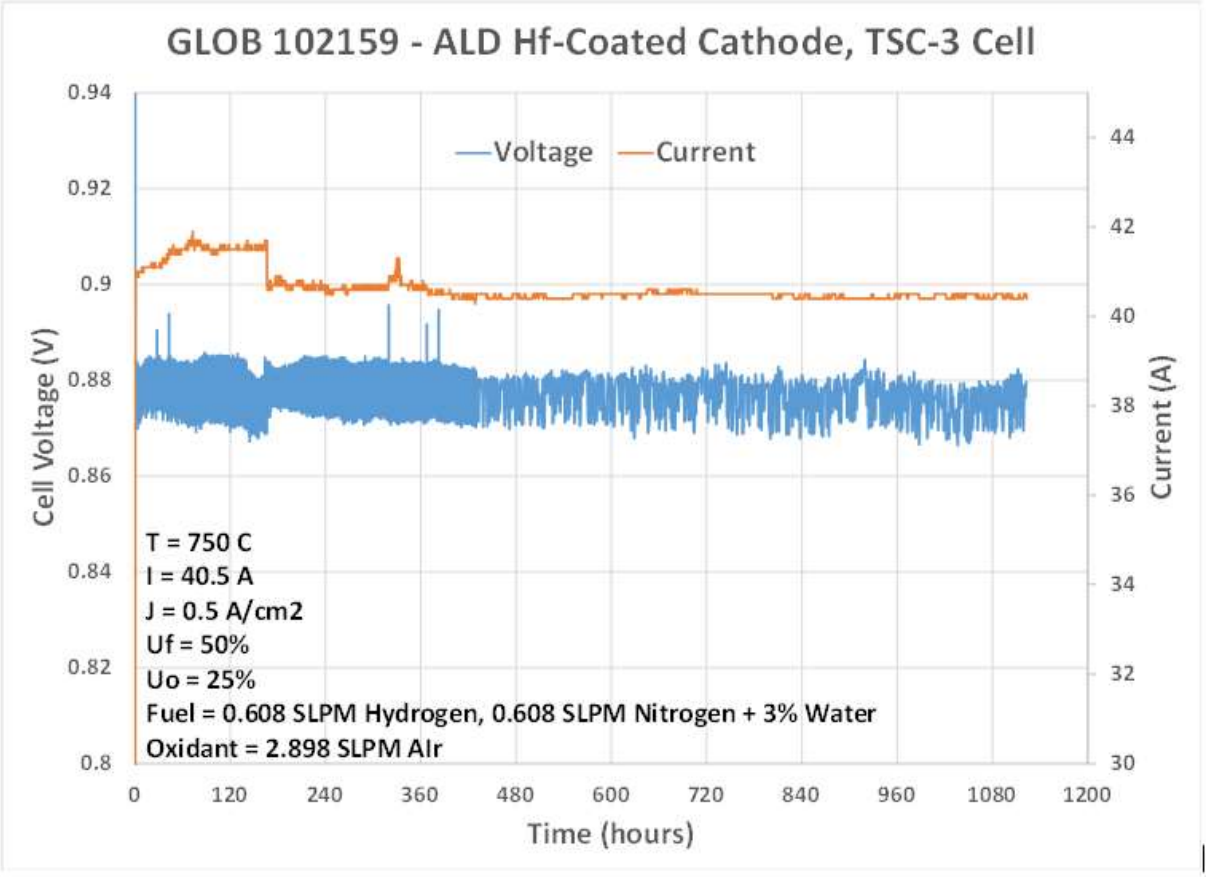

Figure 2.3-2 Steady-State Hold at 0.5 A/cm^2 and 750°C for 102159, TSC-3 Cell with ALD Coated Cathode Powder

After meeting milestones M2.4, M2.5 and M2.6, showing ALD coated cathode cell operating for greater than 500 hours with less than 0.2% per 1000 hours voltage degradation, the cell continued to operate at the time of writing after 3,850 hours operation with a degradation rate of 4 mV/khrs or 0.5 %/khrs (Figure 2.3-3).

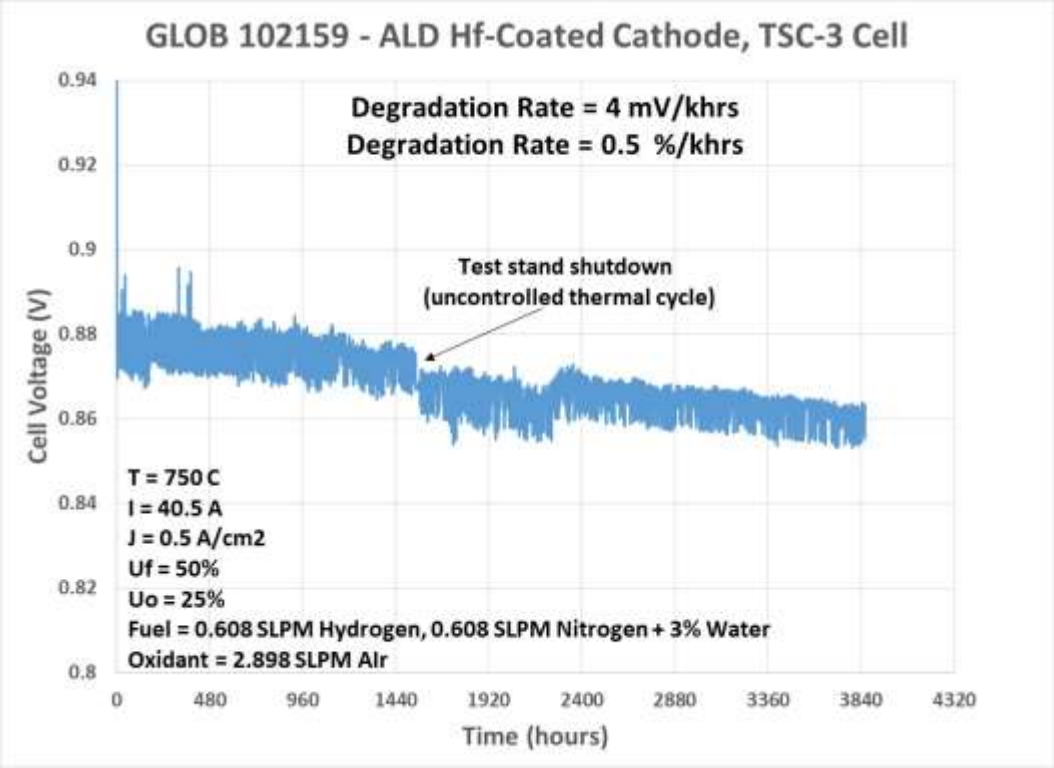

Figure 2.3-3 Steady-State Hold at 0.5 A/cm^2 and 750°C for 102159, TSC-3 Cell with ALD Coated Cathode Powder

3 SOFC Stack Development

Objective:

The objective of this task was to develop and to fabricate 6 x 350-cell 7 kW CSA stacks with a particular focus on control of manufacturing repeatability and reproducibility to improve stack reliability.

3.1 Stack Manufacturing

Approach:

Manufacturing development efforts focused on improving repeatability and reliability of the assembled 350-cell CSA stack. Tooling, use of fixtures, and quality control checks to fabricate seals, sub-assemblies and stack non-repeat parts to ensure stack to stack consistency, were critical to the performance of stacks deployed into arrays assembled into modular units. Methods appropriate to the tolerance allowed of CTQ measures were identified and implemented in inspection equipment and evaluation of technologies for automated inspection of applied seals for profile and volume. The resulting inspection and measurement methods were evaluated through repeatability and reproducibility studies (Gage R&R). The quality control of the seals was maintained by continuous monitoring of measurement data and equipment inspections.

Results & Discussion:

FuelCell Energy's advanced solid oxide technology is the result of decades of development of the solid oxide platform with a focus on a variety of target applications, and we have developed an

approach to a common cell stack platform that can be used in power generation, electrolysis, and energy storage systems. The technology has been demonstrated in bench-scale systems for energy storage and electrolysis, and a 200kW field demonstration has recently completed for the power generation platform.

The solid oxide stack (shown in **Error! Reference source not found.**) is comprised of planar solid oxide fuel cells with glass ceramic seals and sheet metal, bipolar plate interconnects; and has a mix of internal and external gas manifolds. A full height stack is shown in the following figure. Each cell is a 0.30 mm thick annular (donut shaped), cell with 81 cm2 active area made in a process consisting of tape casting, screen printing, and firing cell components. The full height stack consists of 350 repeat units and a set of non-repeat parts. A repeat unit includes one ceramic cell, inner and outer seals, and a metallic interconnect which incorporates flow fields for both fuel and oxidant. Non-repeat parts include the end plates, manifolds, and compression components. The stack is 17 inches high and is capable of producing 6-7kW power when fueled with natural gas, biogas, hydrogen, or other fuels. The same stack is capable of operating at higher power density in electrolysis mode, producing 15 kg/day hydrogen with 22 kW power input.

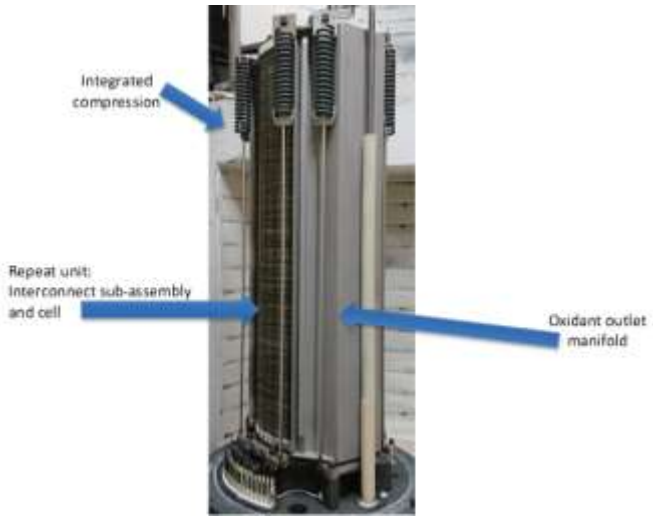

Figure 3.1-1 Solid Oxide Cell Stack

Advanced automated stack manufacturing methods, as shown in **Error! Reference source not found.**, have been developed to ensure that the low material cost of the stack is matched with low labor and overhead cost. The figures below show FCE's automated printing line used for solid oxide cells and robotic cell-stack assembly facility. The automated system performs the stack build at ~12 seconds per repeat layer, including optical part inspection, cell leak test and thickness measurement, interconnect spot weld and leak test, and part-marking for stack quality assurance.

Figure 3.1-2 Automated Stack Assembly Facility

3.2 Technology Stack Testing

Approach:

FCE consolidated improvements from prior tasks to demonstrate reliable stack performance under system representative conditions. Up to five technology stacks were built and tested, with the combined goals of validating the development efforts of Tasks 2.0 and 3.1 and of validating and exploring the anticipated system conditions developed under Task 4. Validation testing included electrochemical qualification and testing, as well as demonstration of stack pressure drop equivalence and a gas integrity leak test.

Results & Discussion:

FuelCell Energy, Inc. (FCE) has been actively developing a new high specific power stack design internally designated the CSA stack. This design offers a 4 to 5x increase in power to weight and a 6x power to volume improvement over the prior generation Large Area Stack (LAS) stack, along with associated cost and functionality benefits. This project was designed around the CSA stack.

As stability of the stack platform has improved, it has become apparent that it is not delivering the full performance potential of the underlying cell materials. Operating on simulated reformate the latest stacks are roughly 65 mV/cell lower performance than the prior generation LAS stacks. Part of the performance difference may be explained by a difference in air utilization where the LAS stacks required 15% air utilization in order to maintain thermal control, whereas the CSA stacks are designed to run at 40% air utilization, or less than half the air flow. However, the theoretical impact of this change in utilization is only a few millivolts shift in the Nernst potential, not enough to explain the majority of the performance gap.

One area that has come to be suspected is flow maldistribution within the unit cell, leading to localized starvation of the cell, having the effect of reducing the useful active area of the cell. The anode side is a particular area of concern. The anode flow starts and ends in the center of the annular cell. Without re-distribution, the flow would tend to short circuit around the inside of the annular cell area rather than flowing to the outer edge. Compounding the challenge is that the outer edge of the cell is proportionally more important as it represents a larger active area of the cell.

Much of the unit cell design is focussed around forcing the anode flow away from the inner annulus and towards the outside of the unit cell. This is accomplished through detailed design of ribs and features that re-distribute the flow. In CFD modelling this effort has yielded very good flow distribution. However, on review it has been realized that there is a potential for flow to bypass the ribs through a secondary contact media that lies between the cell and the interconnect. Figure

3.2-1 shows a CFD study of a short span of representative rib, covered with a detailed model of the contact media. As can be seen, the openings are just large enough to permit localized flow bypass.

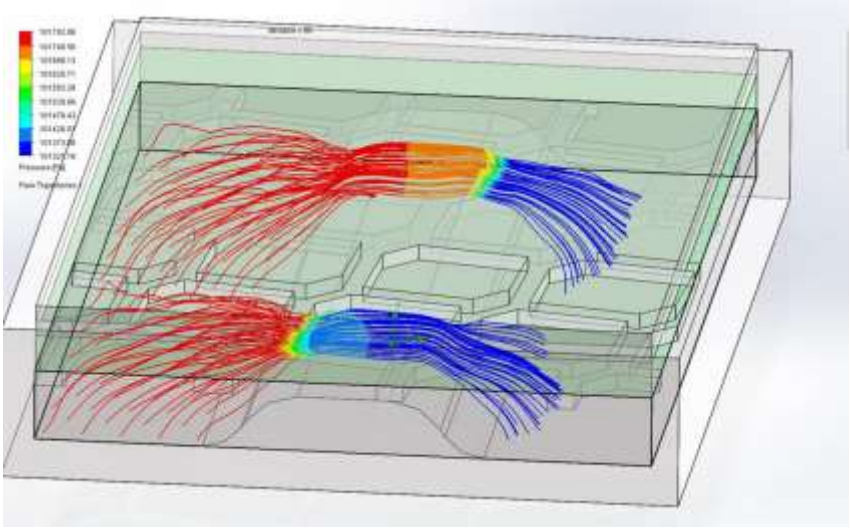

Figure 3.2-1 Rib bypass through anode contact media.

The detailed contact media geometry is too detailed to be deployed in-house across a full unit cell model. Instead, a porous media model was developed that offers the same flow characteristics, on an average basis, as the detailed model. Figure 3.2-2 shows the resultant porous media model at the same total bypass flow as the detailed model in Figure 3.2-1. Although the local behavior on the scale of this small sample is quite different, the average over longer ribs should be comparable. This porous media was then applied to a full interconnect flow model.

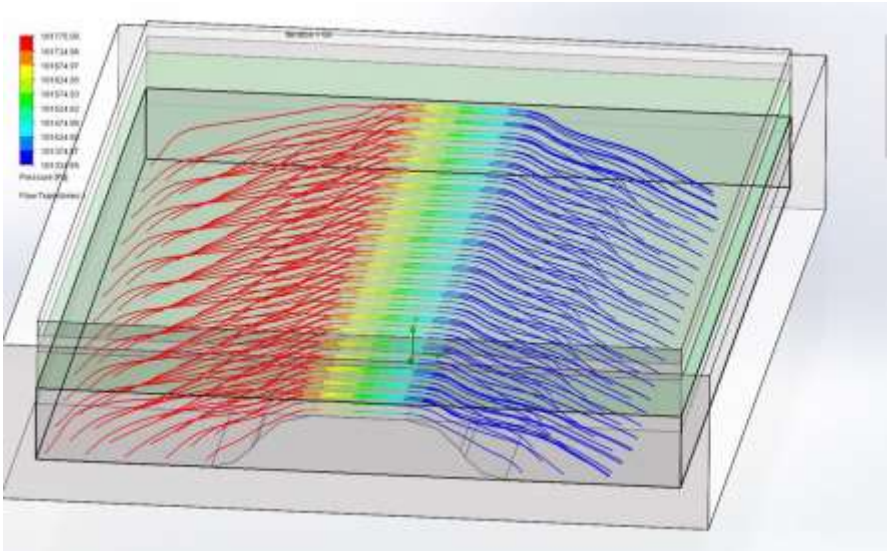

Figure 3.2-2 Bulk porous media model at same bypass flow.

Table 3.2-1 Results of the Flow Distribution Analysis

	As designed (no bypass)	With contact bypass flow		Percentage of active area
Inner channel	101%	331%		8.3%
Channel 2	100%	100%		8.7%
Channel 3	100%	90%		9.9%
Channel 4	101%	87%		10.5%
Channel 5	100%	79%		11.2%
Channel 6	99%	72%		12.0%
Channel 7	100%	66%		12.8%
Channel 8	100%	62%		13.9%
Outer Channel	99%	89%		12.7%

The results are captured in Table 3.2-1 and show a significant flow maldistribution. Over one quarter of the cell (channels 7 and 8) may be receiving less than two thirds of the intended flow. E.g.: If the flow was set for 50% overall utilization, 26.7% of the cell might be running at 75% utilization. If the flow was set for 68% overall utilization, 26.7% of the cell might be running over 100% utilization.

In practice the starved portions of the cell wouldn't run to such extreme utilizations, instead they would shed current load towards the sections of cell that are more favorably fed. As portions of the cell deactivated electrically, the remainder of the cell would be running at higher current density than targeted, leading to lower voltage. This is consistent with the recent utilization performance as discussed in more detail below.

To explore this in more detail, a higher density and thinner contact media was acquired. The higher density mesh has features that are too small to bridge the ribs in the interconnect and should get the design closer to theoretical performance.

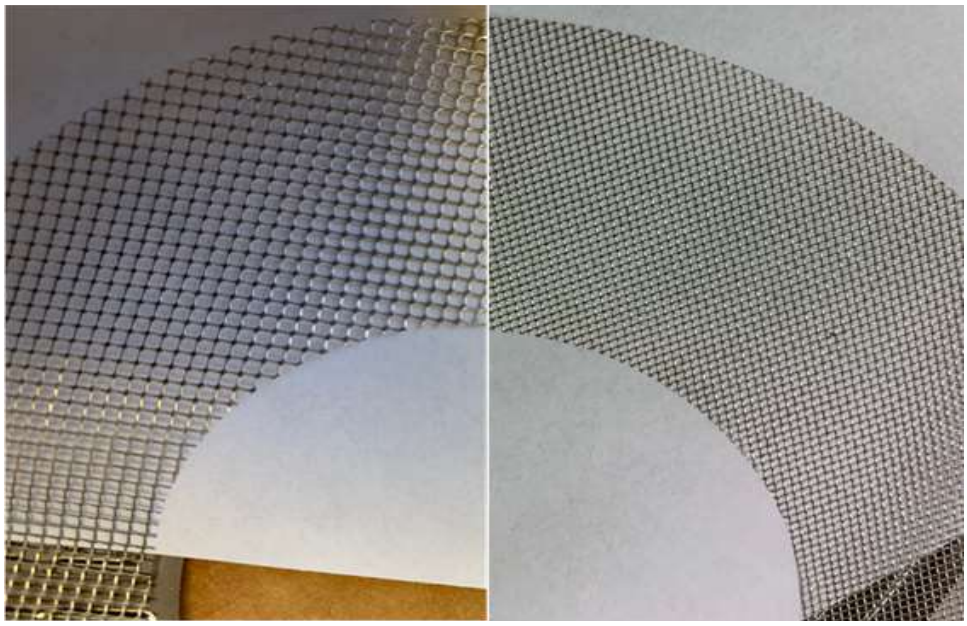

Figure 3.2-3 Comparison of anode mesh geometry – Baseline (left), Higher Density (Right)

A 45-cell parametric stack was built (GT060248-0013) with the higher density mesh. It was parametric in the incorporation of two interconnect materials. A Sanergy HT material which had been the baseline material to date, and a SS441 material which was proposed as a replacement material due to a stop in production of the Sanergy HT. The materials have proven similar in applications at FCE and externally and this was viewed as a low-risk validation of the new material, before incorporating it into regular production.

However, testing showed a significant difference as can be seen in Figure 3.2-4. The blue traces represent the cell layers with SS441 interconnects. The pink traces the cell layers using the Sanergy HT material. At most conditions only the weakest of the SS441 layers was weaker than the strongest of the Sanergy HT layers. At some conditions there was no overlap at all. Ignoring the end grouping of cells 1-5, which is probably a little cold, the SS441 layers were stronger than the Sanergy HT layers at all conditions. There was no technical reason for the base material to have this effect, and these results led to the discovery that a batch of interconnects had been manufactured upside down, putting the protective coatings on the incorrect sides of the interconnects. This error has negatively affected performance where the inverted interconnects were used.

While finding the inverted interconnects is a positive step in that it triggered a review of all interconnect inventory and a sorting and quarantining of inverted parts, it does interfere with the intended focus of this test.

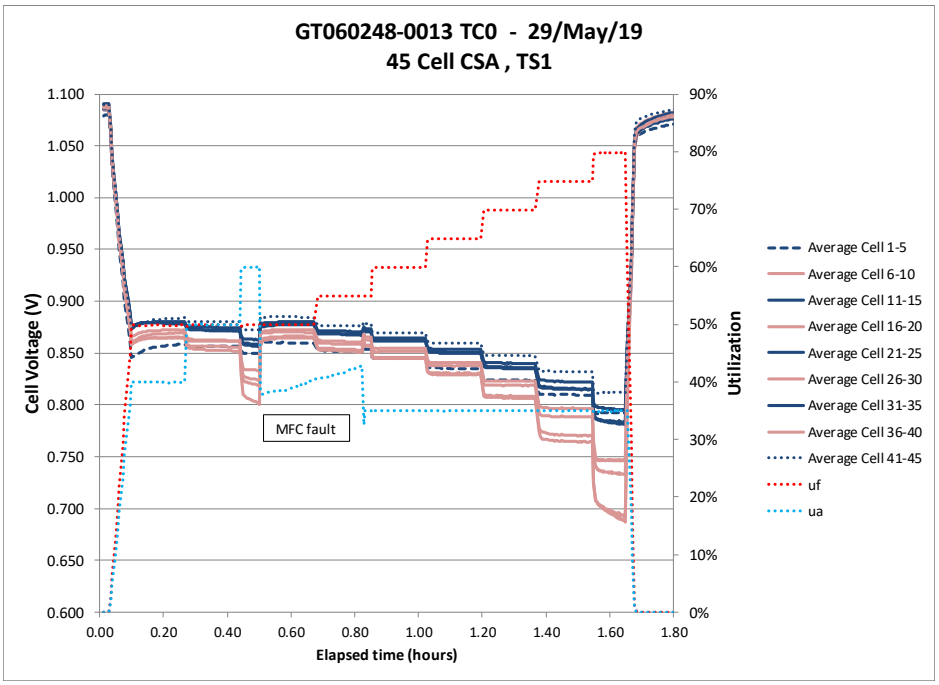

Figure 3.2-4 Utilization testing of parametric stack GT060248-0013

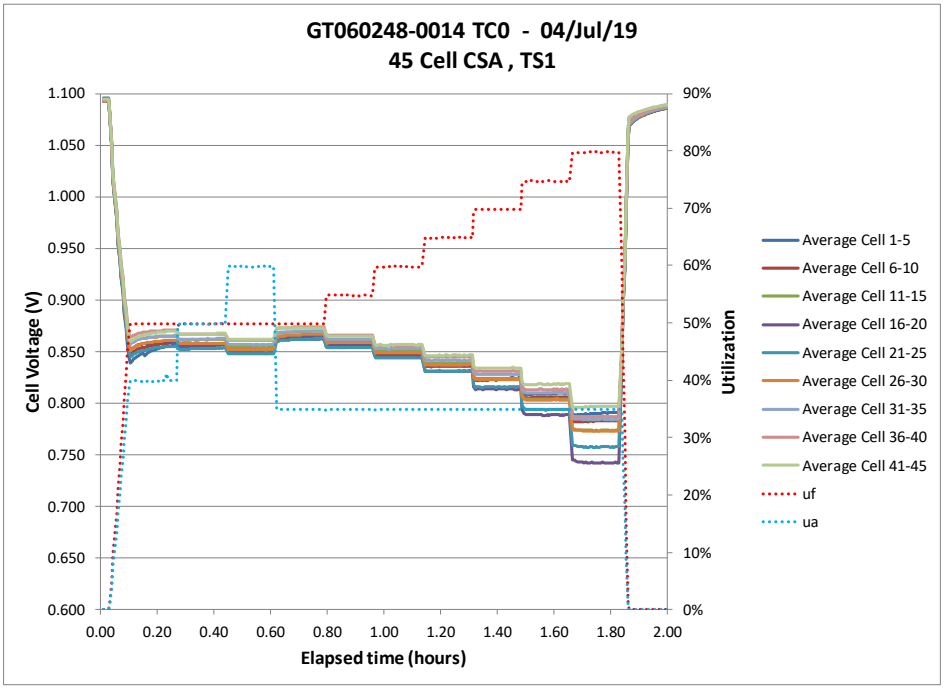

Figure 3.2-5 GT060248-0014 utilization.

Subsequent stack GT060248-0014 was built entirely with SS441 interconnects and the original coarser contact mesh. If we compare the average performance of the SS441 layers between the two stacks, there is a 10 mV to 15 mV higher performance in stack 13 which incorporated the higher density contact layer. Stack 14 results are shown in Figure 3.2-5.

Whether this is truly representative of the performance difference of the two meshes is unclear due to the compromised nature of the first test. For example, the inverted interconnects led to higher electrical losses in those layers and more heating, this would tend to increase the DP in these layers, pushing more flow to the SS441 layers, and therefore lowering their effective utilization. On the other hand, there are indications the SS441 layers were running upwards of 10°C cooler in stack 13 than in stack 14, probably an artefact of increased flow and possibly from lower electrical losses. One of these would tend to increase performance while one would tend to decrease performance – it is therefore difficult to quantify the true effect of the higher density contact material.

Stable operation in fuel cell operation was shown by reducing the current and/or imposing less aggressive fuel utilization conditions. Figure 3.2-6 shows test results on 45-cell CSA stack GT060248-0012 which has the inverted interconnects, it ran for 1600 hours, the last 1200 hours of which at 40% fuel utilization and 40% air utilization, at 0.25 A/cm^2. The fuel side was supplied with a simulated reformate that includes natural gas with on-cell reforming. At the last condition the stack has been degrading at a rate of 9.7 mV/cell/khr overall.

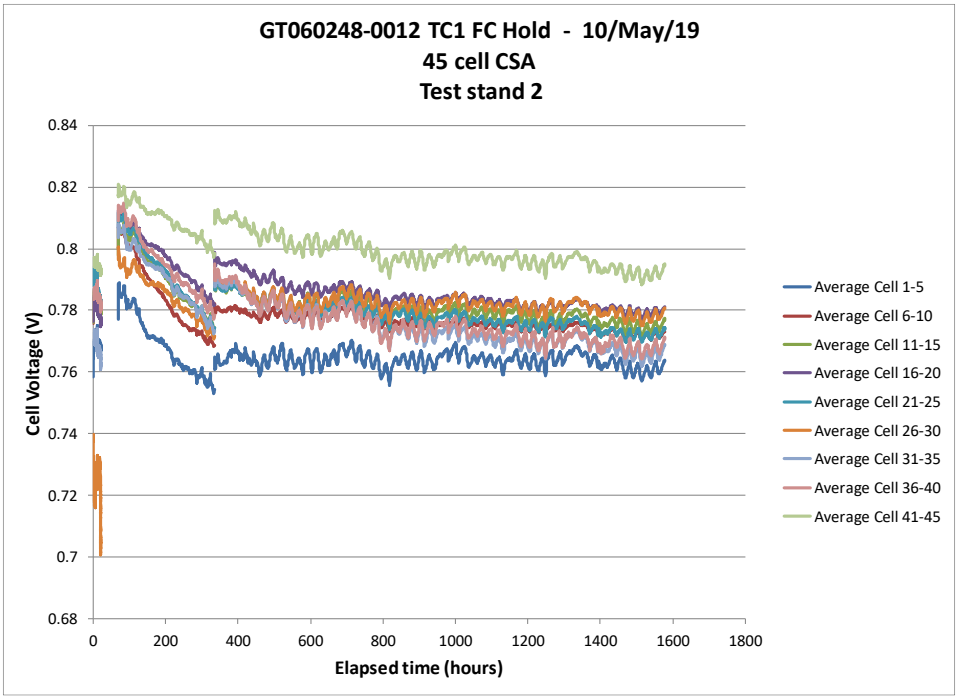

Figure 3.2-6 GT060248-0012 with improperly coating interconnect, running 40% fuel utilization on simulated reformate, 40% air utilization, and 0.25 A/cm^2.

The first full height CSA stack was built and tested in fuel cell mode at greater than 5 kW. This represents the culmination of work under parallel project DE-FE0026093 for the demonstration of the low-cost, high-power density CSA stack at > 5 kWe output while operating on reformate. This was an opportunity to validate the production processes for the full height stack and for the automated stack build. A problem with part feeding arose with the larger quantities but was resolved. The build completed in 52 minutes at an average time of 9.2 seconds per layer, and a production rate approaching 10 MW/year per 7-hour shift.

Figure 3.2-7 shows the stack installed into the test stand. The integrated (hot) compression springs are visible towards the top, as is the compliant current collection connection. One of the air manifolds is visible towards the front right; the second, behind the stack.

Figure 3.2-7 First Full Height CSA Stack Installed in Test Stand

The 350-cell stack is being tested under the following conditions:

- 18 A (0.222 A/cm^2) – limited due to failure of one of the parallel load banks
- 50% fuel utilization, 35% air utilization
- Simulated reformate:
    - 8.6 dry% Natural gas (desulfurized)
    - 59.8 dry% Hydrogen (H2 & CO surrogate)
    - 31.6 dry% Nitrogen (CO2 surrogate)
    - 26% humidity

These conditions are representative of an anode recycle system with recycle sufficient to ensure water independence, corresponding to:

- 37% stack level internal reforming
- 100% system level internal reforming

The resultant cell voltages are as shown in Figure 3.2-8. General observations include:

- The voltage distribution is tight, within 20 mV average cell voltage top to bottom. This is indicative of good vertical flow distribution, validating the manifold sizing and configuration

for the full height stack. This also validates the thermal design and the ability of the stack to present similar thermal conditions top-to-bottom.

- Operation was stable, all cells responded roughly the same with time. This suggests a good overall build with no localized differences that might lead to different degradation characteristics.
- The cells appreciated in voltage over the first ~550 hours. While the cause of this is unclear, there was a shorting event associated with a failure in the original load bank that likely resulted in a short term but aggressive redox event. It is suspected that at least some of the cell appreciation is a slow recovery from this redox event.

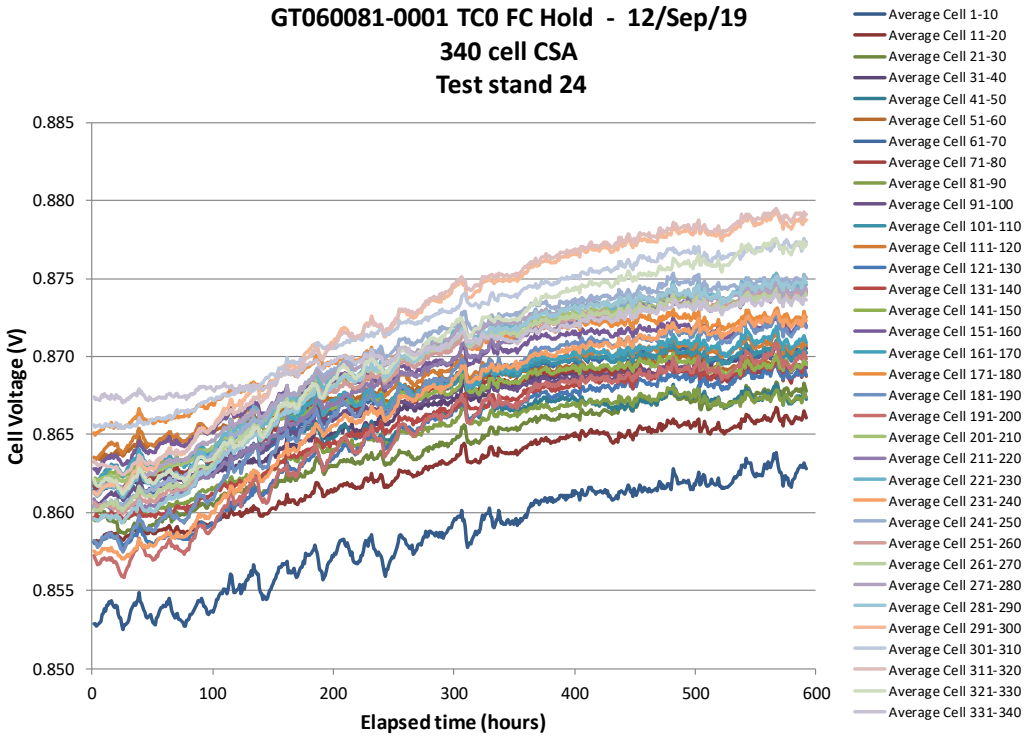

Figure 3.2-8 GT060081-0001 Fuel cell degradation test.

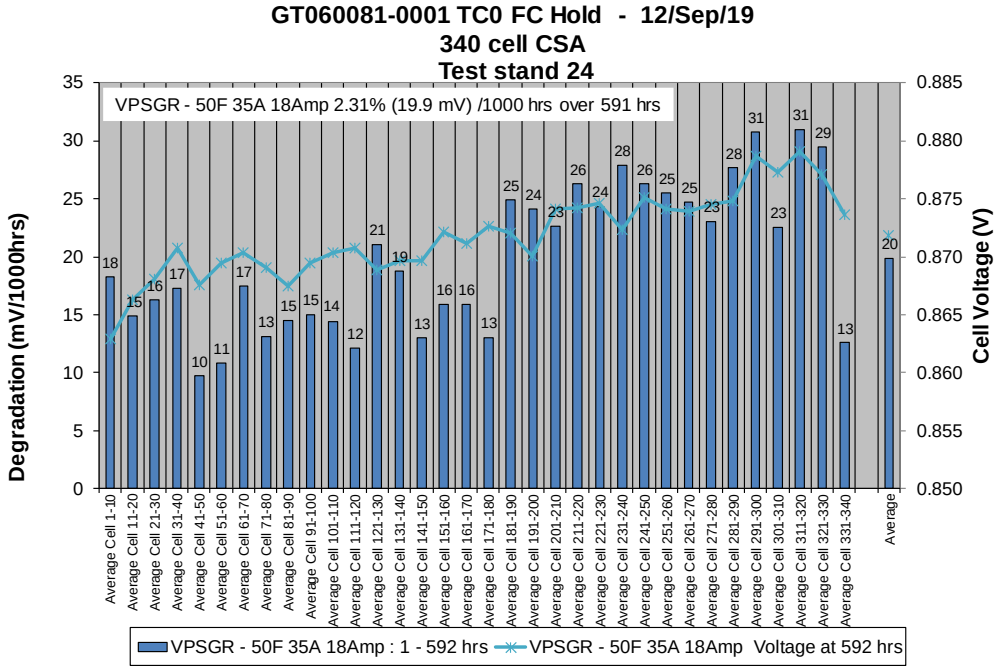

Figure 3.2-9 GT060081-0001 Degradation by cell position, 0 to 591 hours.

Figure 3.2-9 shows the same data replotted as average linear fit degradation rate over the first 591 hours. Positive values indicate an increase in performance over the hold. This graph shows the overall uniformity of the stack. There is a slight trend towards higher voltages with cell number, and a slight trend towards more voltage recovery with cell number. There is a correlation here with cell thickness, which were ordered from thickest (400 micron) to thinnest (290 micron) through the stack height. Generally thinner cells show somewhat better performance, and are less robust to redox, so these results are in alignment with the cell thickness and the shorting event, however it is difficult to determine if there is truly a causal relationship between these events and results.

Performance results of the full height (340 cell) stack suggest that vertical flow distribution and temperature distribution, from stack top to bottom, meet design expectations. However, it appears that within the unit cells the flow is not being distributed as designed; resulting in certain areas of the cell are getting less than the intended flow. It is theorized that this maldistribution could be caused by an interfacing mesh that sits between the interconnect and the cell. The primary purpose of this mesh is to improve electrical contact on the fuel side. An ex-situ test apparatus has been deployed to test alternate mesh solutions in a reducing environment and under current load, mated with representative rib geometry (Figure 3.2-10). The blue plates represent interconnects, the green plates represent cell anodes (with no electrolyte or cathode), and the red convolutions represent the interfacing material under test. Each layer incorporates two identical interfacing materials in symmetric test cells. Multiple repeat units can be built up, much like a real stack, in order to test different materials simultaneously. Figure 3.2-11 shows a CAD view of the overall jig with the test layers to the far left, and the electrical, mechanical load, and gas connections to the right. Figure 3.2-12 shows the jig under test. A reducing gas mixture (4% hydrogen in nitrogen) flows through the jig to keep the cell anodes and the contact media reduced.

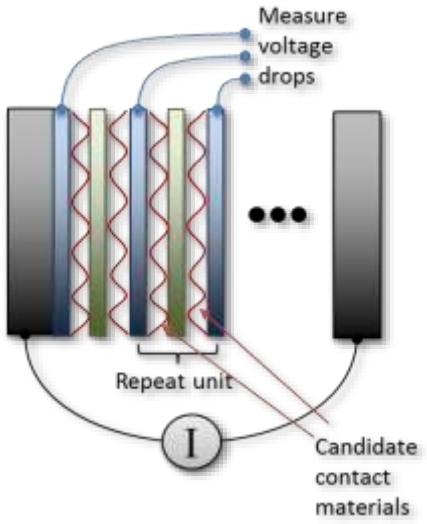

Figure 3.2-10 Electrical contact media tester.

Figure 3.2-11 CAD view of the interface material test jig.

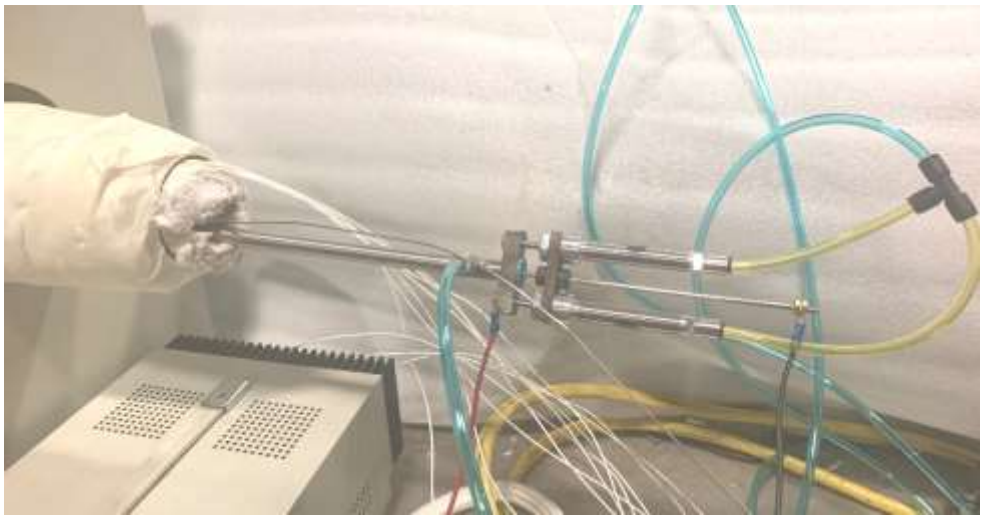

Figure 3.2-12 Interface test jig installed into tube furnace.

The initial electrical contact trials (Funded under parallel program DE-AR0000957 INEGRATE). Results are presented as voltage loss at 0.3 A/cm^2 applied across the full symmetric repeat unit (two full interface sets). This provides an intuitive grasp of the magnitude of the loss. At this current density the baseline solution contributes less than 1 mV loss per component. The following materials are under test:

- bare interconnect against cells (orange, off scale, losses of 0.150 V)
- baseline mesh solution with spot welds (dark blue)
- baseline mesh without spot welds (gray)
- a finer mesh candidate without spot welds (gold)
- flat nickel (red)
- flat copper (green, mostly off scale, > 50 mV loss)

The setup was thermal cycled twice after 70 hours and has otherwise been holding at 750°C. Preliminary results are already interesting. Over this period there was no electrical benefit to spot welding. The finer mesh candidate appears to perform identically to the baseline mesh. It is interesting that the flat nickel form has 1.7x the losses of the baseline mesh. This is not a large loss overall, but it points to a sensitivity to geometry as well as to material.

The testing continued accumulating over 2000 hours of operation and 8 thermal cycles before being shut down and the results are shown in Figure 3.2-13. After 1000 hours the temperature was increased from 750°C to 800°C to increase oxidation rates. There was no indication of increased degradation at the higher temperature. At 1458 hours the current was removed for 300 hours to determine if current was affecting the oxidation rates. There was no sign that the absence of current affected the contact quality from this test, as well as a shorter no current hold 300 hours into the test similarly showed no effect. Overall, there was no degradation observed for the four nickel-based samples (baseline mesh, a finer version of the baseline mesh, baseline mesh spot welded, and a flat nickel sheet). The finer mesh showed the same performance as the baseline mesh to within a fraction of a millivolt for the full test period. Spot welding had no impact on the conductivity. The flat nickel sheet had higher loss in general, although still low overall, showing that electrical losses are a function of both material and form.

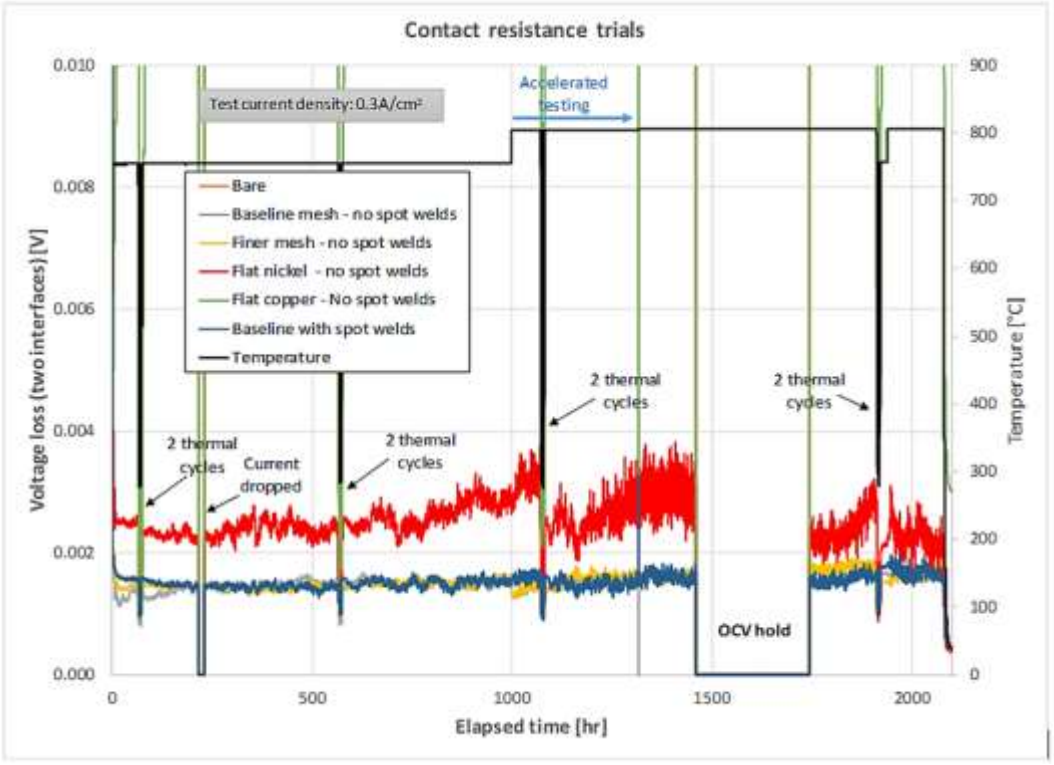

Figure 3.2-13 Electrical contact trials.

Based on the early results of this testing, finer nickel mesh samples were ordered for incorporation into technology stacks. Stack GT060248-0016 incorporated two trial meshes in a parametric test, one mesh with half the opening size of the baseline, 0.050” vs 0.100”, and a second mesh with a further 40% reduction in opening size to 0.030”. When conceived it was anticipated that the relative performance difference between these two mesh configurations would be small. It was also anticipated that the smaller opening would likely be better. Both predictions proved false (Figure 3.2-14). The finest mesh (blue and green traces) was grouped significantly lower, 50+ mV/cell, than the others (red). The root cause is uncertain, but perhaps the smaller openings of the finest mesh are starting to interfere with diffusion to and from the cell active area. With such a disparity in performance the value of this parametric test in generating performance data is limited. The weaker cells tend to heat up, shunting more flow to the (already) stronger cells, thereby exaggerating any differences.

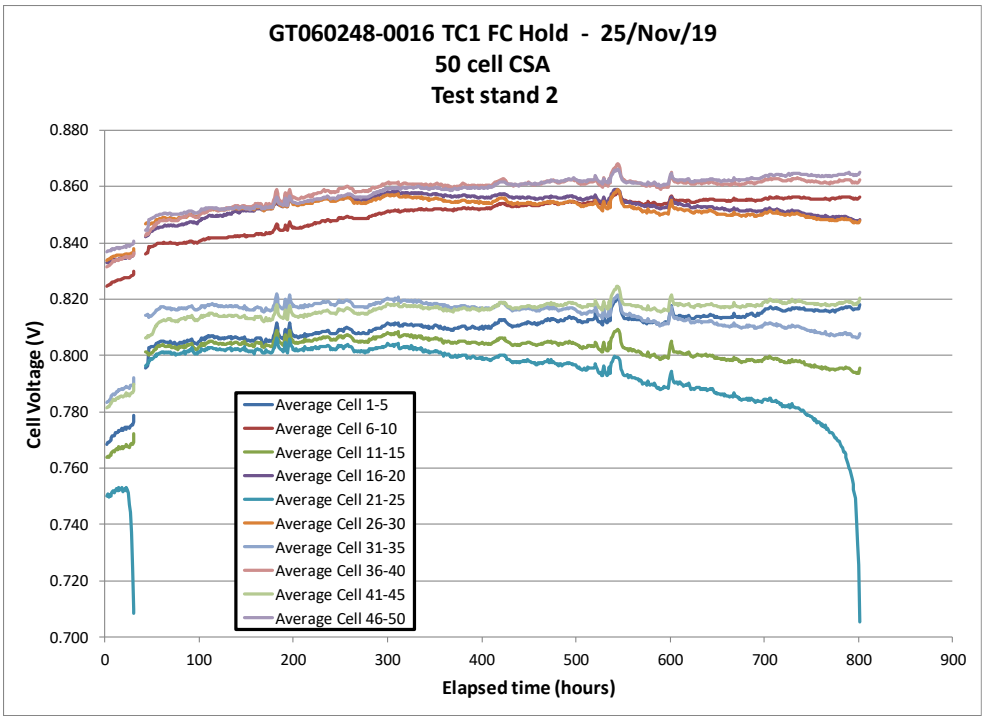

Figure 3.2-14 GT060248-0016 Parametric contact test.

The better contact solutions (0.050" openings) was therefore selected for a follow-on stack testing. This contact media evaluation and technology stack testing was funded under program DE-AR0000957 Adaptive SOFC for Ultra High Efficiency Power Systems but is relevant to this project as well and feed into the stack design for the module demonstration.

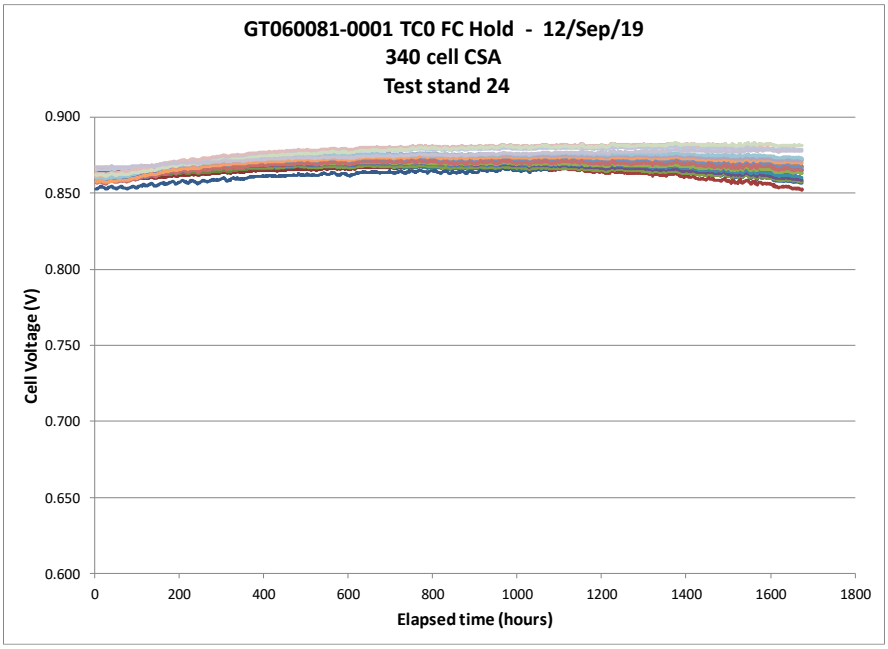

Figure 3.2-15 GT060081-0001 Fuel cell hold on reformate – 1674 hours.

Figure 3.2-15 shows the first hold period. It is evident that by the end of the hold some degradation was occurring. Some cells were showing decreasing voltage with time, starting at around 1000 hours elapsed.

Figure 3.2-16 shows the voltage change rate for each instrumented block of cells, where the value is calculated as the best fit line to the data. The blue bars represent that voltage change over the full test period; the red bars represent only the last 750 hours of testing (where degradation was apparent in the data). In general terms this shows that the stack appreciated overall over the course of the testing, but that cells 41 to 120 had some net degradation, centered around cells 71 to 80. This pattern is repeated in the last 750 hours although for that period most of the stack is degrading to some extent, but more so over cells 41 to 120.

Cells were ordered from thickest (400 micron) to thinnest (290 micron). The observed degradation pattern is consistent with a mild thermal runaway condition. Cells 71-80 start to heat up, local gas viscosity increases resulting in lower flow to these cells, the cells have to work harder (same current, less reactants, and less flow) and start to heat up more, they start to heat their neighbors, and the decrease in performance starts to propagate through the stack in both directions.

Four in-stack thermocouples support this hypothesis (Figure 3.2-17). The nearest thermocouple to the suspected hot cells was at layer 115. All thermocouples show a slight downward trend with time, consistent with a slight increase in flow as it moves away from the hot layers. The temperature at layer 115 stop decreasing at around 1000 hours elapsed and start to increase progressively faster after 1400 hours. The thermocouple at layer 250 failed at ~1100 hours.

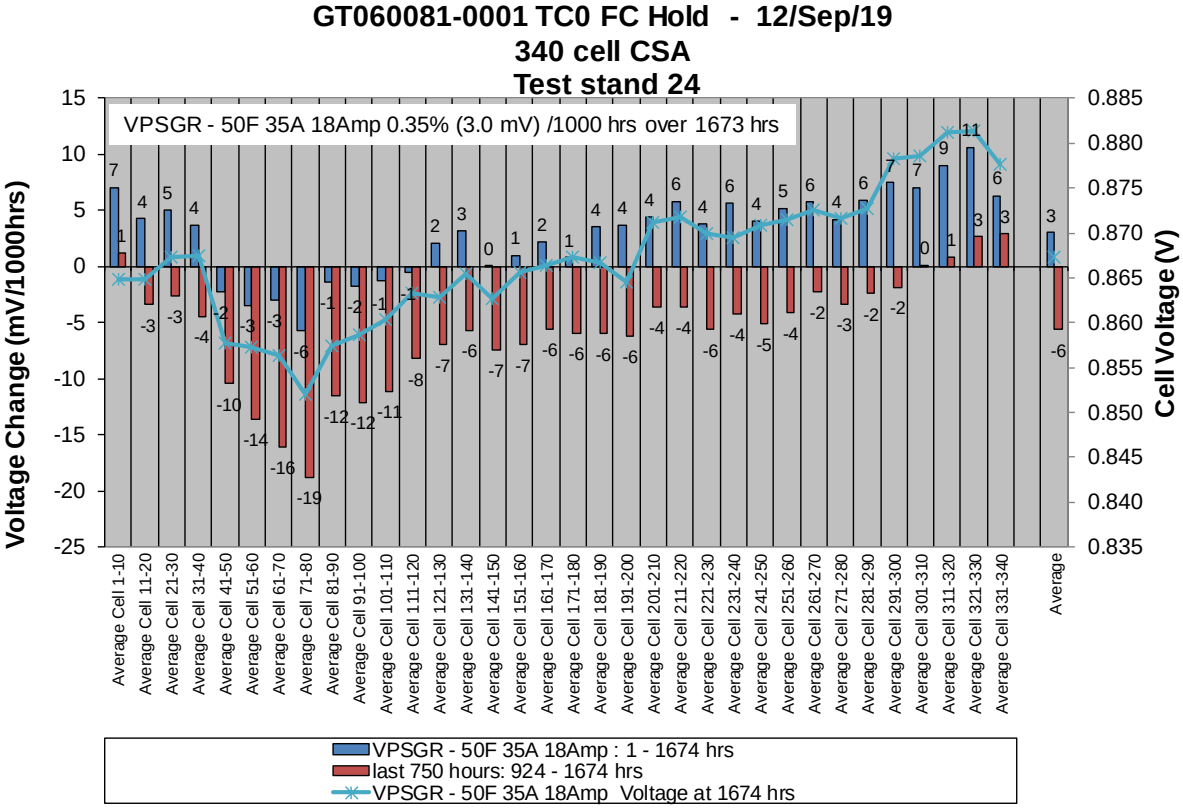

Figure 3.2-16 GT060081-0001 Fuel cell hold – degradation by cell position.

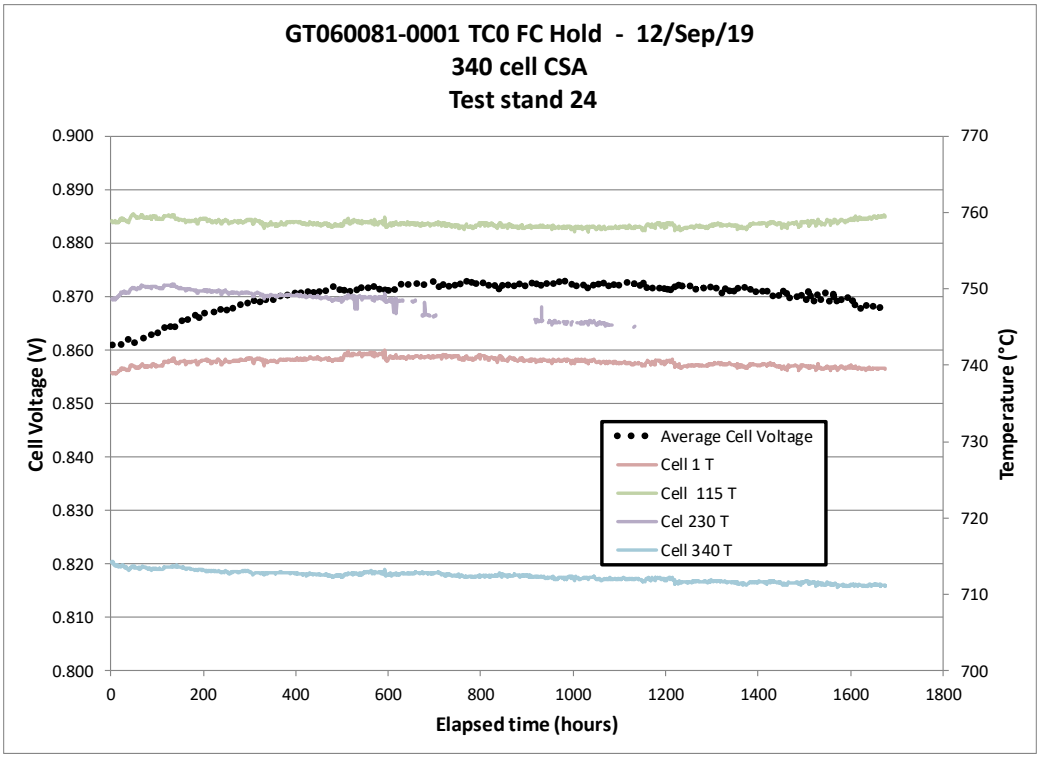

Figure 3.2-17 GT060081-0001 Fuel cell hold – temperatures.

The results over this first hold were positive, with good stability for a first article test, but also raised some questions as to what occurred that caused the layers around 71 to 80 to show the observed behavior. The in-stack temperature data was interesting in that is showed layer 115 was about 20 °C hotter than layer 230. This is the inverse of what is typically observed in bottom fed stacks. Generally, the hottest part of the stack is 2/3 to ¾ of the way up the stack as the sensible cooling from the gas streams is reduced. The performance did not suggest significant starvation, but the temperatures did suggest the lower portion of the stack might not have been getting as much flow to begin with, which prompted a closer look at the air flow to the stack.

A review of the air inlets suggested that flow dynamics at the test conditions were resulting in more inlet air flow towards the top of the stack. A redesign was undertaken on the air inlet geometry to improve the air inlet distribution. Figure 3.2-18 illustrated the original air inlet flow (left) and the redesigned air inlets (right). The redesigned inlets were fabricated and installed prior to reheating the stack for continued testing. While cold, the in-stack thermocouple in layer 230 which had failed was replaced.

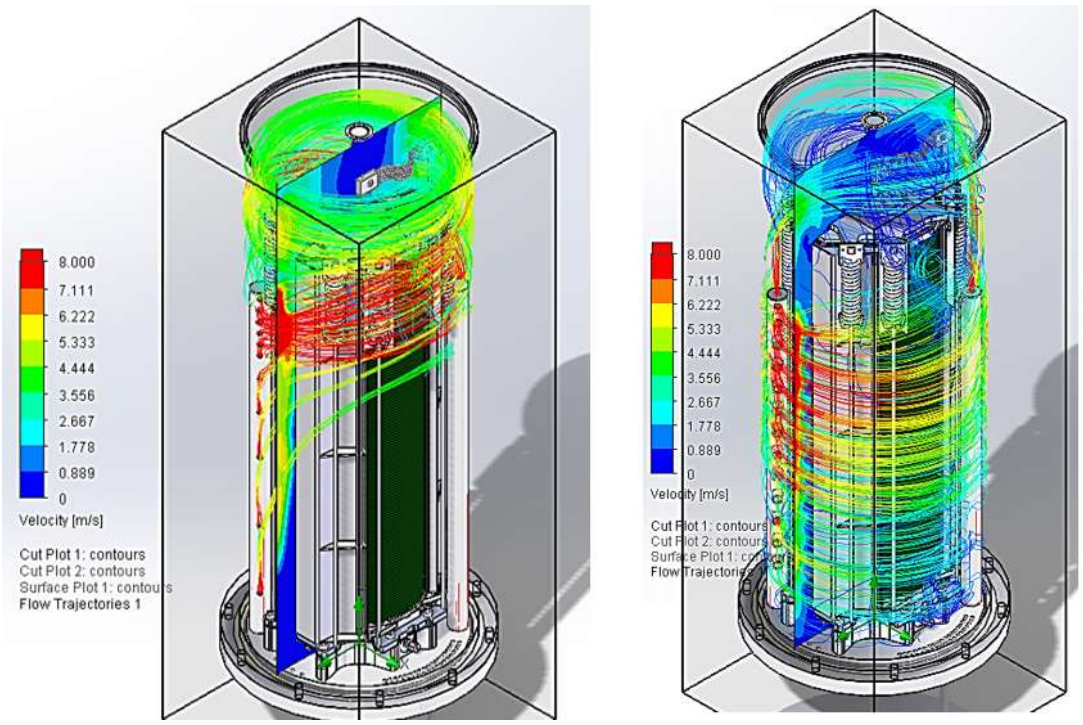

Figure 3.2-18 Air inlet streamlines (left: As built, right: Revised)

Table 3.2-2 Temperatures Before and After Revision

Position	Before Cooldown	After Heat Up	Change
Layer 1 Temperature	740 °C	742 °C	+2 K
Layer 115 Temperature	759 °C	767 °C	+8 K
Layer 230 Temperature	~745 °C	763 °C	+18 K
Layer 350 Temperature	711 °C	717 °C	+6 K
		Average:	+8.5 K
Average Cell Voltage	0.867 V	0.849 V	-18 mV

On reheat and resumption of prior test conditions the in-stack temperatures had changed as captured in Table 3.2-2. The significant increase in temperature at layer 230, in both relative and absolute terms, suggests that the air inlet distribution is behaving as intended, reducing the bulk cooling towards the top of the stack from the relatively cooler air inlet streams. While layer 115 remains hotter, the temperature difference between layer 115 and 230 is much closer than before, more in line with expectations. Normally layer 230 would be hotter than layer 115, but in this case degradation of the cell layers 41 through 120 led to more electrochemical heating in that area of the stack. The top and bottom of the stack remain relatively cooler due to heat loss out the (unheated) top and bottom of the enclosing furnace.

After restarting the stack ran another 977 hours (Figure 3.2-19). The stack was operated at progressively increasing air flows, and each time the air flow was increased the weakest cells recovered substantially and their degradation slowed. This indicates that despite the revised air manifold, the trend observed in the first 1600 hours continues. Perhaps because the weak layers have already been degraded. The stack had been running at a reduced current of 0.22 A/cm^2 due to limitations with the original load bank. With the installation of a refurbished load bank prior to this second hold it was possible to run the stack up to the full current design point of 0.29 A/cm^2. This was done over a 2-day period at about 900 hours elapsed. While initially stable, the voltage

at the weakest cell groups was relatively low and started to rapidly degrade after about 24 hours. At that point the test condition was reverted to the lower 0.22 A/cm^2 load and held. The cell voltages resumed their previous level with the exception of the lower group (cells 71-80) which showed some irreversible damage. It seems likely at this point that there is physical damage in cell group 71-80 (i.e.: Some sort of cross leak).

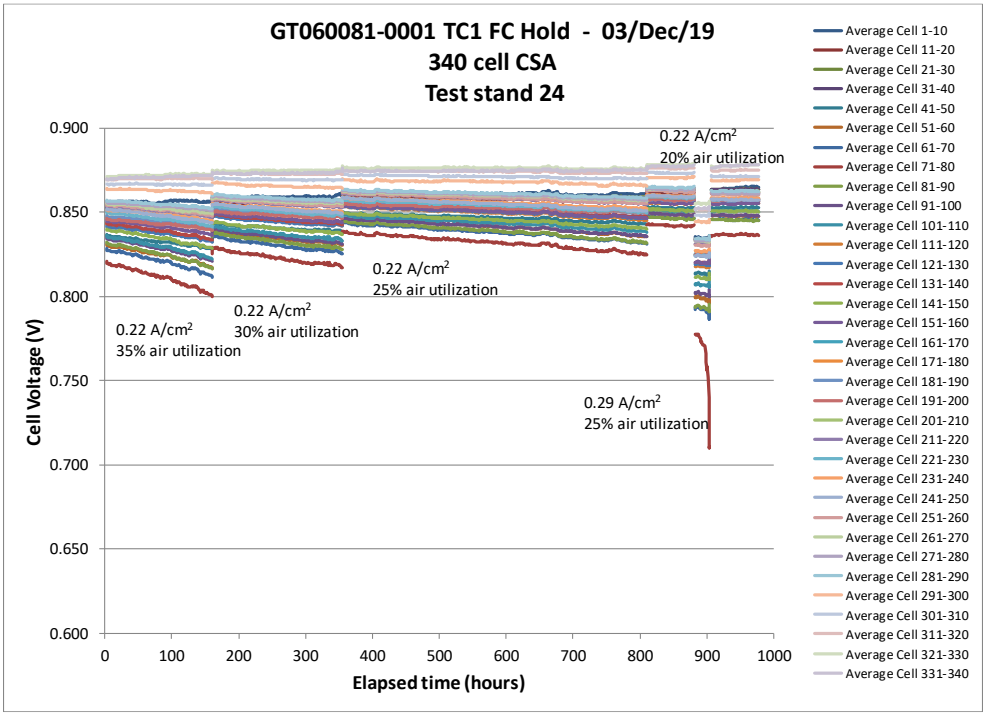

Figure 3.2-19 GT060081-0001 TC1 GT060081-0001 Fuel cell hold on reformate

Improved Interface Sealing

A minor design change was incorporated into stack GT060248-0015, a technology stack that was evaluating waterjet cut cells for final dimensioning. As part of the bottom end plate production process for all stacks the base is sanded to improve seal interfacing. For stack GT060248-0015 a raised surface was added in the sealing area such that the sanding process was easier to carry out. This has no impact on the total sealing surface, it only makes the sanding easier to carry out. (Figure 3.2-20) compares the bottom of the older and newer base plate design.

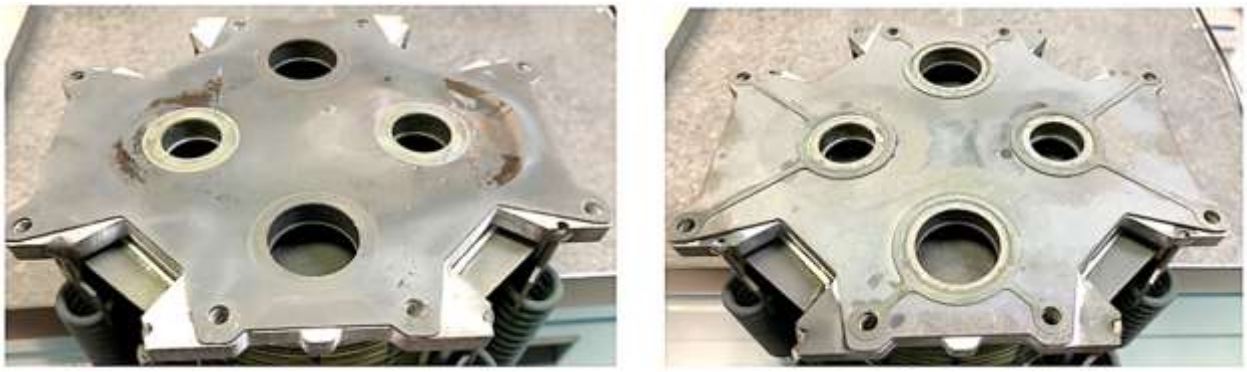

Figure 3.2-20 Original base plate (left) and revised base plate (right)

The impact of this change on stack utilization performance and thermal cycle stability was significant. Figure 3.2-21 shows the fuel utilization characterization curves for stack GT060248-0014 (original base plate) and Figure 3.2-22 shows the same characterization curves on stack GT060248-0015 (revised end plates). Each characterization curve runs through the same utilization steps of (fuel utilization/air utilization): (50/40), (50/50), (50/60), (50/35), (55/35),…,(80/35).

On the air side it is noticeable that the performance at 50% air utilization on the revised plates is better than the 40% air utilization performance on the original base plate. On the fuel side the general trend is that the performance on the revised plate is comparable to the performance at 5% lower utilization on the original base plate. These results point to better sealing between the stack and the test stand with the revised base plate. The other observation is that thermal cycling resulted in a noticeable decrease in performance on stack GT060248-0014, but not on the stack with the revised base plate. The geometry appears to be helping the seals stay fully seated through thermal cycles.

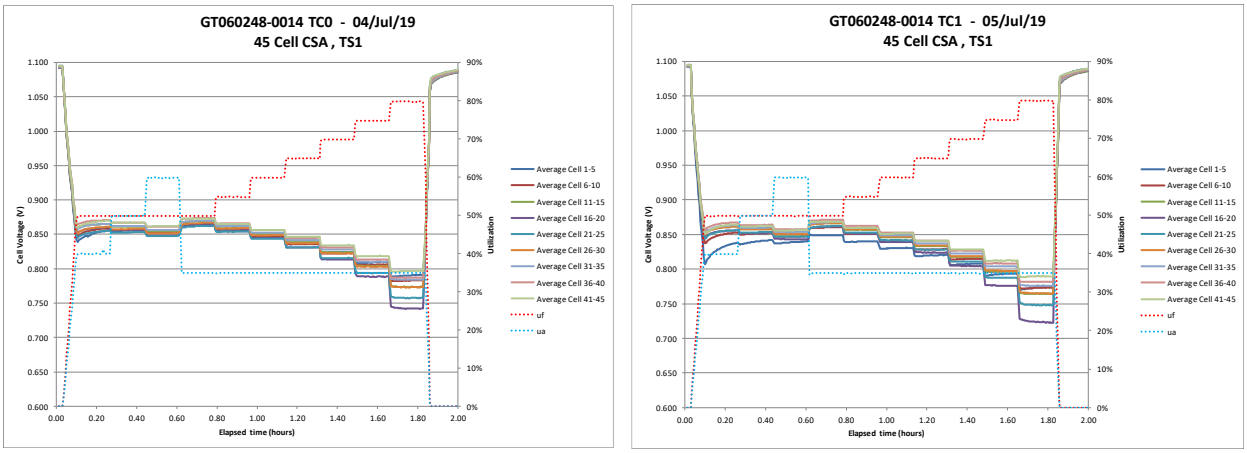

Figure 3.2-21 Utilization characterization of stack GT060248-0014 Thermal cycle 0 and 1.

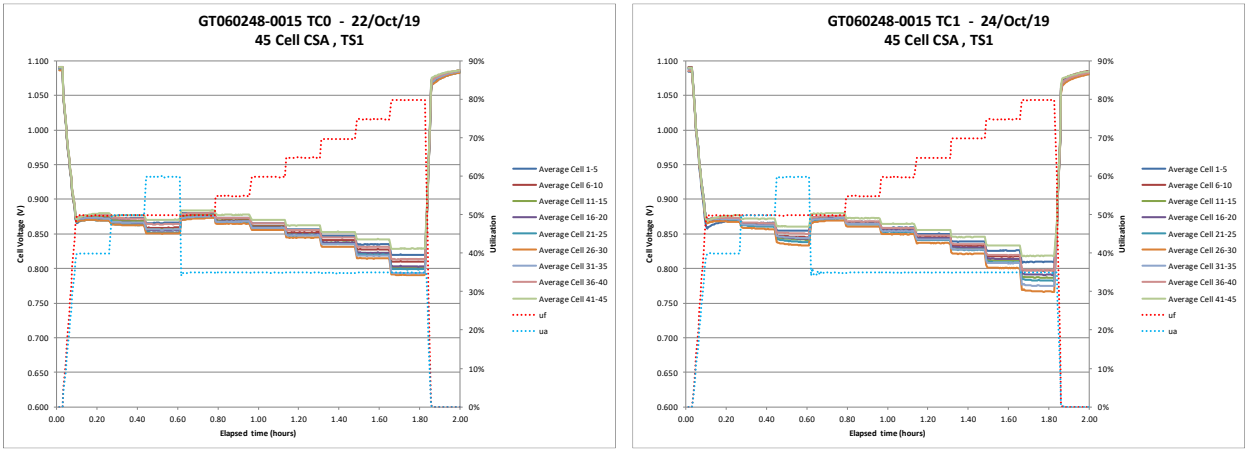

Figure 3.2-22 Utilization characterization of stack GT060248-0015 Thermal cycle 0 and 1.

The revised base plate has been implemented as the new baseline design for all stacks. The full height stack described at the beginning of this section was built before this design change and has the original base plate.

Two technology stacks were built. GT060248-0017 was built with the latest choice of anode contact mesh, based on earlier selection trials. GT060248-0018 was built with opposite electrical polarity (cells and interconnects inverted in the stack) and with a double thickness bottom end plate that aimed to improve base sealing to the test stand.

After a couple of aborted starts due to test facility problems, stack GT060248-0017 was restarted a third time and held for 1200 hours in a fuel cell hold with a simulated reformate feed gas consisting of a humidified methane, hydrogen, nitrogen blend intended to represent in-system conditions, but avoiding the use of CO and CO2 feeds (Figure 3.2-23). The fuel feed contains methane at a concentration corresponding to 37% direct internal reforming, representing a system case where roughly half the inlet methane is reformed prior to reaching the stack, in a system using anode recycle to provide steam to support steam reforming. The operating current was 0.29 A/cm^2, the fuel utilization was 68% (same as would be encountered in-system), and the air utilization was 30%. After an initial period of appreciation, the stack started to degrade and in particular, the centre group of cells (26-30). At 694 hours into the hold adjustments were made to assess what might be driving the degradation and a strong response to air flow was found. The air flow was increased such that the air utilization was 20% and the testing was continued until 1195 hours elapsed. The degradation rate decreased but was similarly characterized by a higher degradation in the group of cells 26 to 30.

Figure 3.2-24 illustrates the degradation distribution within the stack, showing a similar distribution before and after the air flow change. The degradation displayed for the initial hold only includes the data starting at 200 hours elapsed time, in order to remove the initial appreciation. The air flow increases roughly halved the degradation in the cells that were degrading, but did not stop it.

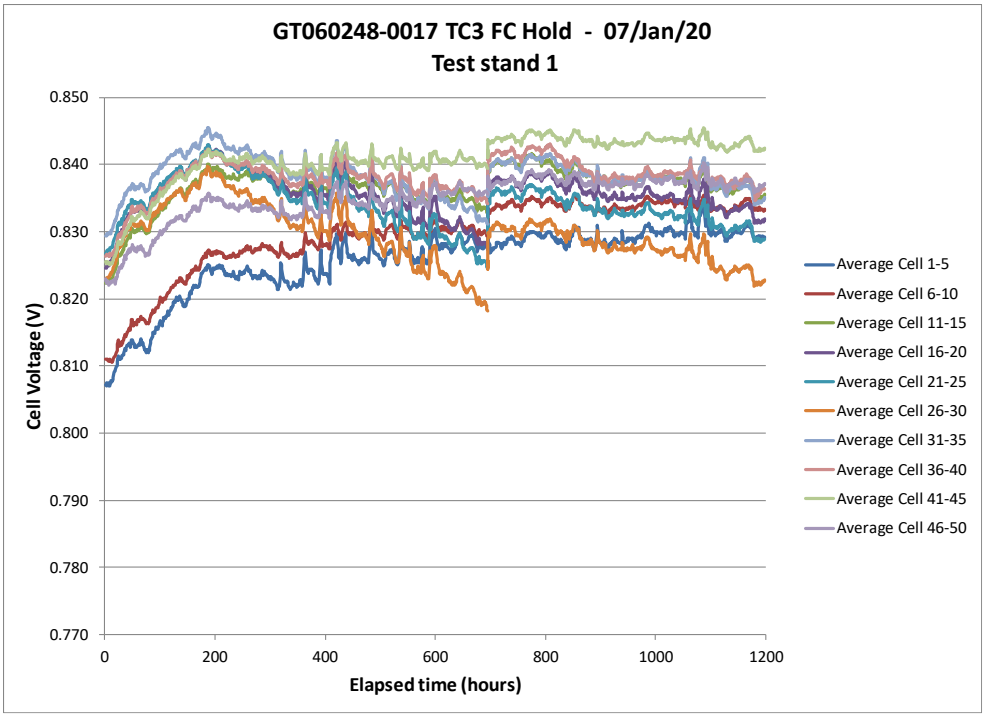

Figure 3.2-23 GT060248-0017 Fuel cell hold on reformate.

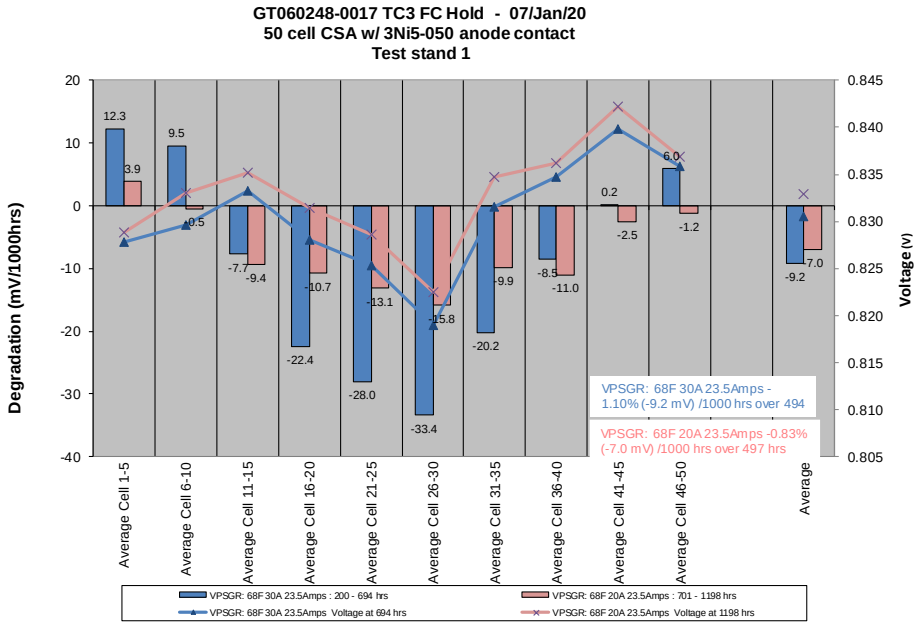

Figure 3.2-24 Degradation distribution over reformate holds.

With the test results clearly indicating a sensitivity to air flow, but still showing weakness at the higher air flow rates, it was thought that perhaps the air outlet manifolds were leaking, allowing inlet air to bypass the stack. Following a strategy that has been previously shown to identify weak manifold sealing, the stack was cooled, and ceramic seal slurry was applied to all the air manifold interfaces, forming a relatively thick seal bead between the manifold and the stack core. The stack was reheated after the caulking application and tested a further 1100 hours (Figure 3.2-25). There is no indication that the added sealing provided any benefit and the degradation on the stack was higher during this subsequent hold than during the initial hold, although the distribution is qualitatively similar (Figure 3.2-26).

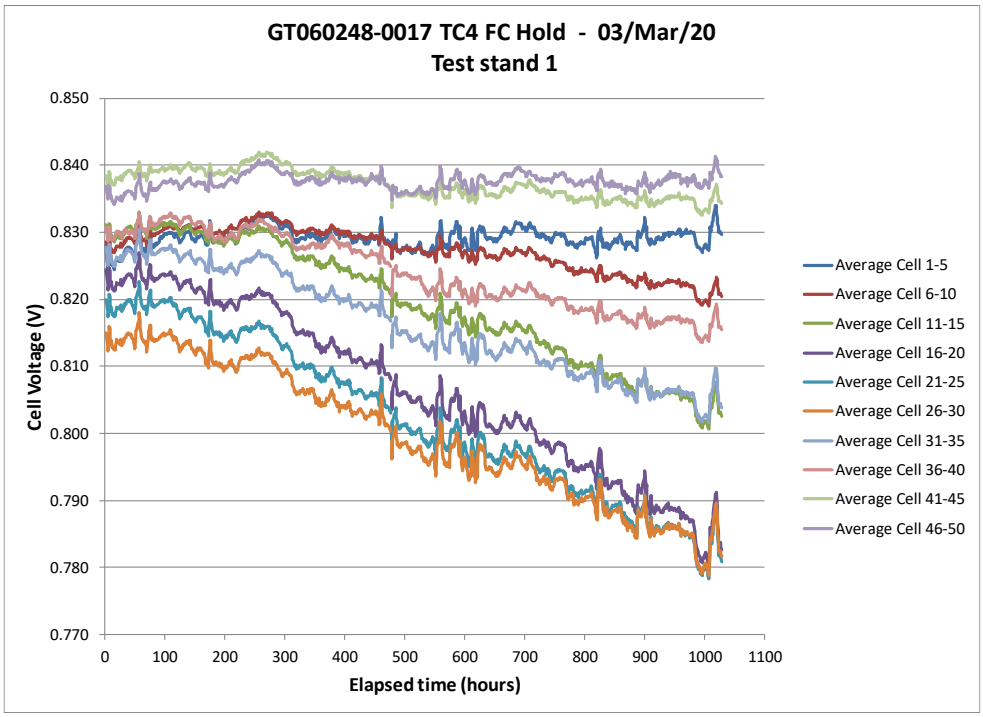

Figure 3.2-25 GT060247-0017 Fuel cell hold on simulated reformate after caulking.

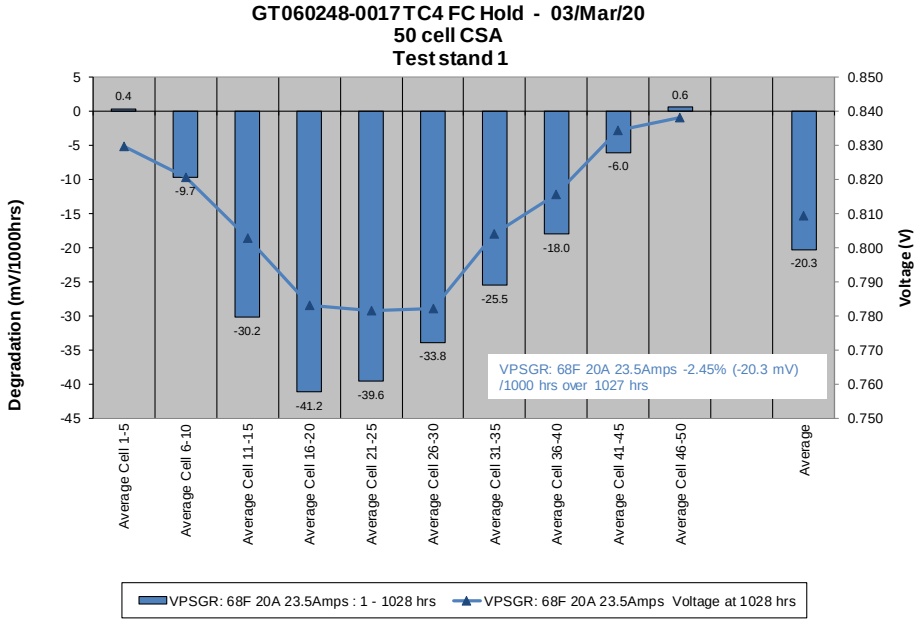

Figure 3.2-26 Degradation Distribution for stack GT060248-0017 after caulking.

In other testing, five stacks that had run over 1000 hours had their integrated compression systems evaluated. This consisted of three short (50-cell nominal), one mid-sized (150 cells) and one full height stack (350 cells). The design intent is to maintain the stack compression above 20 lbf, hot, for the life of the stack. Between stack GT060248-0007 and stack GT060248-0012 there was a change in initial processing that allowed the preload on the stack to increase, and this can be seen by the relatively lower compressive load on the former (Figure 3.2-27). The blue bars

represent the measured load (cold), and the orange bars represent an estimate of the compression load when the stack is at operating temperature, assuming a uniform temperature across the stack and compression system. As the stack gets taller, the reduction in compression load increases. This is driven by a thermal expansion mismatch between the relatively high CTE of the high strength compression elements, and the relatively lower CTE of the stack core. The actual hot compression was somewhat higher than the shown calculated value due to the stack core being at a higher temperature than the compression elements.

Nonetheless, the relatively large drop in compression load for the full height stack prompted a re-examination of the materials in the compression system. The main tension rods carrying the spring force had been made from alloy RA253MA which has a CTE of 18.5 E-6 /K. By replacing these with Haynes 282 rods (CTE 14.6 E-6 /K), the full height hot compression would be 97 lbf instead of the 35 lbf found for GT060081-0001 for the same cold compression.

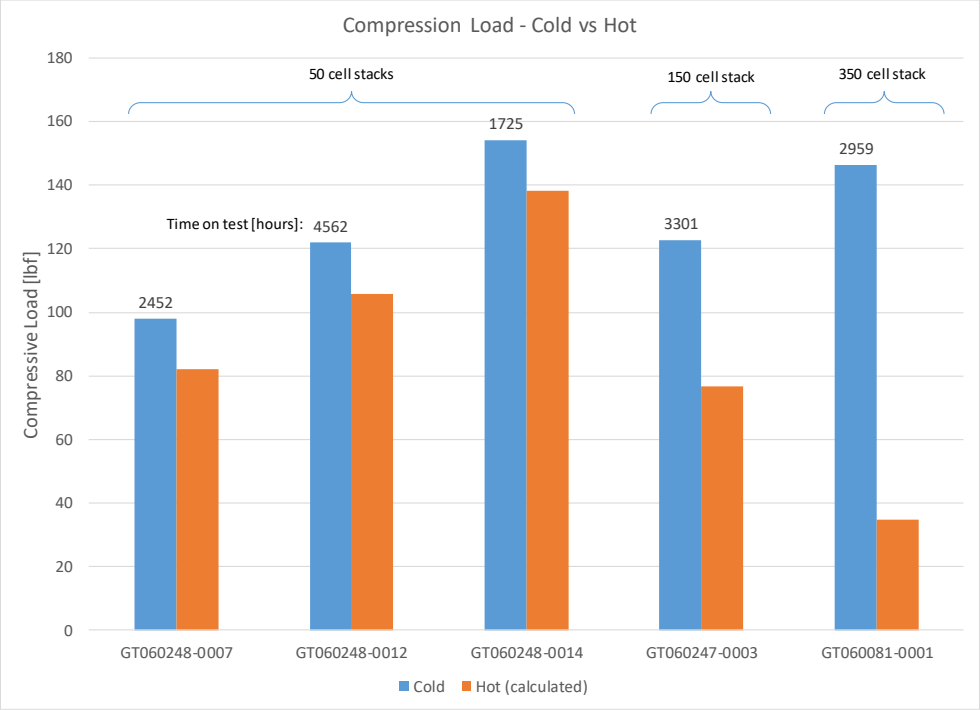

Figure 3.2-27 Post-test Stack Compression Load

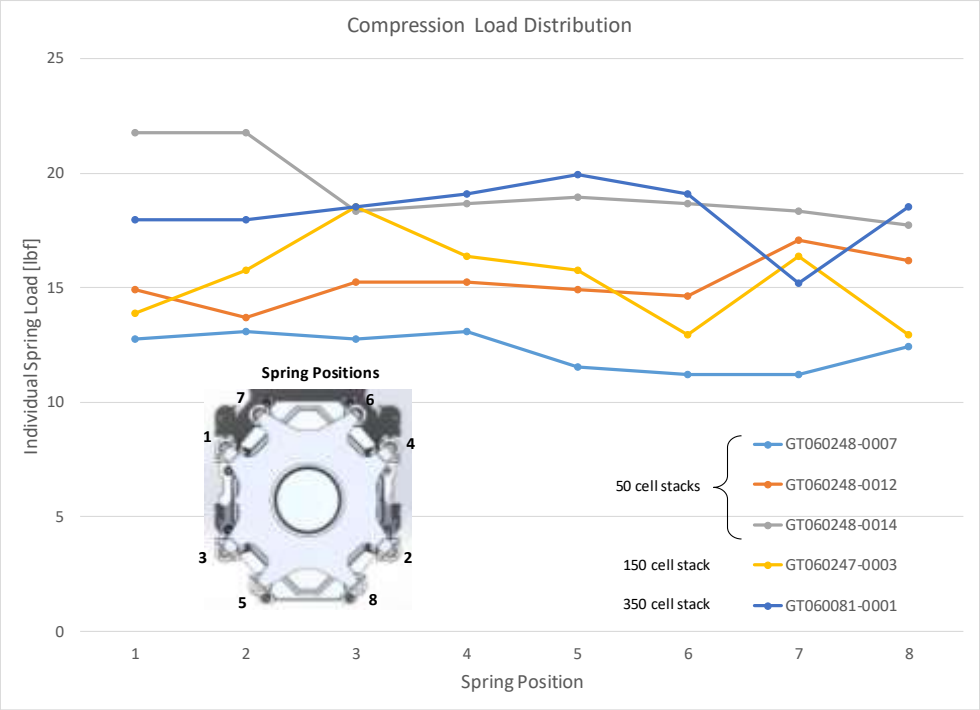

Figure 3.2-28 Post-test compression load on each spring.

Figure 3.2-28 shows the as-found cold compression loads on each of the eight springs that make up the compression system for these stacks. Larger than expected variability was found and this has been attributed to the tooling which applied spring preload as the spring are installed onto the stack. A review of the original tooling revealed that it was subject to stiction that could reduce the applied load. New tooling was deployed that eliminates the stiction point and used for future stacks.

Stack GT060248-0018 was built to test two design variations. It increased the bottom compression plate thickness from 0.25” to 0.50”. The intent of this change was to increase the compressive load that could be applied to the seals between the stack and the test stand or system. As previously reported, there were some indications of leakage between stacks and test stands, and design changes to improve the base seal showed improvements in stack performance. A second change was procedural. This stack was built with opposite polarity to all prior stacks; the cells and interconnects were inverted for the build. This was to validate both the manufacturing processes, and the resulting stack, to show that an inverted stack could be built. Inverter stacks are of interest for system applications where coupling stacks of opposite polarity relative to a common base is an easy way to achieve voltage doubling, which is generally advantageous for the power electronics.

The build and initial testing proceeded without problems, demonstrating that both changes were technically achievable within the current process. Only initial test results are available in the form of utilization test results. If the thicker compression plate had improved base sealing it might be expected that the performance change before and after the initial thermal cycle would decrease, however the main benefit might only arise over longer test periods when material creep in the base plate comes into play. A comparison of the utilization results (a conditioning and characterization test where the stack is subject to progressively higher utilizations at a fixed current) between stack GT060248-0017 and GT060248-0018 does not show any gain for the latter (Figure 3.2-29). If anything, the performance is somewhat poorer. Stack GT060248-0018

was tested on a different test stand and was shifted to a new test stand between thermal cycle 1 and thermal cycle 2. This may partly explain the observed differences.

From these initial results there is no problem with building an inverted polarity stack. While deemed a high confidence change, the sorts of problems that could be attributed to the inverted polarity were thought to be primarily process related. For example, the jigs, fixtures, and handling in the automated work cell or subsequent stack firing and finishing tooling might have directional characteristics which would damage cells or seals. These sorts of problems would manifest early and significantly in the testing.

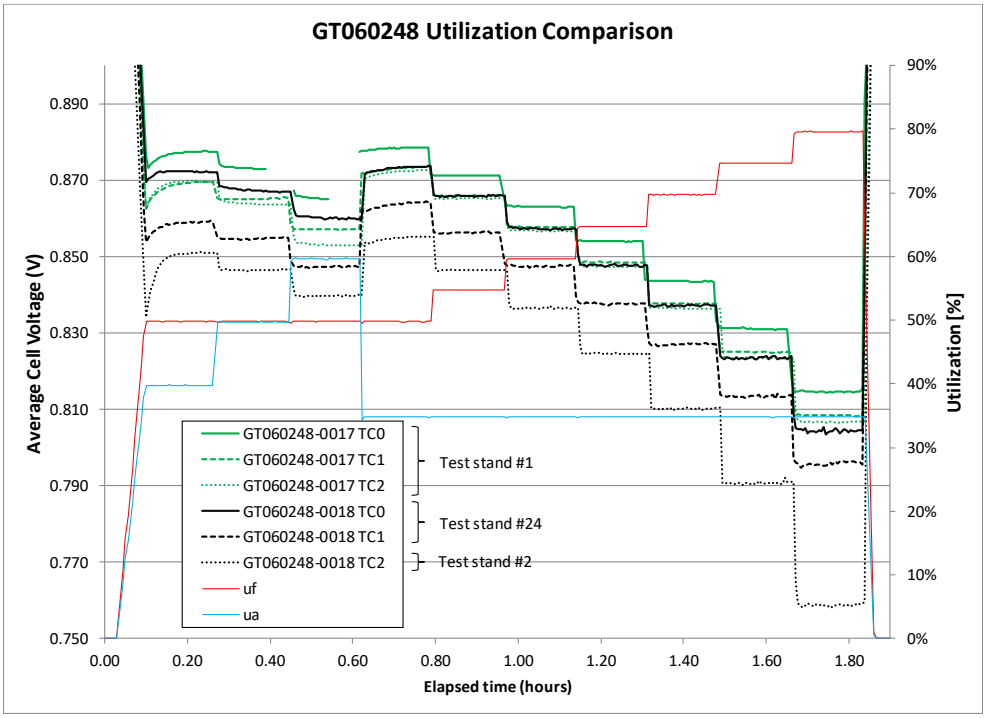

Figure 3.2-29 Utilization Test Results for Opposite Polarity, Thicker End Plate

This stack was operated for 2000 hours in a fuel cell hold (Figure 3.2-30). As described above, there was a concerning trend of degradation; typically starting about 800 hours into testing, beginning at the center of the stack. For example, previous stack GT060248-0017 showed a distinct degradation trend after several hundred hours and testing was aborted after 1000 hours when the three lowest voltage cell groups were clearly separating from the rest of the stack. While the initial results on stack GT060248-0018 appeared positive, with stability out to 1000 hours, a similar point of degradation once again became evident in a similar manner to prior stacks.

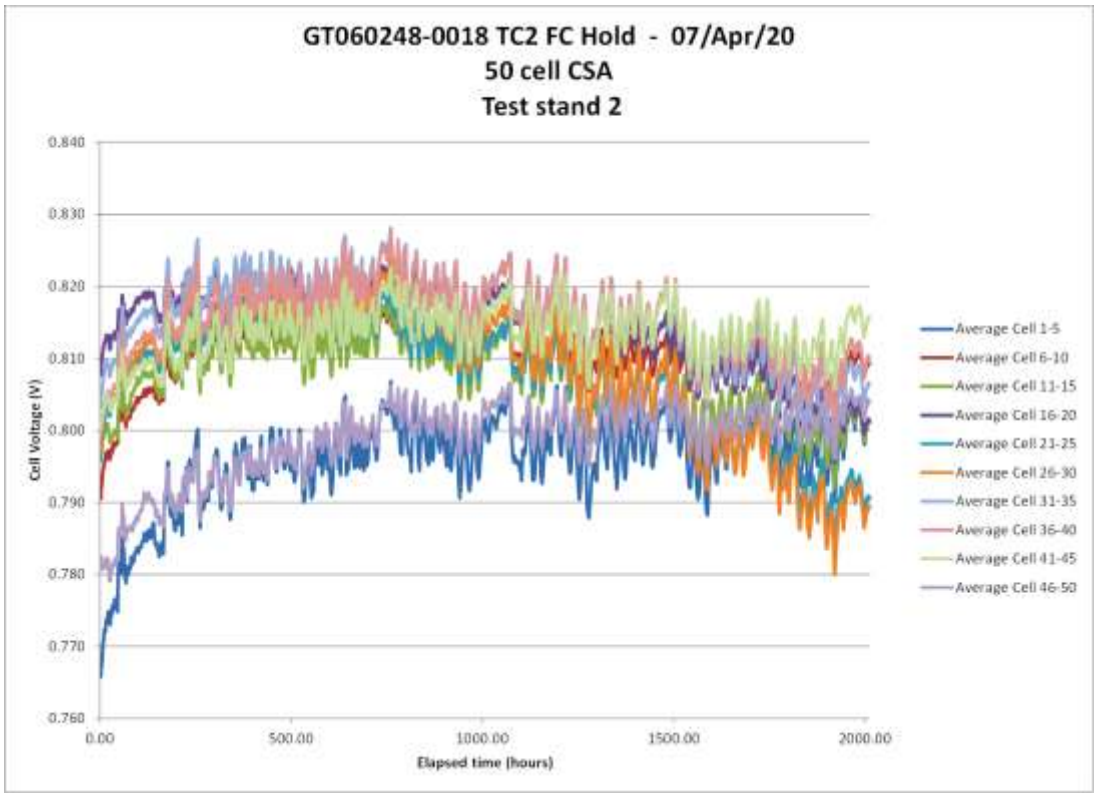

Figure 3.2-30 GT060248-0018 2000 Hour Fuel Cell Hold

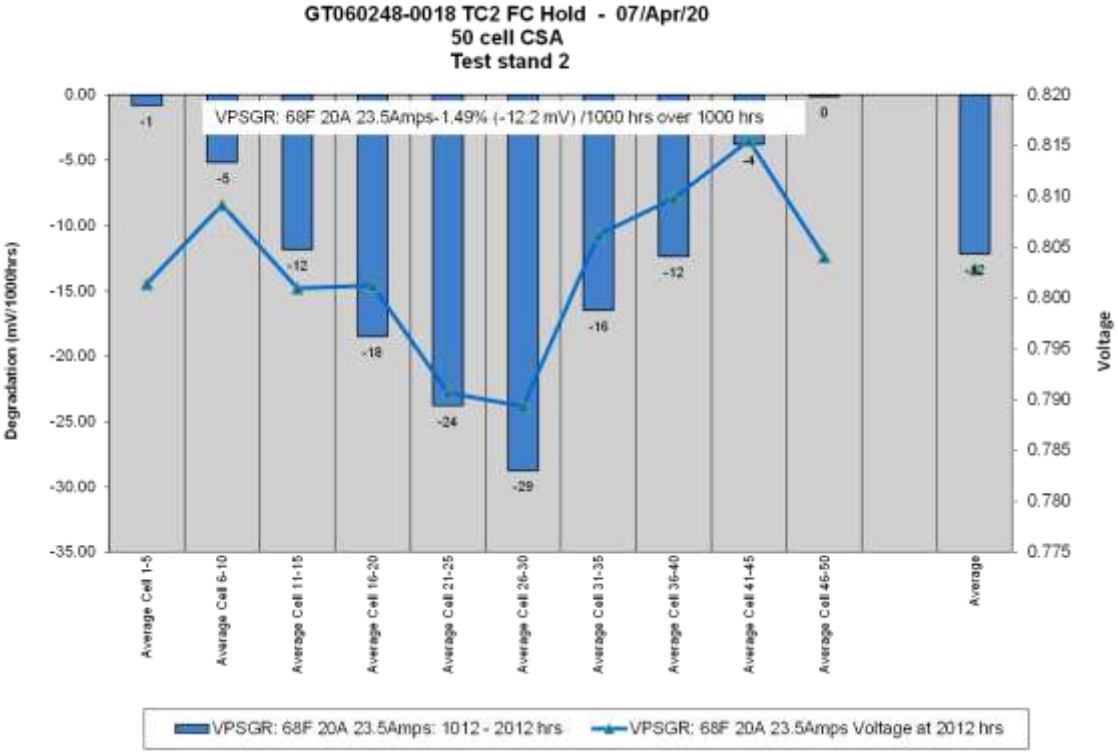

Figure 3.2-31 GT060248-0018 Degradation by Cell Position (last 1000 hours)

Figure 3.2-31 plots the best linear fit degradation for the last 1000 hours of operation of GT060248-0018 (once degradation was obvious). Although the rate is substantially lower than the prior stack, the qualitative behavior is similar with the highest degradation in the grouping 21 to 25 cells from the bottom of the stack. This suggests that while we have improved the situation, we have not completely addressed the root problem. Autopsies of prior stacks have been hampered when the stack was allowed to run to the point of physical damage to the cells and interconnects. In this case the testing was ended after 2000 hours with the intention that this early end of test, before significant degradation occurs, would better preserve the stack for autopsy.

Subsequently, stack GT060248-0019 was built and put into similar test conditions. It is largely a repeat of GT060248-0018 although unit cells were not inverted.

Full height stack (350 cells) GT060081-0002 on test for the Transformational SOFC program (DE-FE0027584) in test stand 24 ran to 679 hours with the majority of the cells appreciating over that period (Figure 3.2-32). At 300 hours elapsed some alternate operating points were briefly tested before returning to the baseline conditions of 45% DIR, 68% fuel utilization, 30% air utilization, 0.2 A/cm^2.

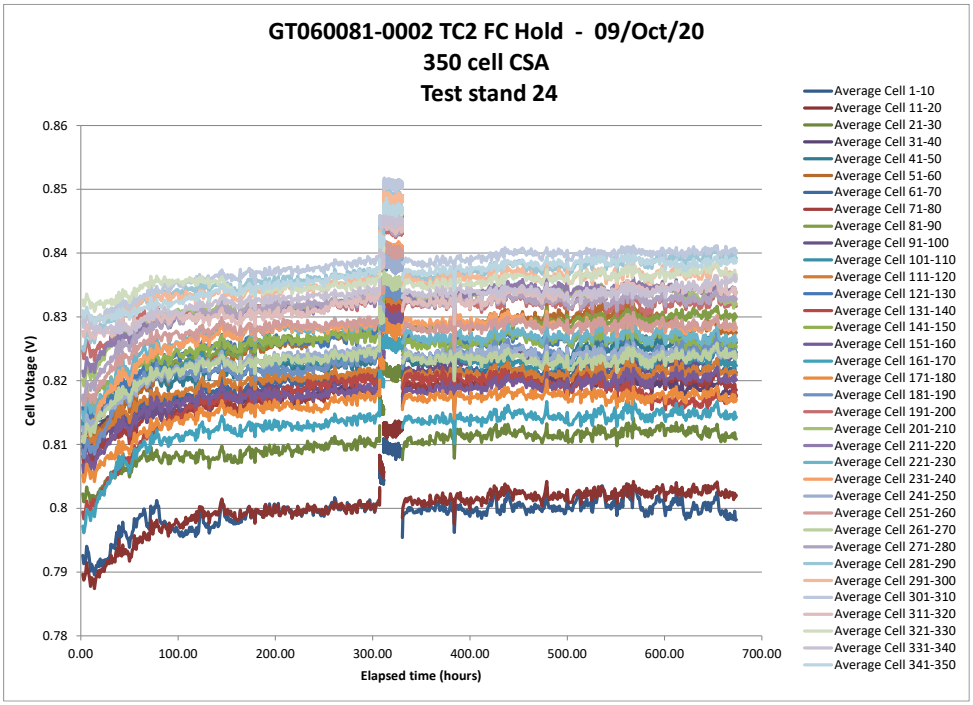

Figure 3.2-32 GT060081-0002 Fuel Cell Hold

At 679 hours the control computer halted and a watchdog timer that was intended to put the test stand into a shutdown condition did not work. Up to that point no test anomalies were recorded. No data was logged after that point. The failure occurred on a Friday night and was not discovered until Monday morning by which time the stack was damaged beyond repair. Testing team members were not able to determine what had gone wrong in what otherwise appeared to be stable operation. The watchdog hardware has been replaced and tested; giving confidence that should a similar case occur in the future the test stand should revert to a safe mode, protecting both the stack and the test stand.

A replacement stack, GT060081-0003 was built and installed for test. On initial testing a DAC isolator failed, shorting cell block 241-250 to ground. The resulting current through the voltage leads melted the interconnect in the vicinity of the load connection and resulted in a hole in the interconnect and damage around and through the adjacent seals. The damage prevented further operation of the stack.

4 Stack Module Development

Objective:

The objective of this task is to develop the 40-kW demonstration sub-module building block that surpasses current SOFC technology in terms of robustness and endurance to meet the long-term reliability goals. Sub-module development consists of four major areas: 1) stack module design, 2) integrated hot balance of plant development, 3) DC-power management and controls development including individual stack current measurement and control, and 4) instrumentation and sub-module controller development.

4.1 Stack Module Design

Approach:

This task focused primarily on the base stack module design and integrated hot BOP development. The base stack module design consists of the stacks, close-coupled heat exchange elements, process and electrical connections, insulation, and structure. Design efforts included multi-stack scale thermal computational fluid dynamics (CFD) modeling (Task 4.2) to evaluate and optimize thermal performance of a close-coupled pre-reformer and close-coupled gas preheat devices, both sourcing radiant heat from the operating stack. The stack module design effort also considered larger arrays, for example designing with feed tube sizes compatible with larger systems but detailed and delivered a design for a 40-kW module.

FCE completed design and production drawings for a 40 kWe stack module with an associated conceptual design for scaling. Integrated hot balance of plant development included the design of hot balance of plant components and their piping, insulation, and support structure. This included gas recuperators, afterburner and exhaust handling, preheater(s), startup water injection and vaporizer, as well as associated instrumentation and piping. CFD analysis (Task 4.2) of the stack module was carried out to evaluate flow and temperature distribution to each stack to achieve uniformity, especially between edge stacks (those adjacent to side walls) and core stacks (those surrounded by other stacks). Finite Element Analysis (Task 4.2) was completed where critical material strength is required and thermal expansion of components needs to be considered and accounted for via use of bellows, material CTE matching, and/or changes in moments of inertia are needed. The opportunity for simplification, integration, and repacking is also significant and was considered.

These design activities were completed with consideration of control systems development (Task 4.3) and process simulation results. The base stack module and integrated hot BOP was revised where necessary to accommodate stack module control strategies that directly impact the reliability of stack module.

Results & Discussion:

The geometrical shape and internal flow distribution of the Compact SOFC Architecture (CSA) stacks may result in a different approach to packaging within the module vessel as well as how

pre-reforming design was integrated. An energy balance was completed for the Compact SOFC Architecture (CSA) stacks. Figure 4.1-1 below shows the results of the energy balance in a Sankey Diagram. The analysis was completed for a configuration of six, 350 cell CSA stacks providing a total of 35.9 kW of DC power. It was assumed that the process design was the same as used in previous FCE SOFC systems that utilized LAS Stacks. The purpose of the analysis was to diagram the methods of cooling the stack and controlling on cell temperatures. The fuel cell is assumed to achieve a 65% fuel to electricity efficiency. Therefore, for a total of 35.9 kW of DC power there is 19.7 kW of heat generated that needs to be removed from the stack. There are three methods used to let heat escape from the fuel cell stacks. The largest amount of cooling comes from reforming the fuel, followed by sensible heating of the gasses, and finally heat lost to the environment.

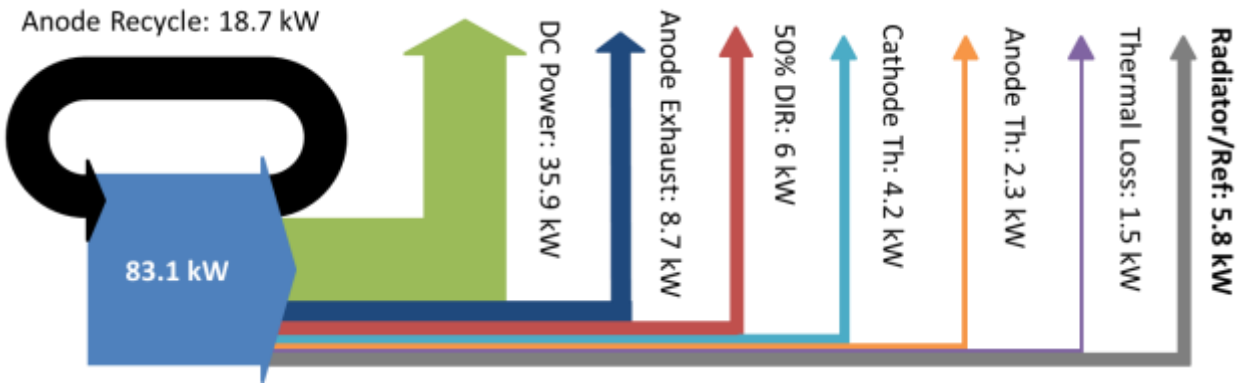

Figure 4.1-1: Sankey Diagram: Stack Energy

The reforming reaction to create hydrogen for the fuel cell is highly endothermic and has the largest impact on cooling that stack and controlling stack temperatures. The reforming reaction can take place in two locations, pre-reforming (reforming upstream of the fuel cell stack) and direct internal reforming (DIR), reforming on the surface of the fuel cell. The optimum amount of DIR is being evaluated experimentally and the results were used to guide the design of the Next Generation module. For this analysis it was assumed that 50% of the reforming occurred by DIR and 50% occurred in pre-reforming. For the pre-reforming reaction to assist in cooling, the stack surface needs to radiate heat to the surface of the pre-reformer. The radiator / pre-reformer design is critical in being able to operate the stacks and maintain temperatures. If the pre-reformer under performs it can drive high amounts of DIR which can lead to cooling the entrance area of the cell and creating high differential temperatures on the cell.

Sensible heating of the Cathode and Anode gas have the second largest effect on cooling the stacks. For the energy balance it was assumed that the two gas streams entered the stack at 650°C and are heated to 750°C. The anode gas flow and temperature are critical to the operation of the fuel cell and are generally fixed in the design. The cathode gas flow rate and inlet temperature can be changed to control the stack temperatures during operation. As seen in Sankey Diagram the sensible heat from the cathode cannot replace the heat that goes to reforming unless the inlet temperature is dropped, or the mass flow is increased significantly.

The Sankey Diagram in Figure 4.1-1 illustrates how critical the design of the pre-former is in this SOFC system. Without a radiative pre-reformer, significantly more energy would need to go into sensible heating of the cathode gas or be lost to the environment.

The ability to transfer heat from the CSA stack through radiation not only plays a critical role in cooling but as a functional system component of the stack module. This heat can then be used for fuel pre-reforming, for heating gas flow streams prior to entering the stacks, or a combination of the two - as has been done the most recent NETL-funded SOFC projects. The geometric form factor of the LAS technology stacks used in those projects was well-suited for radiative heat transfer: 1) as a continuous square, all sides of this stack were external, exposed for possible radiative heat transfer to neighboring surfaces; and 2) the sides are relatively flat, in form, making them readily seen by other surfaces to harness the radiation. For those modules developed with the LAS stacks, it was practical enough to fabricate and install a cross-shaped radiative fuel reformer (RFR) between four stacks; with the sides of the RFR looking at the hottest sides of every stack (Figure 4.1-2). The radiation shape factor for those surface heat transfer pairs is effectively 1.0 in that design. The CSA stack has a different form factor that reduces the surface area available for radiative heat transfer. The inside diameter walls are completely obscured from neighboring surfaces of other stack module hardware, reducing the availability of exposed surface of the cells of the stack by 30%. In addition, the available surface is round and convex in shape relative to possible surfaces to radiate to. That reduces the radiation shape factor. As an example, one of the vessel design configurations being considered is shown in Figure 4.1-2. The shape factor of the exposed cells only is reduced to 0.85.

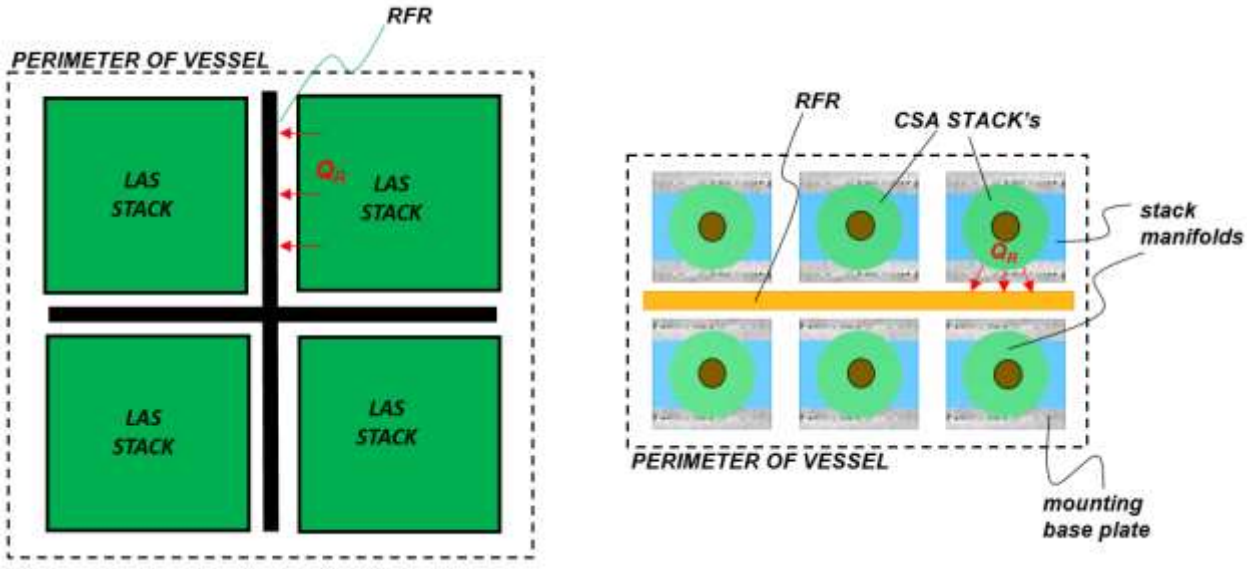

Figure 4.1-2: Form Factor Effect on Radiation Shape Factor

The design concept for the 40kWe stack module is shown in Figure 4.1-1. The module utilizes six, 350 cell CSA stacks arrayed radially in a cylindrical module. The Anode and Cathode gas flows enter from the bottom of the module. Locating the process connections at the bottom of the module allows the internal BOP equipment and stacks to be assembled with the cylindrical shell and insulation removed, leaving access to the equipment. The insulation and vessel shell can then be lowered over the assembled equipment and sealed to the bottom plate.

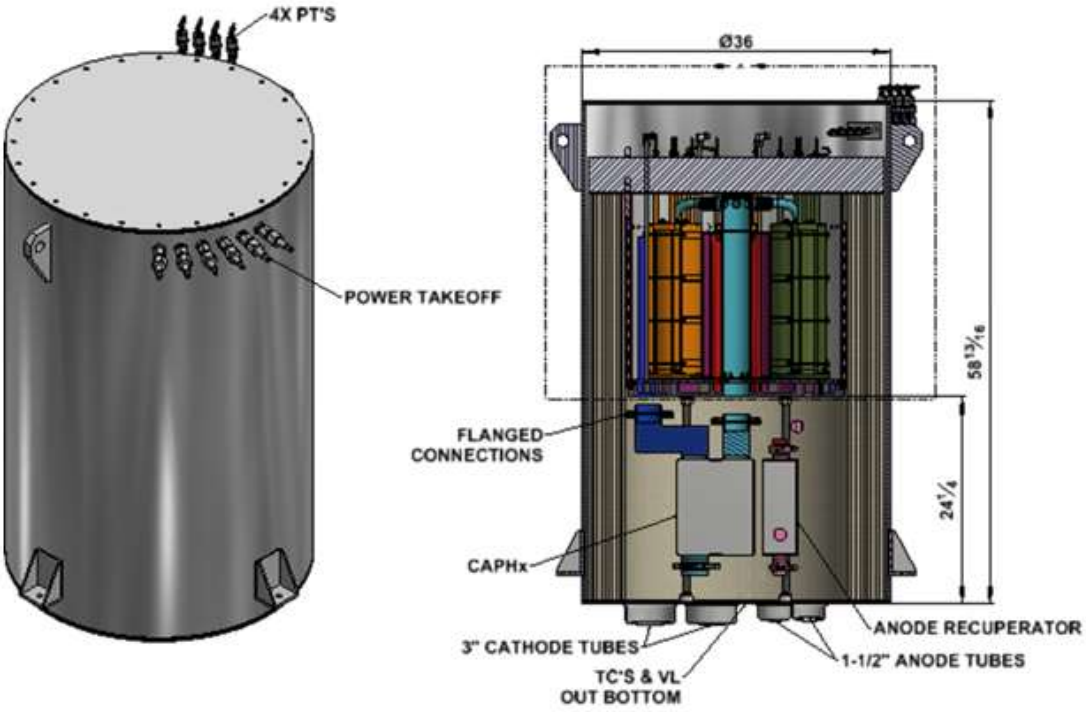

Figure 4.1-3 40kWe SOFC Module

In the pressure vessel described above, in the penetrations there is space to integrate hot process equipment. The concept shows an integrated Anode Recuperator and Cathode Air Pre-Heater / Oxidizer (CAPHx). The integrated heat exchangers minimize heat loss from the module because the gasses pass through the pressure vessel boundary at a lower temperature. Even though there are advantages in integrating the heat exchangers into the pressure boundary, it may be more cost effective to use larger de-integrated heat exchangers in a 1 MW system design. For this purpose, the test vessel has been designed with the flexibility to be operated with or without the integrated heat exchangers.

In order to operate without the integrated heat exchangers, the nozzles for the pressure vessel penetrations are designed to tolerate pre-heated gasses and there are flanges on either side of the heat exchangers to allow them to be removed. Once the heat exchangers are removed, they were replaced with bypass pipes to flow directly to the module baseplate.

The module baseplate is located directly above the process section. The baseplate is multifunctional; it allows the gas to be distributed to each stack via internal flow passages and it also serves as the support for the stacks. The stacks were electrically isolated from the baseplate to allow flexibility in electrical system design. Multiple inverters and control methods are being evaluated for the 1 MW systems and isolating the stacks from the baseplate allows for all the options to be tested in the 40kW test. Above the stacks is an insulated purgatory zone to transition to lower temperature materials and allow access to make final electrical and instrumentation connections.

The design of the 40kWe stack module requires some consideration for how closely the module architecture needs to match a larger kWe capacity version for MW-class SOFC plants. This characteristic is referred to as ‘scalability’. The module architecture includes elements such as the vessel, base plate, upstream and downstream process piping, control instrumentation, and insulation – with the stacks housed within.

The focus up to this point had been a module design configuration sized for the project power generation capacity target of 40kWe. This is a 6-pack circular arrangement of 6.6kWe CSA stacks with an option for integrated anode recuperator and catalytic air preheater heat exchange equipment. The size of the module was decided as 40kWe, as part of the “MW-Class” decision process. However, a design decision matrix completed as part of that project showed the arrangement for this integrated equipment being more expensive than non-integrated, BOP sized, heat exchange equipment. However, this non-integrated equipment has the disadvantage of requiring “hot” module connections and longer “hot” pipe lengths resulting in larger heat losses from process piping.

The final aspect to the module down selection process has to do with the question of scalability. As referenced in the initial “Next Generation” funding application, a strategy was targeted to implement the stack into a sub-array as a low-cost building block for modules of larger systems. The building block (Figure 4.1-4) would include a manifolded mounting base to facilitate upstream and downstream process piping. Larger plumbing connections would be located below the lower decking to facilitate the flow rates of “MW-Class” module size. The stacks were arranged in a rectangular pattern resulting in a number of stacks installed around the module perimeter while others would be surrounded by these perimeter stacks, unexposed to the module vessel walls. One of the unknowns of such a system is how these unexposed stacks perform as compared to perimeter stacks including thermal and flow distribution both to/from and within these stacks. The 40kWe circularly stack array (Figure 4.1-4), covered during prior reporting, is not intended to link up to neighboring 40kWe segments so it’s a physically connected building block like the rectangular array. In order to make a decision on final configuration – circular array versus rectangular array are presented to review the pluses and minuses of each in order to drive a final decision.

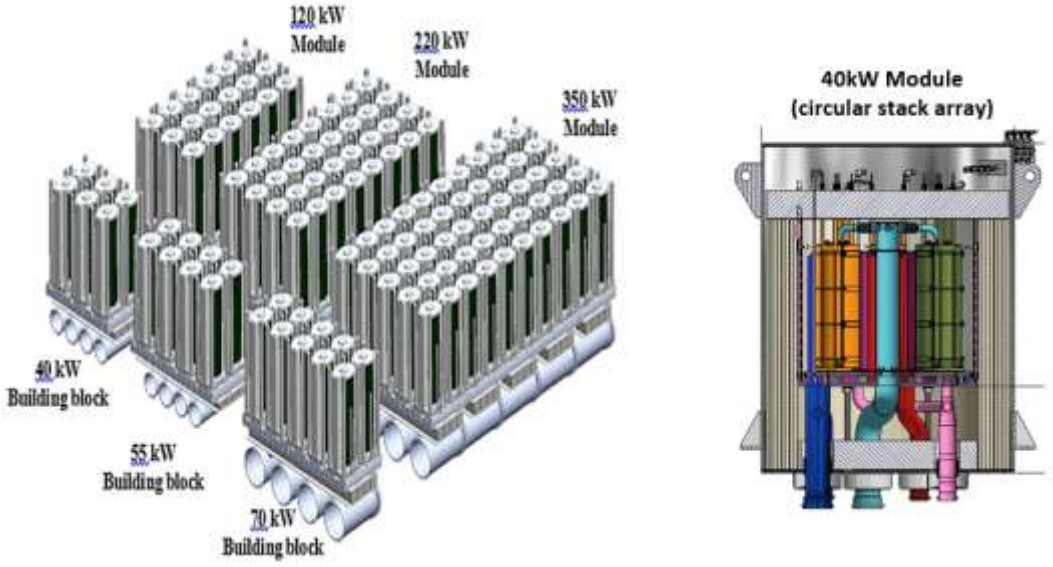

Figure 4.1-4 Final Module Configuration Selections

The 6-stack geometrical array needs to be finalized. Initial concepts included in project proposals illustrated a rectangular array of stacks mounted onto a base plate brazement with integrated flow distribution ducting (Figure 4.1-5). The exhaust and supply gases would flow through large circular ducts at the bottom of the brazement, while flow distribution to the individual stacks would take place through a series of rectangular sheet metal box tubes, sandwiched with insulation between a stack mounting plate and the larger circular ducts. The intent is that segments from six to ten

stacks could be built and connected by the circular ducts in a row to be installed within a module vessel for a range of capacities depending on the customer requirements.

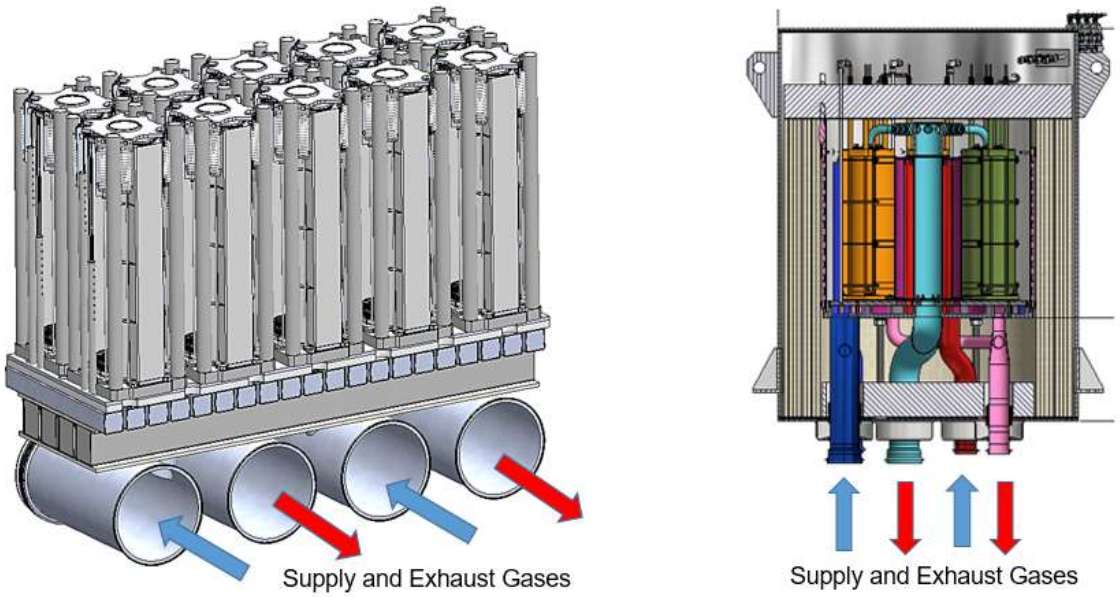

Figure 4.1-5 Initial Proposal Concept (l), Circular Array Concept (r)

Packaging has become a strong design driver for the 40kW building block size selected. This has led to a focus of packaging sections of the module together for practical assembly. The basic layout of the module can be broken into three main sections (Figure 4.1-6): an upper purgatory (intermediate temperature) zone; a middle hot zone housing the stacks and base they are mounted to; and a lower zone for balance of plant (BOP) distribution conduits. The upper purgatory zone allows for power take-off (PTO) hardware to be constructed of more common materials and sealed pressure measurement connectors to be used, by means of an insulated barrier between the purgatory and the hot zone of stacks below it. Instrumentation wires can be passed through this zone as well, reducing the requirements of the vessel penetration. The middle hot zone houses the six stacks, mounting gaskets, mounting base, radiative fuel reformer (RFR) equipment, and air supply tubes. As a compact brazement, the mounting base has plumbing and flow distribution features built into it, allowing stack supply and exhaust gas interfaces within a short distance to the bulk flow of the balance-of-plant (BOP). The lower zone was required to structurally support the stacks and mounting base. The conduits residing here extend to connections on the outside of the vessel. This arrangement strategically allows for multiple modules to be connected in series to the BOP (Figure 4.1-7). This conduit can be increased in size from initial sub-MW demonstration systems to MW-sized plants – as well as for when the module size itself increases during the product lifecycle.

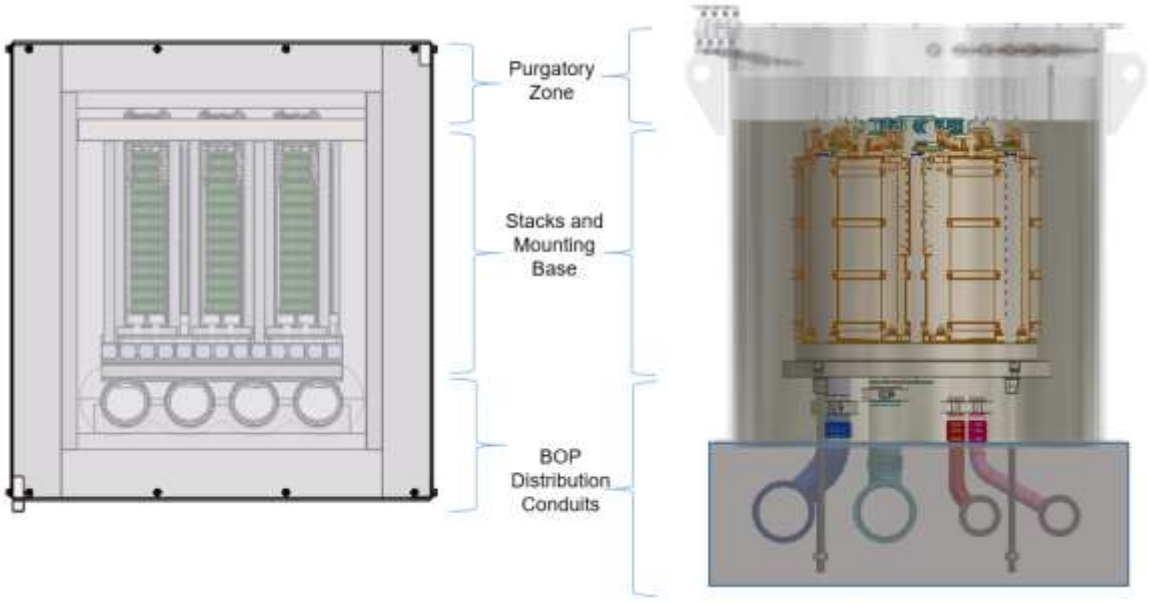

Figure 4.1-6 General Arrangement of the Compact SOFC Module

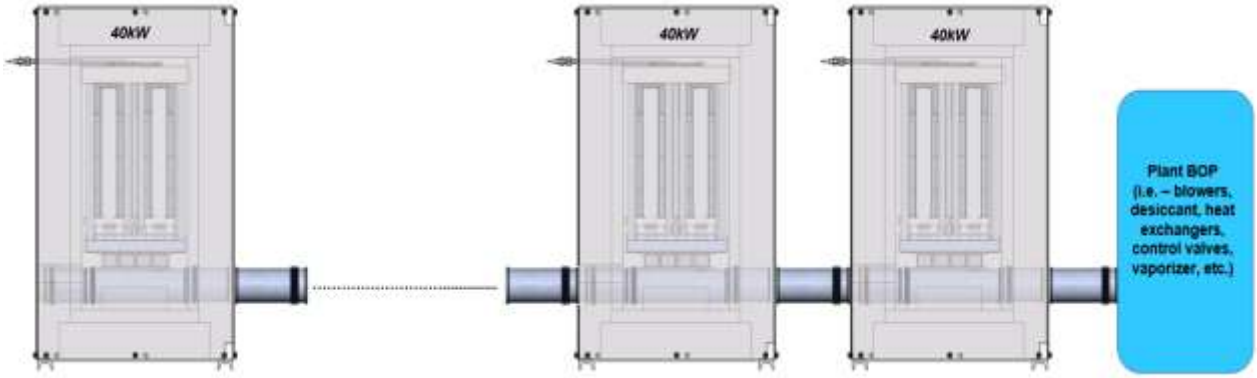

Figure 4.1-7 Multiple Modules Connected in Series to BOP

Both the rectangular and circular stack array module configurations were modeled in detail. Stacks were spaced for practical installation and instrumentation access. Air supply tubes were placed strategically to allow air to be injected tangentially to the outside surface of the hotter cathode out manifolds. The intent here is to help evenly cool the stack when combined with RFR equipment by letting the cooler supply air convectively transfer heat from the outer surface of the manifold. As an initial layout, the RFR equipment of the rectangular array is located within tube-inside-tube fabrications at the four corners of the bottom end plate (Figure 4.1-8) and terminates to an anode in fuel manifold plate mounted to the bottom of the stack. The endothermic reforming reaction provides stack cooling through the outer surfaces of the tubes.

The RFR of the circular array is located within the open space created by the circular spacing of the stacks. This equipment handles indirect fuel reforming for all six stacks and provides surface on the outside diameter of it to pull heat from the cathode manifolds— providing a thermal sink. For each of the concepts, the base plates to which the stacks are mounted are planned to be multiple piece brazements in which the supply and exhaust gases to the stacks (and RFR) are distributed. The rectangular array configuration features several box tubes arranged in two levels

of distribution wherein a main lower level distributes flows to smaller box tubes above them. Each of the smaller tubes feeds two individual stacks. The circular array configuration features a three-piece brazement with nested internal channels to distribute flow. Initial construction for this design can be completed by brazing thinner top and bottom plates to a thicker middle plate which is machined on both sides. Later configurations can feature multiple folded sheet metal pieces brazed together, for a cost reduced design.

The compact size of both the rectangular and circular stack array configurations allows for the possibility of similar lower vessel base designs such that either can be mounted to this lower base for the 40kW validation. Figure 4.1-8 illustrates this concept. Here, the BOP connection plumbing has been sized using hand calculations and is balanced between flow distribution to multiple modules in series and pressure drop along these flow paths. The current strategy would be to connect up to four modules in series, with two full series in parallel connected to the sub-MW sized BOP. This would allow for initial sub-MW demonstration system builds up to 320kWe capacity. The circular array design is currently being evaluated to see how practical and structurally sound it would be to have the lower vessel plumbing fixed to the bottom of the base plate brazement.

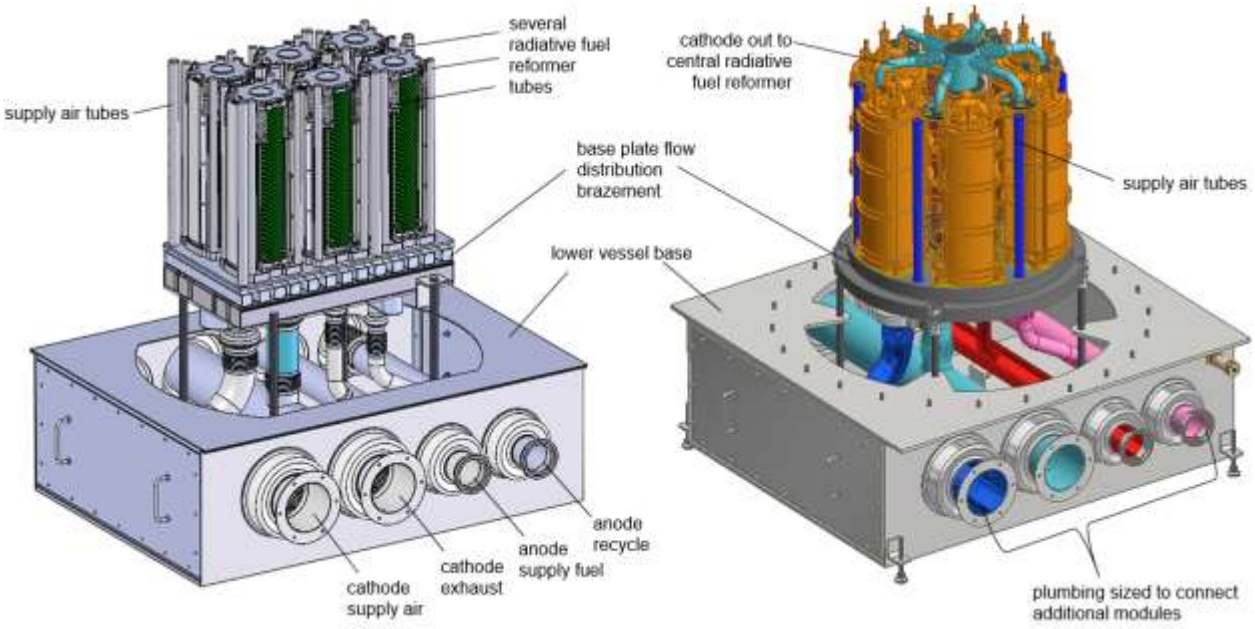

Figure 4.1-8 40kW Module Configurations: Rectangular Array; Circular Array

The module design concept with a circular installation pattern of six stacks was developed with more detail to better assess pros and cons compared with the rectangular installation pattern. The circular array design features a central radiative fuel reformer (RFR), a base plate brazement, and a vessel base weldment (Figure 4.1-9). An upper lid provides access to a purgatory (cooler) zone where power take-off (PTO) hardware, pressure transmitter (PT) tubing connections and other instrumentation can be serviced and inspected. A plenum type weldment is connected to the top of the RFR to collect cathode-out gas from the six CSA stacks. For this design configuration, the top end of the CSA stack would be replaced with one that allows flow from the cathode-out manifolds to exit out top of stacks into this collector hardware. The base plate brazement acts as both a stack mounting piece but also fuel and gas distributor to the RFR and circular array of stacks. The vessel design is illustrated taller than needed to intentionally illustrate the simplicity in adding volume space at a later step in the module product evolution. The idea is

to give some flexibility to the choice of integrating the heat exchangers as individual to each module – a catalytic air pre-heater and an anode recuperator. The height of the vessel base is sized to allow for plenty of access to plumbing connections and instrumentation routing while providing a structurally sound base for installing the upper-level hardware (base plate, RFR, stacks, etc.). An insulation wrap and upper vessel structure would be slid over the assembled stacks and fastened to finish the assembly.

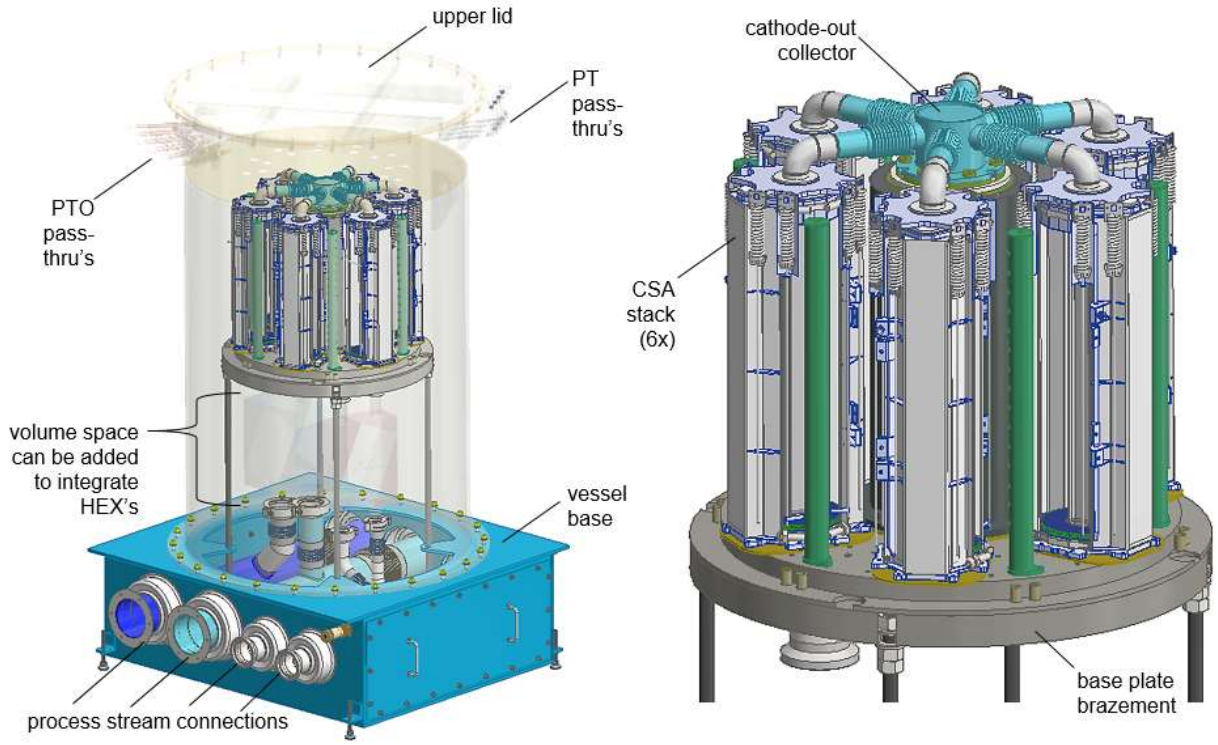

Figure 4.1-9 Layout of a Module with Circular Array Pattern of Stacks

The central RFR of the circular array design features a two-pass flow stream (Figure 4.1-10) that allows for coating of reforming catalyst onto low pressure-drop substrates on the first or second pass. Ideally, it would be the second pass which is exposed to the hot outer surfaces of the stack. Here, there exists a mutual benefit between the stacks and RFR, whereby the colder RFR (due to endotherm) actively cools the stack while the hotter stack provides significant heat duty via radiation to drive the fuel gas reforming reaction to required pre-reforming target. The two passes allow the base plate brazement to supply the RFR with fuel gas while also supplying the CSA stacks with anode-in gas from what exits the RFR. An insulation barrier resides on the inside diameter to prevent significant heat transfer from the hot cathode-out gas, which exits into the base plate prior to continues to plant BOP. The bellows on the cathode-out collector accommodates differences in thermal growth as well as compliance during install for connecting to each stack.

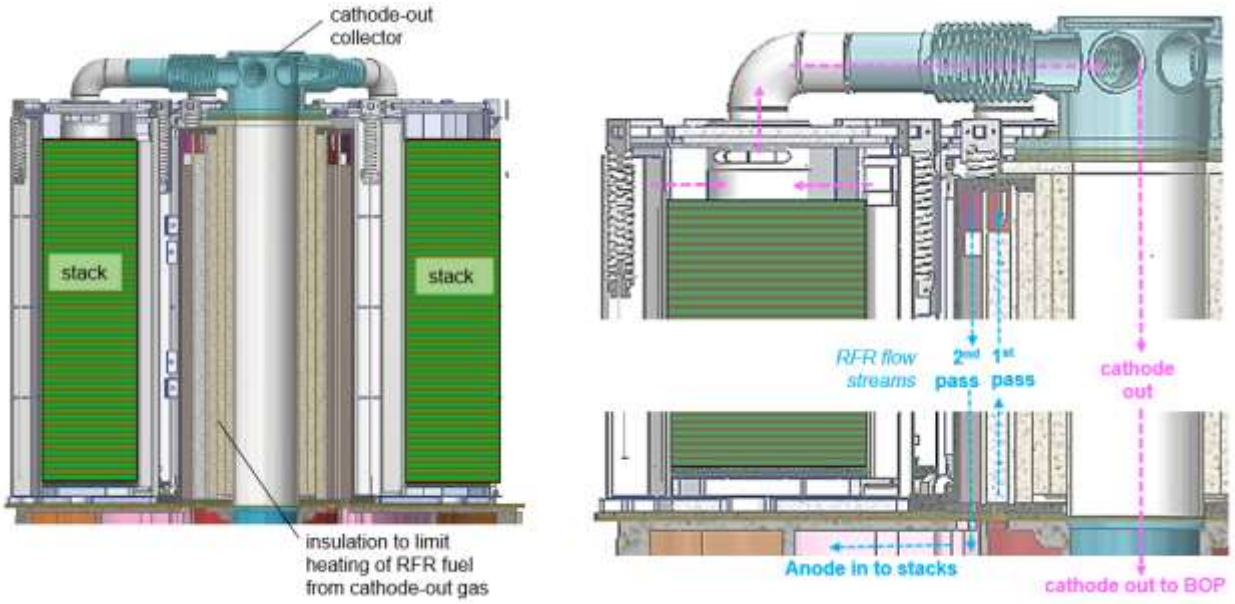

Figure 4.1-10 Flow Streams of Central RFR

The six CSA stacks in this circular array configuration are mounted to a base plate consisting of three main plates, ferrule flange process connections, and detachable air supply tubes (Figure 4.1-11). The cathode supply air flows through these six tubes prior to entering the hot zone flush with the stacks. Inside each of these is a second tube that forces the air through a second pass to help with thermal distribution of the air along the height of the stacks to help limit temperature differences in that direction. The process connections allow for easy install to vessel base with clamps and are also strategically located to connect a catalytic air pre-heater and an anode recuperator in the event that equipment is decentralized from the 250kW AC BOP. The limited number of plates of the base plate allow for straight forward brazement for rapid design introduction as part of a demonstration system. For such a design, a material reduction activity by replacing thick machined plates with bent sheet metal components would replace these heavier parts for larger volume lower cost fabrication. Several CFD studies have been performed on both the upper and lower passages, as well as process gas openings to installed equipment (CSA stacks, RFR, etc.), to ensure good flow distribution to each of the six stacks.

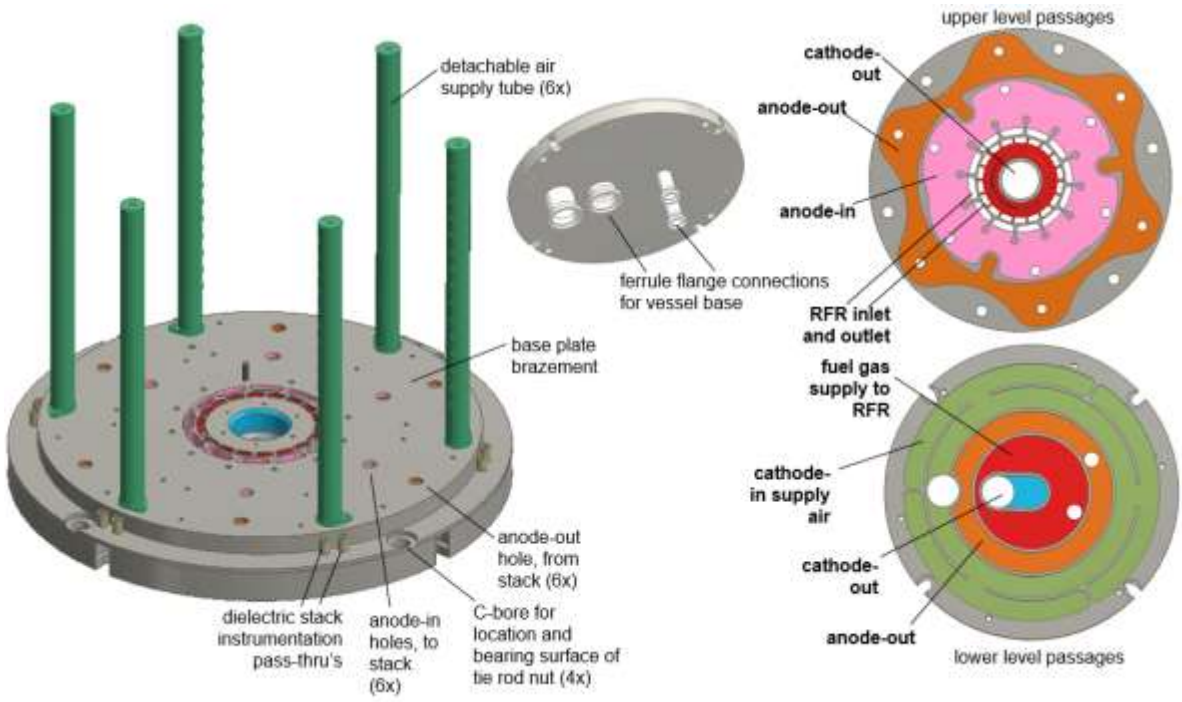

Figure 4.1-11 Design Layout of Circular Array Base Plate Brazement

Lower vessel base for this circular array was designed with attention to adaptability and process gas flow distribution in mind. The pattern of threaded studs makes it possible to receive either a round or rectangular upper vessel. That is, the rectangular array design is more tightly package in one direction such that the interface flange bolt pattern can be the same. The vertical uprights of the process gas plumbing connect to either the circular array or rectangular array design layouts with a design update to the rectangular array brazement connections. These uprights are also spaced strategically to allow for the integration of each of the heat exchangers at a later date in the product evolution if it's determined better for process and/or proven more cost effective. The BOP process gas connections were sized for gas velocities to allow for four 40kWe DC SOFC modules to be plumbed in series to balance flow distribution and pressure drop. The idea for such an array of modules was to have two rows in parallel, four modules each, connected to the 250kWe AC balance-of-plant (BOP). Thermal expansion calculations were completed on the plumbing to complete design of the bellows. And a complete insulation fabrication kit drawing was released.

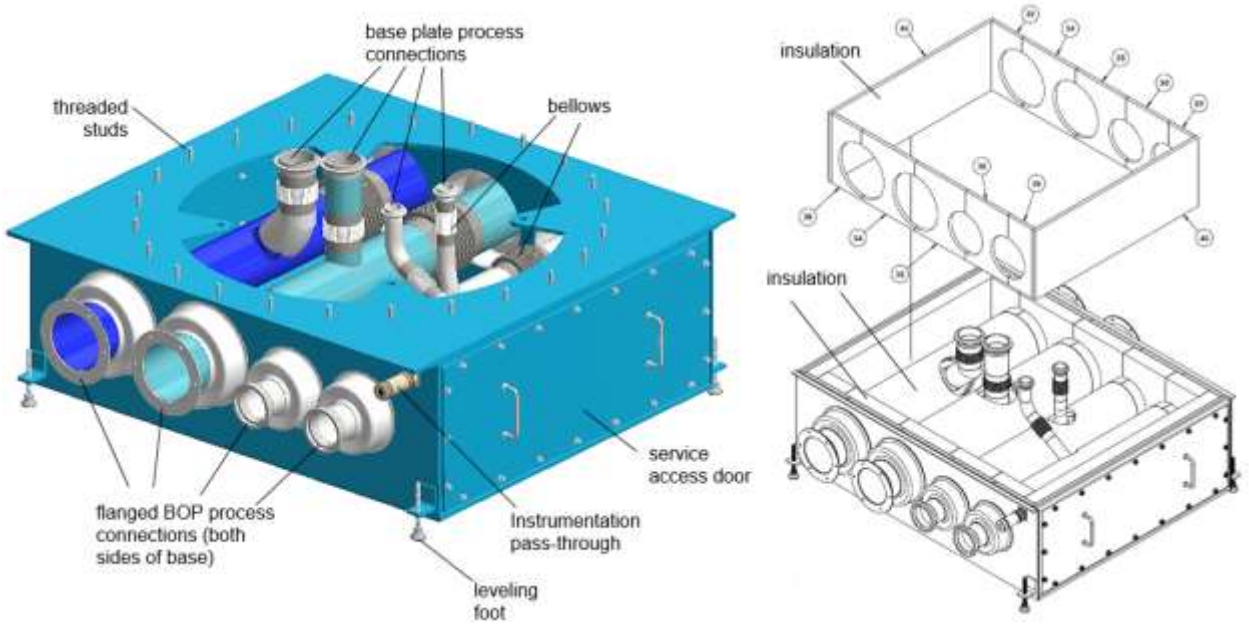

Figure 4.1-12 Design Layout of Circular Array Vessel Base

The plan is to connect a number of these in series to produce 250kWe AC power as a system level building block for MW power plants. These most recent design efforts have been mostly dedicated towards a circular array of stacks (Figure 4.1-13) with a central radiative fuel reformer (RFR). The vessel, being round, would be more suitable for higher pressure applications and protection against deflagration events than a rectangular form of the same wall thickness. The rectangular form would require a thicker wall as well as stiffeners for the corners where induced stresses would be highest. However, FCE has experience designing in deflagration protection for rectangular vessels. Also, the form and function of the components of the rectangular array vessel fit better with the projected SOFC technology evolution whereby future modules would have up to 50 CSA stacks. This can be achieved by extending the length of most of the components while assembling segments of stacks much closer together when packaged in a larger vessel. The circular array wouldn't pack as close together when scaling up module size. It also became a question as to whether the circular array's central RFR would result in a significant temperature differential across the diameter of the stacks. The rectangular array breaks up the RFR reforming duty into a number of smaller units, constructed as smaller diameter tube forms; in close proximity to each of the stacks. Thus, a rectangular array design concept has been chosen to detail further for the purposes of completing this project's validation test, mainly due to product life cycle future demand for larger modules.

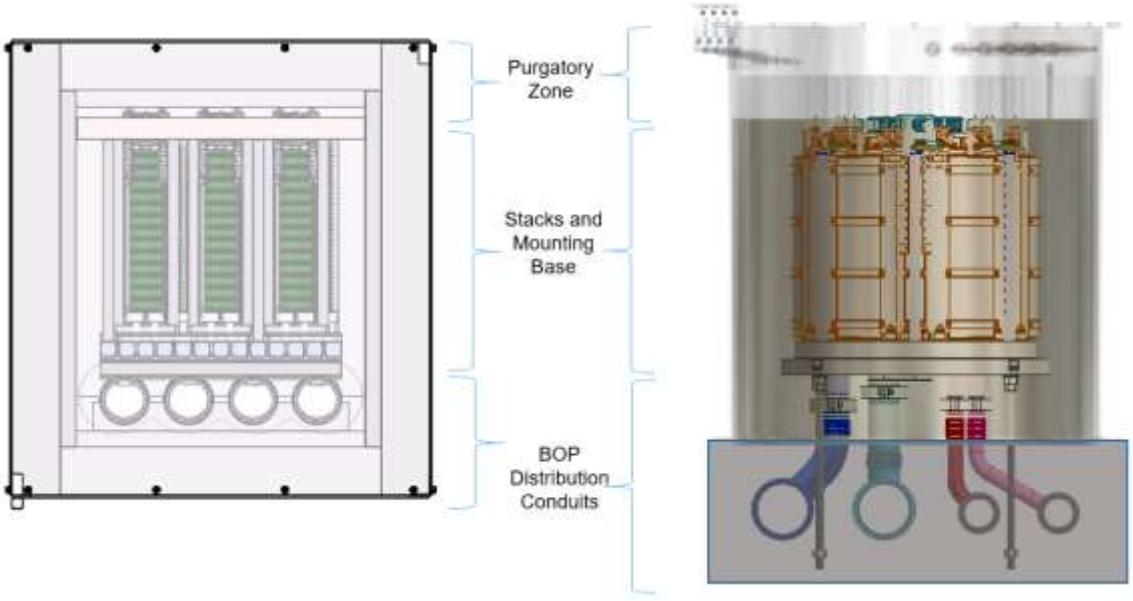

Figure 4.1-13 Stack Array Configurations: Rectangular (l); Circular (r)

It was reported last quarter that a rectangular array design concept has been chosen to further detail, for the purpose of completing this project's validation test. This was chosen over a circular array of stacks mainly due to product life cycle future demand for larger modules. The rectangular array module (Figure 4.1-14) features a removable upper enclosure with no plumbing or instrumentation attached to it. This allows for inspections with minimal effort as well as accessibility for technicians to perform install of the hardware required of operating SOFC stacks. This includes insulation, the base the stacks are mounted to, routing of instrumentation wires and gas sampling lines, and installation of plumbing connection clamps; all of which can be built onto the module lower enclosure weldment. For this first fabrication, there has been additional space added between the rectangular array of stacks and adjacent wall of insulation to aid the assembly nuances and accommodate RFR fuel bypass lines which would be removed on future builds. This extra space allows for the option to either reduce the size of the module at a future date or use the extra space to add two more stacks, increasing power generation capacity to $50kW_{DC}$. The level of instrumentation of the stacks has been greatly reduced compared with what is typically used during technology stack testing in single stack test stands as well as compared to the 200kW SOFC demonstration system. This moves the design much closer to the expectations of future products, where further learning in development would allow the engineering rationales afforded to eliminate these further. This would include voltage and temperature instrumentation connections as well as pressure measurement and gas chromatography sampling lines.

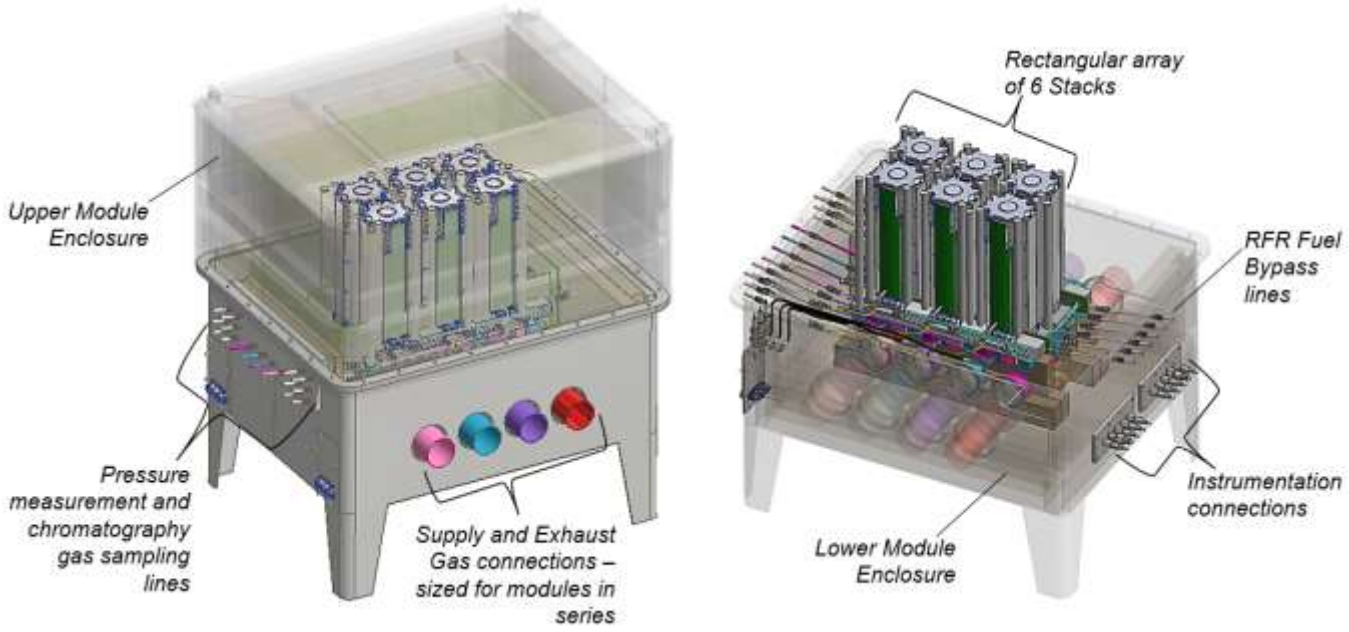

Figure 4.1-14 Rectangular Array Module Arrangement

The stacks, instead of being mounted directly to a base plate, are installed in individual interface plates (Figure 4.1-15). These interface plates have multiple functions: distribution of anode supply gas to four separate RFR tubes; consolidating and routing reformed fuel gas to the anode inlet of the stack; access for gas sampling to evaluate the performance of the RFR's; routing cathode exhaust gas; and serve as a rugged carrier of the CSA stack to be directly mounted to the base brazement. RFR tubes of the stack interface plate also provide potential strain relief tie-ins to protect the sensitive voltage and temperature instrumentation. Compression fittings are welded to the rectangular distribution tubes of the base brazement to provide a means to take critical measurements of pressure, temperature, and gas composition.

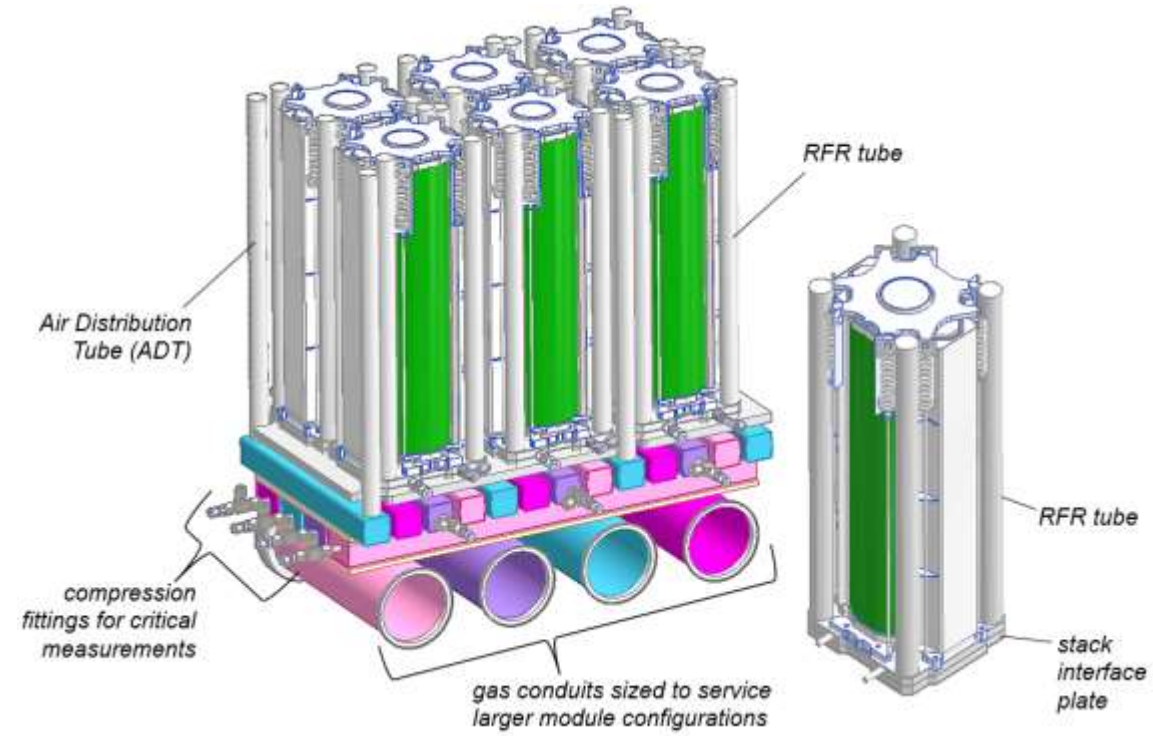

.

Figure 4.1-15 Stacks Mounted to Base Brazement

The base brazement fabrication takes advantage of compact rectangular tube arrangements to keep packaging space reduced. An overhead view of this with the CSA stacks (and associated interface plates) is shown in Figure 4.1-16 below. The mounting base brazement features include removable air distribution tubes to provide clearance and flexibility of sequence for stack installs; a high strength alloy mounting plate for stability under higher temperature long duration operation; thoughtfully placed insulation pieces to limit thermal effects from the hot zone of the stacks; and two levels of gas distribution tubes. The gas distribution tubes are made of easily formed sheet metal and provide a means to evenly distribute (and exhaust) process stream gases to individual stacks.

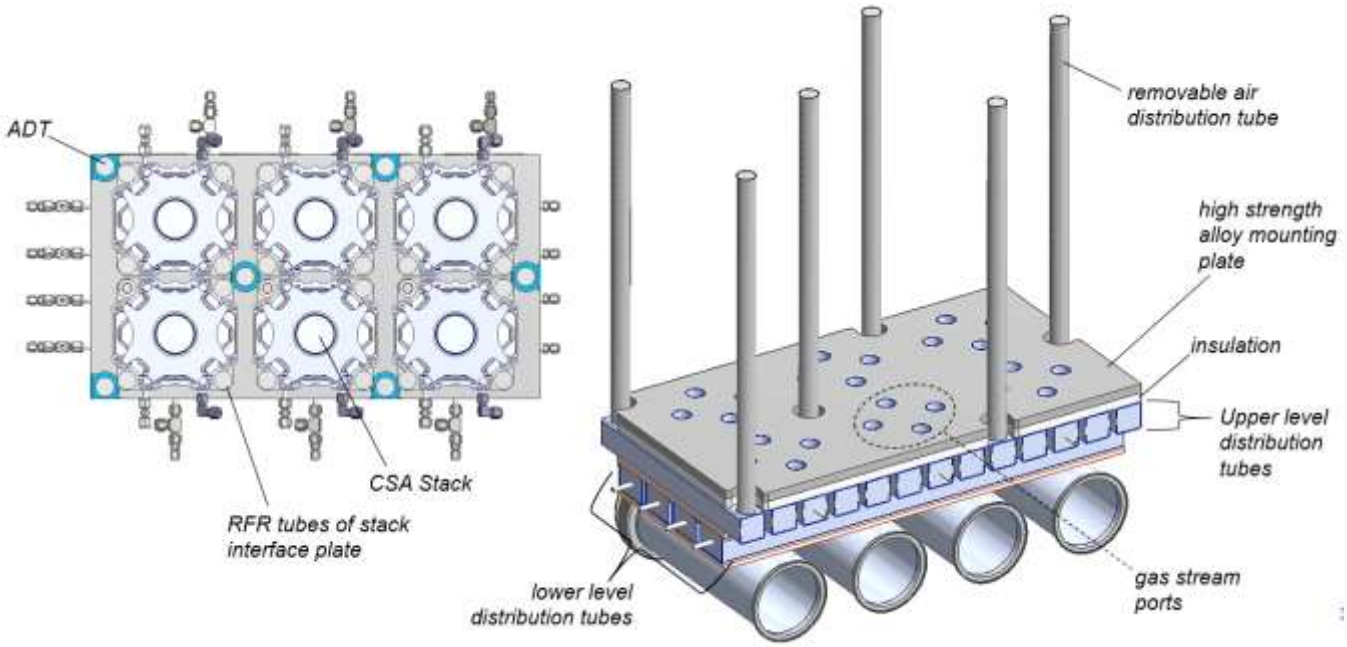

Figure 4.1-16 Base Brazement Construction

Part procurement has begun for the demonstration 6 stack module which is a sub-scale implementation of the full-scale concept illustrated in (Figure 4.1-17). This assembly consists of a base brazement onto which are mounted the stacks. Ten stacks are shown to illustrate a full-scale design. The brazement uses sheet metal plenums joined by expanded tube sections that are brazed at the junctions. The nickel brazing process is implemented with nickel plated components such that the parts can be assembled and brazed with a minimum level of handling and with well controlled braze placement.

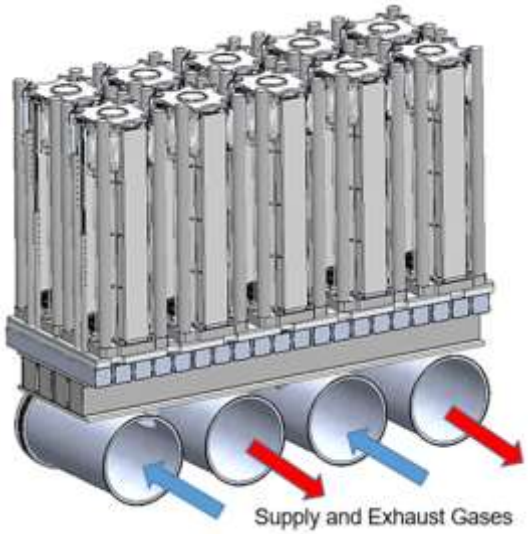

Figure 4.1-17 Conceptual stack array layout.

Braze trials were carried out on sample parts with success before committing real parts to brazing. Figure 4.1-18 shows some real parts as well as a brazement sample showing the successful positioning and brazing of two components. From these trials, a small adjustment to the expansion tooling was carried out for increased expansion. Overall, the results have demonstrated the basic

approach and provide confidence to finalize the design and procurement of the balance of the brazement components.

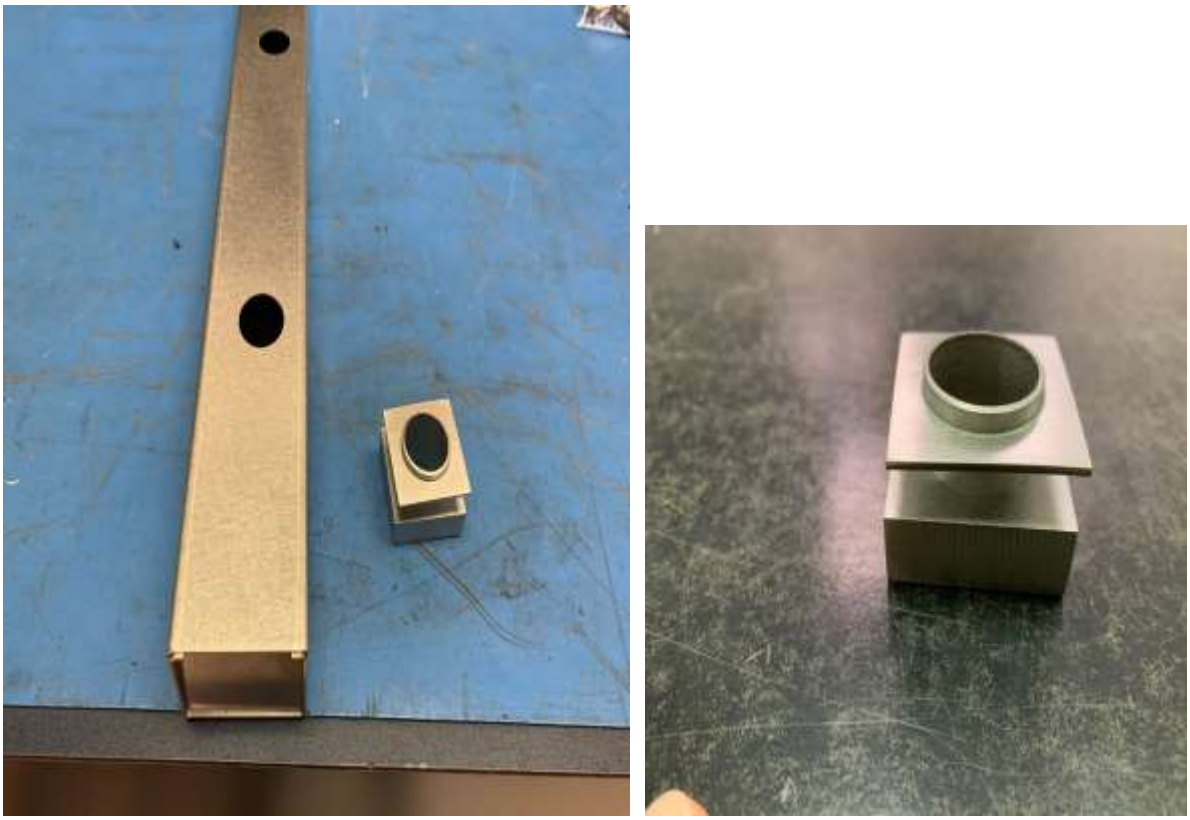

Figure 4.1-18 Manifold Base Plenum (far left) and Brazement Sample (center and right)

Prior quarterly reporting summarized the arrangement of the module components, including an interface brazement fabrication to which each of the CSA stacks are mounted (Figure 4.1-19). As stated in prior reporting, these interface plates have multiple functions. These include distribution of anode supply gas to four separate radiative fuel reforming (RFR) tubes; consolidating and routing reformed fuel gas to the anode inlet of the stack; access for gas sampling to evaluate the performance of the RFR's; routing cathode exhaust gas; and serve as a rugged carrier of the CSA stack to be directly mounted to the base brazement. The most critical function is pre-reforming fuel gas; actively cooling the stacks in the process.

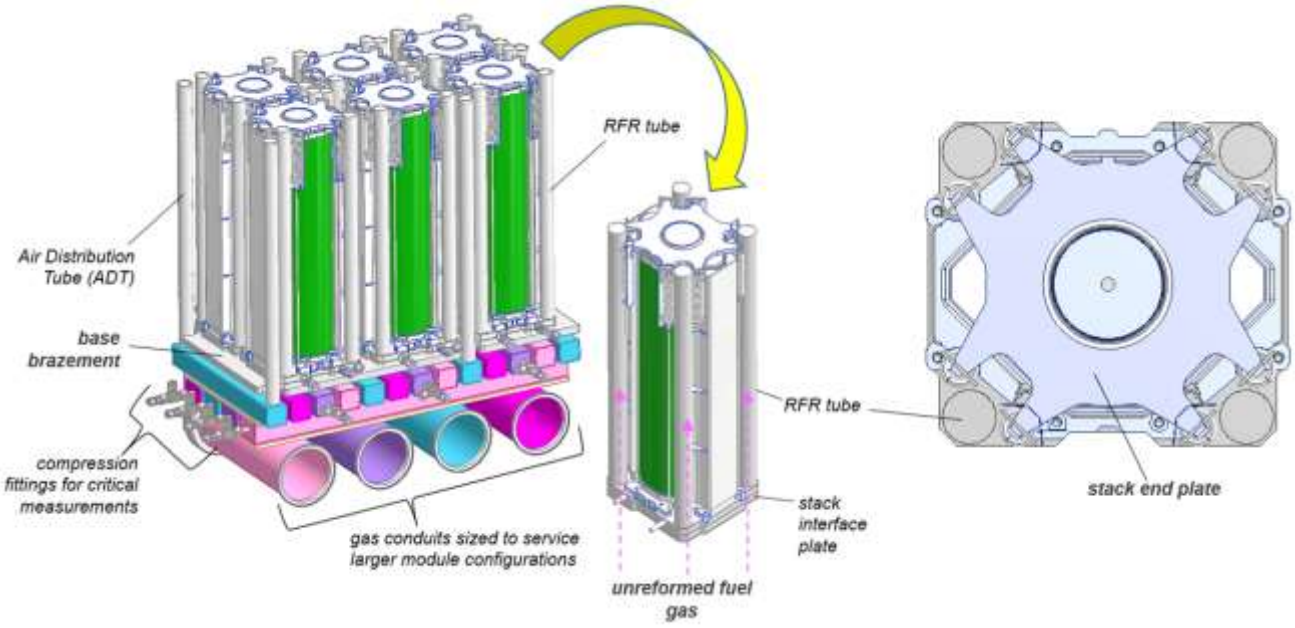

Figure 4.1-19 Stack Array on Base Brazement, Interface/RFR Tubes

The RFR technology to be implemented builds upon reforming technology developed during past DOE NETL funded projects – for 50kW$_{DC}$ and 100kW$_{DC}$ SOFC modules. For these, a four-paneled weldment was constructed with catalyst-coated substrates packaged within the channels inside the panels (Figure 4.1-20). During operation, fuel gas flows over these substrates within these panels. For the 100kW$_{DC}$ SOFC module, the cross-arrayed panel weldment, or RFR, was placed between the four stack towers. As the stack towers generated power, the RFR panels provided radiative cooling of the stacks; enhanced by the endotherm phenomena of the fuel gas reforming. Similarly, catalyst-coated substrates are packaged within each of the four RFR tubes surrounding the CSA stack, where the outer diameters of the tubes provide the radiative cooling surfaces.

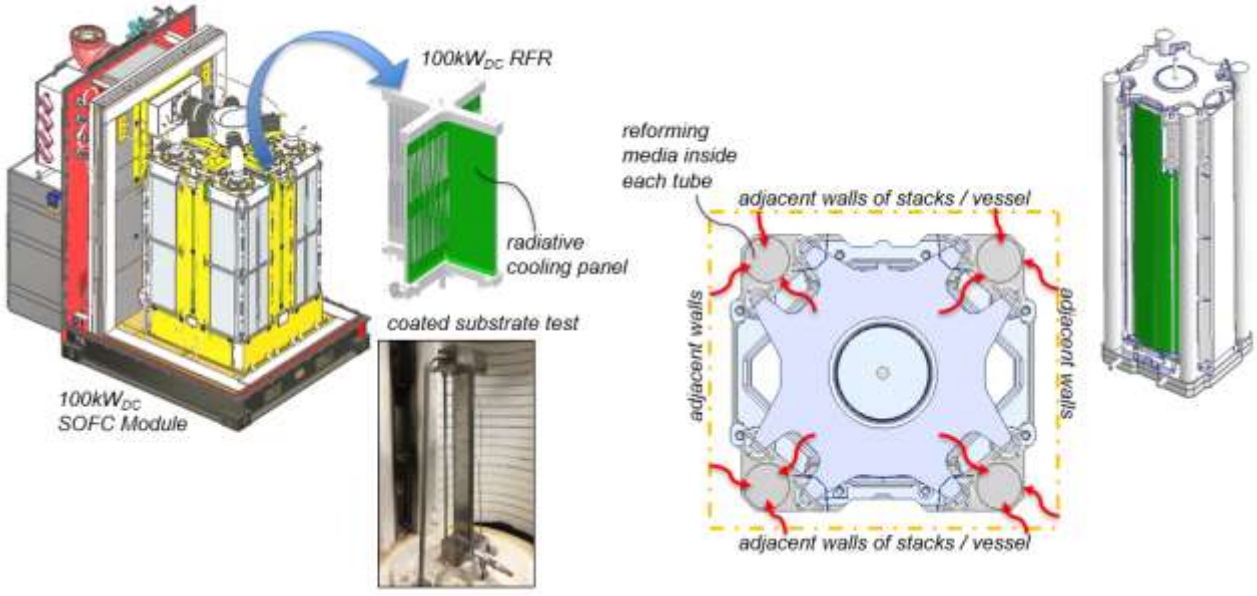

Figure 4.1-20 Incorporation of Prior Developed RFR Technology

The final design verification and procurement of the Stack Interface Plate, with RFR tubes, was completed in parallel with procurement of the Module Enclosure assembly parts, including insulation kits, instrumentation connectors, and the metal enclosure itself. RFR development activities that have been under way include identification of suitable catalyst/substrate design configurations, procurement and assembly of prototype parts, and construction of a small-scale test facility. The general design configuration (Figure 4.1-21) is a tube-in-tube arrangement whereby fuel gas is fed through an inner tube and then flows in opposing direction through an annulus created by addition of an outer tube. Reforming catalyst/substrate is fitted within the annular gap. The general method of design verification utilized a clamshell heater to simulate hot surfaces within the module. Simulated fuel gas, representing replenished recycled system anode out gas, is fed to the inner tube. Temperature of the fuel gas was adjusted until the minimum reforming requirement is met, verified with gas chromatography. The temperature of the outlet gas and pressure drops was recorded. The pressure drop was compared to the allotted pressure drop budget and the outlet temperature resembled that of the gas entering the fuel manifold within the CSA stack itself. Minimum reforming requirement is 65% with the potential for a lower reforming duty allowed depending on concurrent CSA stack direct internal reforming (DIR) evaluations.

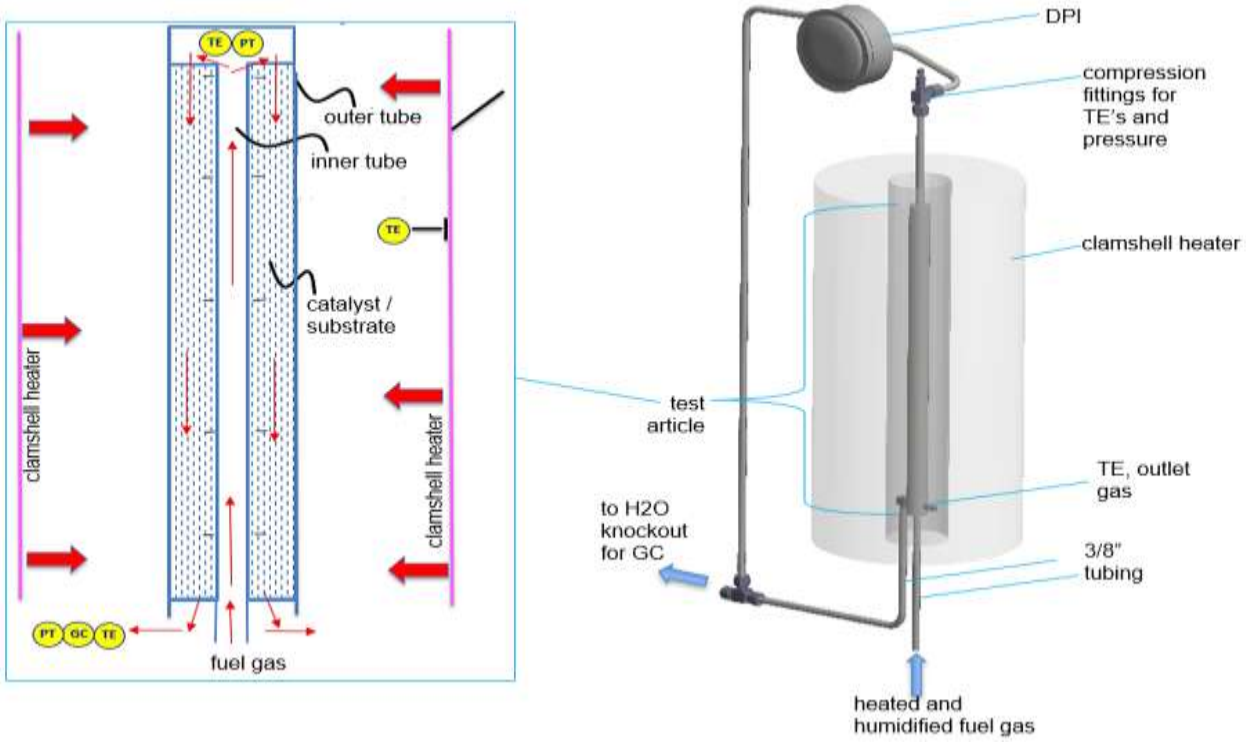

Figure 4.1-21 RFR Configuration and Design Verification Method

An initial configuration with reforming catalyst pellets was evaluated as part of a cold test to measure pressure drops. Using a readily available, easy to control gas, such as nitrogen, allows for the method of Reynolds number scaling and Darcy Weisbach equivalent pressure drop calculations to be used to sufficiently evaluate anticipated pressure drops. The results can be assessed prior to investing the time and resources into subsequent hot testing with actual end use gases. Results with and without loading of catalyst pellets are shown in Figure 4.1-22 below. The results show that use of the pellets in this current configuration of tube diameters surpasses the allotted pressure drop budget for the RFR tubing equipment. Though, only a small adjustment

in these diameters should meet this requirement. Some higher than expected pressure drop was noted through the portion of just the inner tube that was attributed to spill over, or sugaring, of weld joint choking the flow. This won't be a risk when the inner tube feature is brazed to the bulk of the actual Stack Interface Plate. Pellets are being used as a baseline design that has high confidence of meeting reforming requirements. They are not an ideal solution for long duration use due to the settling of materials when exposed to high temperatures. Coated metal substrates were being coated at the time of quarterly writing. These are designed to fit in the annular space created by the inner and outer tubes with the goal of providing a longer-term solution. Use of pellets were developed as a risk mitigation in case initial low-cost, low pressure drop, coated substrate specimens do not meet these requirements.

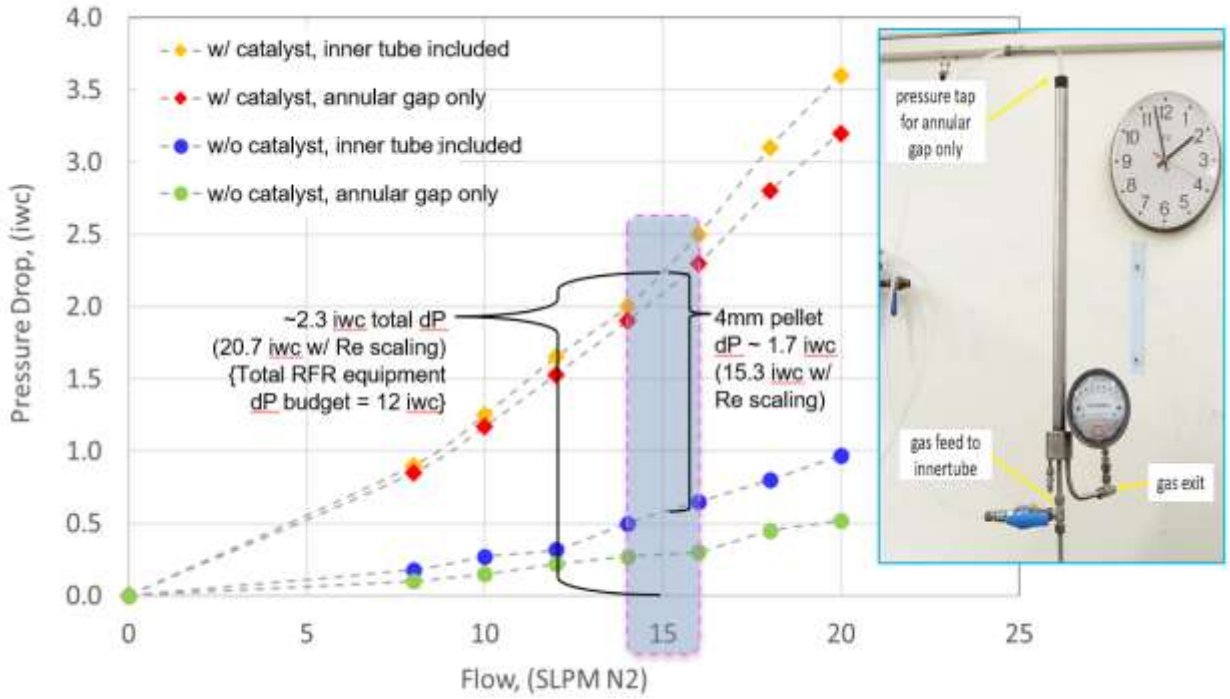

Figure 4.1-22 Results of Cold Pressure Drop Cold Testing of Catalyst Pellets

Prior to running the 40kW SOFC module a single loaded RFR tube was tested under simulated operating conditions. Hot RFR testing is necessary to understand the expected pressure drop that the RFR tubes have on the anode inlet gas. Determining how much methane gets reformed in the RFR tubes was the primary performance metric during testing. The inlet gas blend (recycle) consisted of CH4, H2, CO, CO2 and Steam. The embedded picture (Figure 4.1-23) shows the bubbler humidifier, clamshell heater, and Alicat mass flow controllers for this test.

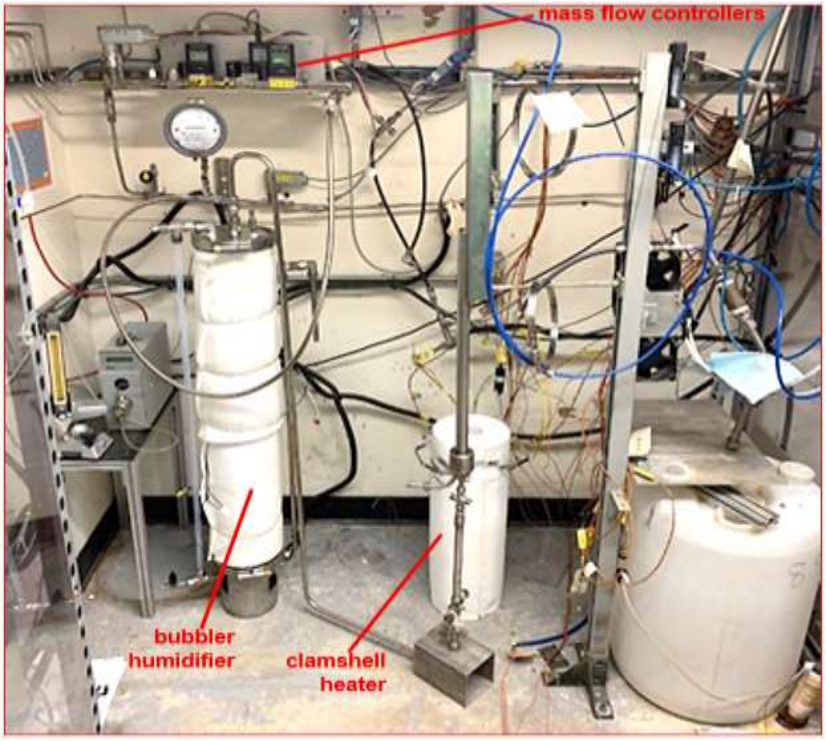

Figure 4.1-23 Small-scale RFR Test Facility

The test system consisted of three actively controlled heaters in addition to some heat trace. The reformate gas was simulated via three dry gases, CH4, H2 and CO2. The reformate gas blend was humidified to a temperature of ~75°C corresponding to nearly 40% steam. This small system was run under several inlet temperatures as well as several different reactor temperatures to better understand the reactor performance envelope. Two types of reforming catalyst are being considered in this reactor: pellets and monolith inserts. Several thermocouples were installed to monitor the thermal behavior of the reactor along the catalyst tube.

Final design details have been worked through on the overall Module Enclosure and major contents. Some reconfiguring of the insulation arrangements and addition of a dedicated purgatory space has allowed for ease of installation of insulation kits and routing of instrument wires (Figure 4.1-24). This inaugural build of a multi-stack (CSA) requires more instrumentation than that of a final product in order to sufficiently assess the performance of the module (and stacks). This additional instrumentation allows for such items as fine tuning the active stack-cooling and reforming capacity of the RFR's as well as how temperatures vary in different regions and stack positions within the module. Follow-on module constructions are expected to be noticeably more compact and less instrumented after assessing lessons learned from this first unit being built and operated. Attention has been given to the layers of the insulation vertical and horizontal pieces to limit heat loss at seams created where the pieces meet; typically achieved by having neighboring pieces overlap one another.

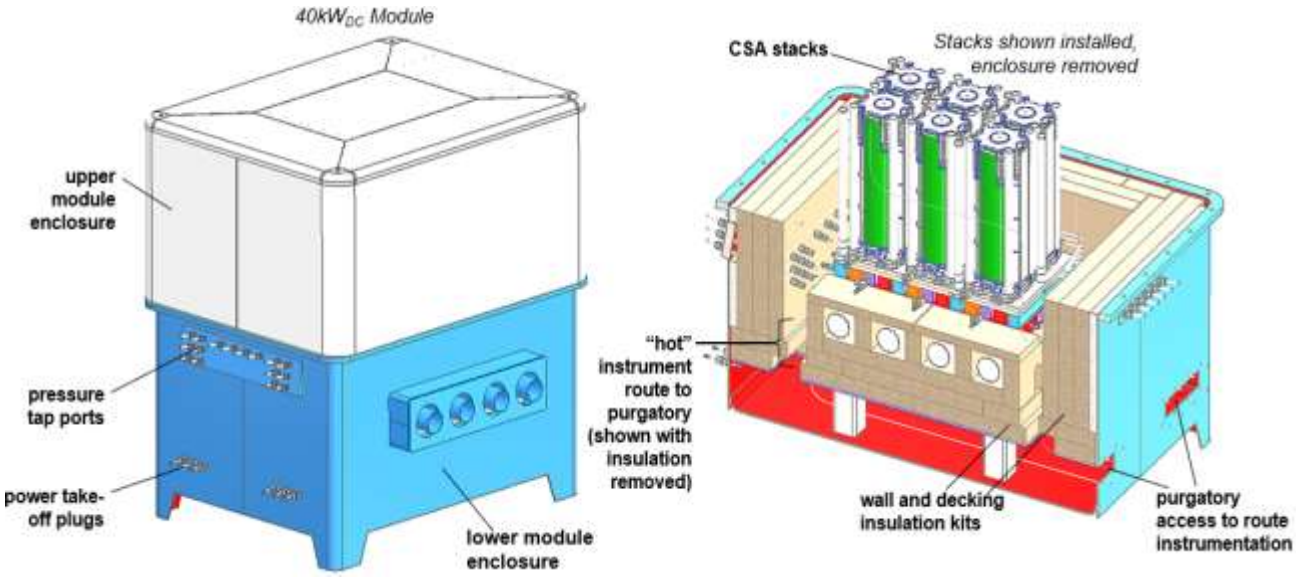

Figure 4.1-24 Updates to Module Enclosure and Contents for Instrument Routing

Final design details of the Stack Mount Brazement were worked through as well. The brazement is constructed of multiple levels of rectangular sheet metal components; brazed together with sheets of insulation creating a thermal shunt between each layer (Figure 4.1-25). The top plate acts as the mounting surface for the CSA stacks (with accompanying Interface Plate) and tube stub connections protrude above this plate to provide a means to assemble air distribution tubes (ADT) at a later assembly step. The lower level of tubing needed to be changed from circular tube to a rectangular sheet metal arrangement to provide level seating surface and distribute better the weight of the stacks. The rectangular form also makes better use of volume space for flow of process gases, making for a more compact module arrangement and better control of gas temperatures. Tabs were added to these lower-level tubes to provide a means of shipping retention. The hardware for retention is designed to become less restrained at higher temperatures to allow the brazement to grow laterally during thermal expansion without inducing elevated stresses and/or adversely warping components. More detailed activities regarding flow distribution and pressure drop through these flow passage tubes can be found in Task 4.2 of this report.

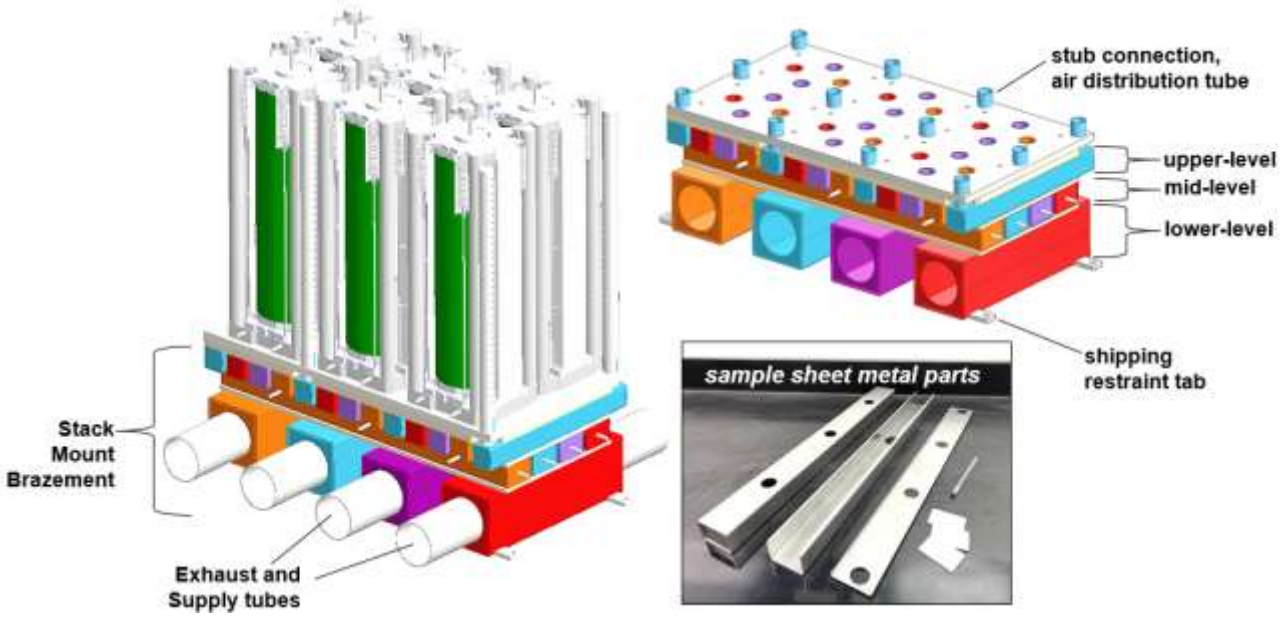

Figure 4.1-25 Final Stack Mount Brazement Updates

A single tube radiative fuel reformer was installed and heated up in a test stand, in early December, to observe its performance characteristics, reduction stability, pressure drop and reforming performance. The initial catalyst selected was a pellet type reforming catalyst from onsite inventory. The specific test stand (Figure 4.1-23) assigned to carry out reforming testing utilizes a new bubbler style humidifier for steam supply, an inline gas preheater, and a radiant heater for the reactor tube. Some areas for improvement for the test stand system were identified and resolved. The pressure drop through the preheating section was found to be higher than expected so a replacement preheater slightly larger in diameter with much lower pressure drop was selected, procured, and installed in its place.

Initial flow testing revealed that higher than anticipated bubbler humidifier pressures led to low water fill level inside the bubbler. The bubbler originally had a simple passive liquid level control scheme. A bubbler over fill drain tube limited the highest liquid level inside the bubbler. Since the overfill tube references ambient pressure the bubbler must run at pressures relatively close to ambient pressure to function properly. Humidifier level control was upgraded by means of adding a normally closed solenoid valve to open when the water level drops below a predetermined setpoint as measured with several pressure transmitters. The pressure transmitters are arranged with two pressure transmitters mounted at the top of the humidifier vapor space and two more mounted at the base of the humidifier. This upgrade permitted a greater range of possible test conditions, including running at higher flow rates. Testing at elevated reactor flow rates, beyond the planned rated power flow rate is necessary to simulate low fuel utilization in the SOFC system.

Replacement over temperature alarm controllers were added to the test stand to replace existing legacy units. The three temperature alarm controllers serve to interrupt heater power to the process heaters specifically the Humidifier, Gas Preheater, Main Reactor Tube Heater if their over temperature setpoints are exceeded. A single tube reactor test plan has been created to ensure the correct order of testing occurs, as well as all desired test conditions including temperature, composition, and flow rates in one document. A gas chromatograph was utilized to measure the product gas composition.

The reformer ran for more than five weeks in the Reformer Test Stand; benchmarking monolith performance in the Radiative Fuel Reformer. Reformer performance has been extremely stable as shown by reformer exit samples tested by gas chromatography on a weekly basis. This indicates that the reforming catalyst is very stable. Additional reforming and elevated temperature were realized when FCE replaced the 18" Long RFR Main Reactor heater with 24" Long heater to better represent the Next Gen Module thermal environment; specifically reducing test article heat loss at either end of the reactor.

GC data indicates that the reactor is reforming more methane than necessary but was not quite providing sufficiently hot reactor exit temperature. The reactor exit temperature is important as it directly feeds reformate into the SOFC anode inlet where on-cell temperatures differentials need to be minimized. For optimum fuel cell performance, it is critical for the anode inlet gas temperature to be well within 100°C of the stack temperature. Also noted, test results showed the inlet tube supplying gas to the reformer reactor section pressure drop higher than expected. The Flow Lab RFR Test Stand HMI (Figure 4.1-27) allows the user to monitor performance and control the reactor test stand.

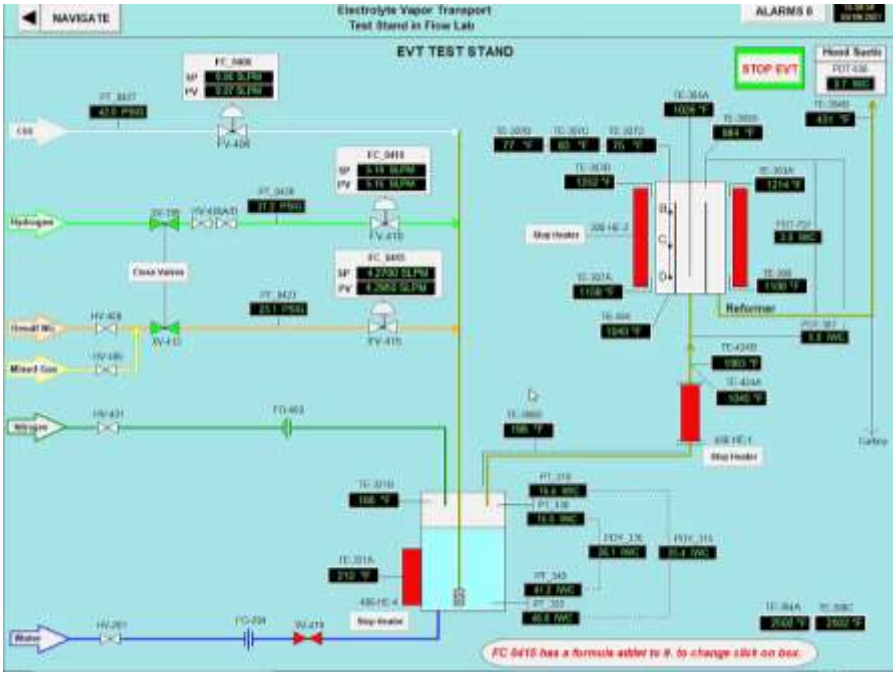

Figure 4.1-26 RFR Test Stand HMI

A plot of exit stream properties is illustrated in Figure 4.1-27 below. Here, it is shown that the results, captured at Rate Power flow conditions, are promising. Dry composition of methane in the exit stream is around 9.5%, while the temperature is around 630°C.

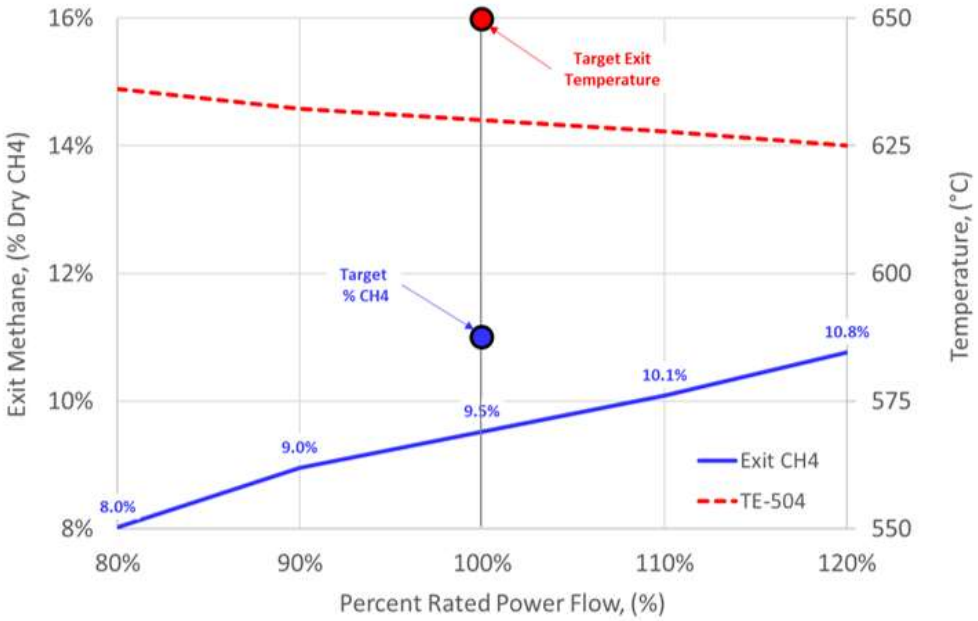

Figure 4.1-27 RFR Test Results: %CH4 and Temperature of Exit Stream

Pressure drop results are shown in Figure 4.1-28 below. Here, it is shown that pressure drop across the RFR annular tube arrangement is within the allotted pressure drop budget of 12 inches of water column. There are opportunities for improvement in pressure drop budget margin and exit stream temperature. These have resulted in some minor adjustments to the RFR design configuration which included: increasing the inlet tube diameter from 3/8” to 7/16” and positioning the coated monoliths higher in the annulus to allow for a region of sensible heat duty. This simultaneously reduced the estimated inlet tube pressure drop and slightly increase reactor space velocity in the annular reformer section with the expectation of reducing overall methane reforming in the reactor. A second monolith reformer was received from the catalyst manufacturer reflecting these changes and evaluated for efficacy.

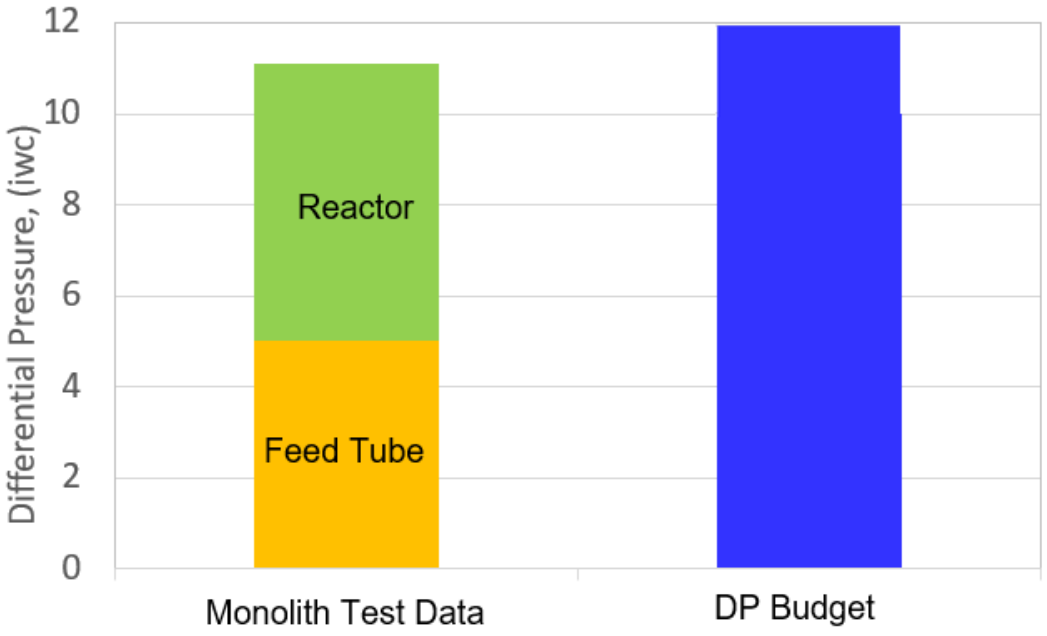

Figure 4.1-28 RFR Test Results: Pressure Drop vs Budget.

4.2 Design Analysis and Process Simulation

Approach:

In this task, CFD and finite element analysis (FEA) techniques were used to model and evaluate the thermal performance the stack arrays and heat exchange elements, such as pre-reformer and gas preheat devices. These tools were employed to better understand radiant heat generation from these elements, determine insulation strategies and structural requirements, maximize the performance of a close-coupled modular building block, and optimize spacing as input to the Stack Module Design layout work of Task 4.1. CFD analysis of the stack module was critical to evaluate flow and temperature distribution to each stack with a focus on designing to achieve uniformity, especially between edge stacks (those adjacent to side walls), and core stacks (those surrounded by other stacks). These results feed directly into process simulation models to be used to analyze anticipated modes of operation such as fuel-enable, hot-stand-by, and rated power. Process simulation results were used to optimize the stack module design (Task 4.1) and stack modules controls (Task 4.3) and be utilized iteratively to refine analyses (CFD, FEA) to continually verify stack and stack module performance requirements are met.

Results & Discussion:

The flow configuration of the process gases is an important aspect to evaluate for potential risks and benefits associated with a specific design. There are a number of ways to supply and exhaust both air (cathode) and fuel (anode) streams; each having the potential to be a better or worse fit for the module design and performance than other competing configurations. For example, the module could be designed to provide supply air flush to the stacks or could have the air supply through the bottom ends of the stacks depending on the trade-offs of flow and temperature distributions, fabrication choice, ease of assembly, and cost. Another example would be reversing the flow of anode gas through the center of the stack and what that does to the mounting base thermal and flow distribution to the anode supply and exhaust streams passing through it. The

CSA stacks have not been run in a module configuration so it's important to examine whether the current flow direction of supply and exhaust gases are appropriate for the selected module design. Other considerations include how the interfacing equipment hardware within the module should be configured best with the choice of flow direction; including the radiative fuel reformer, the stack mounting base which handles anode flow, and non-repeat stack hardware such as end plates and manifolds.

The baseline design of the CSA stack utilizes air supplied flush to the outside diameter of the stack; not plumbed directly to non-repeat hardware of the stack. A CFD study was initiated to determine how well distributed the air would be to six stacks in a modular configuration. Also of interest, was whether there is a significant difference depending on the two sides of the stack the air enters, and what this distribution looks like along the height of the stack. Distribution aspects inspected were both temperature and flow rate. An initial stack layout configuration, with six stacks in a circular pattern along with accompanying air supply distribution tubes, was modeled within CAD space. Then, a model with representative fluid bodies was generated in CAD space and imported into CFD software analysis tools. Figure 4.2-1 below illustrates this model and high-level aspects. Fluid space bodies for cathode manifolds are included which provide the ability to turn each set of fluid bodies on or off - or used as vessel air space - depending on installation orientation. These also include small porous media bodies along the height of the stack to model downstream back pressure of stack interconnect flow channels. After meshing the required fluid bodies, the model was imported into CFD software and boundary conditions were applied (Figure 4.2-2).

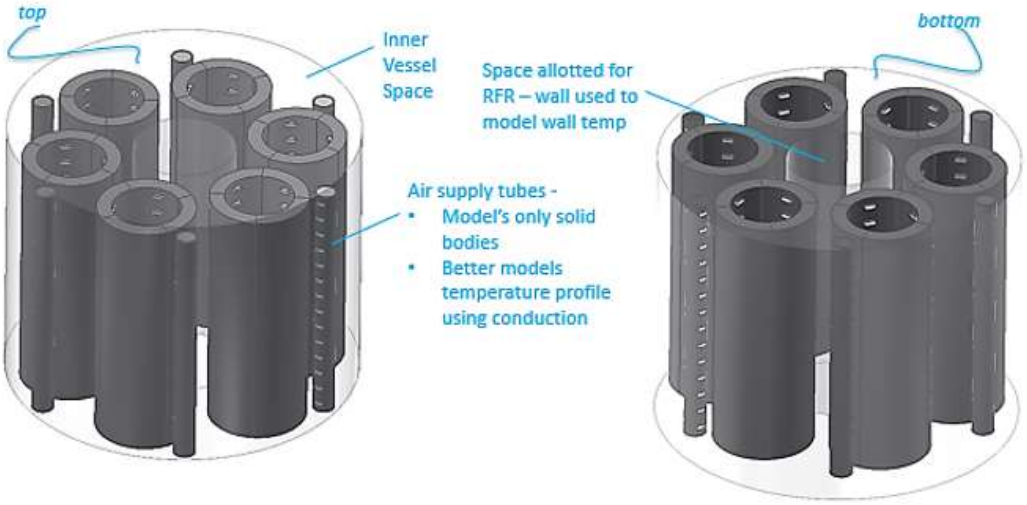

Figure 4.2-1 Supply Air Flow Distribution Model

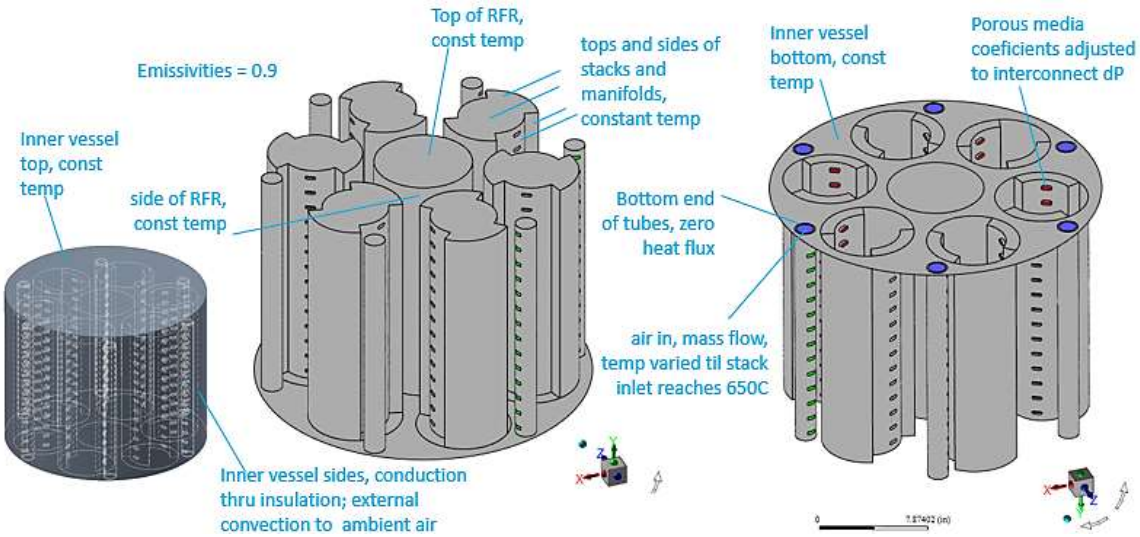

Figure 4.2-2 Summary of CFD Model Boundary Conditions

Flow rates equivalent to 40% air utilization for six stacks were used as a boundary condition. The air supply temperature was adjusted until the temperature of all inlets into the stacks were a minimum of 650°C. The flow rate and temperature distributions were then evaluated. A sample plot of first several hundred steps of simulated flow stream is show below (Figure 4.2-3). It can be seen how the initial jet of air supply into the vessel flow between the tight gaps between the stacks and vessel wall, picking up heat from the stack and vessel manifolds along the way. Qualitatively, the flow rates appear to be very uniform between each of the six air supply tubes and between each of the stacks. A screening of the data showed these flow rates to be within 1% of one another. The data also shows that the counter-clockwise cathode-in flush side of each stack receives about 1% more flow than the clockwise side. This is good enough for the level of air utilization flow rates being targeted for module operation. The average temperatures entering each side of the stack for all six stacks are all within 10 degrees of each other.

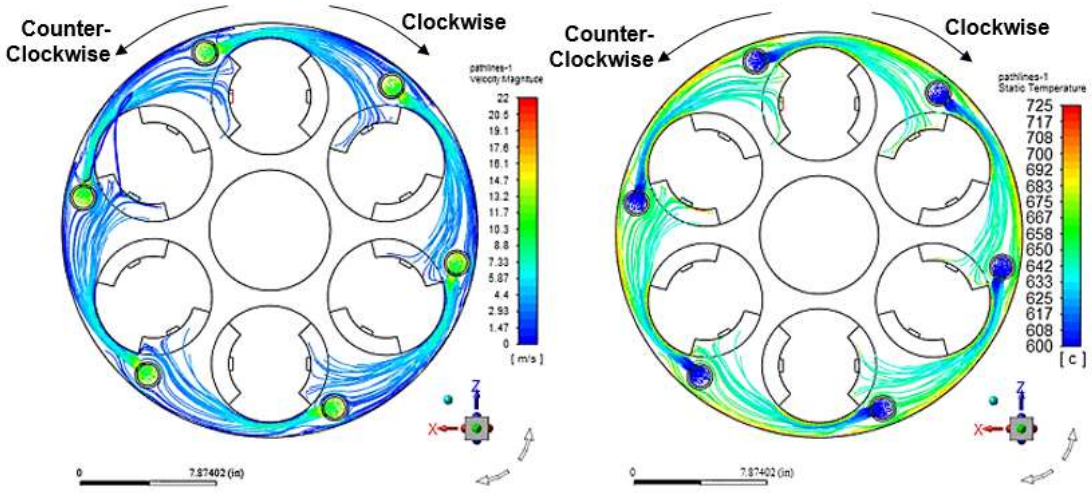

Figure 4.2-3 Sample Flow Streams Plots of Velocity and Temperature

The air being supplied into the inner vessel was able to enter the supply tubes as low as 550°C while maintaining a stack inlet tempeature of 650°C. This is an important aspect as this provides

a measure of how much heat duty is required from the cathode air heat exchanger. This heat duty has historically been provided by a catalytic air pre-heater (installed in a 200kW SOFC plant system currnetly operating in Pittsburgh). A closer look at the temperature of air exiting the air supply tubes shows that a substantial portion of this heat duty is being transferred to this stream withiin the air supply tubes themselves (approximately 40°C of temperature increase). This is heat being picked up by radiation from the open faces of the stacks, the stack manifolds, and vessel walls to the tubes and then into the air via convection. Temperature plots show the tube temperatures to be between 675 and 700°C (Figure 4.2-4). The temperature distiribution along the height of the stacks appears to need some improvement. Thus far, it appears that there is no critical to need to change the flow configuration of cathde-in flush to cathode-out flush.

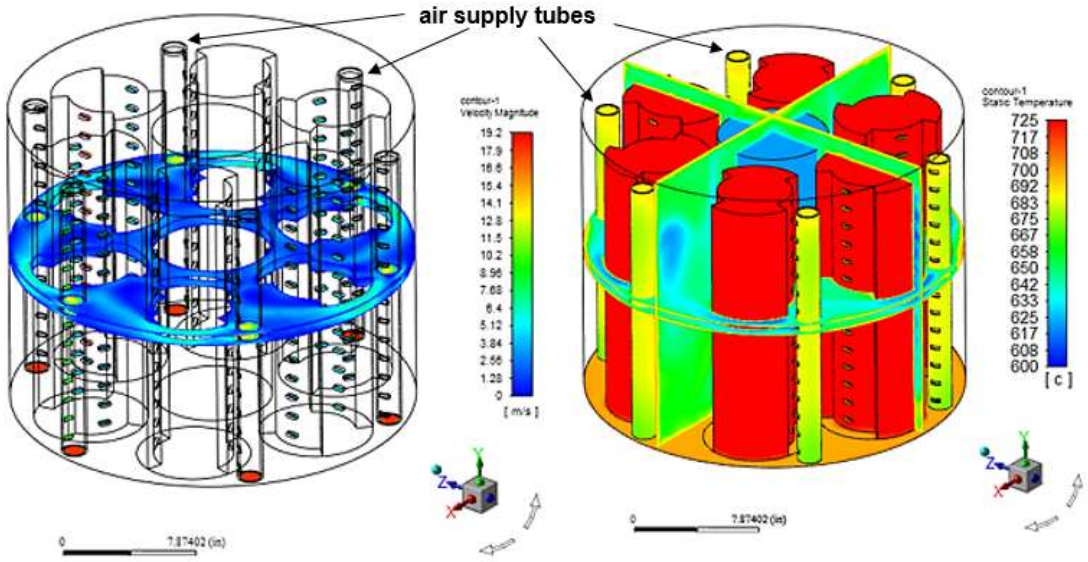

Figure 4.2-4 ISO View Plots of Velocity and Temperature

Due to the intricate level of design detail, it is difficult to carry forward detailed CFD cell level models to the module design environment. As such, work was carried out to build and verify a simplified full 350-cell stack model. Key requirements for the simplified stack and stack module simulation were to have a mesh size (overall module problem statement) be small enough to be practically operated by the workstation CPU. However, the model needed enough detail to capture stack thermal features and be able to approximate on-cell delta T (dT). The resulting CFD CAD model to mesh is shown next to CSA stack CAD model in Figure 4.2-5 below.

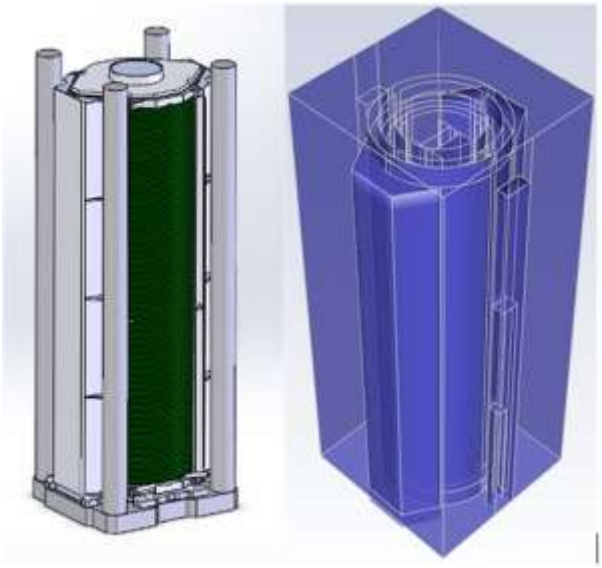

Figure 4.2-5 Single-stack (CAD in details, compacted 350-cell, 9 shells, 4 shells)

The full height of the 350-cell CSA (6.6kW) CAD model mesh consists of nine concentric shells of porous media for the active area of the stack. Realistic flow within the stack is accomplished with low flow resistance, laterally, along the cell plane and high flow resistance, vertically, along stack height, to simulate radial flow within these concentric shells. The mesh size is 0.4 M for the stack. The nine concentric shells are split: four outer shells for air, five inner shells for fuel, and impervious separator layers between the shells. This keeps the fuel towards the core of the stack and the air in the outer shells which helps simplify the model to be meshed. For initial thermal analysis, conditions that simulate a rated power condition, similar to the 100 kW RELISS stack module, were carried forward. These operating conditions are listed below with boundary conditions highlighted in Figure 4.2-6:

- Simulated CH_4-H_2-N_2-H_2O fuel with a direct internal reforming rate of 36%.
- 0.29 A/cm^2 (23.5 A), 0.85 V/cell
- 68 fuel utilization, and 40% air utilization
- 600°C inlets, with 25°C ambient

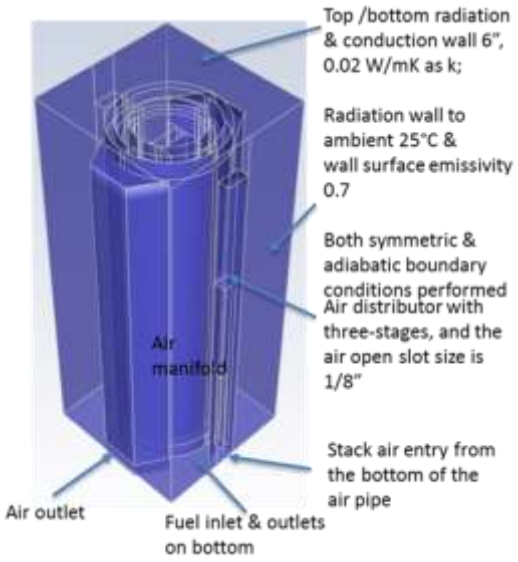

Figure 4.2-6 Boundary conditions and module components description.

The stack core was simulated with a bulk thermal conductivity of ~ 5.4 W/m-K and a tuned pressure drop of ~0.2 psi for reactants through the stack core. A net core heat generation (W/m^3) is calculated based on the operating conditions, with a DO (discrete ordinates) radiation model for heat exchange within the stack module. For air feed and distribution to each stack, a simple 3-stage air distributor is utilized. Figure 4.2-7 shows the air flow distribution around the stack inside the module.

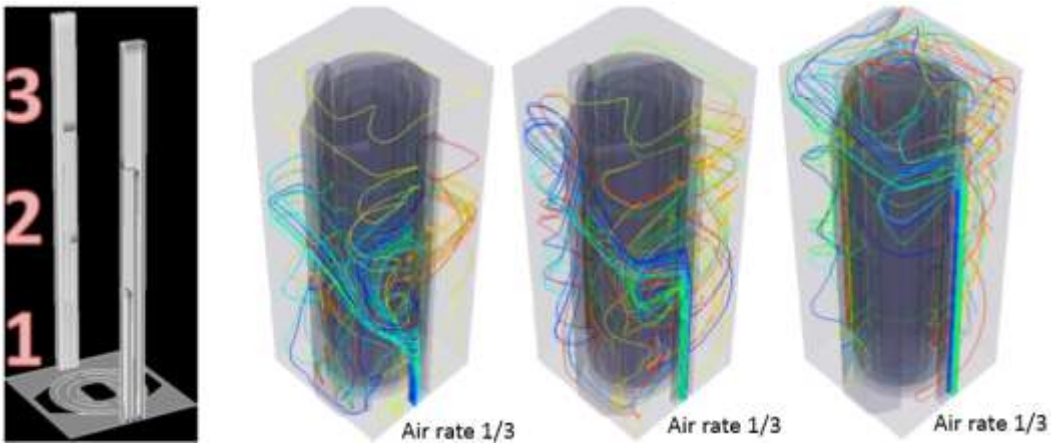

Figure 4.2-7 Flow path lines of a 3-stage air distributor (placed on opposing sides of stack)

For initial model validation, a single stack was modeled prior to progressing to multi-stack arrangements. The thermal profiles on symmetric planes as well as a middle cross-section are as illustrated in Figure 4.2-8. Species distribution mole fraction profiles are shown in Figure 4.2-9. In summary, a pair of three-stage air distributors with a single stack (350-cell tall) has been modelled numerically. Results indicate that the air distributor design works well for preheating air and stack cooling evenly. However, the reforming (36% DIR rate) performed by the stack needs fuel inlet temperature 600°C or below to maintain the peak stack temperature below 800°C.

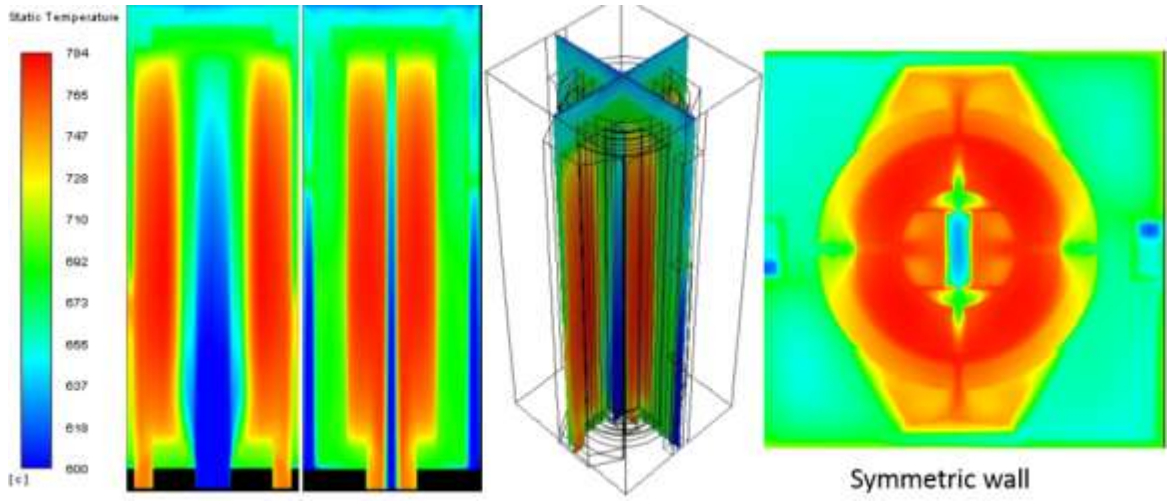

Figure 4.2-8 Temperature Profiles for a Single Stack Module

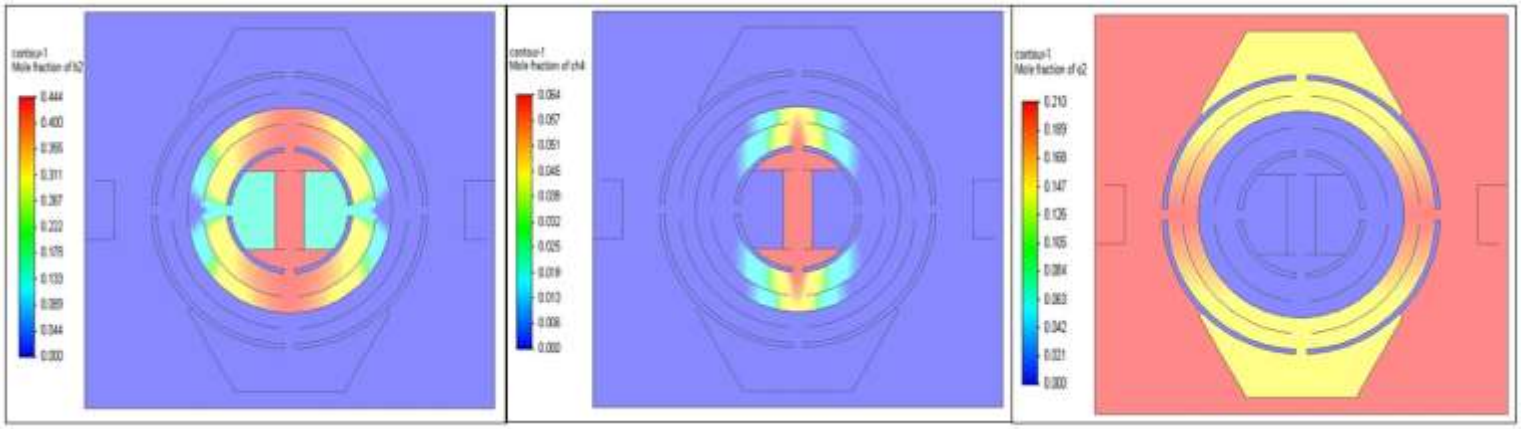

Figure 4.2-9 Species Profiles: H2, CH4, and O2 Mole Fractions

Stack Thermal Control Assessment

One of the more critical questions to answer initially is to what configuration of active cooling of the stack should be chosen. There are two main methods to be used as control knobs means of thermal control (current control is covered in later section). One method consists of use of flowing cathode in air flush to the surrounding stack environment versus cathode out oxygen-depleted air flush. The second method consists of radiative fuel reforming, a method validated for use during prior DOE-funded SOFC projects. Here, it is of interest to see whether there is a preferred side of the stack to place the RFR; the open, un-manifolded side or the covered, manifolded side. For initial assessment, the simplified single-stack CFD model was utilized to run the four different stack cooling configurations as shown in Figure 4.2-10. Of specific interest for this exploration was the stack on-cell temperature differentials as well as minimum/maximum temperatures. The goal is to minimize on-cell dT as well as control maximum temperature to less than 800°C – the current materials system limit for sustained operation. Three different temperatures were chosen for each cooling configuration to illustrate the effect RFR surface temperature and help identify a design temperature to match the indirect reforming design point (total reforming minus target DIR).

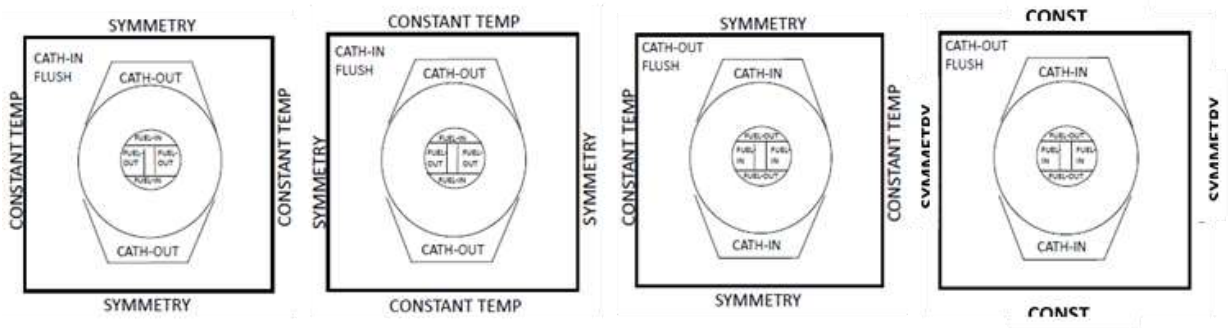

Figure 4.2-10 Four Boundary Condition Cases

A comparison of temperature plots, inclusive of manifolds and simulated module environment outside stack, is shown in Figure 4.2-11. Here, it can be seen that cathode out flush cooling configurations (cases 3 & 4) keep the de-oxygenated air environment surrounding the stack anywhere from approximately 50-to-750°C hotter than that of the cathode-in flush cooling configurations (cases 1 & 2), depending on simulated RFR surface temperature. The effect of this on maximum cell temperature is shown more dramatic with decreasing RFR surface temperature.

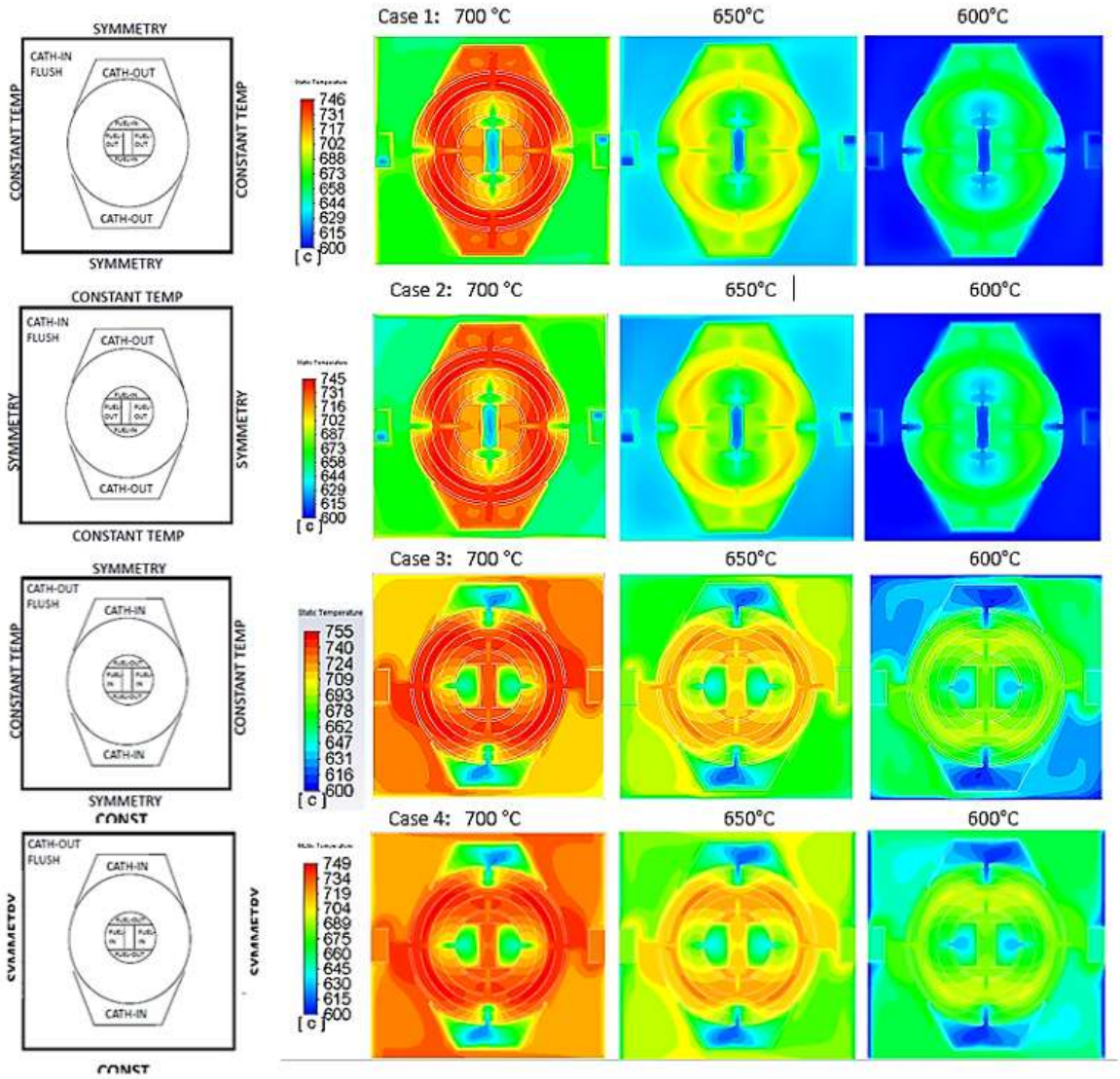

Figure 4.2-11 Comparison of thermal cases 1, 2, 3, 4 respectively.

To best see the effects on the on-cell temperature differential, a critical aspect to preventing thermally induced cell damage and fractures, derived temperatures plots were scoped to only include the region bounded by the inside and outside diameters of the cell. Plots shown include only the cathode in flush cases since cathode out flush cases show relatively poor capability to lower on-cell maximum temperatures (Figure 4.2-12). Results show that as RFR surface temperature is significantly lowered, the on-cell temperature differential is lower for the RFR being located on the open side of the stack versus the cathode manifold side of the stack. However, the values are relatively close to one another. To further discern whether there is significant difference between the two configurations, the five-cell fully detailed CFD modeled was used to provide sufficient accuracy.

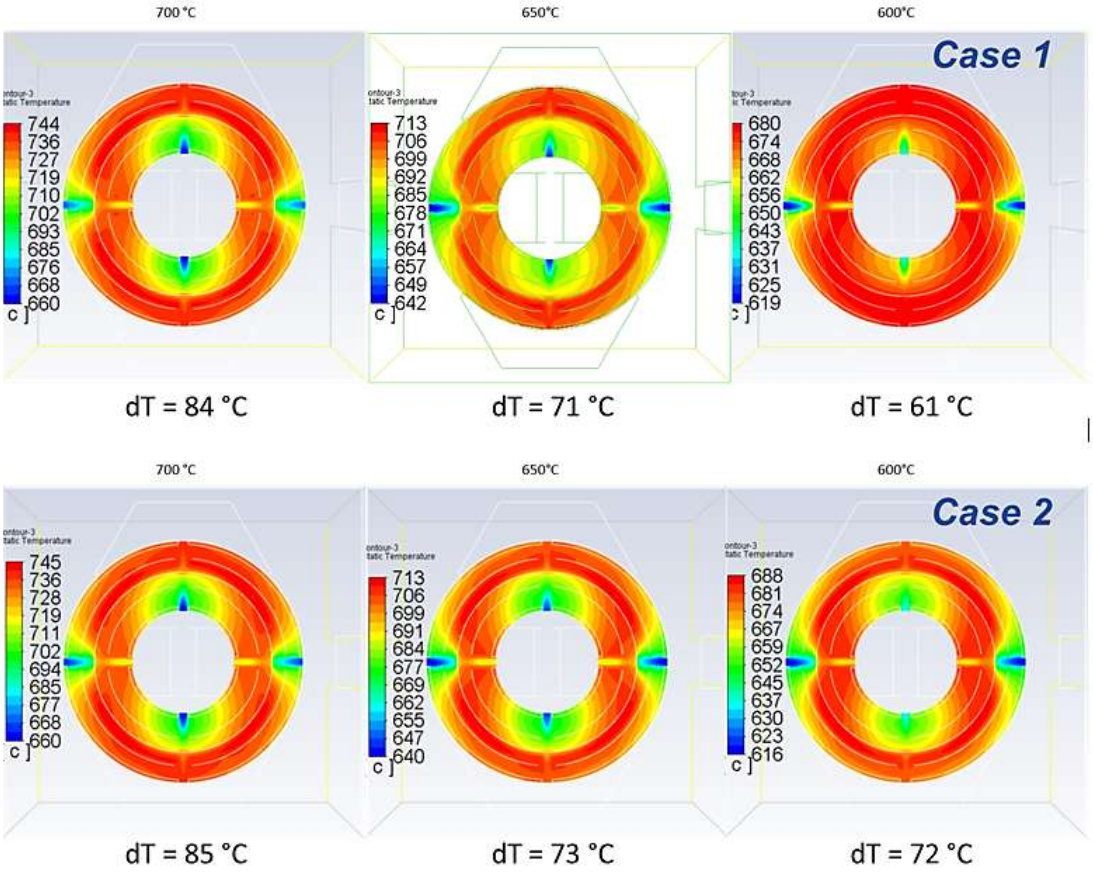

Figure 4.2-12 On-cell Temperature Profiles for Case 1 and 2 only.

CSA 6-stack Module Modeling

A 6-stack module utilizing a tightly packed 2 x 3 array was modeled using CFD software. With each stack having approximately a 7 kWe output, a 6-stack array met the 40 kW project requirement. The 6-stack module pack design leads to a mesh size of 2.1 M. Sample images of the CFD model bodies, as well as isometric and cross-sectional temperatures plots are shown in Figure 4.2-13.

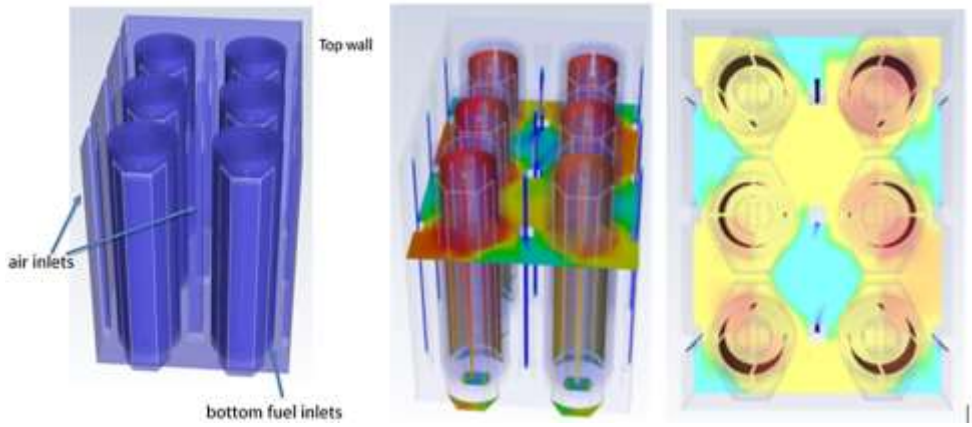

Figure 4.2-13 Rectangular 6-Stack Module, Sample Thermal and Flow Speed Profiles

As shown, the 6-stack module has 6 individual stack models arranged in array. As for operating condition change, air utilization was decreased from 40% to 20% to assist with thermal control. A more realistic detailed insulation design was added with sides and top comprised of six inches; with eight inches along the bottom to accommodate hot plumbing passing through that region. Outsides walls of the vessel were setup as the condition of convection plus radiation to ambient T_{room} = 25°C. The initial results of module thermal performance are illustrated as various module thermal profiles of module cold face, module hot face as well as a full cross-section through stacks, insulation layers, and outside wall are as shown in Figure 4.2-14 and Figure 4.2-15. For this initial modeled condition, the total module heat loss to environment has been calculated to be 416 W. This matches closely with prior hand calculations and results in roughly 1% of the rated DC power. For comparison, system simulations of both the 100kW SOFC module and an application under consideration for the FCE molten carbonate product have budgeted for up to 2.5% of rated DC power as being acceptable to hit plant electrical efficiency targets. Hence, a module design with a reduction of a few inches of insulation through each of the walls is being considered to help reduce cost and packaging.

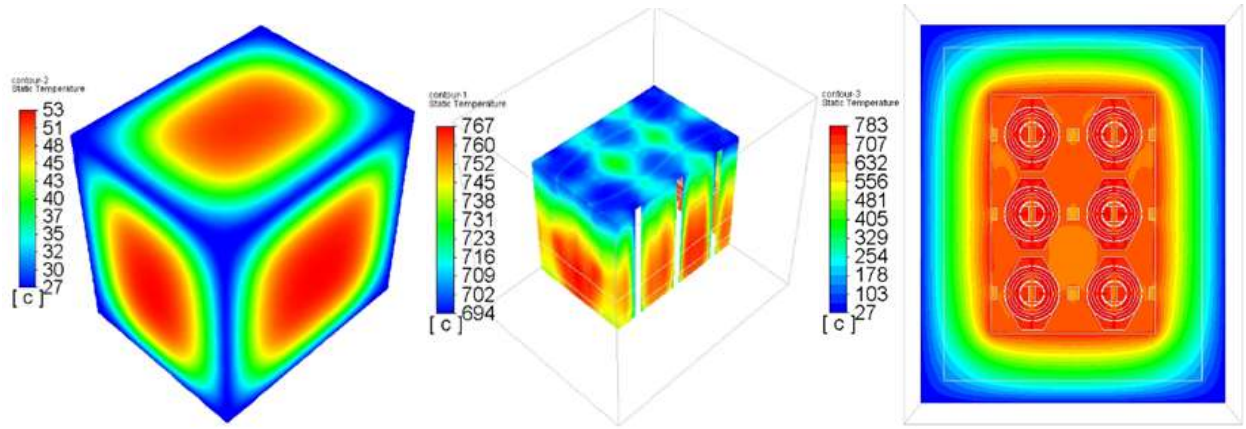

Figure 4.2-14 6-stack rectangular module: Sample Thermal Profile, Initial Conditions

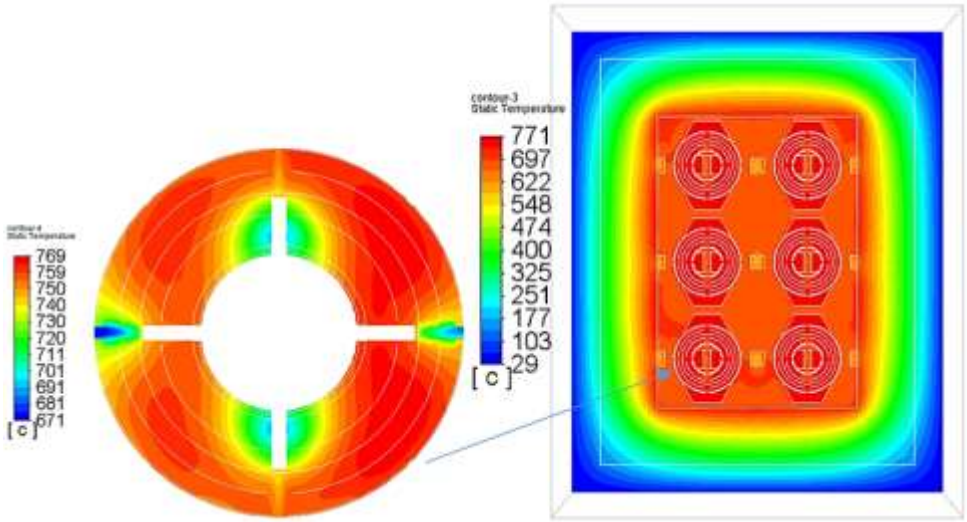

Figure 4.2-15 Bottom Left Stack Thermal profile in zoomed-in view.

Also, the temperature difference among the 6 stacks is currently less than 10°C (stack to stack).

CSA 40-stack Module – Extrapolation of Array Design

Earlier in 2019, work was also completed to prove that the simplified stack model could be implemented at a 40-stack module case (~280 kWe) as shown in Figure 4.2-16.

Figure 4.2-16 40-stack module with 280 kWe electrical power.

Sample results are as shown in Figure 4.2-17 through Figure 4.2-19.

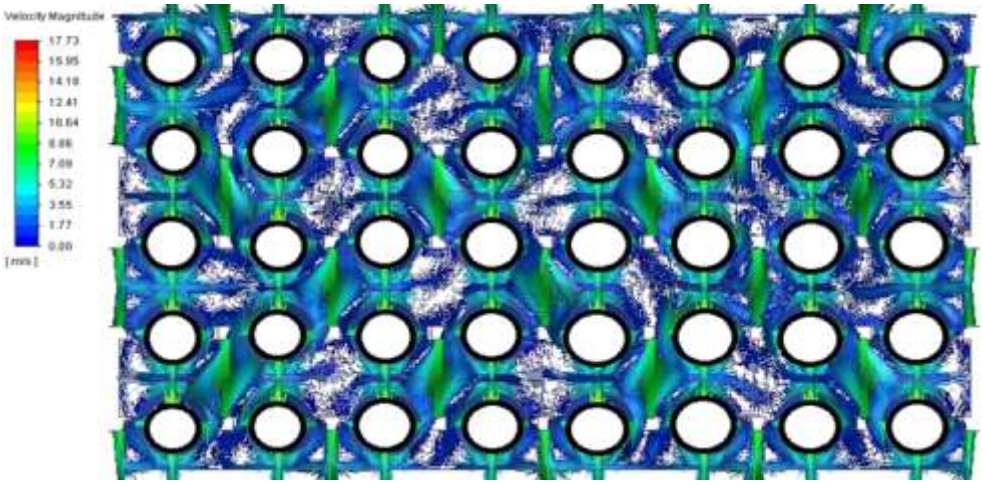

Figure 4.2-17 Air flow field inside the vessel.

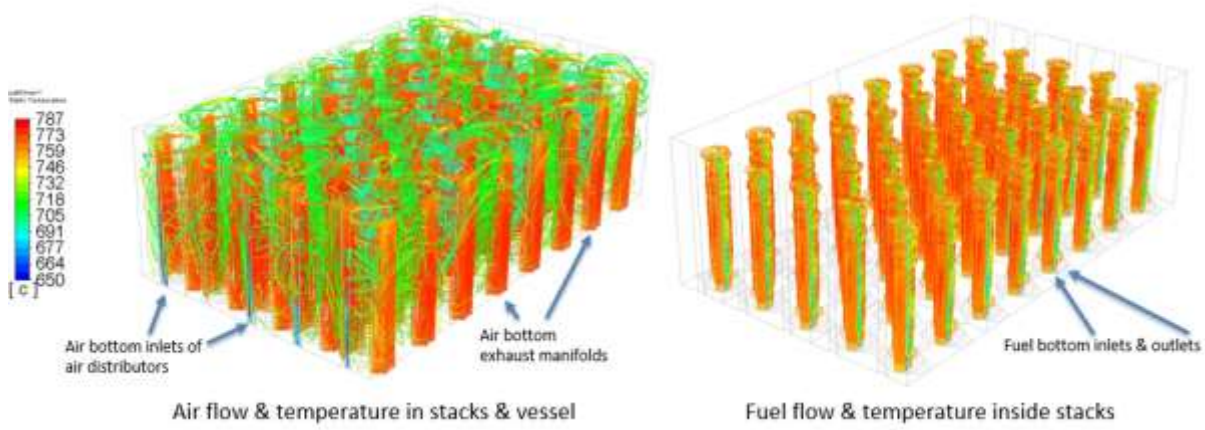

Figure 4.2-18 Air flow field, fuel flow field, and thermal field inside the vessel.

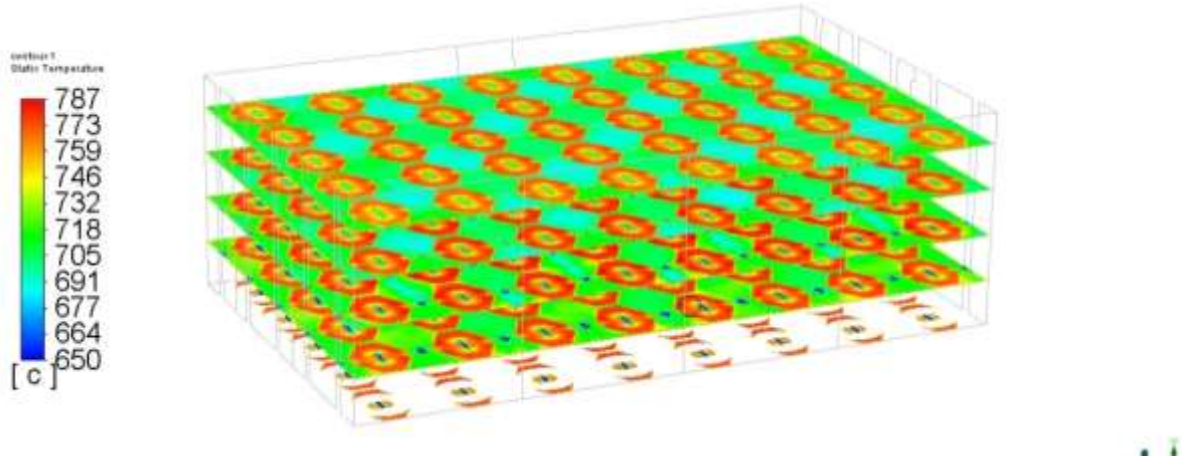

Figure 4.2-19 Temperature profiles in different layers.

These initial modeling results indicate that analysis of the rectangular multiple-stack module at ~280 kW level is achievable; thus, realizing the intent of the simplified stack model approach. In addition, it is believed that these results also showcase the scalability of an array-type structure utilizing the current CSA stack.

A 6-stack module utilizing a tightly packed 2 x 3 stack array with 24 RFR double shell tubes and 6 air distributors was modeled using CFD software. With each stack having approximately 7 kWe output, a 6-stack array met the 40 kW project requirement. CAD modeling of the solid and fluid bodies of this design requires a mesh size of 2.4 million elements to provide sufficiently accurate performance results for various design aspects. Sample images of the details of these CFD model bodies including 6 stacks, 6 air distributors, 24 fuel reformers, piping structure, and 4” insulation layer are shown below in Figure 4.2-20.

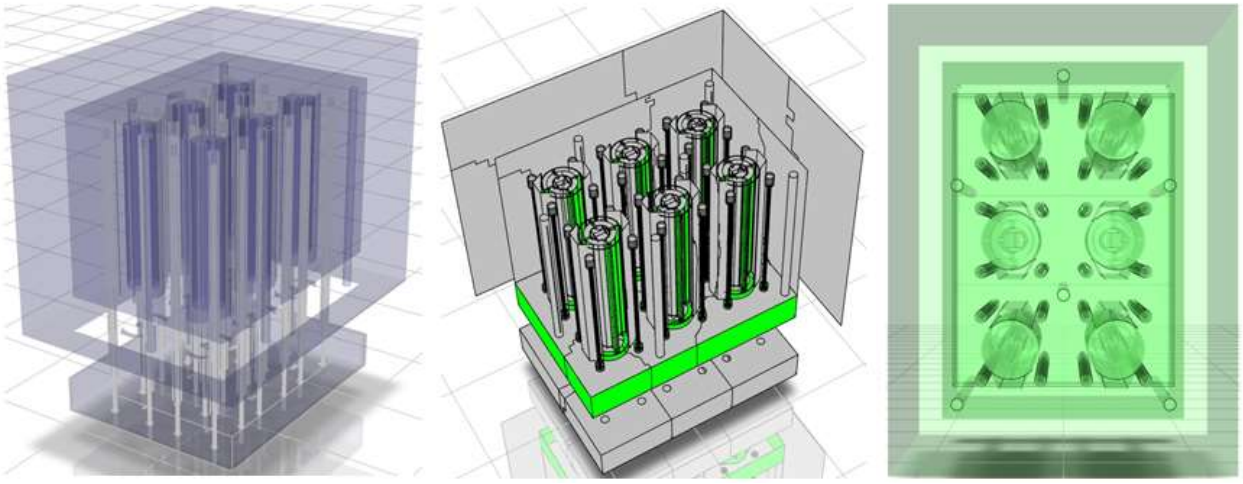

Figure 4.2-20 CFD Model Fluid and Solid Bodies for Pre-Process Meshing

Based on modeling results, four inches of insulation was added to this model to the sides, top and bottom (where the hot plumbing passes through underneath). Air utilization range of increased was expanded from 40% to 20% to assist with thermal control. Also, outside walls of the vessel were setup as the condition of convection plus radiation to ambient temperature of 25°C. Part of the process of in methodically setting up a CFD model for simulating the module, requires various quality checks at several steps of the process. Items such as the mesh element quality, CFD flow stream checkouts to ensure flow streams are separated (fuel vs air stream sides), and reviewing the thermal profiles, to ensure modes of heat transfer are correctly modelled, was part of this process (Figure 4.2-14). These quality checks have now been completed and shown to be acceptable. Some of these numerical testing results of module flow and thermal performance are illustrated as various module air flow, fuel flow and thermal profiles (Figure 4.2-15); with noted attention to the module cold face, module hot face as well as a full cross-section through stacks, insulation layers, and outside wall. The temperature difference between the stacks is currently showing less than 10°C difference as similar heights.

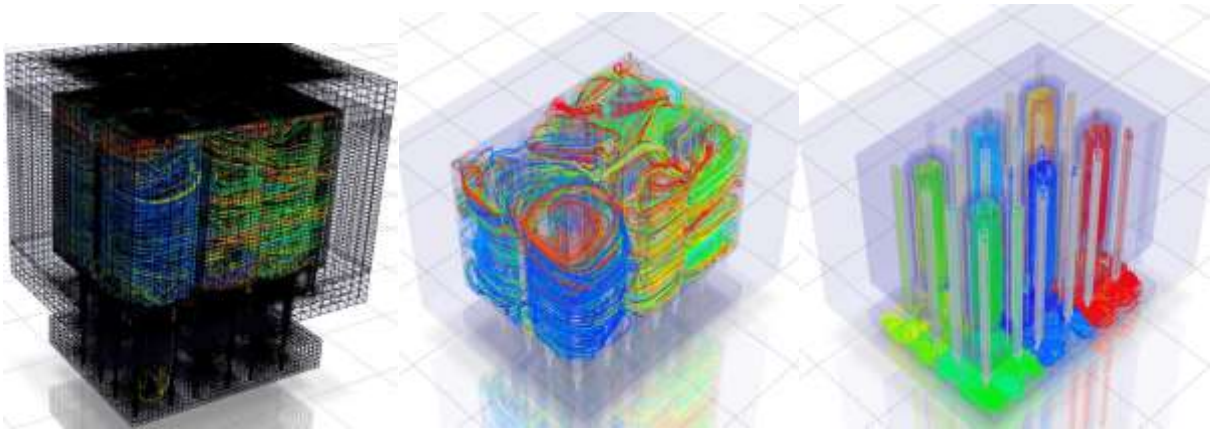

Flow fields with mesh Air flow field Stacks/RFR/Base mixing zone

Figure 4.2-21 6-stack rectangular module: Sample flow Profile, Initial Conditions

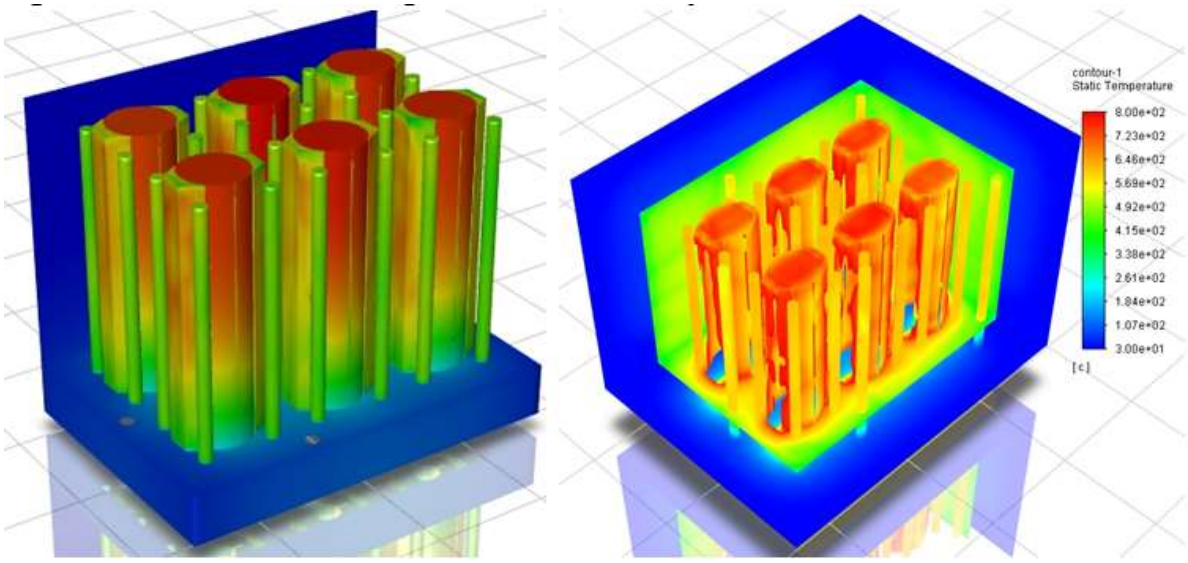

Figure 4.2-22 Stack, RFR, ADT Thermal Profile, Testing Conditions

A 3D model of the 6-stack module has previously been built and integrated into a CFD model for investigating the fluid flow distribution inside module, as well as the integrated thermal performance of the module. That CFD model utilized nine air distribution tubes (ADT's) with an adiabatic boundary condition applied to the wall of these tubes. The results showed reasonable air flow distribution (<1% mass flow rate variation) with the expectation that this could be improved further with a different tubing configuration. However, the results thus far provide an initial first pass for different configurations of ADT's. An additional CFD model using six ADTs was simulated, with adiabatic boundary condition applied to walls of these tubes, resulting in poorer stack-to-stack mass flow variation (~5%) than the nine ADT configuration. Results of this are shown in Figure 4.2-23 below where gas streams can be shown exiting from one or two sides of each ADT.

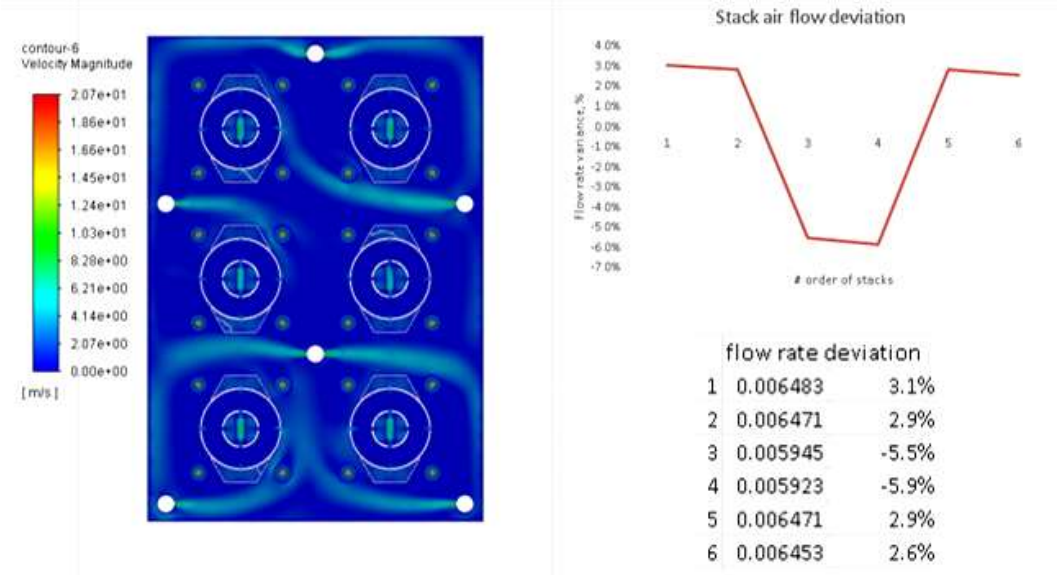

Figure 4.2-23 Air flow distribution of the 6-ADT design.

It was considered that an ideal approach would be to have air exiting from around the entire circumference and lengths of these tubes. To illustrate this, the CFD model was adjusted to allow air to exit in such manner by changing the ADT from a single opening slot, on one or two sides, to the entire tube being represented by a porous media body. Figure 4.2-24 shows the idea and the CFD modeled air flow distribution. CFD results showed that such an "all-direction" ADT tube design can provide an air flow rate variation less than 1%. The results showed thermal variation among the six stacks to be less than 6°C (Figure 4.2-25) when comparing same stack locations.

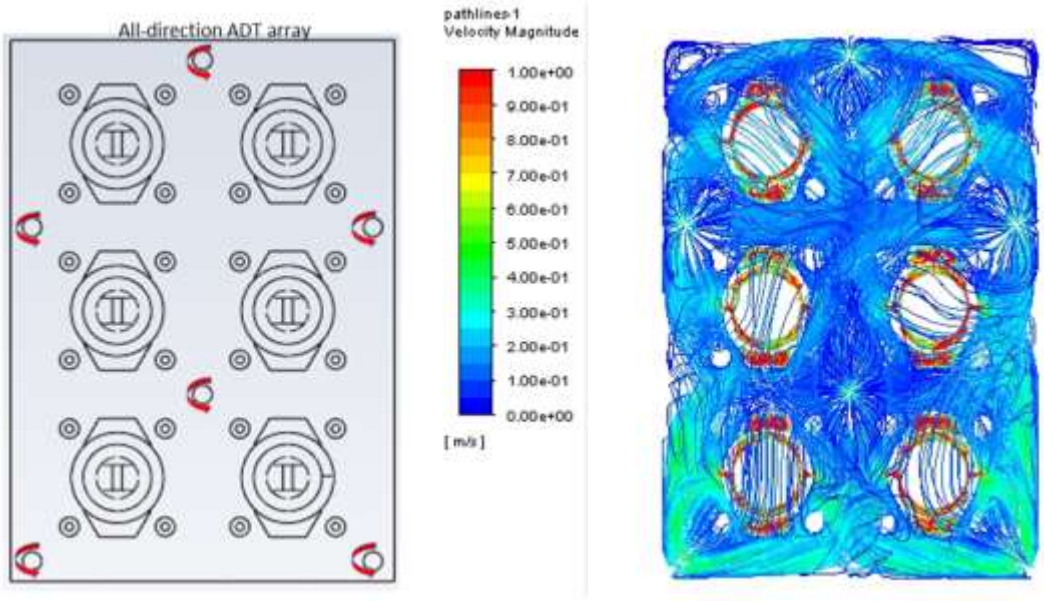

Figure 4.2-24 All-direction ADT Array Idea and Resulting Flow Path Lines

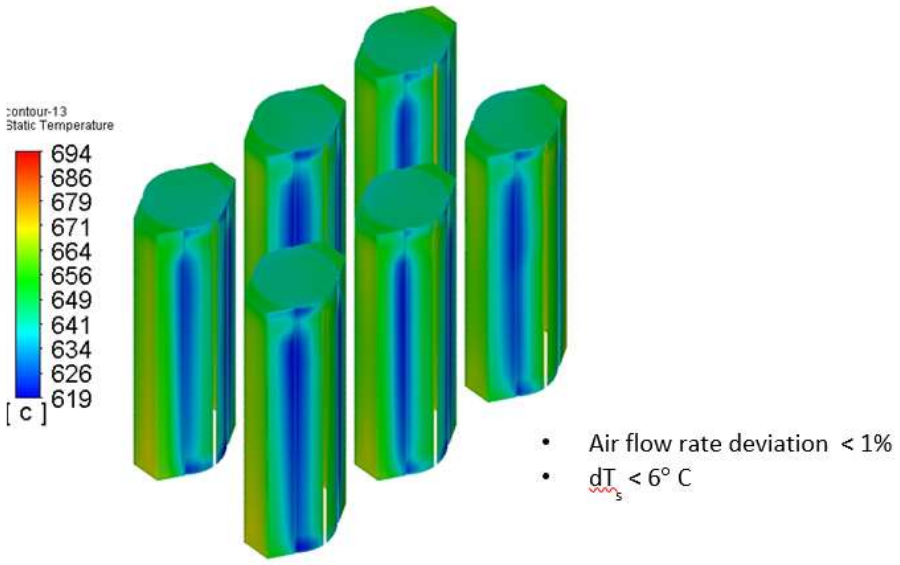

Figure 4.2-25 6-stack Temperature Profiles from "all-direction" ADT Array

A realistic tube configuration was then explored whereby the number of openings varied from two to four sides of tubes amongst twelve and six total ADT's (Figure 4.2-26). This moves the design in more preferred direction than the original concepts which only had one or two sides with openings and much fewer ADT's. The effect of this is illustrated from CFD results of the twelve

ADT version (Figure 4.2-27). Here, stack-to-stack mass flow variation of less than 0.5% is achieved.

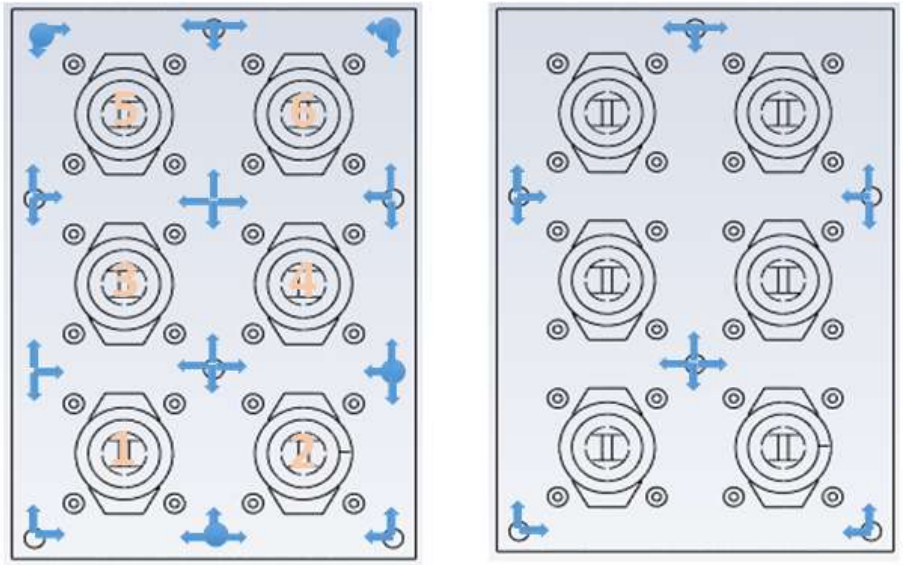

Figure 4.2-26 ADT's with Two, Three, and Four Sides of Flow: 12-ADT (L), 6-ADT (R)

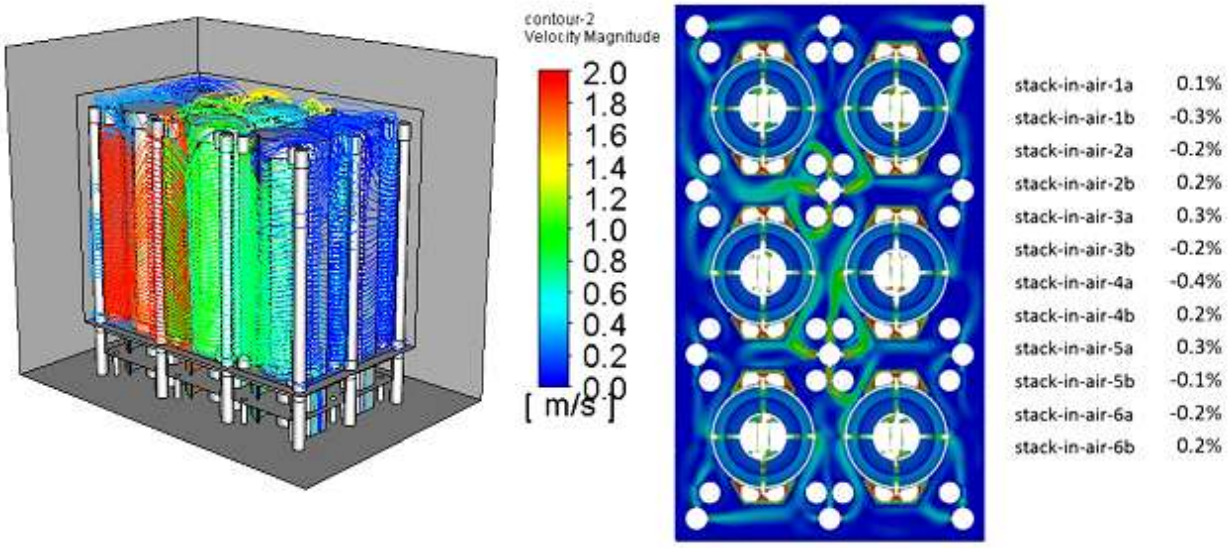

Figure 4.2-27 12-ADT (2-3-4 Direction): Stream Plot (L); Velocity Plot (C); Flow Variation (R)

Structural Analysis, Module Enclosure

One of the critical functions of a fuel cell module is to be able to handle an assortment of operational hazards. These hazards become identified during a hazard and operability study of any new fuel cell system design; the scope of which includes everything identified within the process and instrumentation diagram (P&ID) of that design. A standard range of component failures are identified which would result in abnormal conditions. Those conditions are usually some level of a variable such as flow, gas composition, pressure, voltage, current, and temperature. The consequences of such abnormal conditions are considered along with the

likelihood of such event occurring with the designed-in controls. It is then concluded whether the resultant risk requires a corrective action, typically an additional level of control, to lower the risk to an acceptable level. One particular hazard circumstance is typically, a challenge to reduce to acceptable risk levels with controls only, is component failure within the module enclosure that results in leaking of fuel gas. The hazard considered of such a leak is the accumulation of fuel gas within the module enclosure, surrounding the fuel cells stacks, to worst case stoichiometric fuel-to-oxidant ratio that results in a deflagration.

The containment of this deflagration by the module enclosure results in a rapid pressure rise that could cause a catastrophic breach of the enclosure risking human life. Example methods of control usually considered are as follows: devices like relief valves and rupture disks or a control loop utilizing a gas sensor that sends a signal to rapidly adjust the composition and flow rates of supply gases. Typically, these control measures are insufficient in lowering the risk; and a structural, or deflagration, analysis is required. Making the analysis more challenging is when it is required of a fuel enable operational case, where the gas temperatures are much cooler than normal operating conditions, resulting in a much higher pressure rise.

It was determined that such a risk remains with this 40kW SOFC module design and a deflagration analysis was completed. The magnitude of this pressure rise was determined by the adiabatic isochoric complete combustion calculation for a stoichiometric mix of hydrogen and air. To simplify the analysis, the upper enclosure was chosen to be analyzed separately from the lower enclosure in addition to taking advantage of quarter symmetry of the design (Figure 4.2-28) beginning with a model in CAD space.

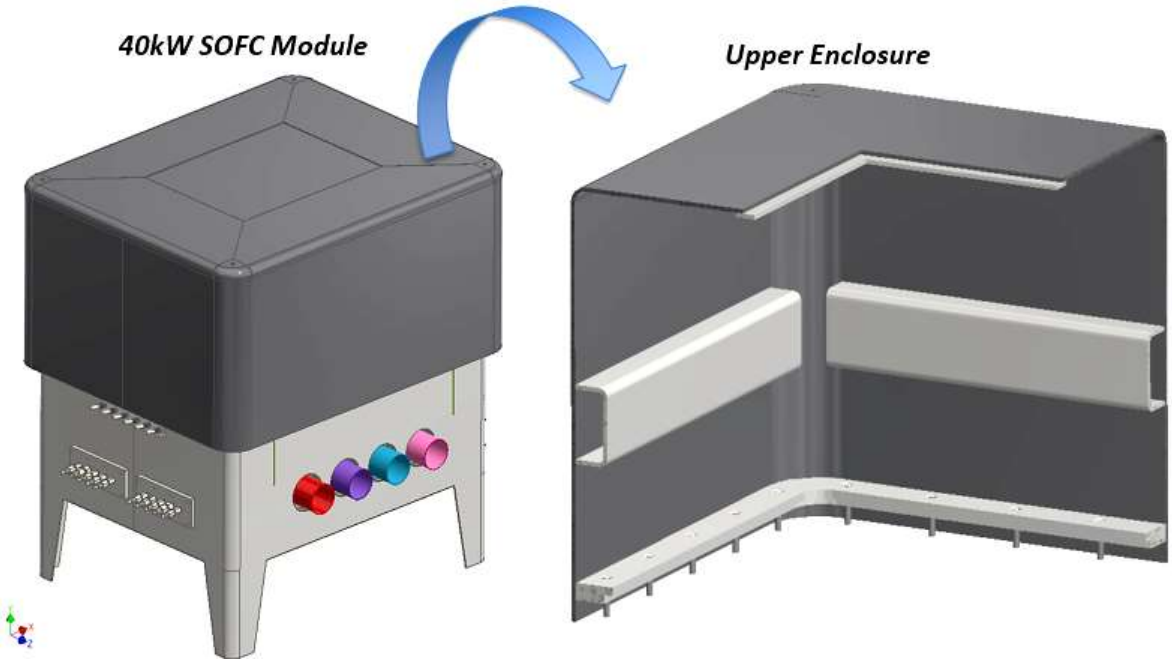

Figure 4.2-28 Quarter Symmetry CAD Model of Module Upper Enclosure

The CAD model was then discretized using the meshing functionality of finite element analysis (FEA) software (Figure 4.2-29). The meshed model utilized shell elements due to the small wall thickness to span ratio which greatly reduced the mesh size. Low carbon steel material was chosen strategically for cost savings (40% to 75% less than stainless steel per pound) as well as better weldability and less likely for welds to crack as compared to medium- and high carbon steels. This analysis was performed with guidance from the ASME boiler and pressure vessel

code where nonlinear effects are evaluated using material plasticity properties (true stress vs true strain curves) where resultant strains are the main focus. This is due to requirement of “no rupture” being acceptable as defined in Section VIII, Division 1 of the SME BPVC code. Since the likelihood of a deflagration event in the case of the SOFC module is very low, it’s considered an acceptable criterion as opposed to overdesigning using no yield criteria. Figure 4.2-29 illustrates how it is expected to observe a number of regions where plastic strain has occurred. Allowable membrane and peak strains were identified from the true stress-true strain curve of the material, as specified in Section III Appendix F, where 70% and 90% of ultimate true stress occur, respectively. The FEA simulation was run with an initial wall thickness and resultant strains were observed. Iteratively, the wall thickness was adjusted and simulation re-run until getting close to the strain requirement criteria, using standard industry wall thickness options. Figure 4.2-30 shows sample resultant peak and membrane strain plots with color scale reflecting the allowable strain criteria.

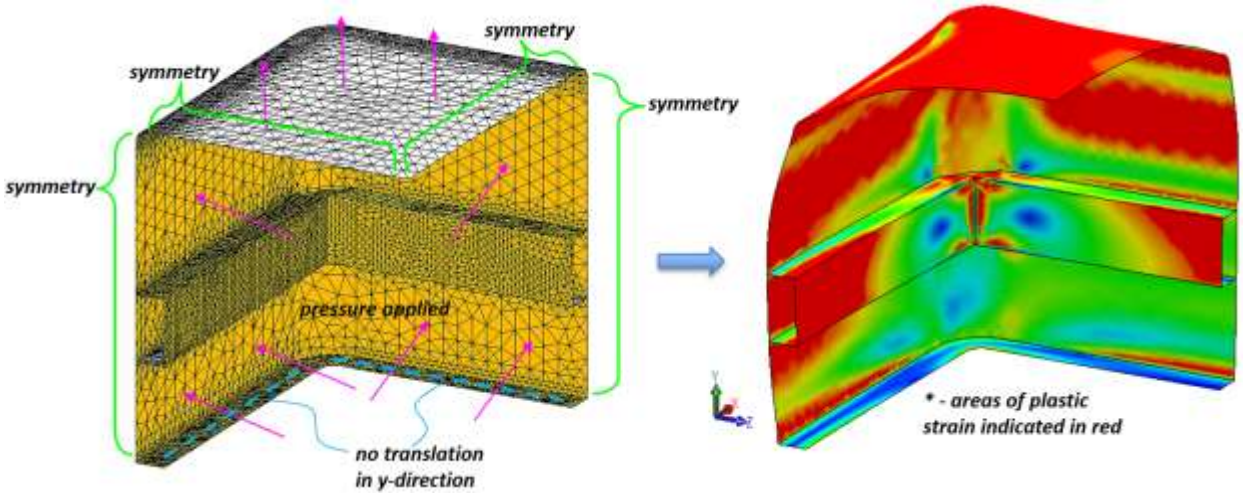

Figure 4.2-29 Meshed Model with Boundary Conditions (l), Resultant Plot of Plastic Strain

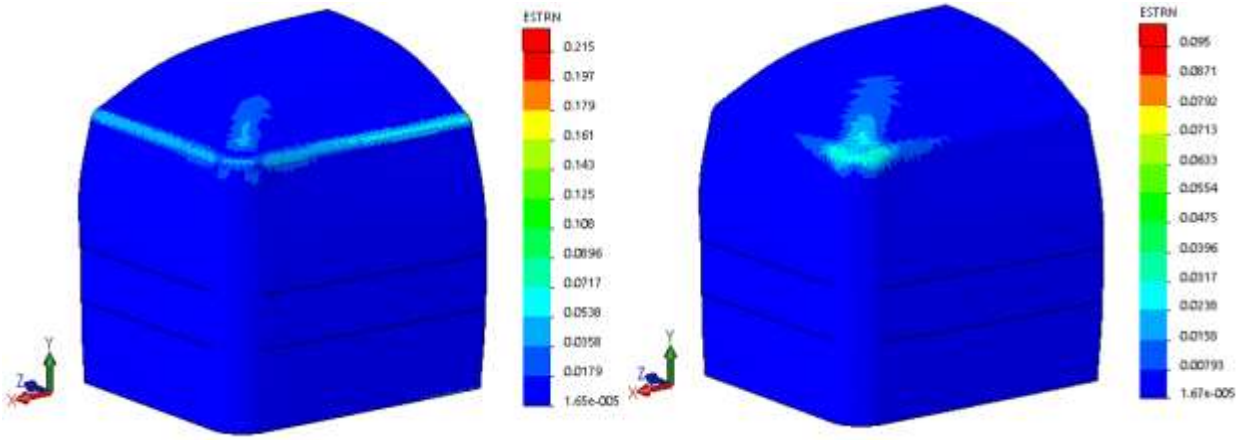

Figure 4.2-30 FEA Result Plots: Peak Strain (L), Membrane Strain (R)

It is of interest to note that it can be challenging to source low carbon steels in sheet form (< 1/8” thick) other than A36. Even with reinforcing members, it can also be challenging attempting to use A36 in these thinner forms without compromising manufacturability, heat losses, or ease of

assembly. For these reasons, some consideration was given to stainless steel options to see where cost tradeoffs are worth using a grade of this instead. As an example, using the assumption that the pressure rise results in a force spread over the hot-facing innermost insulation which then, distributed over the inside wall of enclosure shell, translates to a lower magnitude of pressure. A scenario like that can reduce the deflagration pressure by 60%, which can reduce the enclosure shell thickness by more than 50%.

Design analysis activities focused on computational fluid dynamic (CFD) studies of Stack Mount Brazement. As an initial CFD study focus of interest, the junction tube connecting the lower- to mid-level sets of tubing needed to be evaluated for pressure drop. There is a pressure drop requirement of the cathode gas stream through the entire 40kW SOFC Module that needs to be budgeted for in order to reach plant operating efficiency targets. Cathode pressure drop directly effects the amount of power required to run the plant system air blower. This adds to the parasitic losses that drive down plant operating efficiency. A decent first sizing of the baseline design arrangement of the Stack Mount Brazement resulted in a 1 ½ inch diameter short tube junction, connecting the lower- and mid-level tubing (Figure 4.2-31). Results of follow-on hand calculations had shown there to be a potential risk to meeting this pressure drop budget. Hence, a CFD study activity was initiated for a closer look.

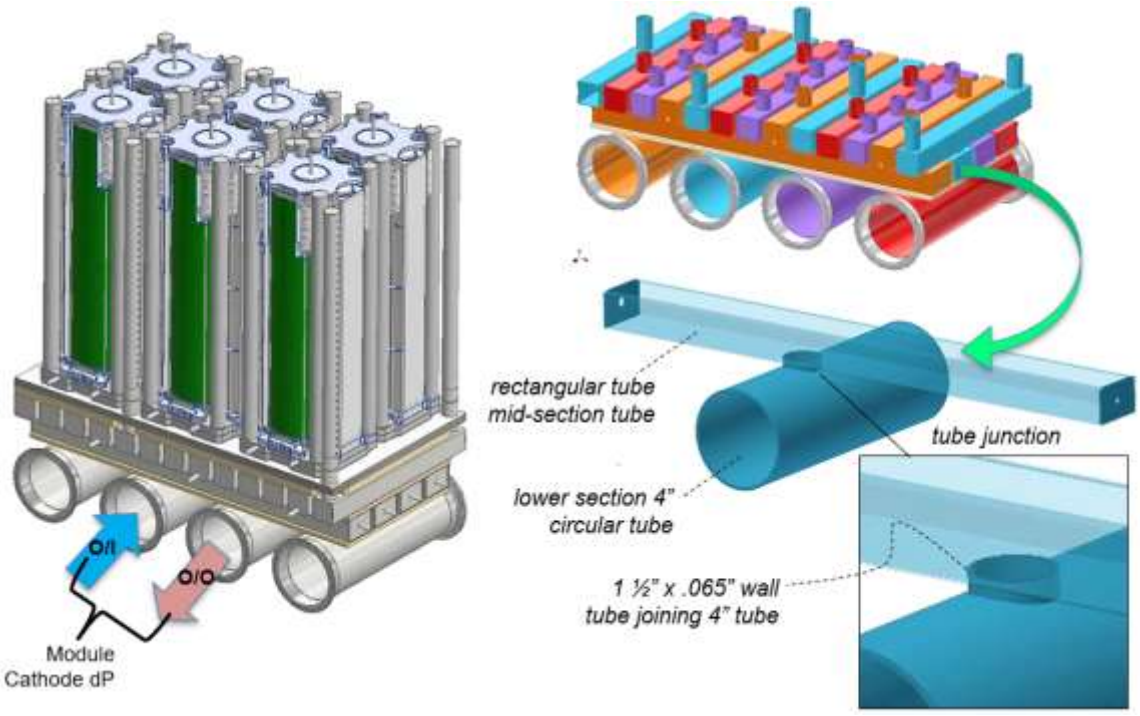

Figure 4.2-31 CFD Focus of Interest: Tube Junction from Lower- to Mid-Level

A fluid body model was constructed to represent the fluid stream passage from the lower- to mid-level rectangular tubes, meshed, and then imported into CFD-software for analysis. Results showed a pressure drop of 21 iwc through the 1 ½" junction tube connecting these two levels (Figure 4.2-32). This far exceeded the allotted cathode pressure drop budget. Some alternative design solutions were considered before pursuing a solution that took advantage of the stock of inventory 1 ½" tube already purchased. Here, the lower level of tubing was just large enough to allow for a total of two 1 ½" tubes. The CFD fluid bodies were updated to simulate this potential solution. The results showed only a pressure drop of 5 iwc (inches of water) through the two 1 ½" junction tubes (Figure 4.2-33). This was well below the total allotted cathode pressure drop

budget; enabling the potential for the entire fluid path circuit – including CSA stacks – to meet this budget.

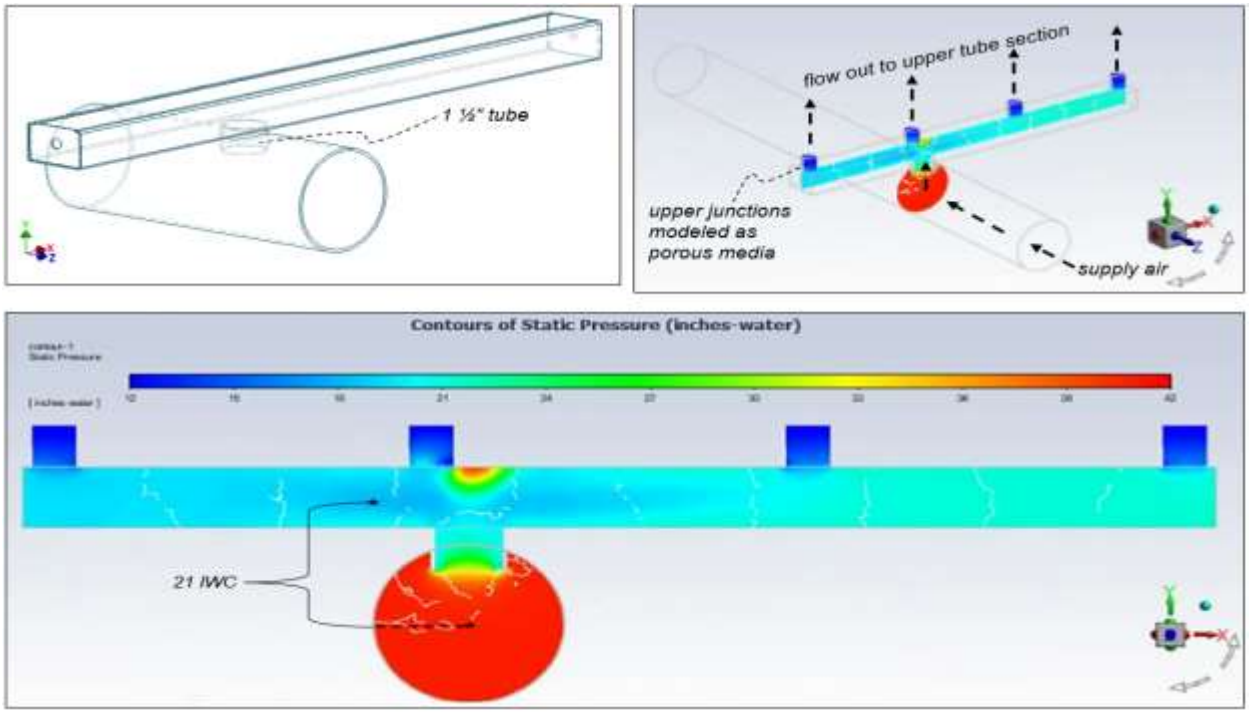

Figure 4.2-32 Junction Tube Initial Baseline CFD Results, Pressure Drop

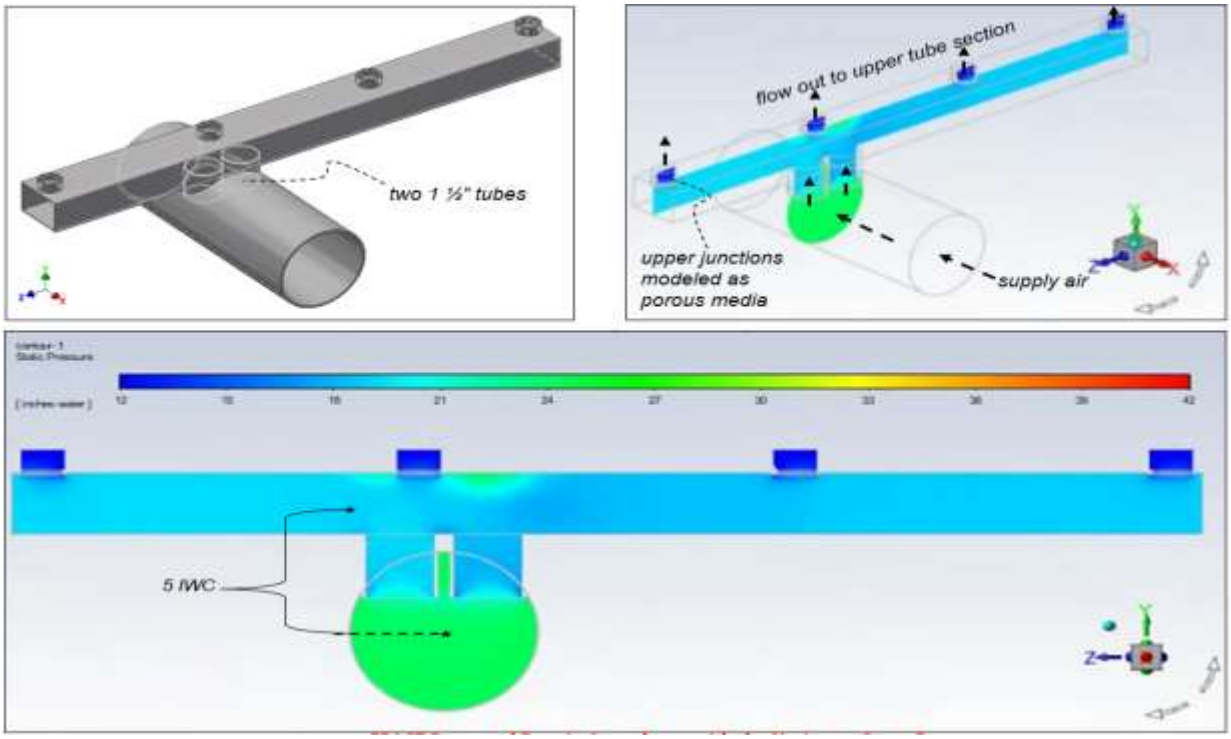

Figure 4.2-33 Junction Tube Revised CFD Results, Pressure Drop

An additional study focused on the anode fuel gas circuit. The anode fuel gas flow rates are significantly lower than the cathode oxidant flow rates so current sizing of the Stack Mount Brazement tubing cross-sections was expected to be sufficient to meet pressure drop requirements though flow distribution requires some level of down stream back pressure to achieve sufficient targets. An arrangement of 3D fluid bodies was assembled and meshed prior to import into CFD analysis software. Porous media controls were applied to mock fluid bodies in order to simulate the anticipated pressure drop across both the Stack Interface Plate and CSA stack (Figure 4.2-34). Operational fuel gas conditions (flow rate, temperature, composition) were applied, and results showed a very low pressure drop of ½ iwc; significantly below the allotted pressure budget. Results also showed less than 1% flow variation from average fuel gas flow between the six upper-level supply tubes connecting to the CSA Stacks and associated Interface Plates; close enough to enable some final optimization without significant changes.

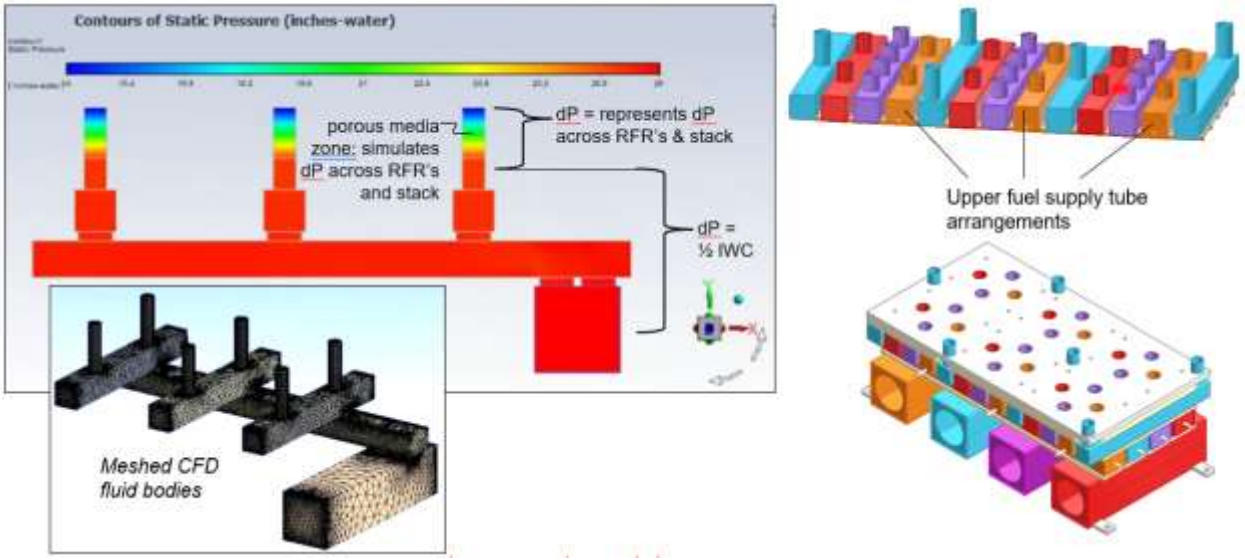

Figure 4.2-34 CFD Focus of Interest: Fuel Gas Flow Circuit

Design analysis and process simulation this quarter focused on computational fluid dynamic (CFD) studies of the cathode inlet flow in the Stack Mount Brazement. The analysis focused on improving flow distribution and minimizing pressure drop due to a need to increase flow rate to reflect CSA stack technology readiness. This analysis uses flow rates for 30% air utilization in the stack rather than the 40% air utilization used last quarter due to the maturity of the stack design. As shown in Figure 4.2-35, a simplified CFD model represents the lower and middle levels of tubing of the cathode inlet flow. This CFD study focused on iterating through several designs of the flow diverter plate to equalize the flow distribution to the upper-level tubing.

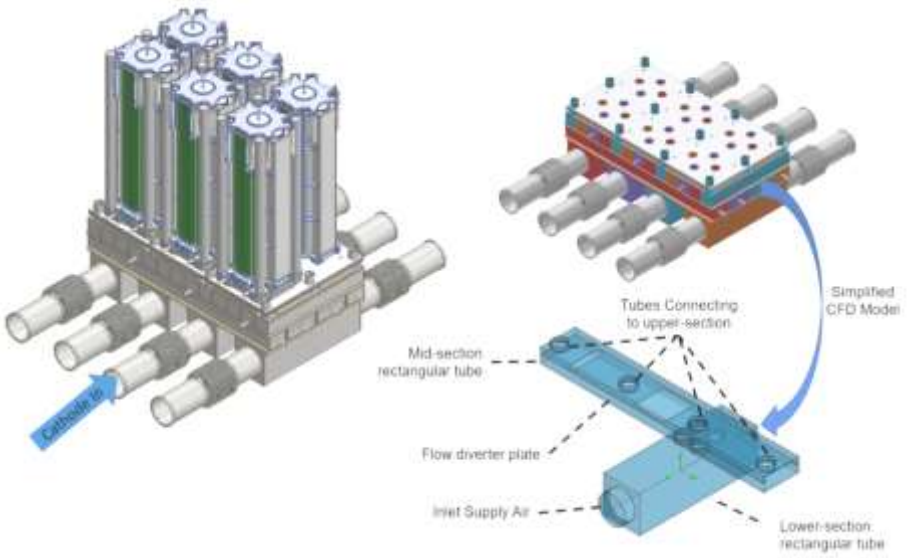

Figure 4.2-35 CFD Focus of Interest: Tube Junction from Lower- to Mid-Level

The simplified CFD model went through several iterations of modifying the flow diverter plate to achieve a mass flow rate variation from average of less than ±5%. To set up the model, the tubes connecting to the upper section induced a 7 IWC pressure drop to simulate down stream effects. Results from Figure 4.2-36 show a pressure drop of 6.4 IWC from the inlet supply air to the upper-level tubing and a mass flow rate variation from average of less than ±5%.

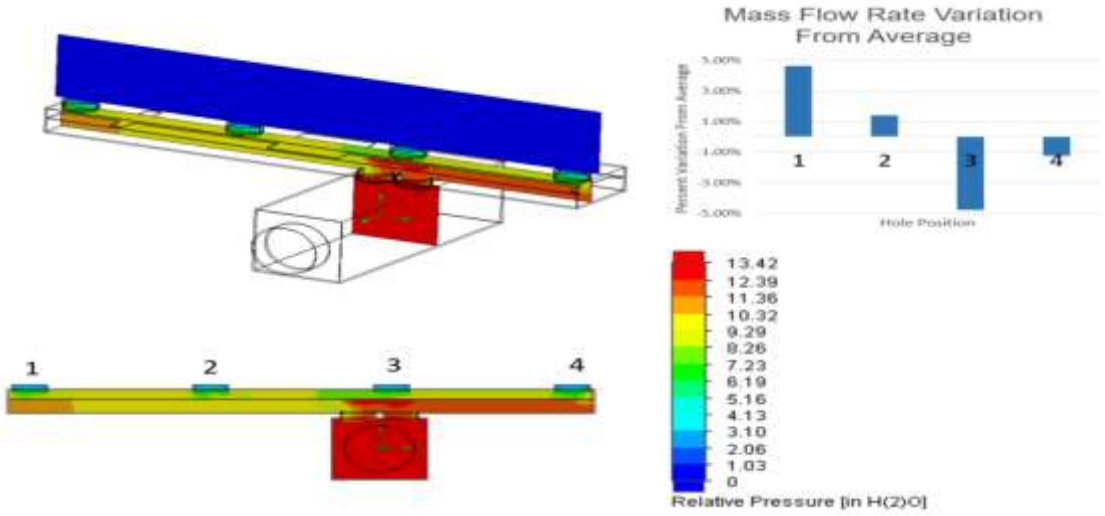

Figure 4.2-36 Junction Tube CFD Results: Pressure Drop, Mass Flow Rate Variation

An additional study focused on air distribution tubes (ADTs) further downstream. Several air supply tubes, shown in Figure 4.2-37, help even out the distribution of air inside of the module; both in vertical and lateral directions. This is to ensure each cell in a stack has an equal amount of supply air. Limited temperature variation is also important as that can affect the on-cell temperatures. The target requirements were as follows: vertical mass flow rate variation from average of <±10%; and the vertical temperature variation from average of <±10°C. These goals drove the need to analyze the air distribution tubes using CFD methods.

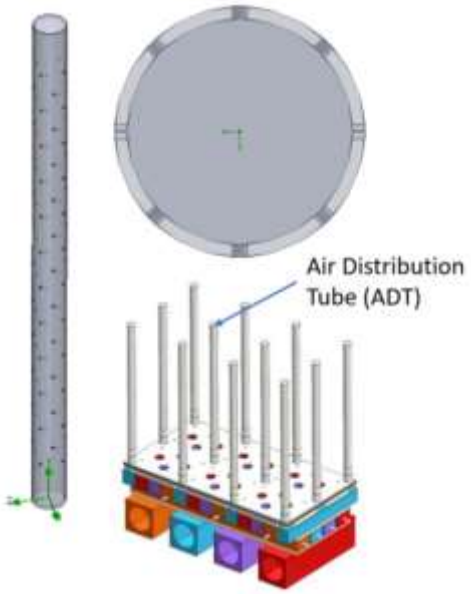

Figure 4.2-37 CFD Focus of Interest: Air Distribution Tube (ADT)

The ADT went through several iterations modifying the number and location of exit holes until finalizing on an 8-column hole arrangement as seen in Figure 4.2-38. Results show a maximum pressure drop of 4.2 IWC from the inlet of the ADT to exit holes. Figure 4.2-39 shows the mass flow rate variation from average and the exit temperature variation from average of the exit holes. Results show that a mass flow rate variation of <±5.7% and an exit temperature variation of <±3.2°C, which is much lower than initial goal of <±10% and <±10°C.

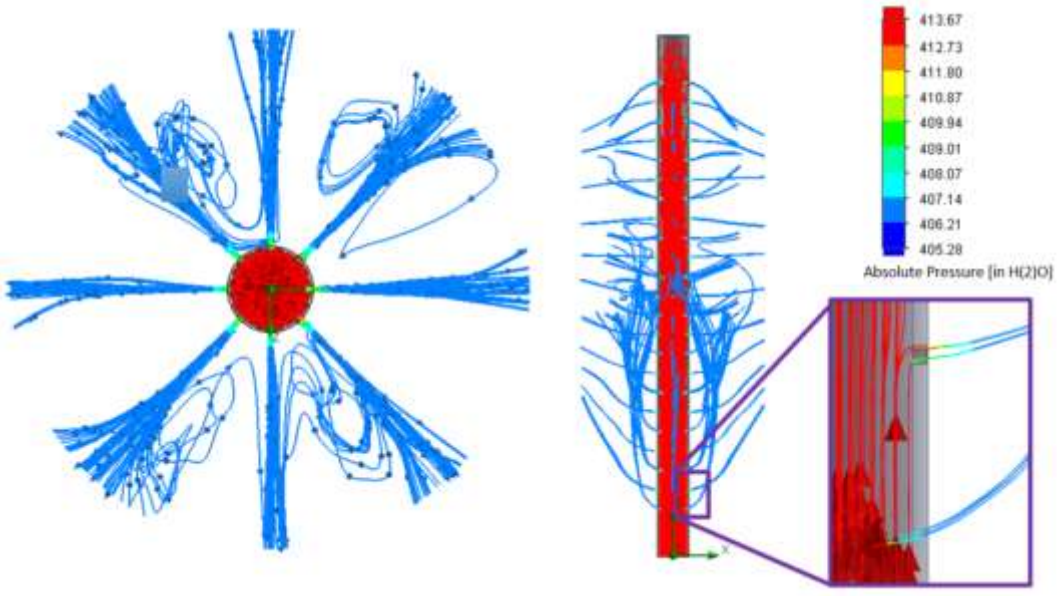

Figure 4.2-38 Air Distribution Tube, Pressure Drop

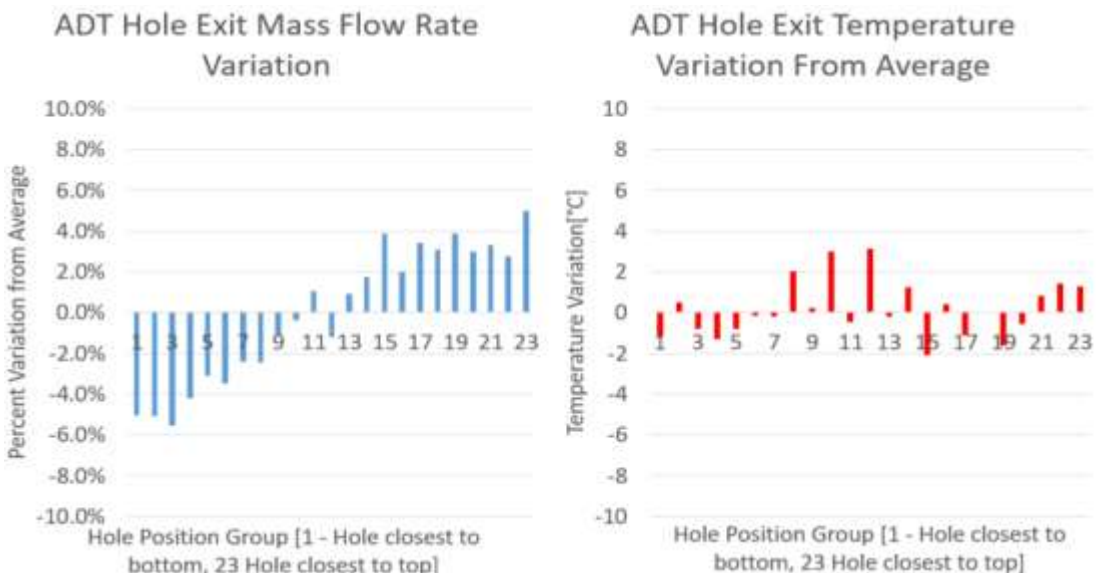

Figure 4.2-39 Air Distribution Tube, Mass Flow Rate and Exit Temperature Variations

4.3 Stack Module Controls

Approach:

This task focused on both the DC-power management and controls development, as well as instrumentation and sub-module controller development. Electronic hardware and associated control system were developed and demonstrated (Task 5.2) to show the capability of modulating power distribution between an array of stacks and a common DC bus. Development of the controller hardware, software, and instrumentation integration was completed to provide adequately granular data across the individual stack and module. Initial work focused on identifying attractive control hardware with capabilities in line with the desired system control operation and instrumentation capabilities. In parallel with hardware development, software architecture and testing utilize simulated module inputs for validation purposes. Finally, the control and instrumentation package was integrated and validated in the 40 kW module prototype (Tasks 5.1 and 5.2).

Results & Discussion:

Power management and controls development focused on researching technologies to extend the life of stacks and possible power conversion plant architectures that would work well with this technology. The fuel cell stack is, for all but the smallest applications, a device that operates with many cells electrically in series in order to build to higher voltage. All series connected cells must carry the same current and as a consequence, stack operation must cater to the weakest cell. While economic pressures have pushed fuel cell developers to maximize cell active area in the pursuit of lower costs, the CSA stack proposed in this project pursues miniaturization as a path to low cost. A key benefit of stacks built of lower active area cells and operated with multiple stacks electrically in parallel, is an ability to de-rate individual stacks. If any series electrical connection of cells were to be de-rated to protect the weakest cell, the larger the number of parallel branches of series connected cells (i.e. – stacks), the smaller the impact of this de-rate on the overall system.

CSA stacks offer the opportunity to de-rate individual 6 kW portions of the system and while the minimum power block prior FuelCell Energy SOFC systems could de-rate were 55 kW. The opportunity this represents is significant. For example, some stack testing has shown a near doubling of effective stack life if the power output is reduced by 20% to protect weak cells. As an example, de-rating one stack in twenty to 80% of rated load only reduces overall system output by 1%. If a 1% de-rate offers a doubling of system life that is a very attractive tradeoff. The goal is, therefore, to capitalize on this theoretical benefit offered by the CSA stack and its relatively low current (low active area) and high voltage, by developing and demonstrating a DC stack switching strategy that is both low cost and high efficiency.

The basic approach was to modulate the DC current from each stack through pulse width modulation (PWM) of the DC load. This is a standard approach to numerous marketplace DC power matching applications (from dimmable LEDs, to audio amplifiers, to power supplies, to battery charging, etc.). As a result, the controlling hardware is both available and low cost, especially for lower switching loads. Use of PWM is a digital strategy that operates by alternating between a full-on condition and a full-off condition as a way of producing some desirable intermediate condition. Dimmable LEDs are an instructive application of this where the intrinsic diodes mean an LED doesn't operate at 50% of the input voltage, but if it is operated 50% of the time at full voltage and 50% of the time off, then the light output is 50%. In this case, a PWM controller is offers functionality that would not otherwise be available.

Time constants and switching frequency are important aspects of PWM that need to be well understood for use in fuel cell power generation applications. As an example, if an LED is switched slowly from on to off it is a blinking LED; not a uniform light source at 50% brightness. Switching frequencies must be high enough to match the physical requirements. The same is true of fuel cell stacks which have three physical time constants of relevance:

1. Thermal: The time it takes for temperatures to change in response to a load change, a function of mass and heat capacity of the component. On the order of seconds to minutes.
2. Flow: The time it takes for flow through the cell to bring new reactants to the active sites in support of electrochemistry. A function of the flow conditions and the physical dimensions of the flow passages. On the order of 1/10 of a second.
3. Electrical: The time it takes for any intrinsic energy storage in the device (e.g.: stray capacitance or inductance) to dissipate. i.e.: At switching frequencies high enough, the cell doesn't "see" the switching at all. On the order of frequencies above 10 kHz.

Any switching, therefore, must be faster than the time constant associated with flow in order to operate without compromising overall reactant utilization and without risking damage to the cell. This intrinsically also protects against imposed thermal cycling since it is faster than the thermal time constant. However, while there are benefits to switching faster than the flow time constant, there are also reasons to keep switching frequency low: 1) offering operational benefits in electrolysis operation; and 2) keeping any potential risks of noise to the switching controls of the inverter hardware. Many of the stack operational requirements are identical between the two modes (fuel cell and electrolysis). Strategically, FuelCell Energy would like to develop a single solution that addresses both needs. i.e.: Solutions are sought that operate at a high enough frequency that flow related impacts are avoided, but not necessarily higher.

An example of use of PWM in electrolysis mode is shown in Figure 4.3-1 below. This was from preliminary work (IR&D funded) looking at the effect of switching frequency on electrolysis operation. From left to right are 10Hz, 63 Hz, and 125 Hz switching frequencies, all at 50% duty cycle. It can be seen that at 10 Hz there remains a strong increase in voltage (corresponding to poorer electrolysis performance) during the 'on' period. This is an indication of flow starvation.

The effect increased at lower frequencies. At 63 Hz (middle image) the voltage no longer increased with time, and the same at 125 Hz. While these results are specific to the single cell geometry (for example the flow passage depth has an impact on local flow velocities and volume of reactant adjacent to the cell), they give a first order indication of the lower limit in switching frequency. While 10 Hz is too low, 100 Hz might be a safe lower switching limit.

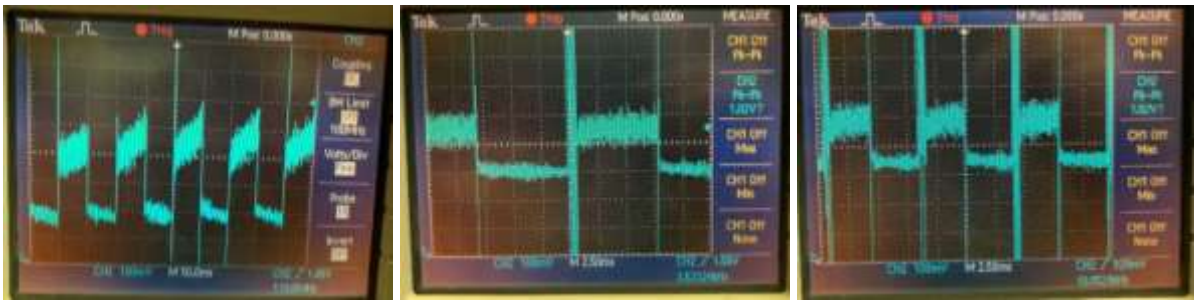

Figure 4.3-1 Electrolysis Single Cell Response, 50% steam utilization, 50% duty cycle, left-to-right 10 Hz, 63 Hz, 125 Hz

Two main electrical topologies are being considered:

1) A buck-boost topology as used in solar string inverters (Figure 4.3-2, left), with the advantage that much of the development work has already been done, and there are attractive efficiencies and costs available on the market now. The challenge here is to work with a string inverter company that would modify their operations away from MPPT and towards operation where string current can be externally commanded from the fuel cell control system.
2) A per-stack switching topology, without buck-boost (Figure 4.3-2, right), which has the advantages of closer stack integration and more granular control, the potential for lower cost, and more flexibility, but for which more in-house development is needed.

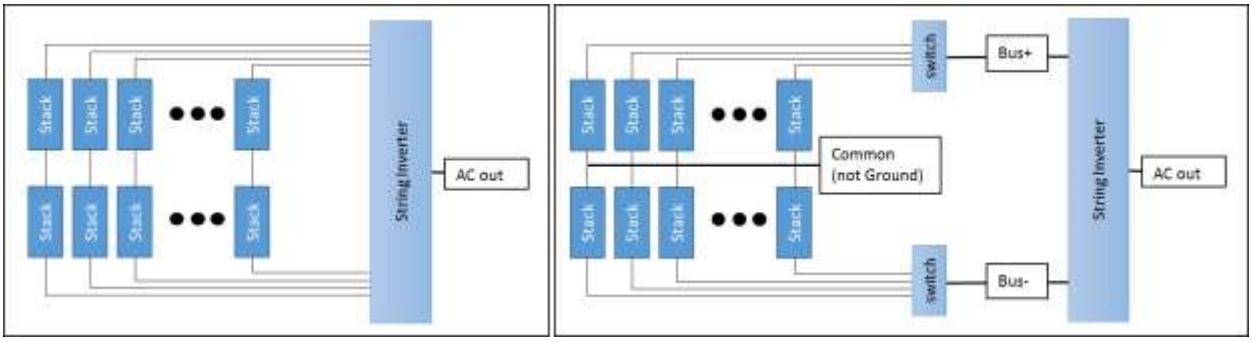

Figure 4.3-2 Power Management Topologies under Review

These two topologies were investigated further. While single-cell experiments were conducted in fuel cell mode with in-house designed hardware, assessments of power conversion options, and associated costs, were vetted through contacts established with industry leading hardware fabricators. From this, a more focused plan of development was realized for this project with strong consideration of use in MW-class power generation applications.

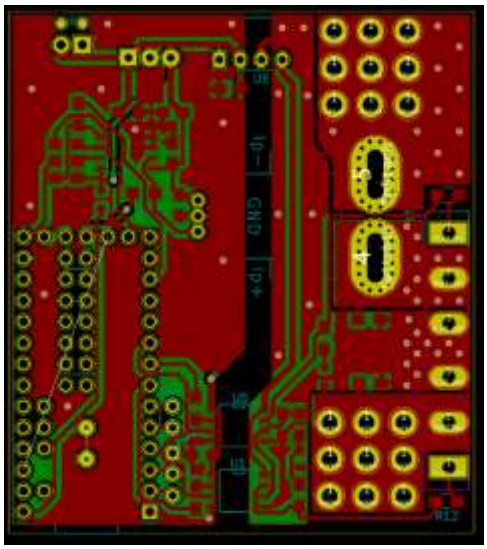

Figure 4.3-3 High side 100A stack switch with current sensing and local control.

Figure 4.3-3 shows a layout for an Ethernet and CAN bus enabled intelligent switch, rated at 100A peak and incorporating current feedback. The board measures 56 mm x 62 mm.

A switching model of a 20-stack electrical configuration was developed on LTSpice. Figure 4.3-4 shows the overall model with the stack array to the left, a capacitor smoothing bank in the middle, and the load (representing for example a module level inverter or inverter branch) to the right. As the number of active switches is increased the numerical stability of the model suffers. For this reason, active switches are only placed on four stacks in total, and generally only two are activated at any one time for simulation. This is sufficient to explore the behavior and especially the induced noise.

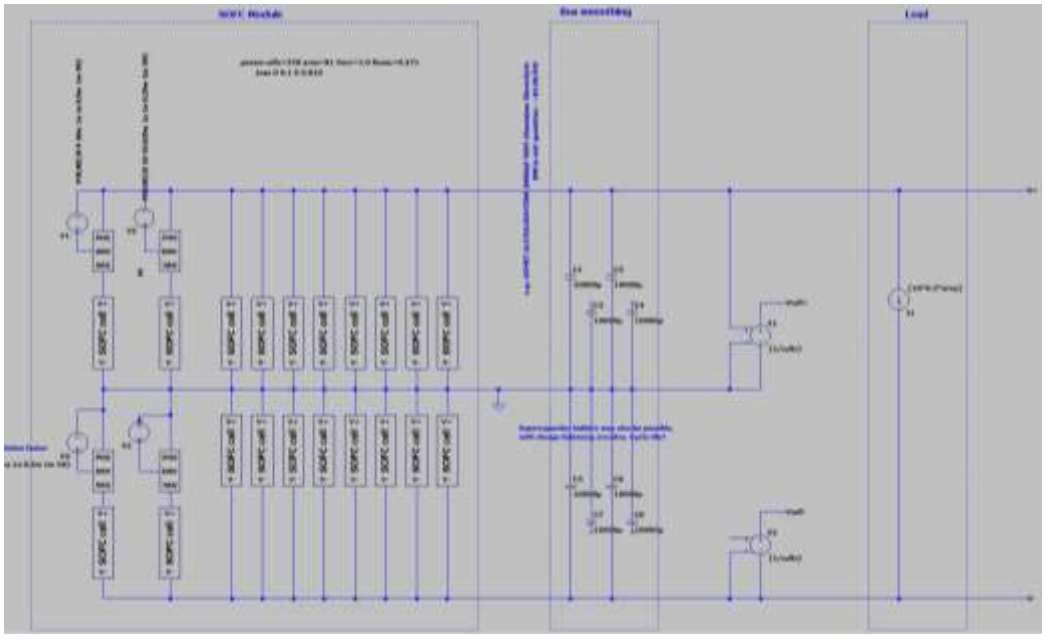

Figure 4.3-4 LTSpice model of 20-stack array, electrical switching and load.

Figure 4.3-5 shows the modelled bus voltage response to 1 kHz switching of one stack of 20 transitioning from 100% duty cycle to 50% duty cycle and back to 100% duty cycle after 60 ms. A 50% duty cycle is the most aggressive case in terms of imposed noise and isn't too extreme even with relatively little in the way of smoothing capacitor (less than $5 in capacitors per kW of system output).

Figure 4.3-6 shows the modelled bus voltage response when two stacks in parallel are switched from 100% to 50% then back. The stack switching occurs out of phase and as a result provides a smoother overall voltage response. As additional stacks are switched, careful selection of timing relative to the different duty cycles can be used to minimize the imposed voltage swings on the bus.

Figure 4.3-7 shows the modelled bus voltage if two stacks in series are switched (out of the 20) from 100% to 50% then back. The first stack switches back at 30 ms elapsed, and the second stack switches back at 60 ms elapsed, making obvious the smoothing benefit available when switching multiple stacks out of phase.

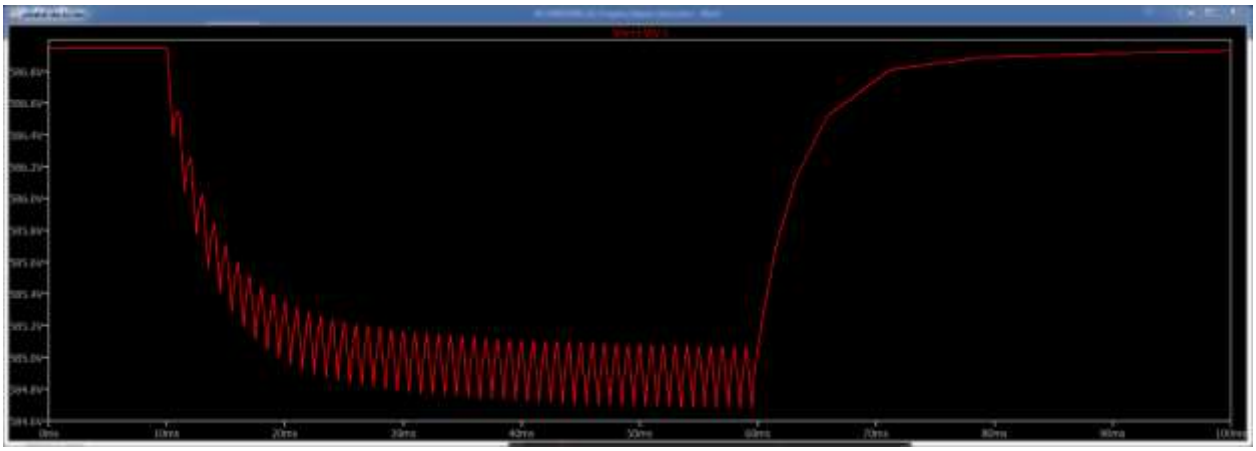

Figure 4.3-5 Bus voltage switching one stack to 50% duty cycle then back to 100%.

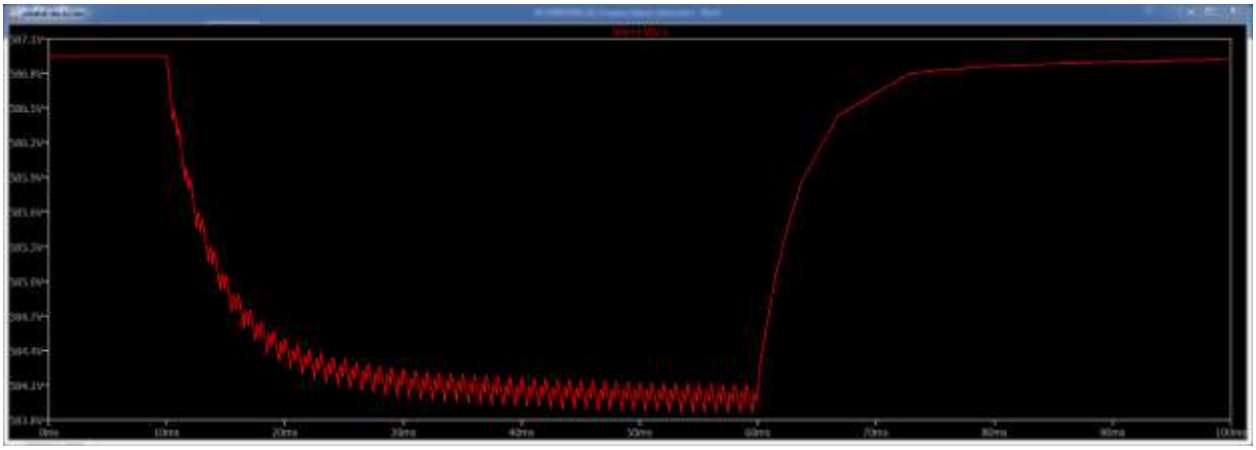

Figure 4.3-6 Bus voltage switching two stacks to 50% duty cycle then back to 100%, out of phase.

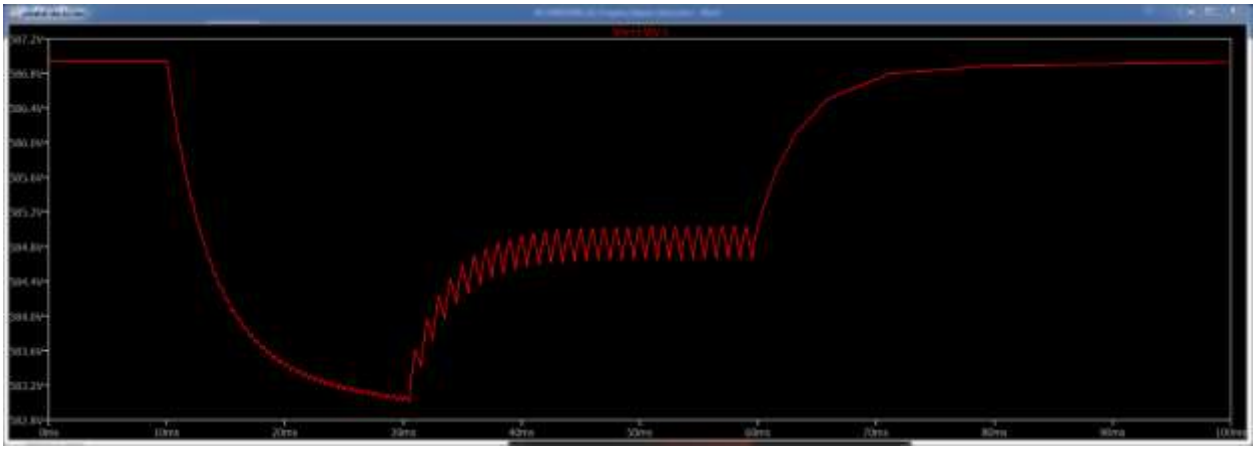

Figure 4.3-7 Bus voltage switching two stacks in series, but out of phase (10 to 30 ms), then only one stack (30 ms to 60 ms) then all stacks full on again.

If no filtering is applied, then the bus is of course much noisier. Figure 4.3-8 shows the bus voltage if only the intrinsic capacitance of the stacks is used, with no external filtering. The benefit of some external filtering is obvious.

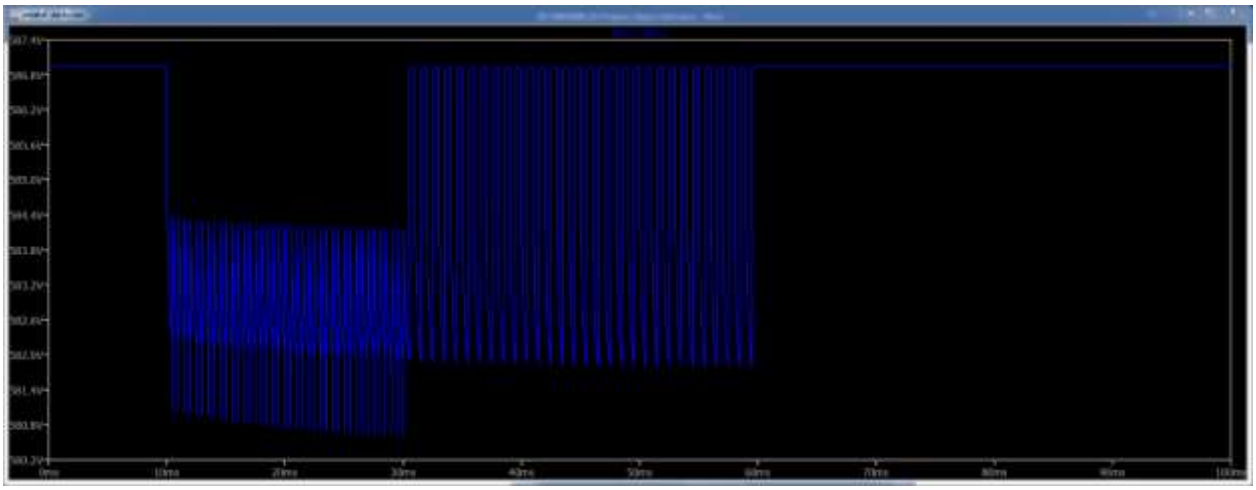

Figure 4.3-8 Bus voltage switching two stacks in series, with no external filtering.

While preliminary, this work sets a foundation for further development. The low-cost switch design is intended to be simple and low cost, for deployment and testing at the prototype level.

Next, an investigation was completed to see what commercially available hardware would be available that could provide this functionality; with some firmware modifications, if needed. Screening of available commercial inverter hardware showed there are several inverter options for the 40kW+ size range. But few of them were able to meet the entire array of capacity requirements (voltage, amperage, power) and ideally be transformer-less for a more compact BOP arrangement. Out of these, one particular vendor meets the needs but likely would require some modification to the firmware at a minimum. Strategically, for this “Next Generation SOFC” project, one of these would be procured to be installed and tested in the 40kWe module test facility to prove out the merits of use of such hardware. Whether a development arrangement can be

agreed upon with this vendor is something that is being flushed out during this next reporting quarter. An initial topology drawing specification has been created to communicate the hardware system needs in order to have productive vendor discussions (Figure 4.3-9).

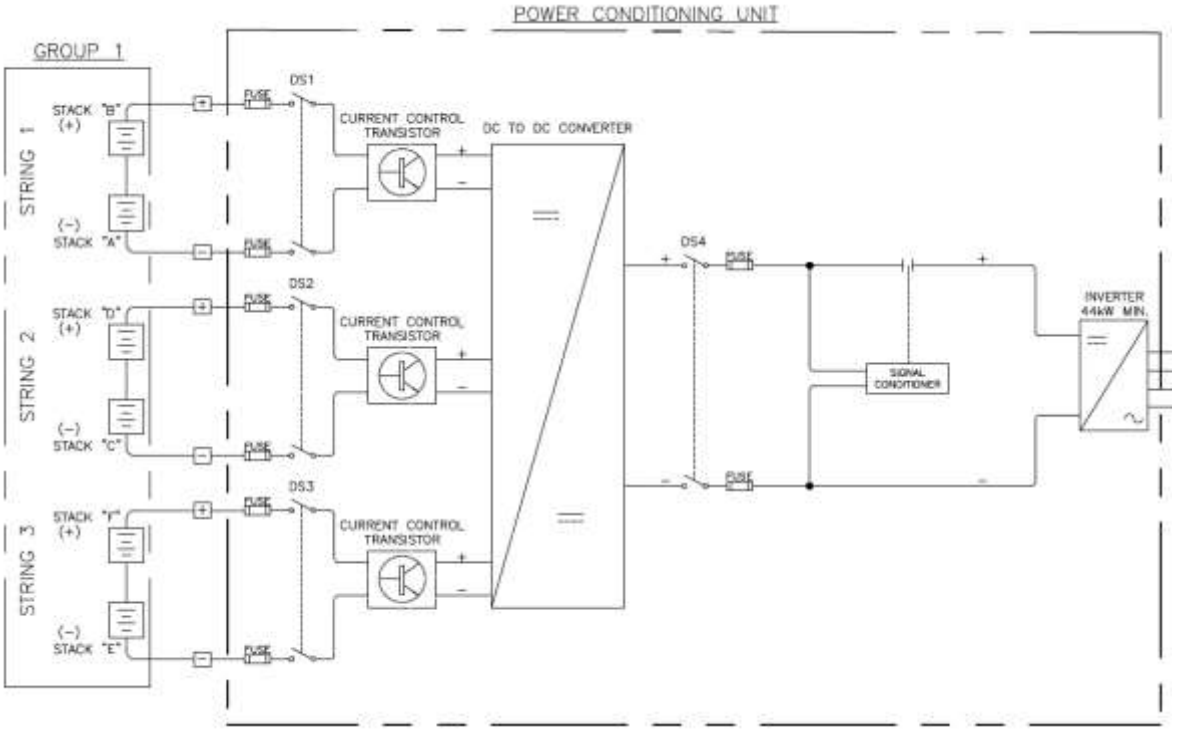

Figure 4.3-9 Current Control Hardware Topology for SOFC

More promising commercial hardware discussions have occurred with an external vendor that develops compact DC-to-DC conversion hardware with current control. Some of the benefits of this hardware are as follows: it provides isolation between the stacks and the inverter which leaves options for whether stacks are floating or grounded; it provides DC boost (or reduction) so the inverter can be transformer-less; and it opens up a wider range of inverters to be connected to. This vendor believes they can easily adapt the firmware of this hardware, typically used for maximum power point tracking of solar arrays, to provide the switching control of current being sought for SOFC load modulation. While it remains to be determined if such a system would be deployed in larger and commercial applications, an initial review suggests it could provide the desired controllability with minimal vendor effort and become a test bed for evaluation of the general approach. Quotes from the vendor have been provided for cost estimating activities and also using their in-house simulation software to completely verify the hardware is capable of performing this current control functionality.

Single Cell Validation Testing

Pulse-width modulation (PWM) control, time phasing of operating and non-operating time period, of a solid oxide stack in either electrolysis mode or fuel cell mode is expected to realize significant operational benefits for future solid oxide products. With the Compact Solid Oxide Architecture (CSA) stack, FCE expects to array and combine a number of these stacks into a high-power stack module to achieve 10's or 100's of kW. Traditionally, stack module lifetime and maintenance intervals are defined by the performance of one or two weakest stacks within the module. In

implementing low-cost stack current control, FCE seeks to have stack module lifetime now defined by the average stack degradation as opposed to these outliers.

At beginning of life, stack performance is very similar stack-to-stack, and all stacks are likely to provide a similar voltage at a requested current. However, because of small performance differences of individual stacks, or cell blocks, as well as imperfections in the thermal or flow elements in the stack module design, performance variations increase occur over time. Having PWM control and more specifically current control of all stacks within the module allows for new operational strategies such as:

- Requesting identical stack currents from each stack in the module, rather than having currents determined by stack impedances.
- Shifting current away from a problem stack or stacks to well performing stacks so that there is no reduction of overall power output.
- Advanced strategies such as utilizing the brief millisecond period at OCV and transient to assess individual stack health.

After an earlier SOEC test, an SOFC test was run in Q4 2019. The goal of this SOFC test was to assess if operating at fixed output or with PWM switching at the same net output caused any increase or decrease in degradation. In addition, at the start of run, different PWM frequency testing was performed to confirm cell voltage stability during the cycles. A pilot production type 10 cm x 10 cm cell was selected for the test with the test jig not having any special chromium layer protective coatings. Test equipment utilized is as shown in Figure 4.3-10, where a looped sequence program is utilized on the Kikisui load bank to carry out the PWM loading of the cell. A power supply is included in the circuit only to meet the minimum input voltage requirement of the load bank.

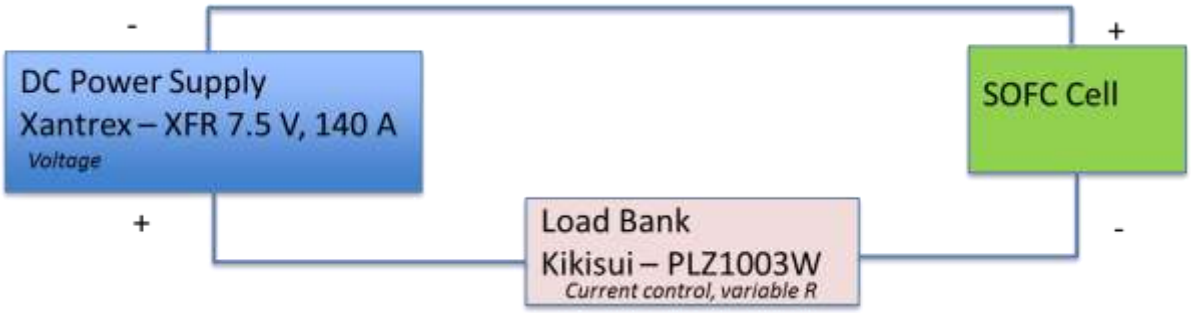

Figure 4.3-10 Test Circuit and Equipment for Pulse-Width Modulation Single Cell Testing

Test conditions were selected for single cell as shown in Figure 4.3-11 to firstly examine the effect of variable frequency on the testing. Frequencies from 250 Hz to <1 Hz were selected. Note and as shown in the figure, the fuel utilization in the “on period” is 104%, thus there is insufficient fuel to operate the fuel cell. Thus, with longer on periods, it is expected that the cell voltage is not sustainable. In contrast, with the faster switching, a blending and averaging occurs where the operating condition is more like pseudo- steady state.

	Flow Calculations					64.8 A	0.800	A/cm^2		
Uf =65% avg. (104% while on)	H2 flow	0.468	SLPM			40.5 A	0.500	A/cm^2		
Stack current = 64.8 A (40.5 A average)	N2 flow	0.468	SLPM							
48.5% H2, 48.5% N2, 3% H2O	Total flow	0.964	SLPM							
Frequency - Hz	250	125	62.5	40	20	10	8	5	1	0.8
Duty Cycle (%)	62.5%	62.5%	62.5%	62.5%	62.5%	62.5%	62.5%	62.5%	62.5%	62.5%
Full Cycle Time (msec)	4	8	16	25	50	100	125	200	1,000	1,250
Program A - on load Time (msec)	2.5	5.0	10.0	15.6	31.3	62.5	78.1	125.0	625.0	781.3
Program B - off load Time (msec)	1.5	3.0	6.0	9.4	18.8	37.5	46.9	75.0	375.0	468.8

Figure 4.3-11 Test Conditions for Pulse-Width Modulation Single Cell Testing

For the frequency testing, a mixture of results is shown in Figure 4.3-12 highlighting the main findings. A Tektronix TDS 2014 digital oscilloscope was utilized for the testing.

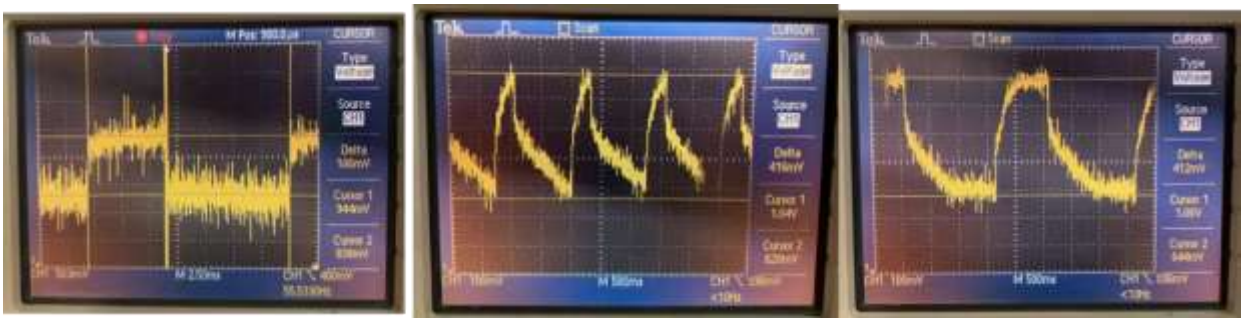

Figure 4.3-12 Oscilloscope Cell Voltage Results: 62.5 Hz (left), 0.8 Hz (middle), 0.4 Hz (right)

As was found with SOEC testing, at a higher frequency such as 62.5 Hz, the cell voltage is relatively constant at both the open circuit and electrically loaded condition. However, at low frequencies such as below ~10 Hz, the cell voltage is no longer stable and sees the impact of the instantaneous 104% fuel utilization condition. The y-axis measurements are shown for voltage, with 838 mV, 628 mV and 644 mV as in the figure above. Also interesting for the 0.4 Hz case, is that the cell voltage is stabilizing at ~0.64 mV in the loaded condition. It is theorized that the Ni – NiO equilibrium may be in fact helping to stable the voltage in this case with the nickel offering itself as reactant fuel to maintain voltage. This is what causes the relatively slow recovery of the open circuit voltage due to nickel redox once the current load is removed from the cell.

Focusing on the 62.5 Hz at 62.5% duty cycle (10 msec on @ 64.8 A (0.80 A/cm^2), and 6 msec @ OCV), a long-term single cell test was completed as shown in Figure 4.3-13. For the figure, only the non-PWM (steady state) portions of the test are illustrated. The PWM voltage measurements are quite noisy due to the frequency differences between the cyclic current demand (62.5 times per second) and the test stand logging rate (1 time per minute). For the continuous current demand sections of the degradation study, a degradation rate of ~0.7% or 6 mV / kh was measured. From this test, at least considering a macro perspective, it is suggested that the PWM loading of the cell did not have a negative impact on the cell degradation result.

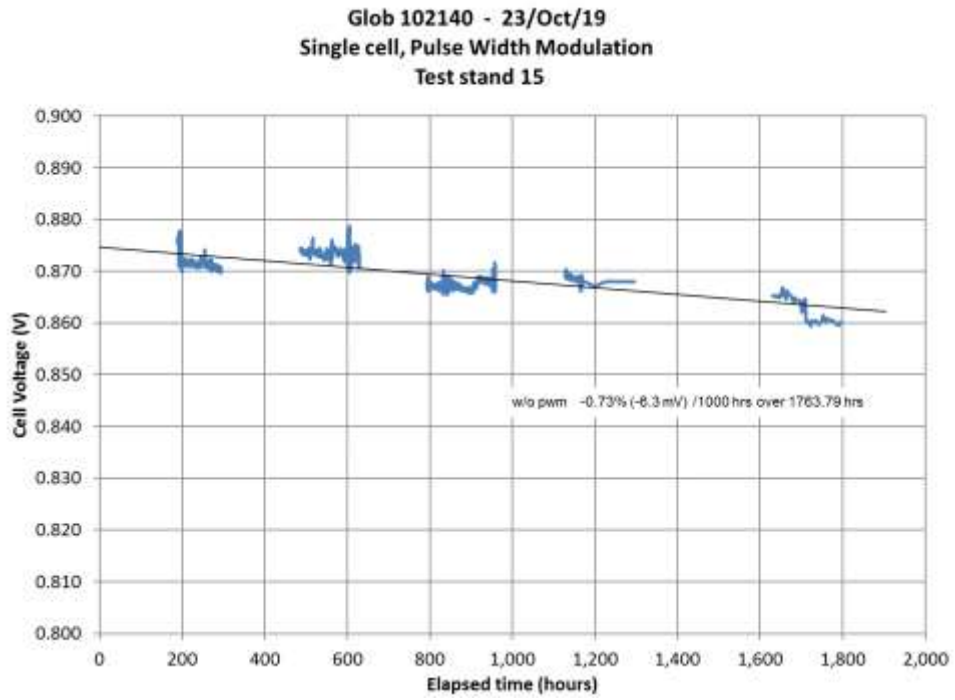

Figure 4.3-13 Single Cell Test: Alternating weeks of PWM (not shown) & No-PWM (shown)

Module Current Control

One avenue that was explored was a compact DC-to-DC optimizer that would provide isolation between the stacks and a downstream inverter while providing current control of individual or string of stacks. This particular piece of hardware would also allow the use of transformer-less inverters since it also provided DC boost (and buck). After a number of reviews of possible topologies, it was determined that the vendor could not provide a viable solution in light of changes required by this hardware. A second avenue that was explored was to identify a family of transformer-less inverters offered by a vendor with whom FCE has a good working relationship. The intent was that by further identifying specific models that would meet the current, voltage, and power requirements of the 40kW module, the changes required to the hardware would be limited to a firmware update. After a number of discussions with how this could be done with the vendor's hardware, it was determined by the vendor that the amount work to provide a solution would be too large of a scope for the anticipated volume. Thus, a third avenue has been chosen that meets the needs of demonstrating stack level current control. This approach is to procure three separate smaller inverters, each providing current control to a string of two stacks each of the six stack SOFC module.

A review of the FCE test facility by electrical contractors has determined that 208 VAC inverter hardware is the most practical approach to meeting the project budget and timelines and a 208 VAC inverter solution has been quoted and procured. A rough layout of the test facility being updated is shown in Figure 4.3-14 below. Since a next generation catalytic air preheater is being tested as part of this project (to provide data for integrated configurations), the current strategy is to procure the lower vessel base ahead of the upper vessel. This allows it to be used for both individual heat exchanger and full module tests. This is possible due to how compact this lower vessel is and how closely matched the upper vessel footprints are when comparing the rectangular array and circular array module concepts.

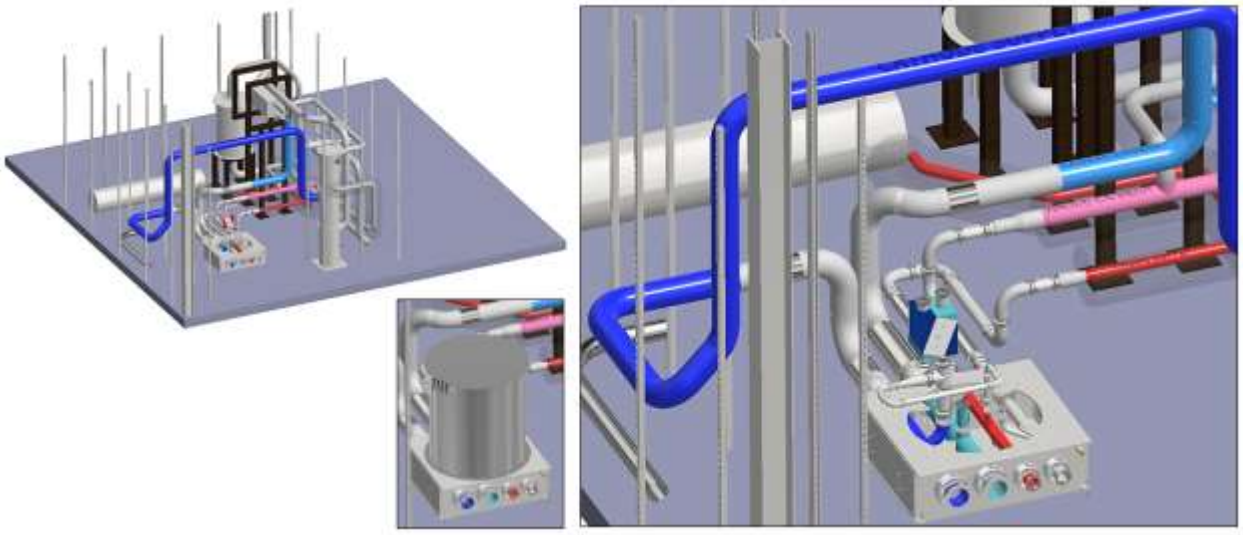

Figure 4.3-14 Early Stages of Test Facility Layout

The power system architecture needs to be designed in a way that allows control of the output current at each string (two stacks in series are called string) of the module. Figure 4.3-15 shows the power curve for single string, it serves as a basis to select hardware needed for output current control. This curve is derived by forecasting results for the string from the test on single cell. Design point in the figure represents the desired point of operation. There are two simultaneous approaches being pursued at this time to design this: 1) using DC-Load Banks; and 2) using inverters.

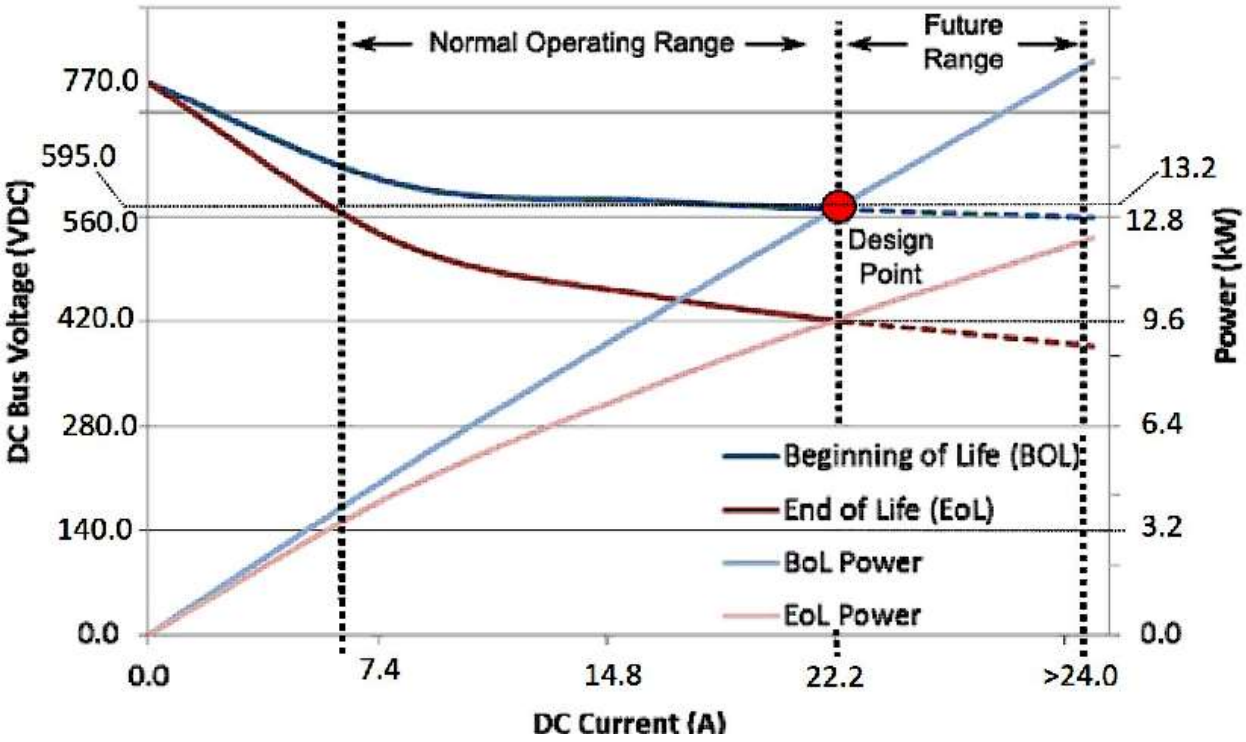

Figure 4.3-15 Power Curve for Single String

Figure 4.3-16 shows a one-line diagram to illustrate use of output current control using DC load banks. Here, each string of two stacks is connected to an individual DC load bank, via a DC disconnect. The load banks would require current control functionality. A DC load bank from Neptune has been identified with this capability (Figure 4.3-16), designed to operate at 600 volts DC and 24 amps, with 0.1 amp load step resolution controlled via MODBUS TCP. It also has a maximum open circuit voltage capability of up to 800 volts DC which is enough to handle the maximum possible open circuit voltage of 770 volts DC for two stacks in series. Three of these were procured along with a power supply. The power supply was used as a check out device to demonstrate proper functionality of use of these load banks using anticipated range of operational DC voltages.

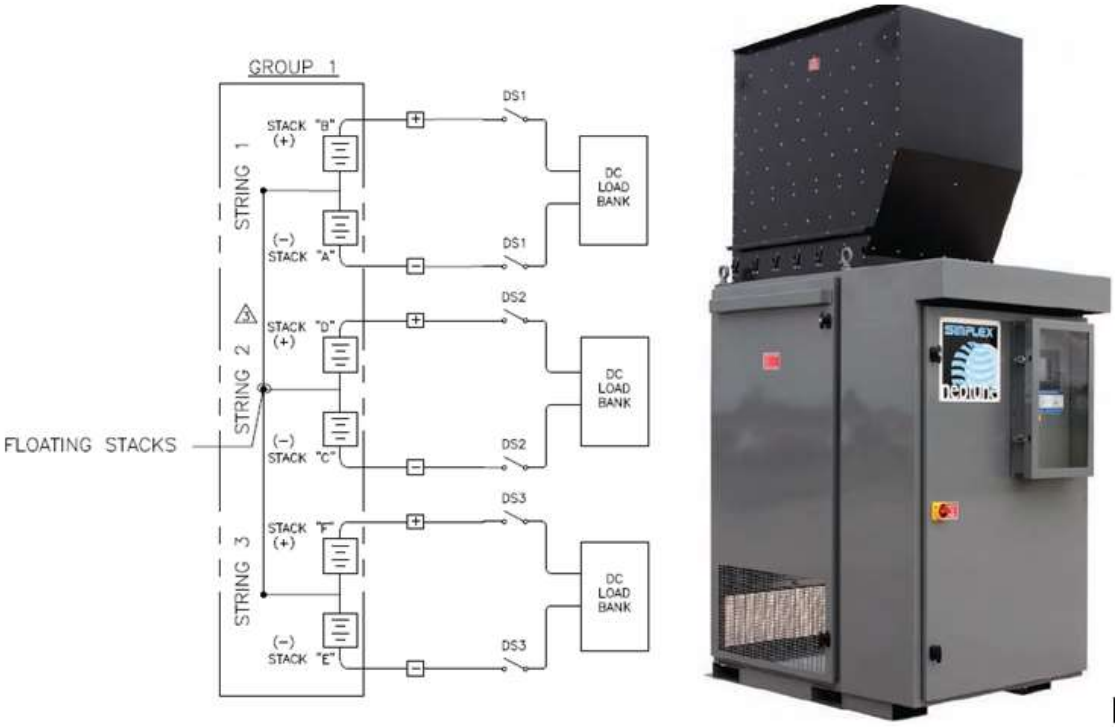

Figure 4.3-16 One-Line Diagram Using DC Load Banks; Simplex DC Load Bank

A one-line diagram of the solution using inverters is shown in Figure 4.3-17. Each string of two stacks is connected to an individual inverter via a DC disconnect. The Yaskawa Solectria PVI 25 TL inverter (Figure 4.3-17) has been identified as an inverter with potential capability to provide current control. One of these was purchased and evaluated to verify it can operate at 600 volts and 24 amps with fine load step resolution. This can also be controlled via MODBUS TCP. As part of this evaluation, it was necessary to utilize a power supply to simulate the DC voltage provided by two stacks in series and map the current response of the inverter.

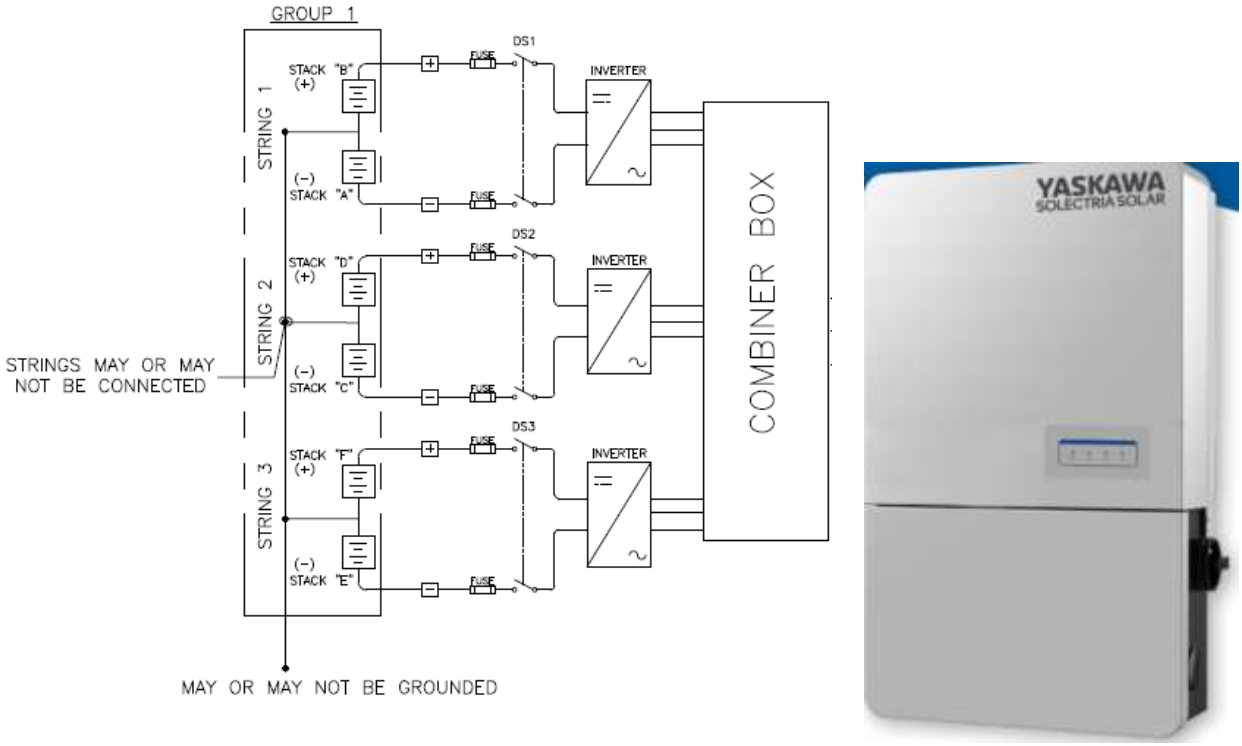

Figure 4.3-17 One-Line Diagram Using Inverters; Yasakawa Solectria Inverter

Controls HAZOP

A Hazard and Operability Study (HAZOP) is an organized exercise to analyze a complex planned or existing process to systematically evaluate problems that could represent risks to either personnel or equipment. In order to complete a HAZOP a group of interdisciplinary team members are required to bring together a wide variety of experience and knowledge of the HAZOP process. Using the P&ID drawing (Process and Instrumentation Diagram), the planned, or existing, process is divided into nodes to easier organize the HAZOP process. An example of a P&ID that is sectioned into nodes is shown below (Figure 4.3-18).

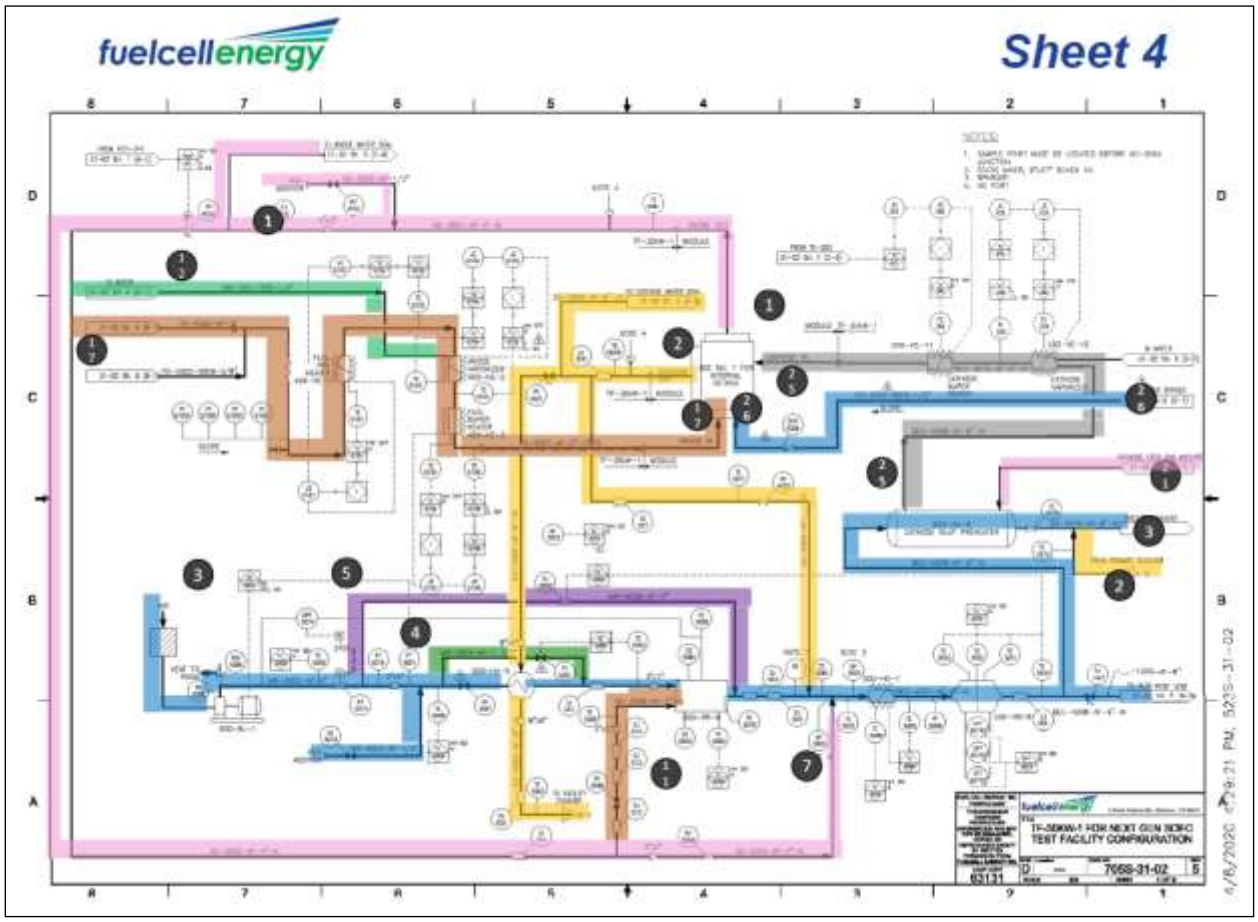

Figure 4.3-18 Next Gen SOFC Test Facility P&ID with HAZOP nodes.

Each individual node is reviewed by the team members as a group. Specifically, risks associated with deviations in flow, pressure, temperature, composition, leak to environment, etc. are identified and listed in table format. For each deviation, there is a cause (component failures) and the consequences of that deviation (assuming no safeguards are in place). Each consequence is rated on a scale of 1-to-4 for the severity of the incident (extent of equipment damage or personnel injury) and likelihood of 1-to-4. The likelihood captures the number of safeguards currently present to stop the consequence from occurring. The combination of these ratings generates a safety rating of A-to-D. Here, A and B are unacceptable hazard levels, C is only acceptable when there is no personnel injury, and D is the safest and therefore the preferred result. The table used by the HAZOP team for this project is shown below in Figure 4.3-19 illustrating the resulting safety ratings based on severity and likelihood combinations.

Likelihood↓\Severity→	**1**	**2**	**3**	**4**
1	**A**	**A**	**B**	**C**
2	**B**	**B**	**C**	**D**
3	**C**	**C**	**D**	**D**
4	**D**	**D**	**D**	**D**

Figure 4.3-19 FuelCell Energy HAZOP Result Look-up Table

The test station being used for testing the 40kW SOFC module, located at FuelCell Energy in Danbury, Connecticut, was configured for other testing purposes. Therefore, a P&ID was created from existing documentation adding in required process lines and equipment for the upgrade for the solid oxide fuel cell module. If there are any A's, B's, or (unacceptable) C's then recommendations to the layout, or addition of interlocked alarms from new or existing components, were recorded in the HAZOP excise table. (i.e. adding a High-High alarm for a temperature for a plant shutdown state) After all of the nodes were completed, the P&ID was updated with the agreed upon changes and the action items are closed out after they were evaluated by the HAZOP group and are accurately represented on the newest revision of the P&ID.

A node (node 27, Figure 4.3-20) that was added, based on an upgrade to the test facility, was a nitrogen feed that would enter a natural gas bypass to the solid oxide fuel cell's radiative fuel reformer. This was a case of special interest because, usually a HAZOP is run under the assumption is that all equipment has its integrity. However, the nitrogen line is present to ensure no moisture is in the line during a shutdown condition. Usually, a HAZOP does not allow two failures to occur at once. But since this was a special instant of a line's that's purpose only occurs during an upset condition of the test facility, it was encouraged to be reviewed (Figure 4.3-21). Although the node was satisfied based on its inherent design it was a good point to review the potential ramifications of a valve not being open when it is required.

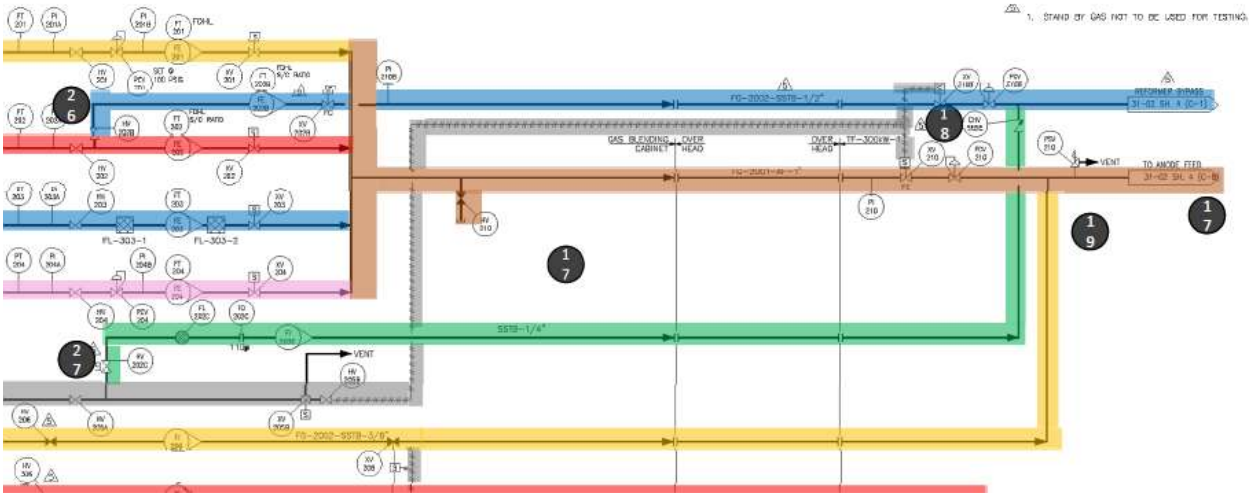

Figure 4.3-20 Node 27 (in green) Nitrogen Purge through Reformer Bypass

Node: (27) N2 to Reformer bypass line
Drawings:
Parameter: Flow Intention:

GW	DEVIATION	CAUSES	CONSEQUENCES	SAFEGUARDS	S	L	R	RECOMMENDATIONS
No	No Flow	1. HV202B closed in error	1.1. moisture in anode on plant SD, potential slug of water into a hot pipe, potential FCD	1.1.1. Line is sized not too big to be able to hold significant moisutre upon SD 1.1.2. OTP 1.1.3. Line is sloped towards Anode inlet so water will not stay in RFR bypass line 1.1.4. FI-202B physically indicates flow of N2	1	4	D	1.1.1. Show valve as locked open on P&ID

Figure 4.3-21 PHA Works Node 27 No Flow Deviation

The P&ID evolved originally from the DFC 30kW Subscale test stand; typically used for single DFC stacks up to 30 cells and 30kW in DC power. The 40kW SOFC system consists of six stacks with 350 cells per stack. There are significant departures from the original DFC Subscale stack test stand in order to test this project's 40kW SOFC Module. Separate current control in the form of three groups of two stacks each was implemented. The cathode side is exclusively dry air compared to a humidified blend of carbon dioxide, nitrogen and air used previously. The anode side is a reformate mixture of steam, carbon dioxide, hydrogen and natural gas. Plus, a second dry natural gas inlet was installed on this test system. The reason for the second mass flow controller is to trim the amount of reforming that occurs in the radiative fuel reformer. To ensure that the steam does not back flow and condense, nitrogen purge was used when the natural gas of this second inlet is not in use. A check valve close to SOFC module install connected was used as well. After reviewing the required anode and cathode flowrates, several upgrades were required of the test stand. The hydrogen and compressed air mass flow controllers required upgrades. And the compressed air line supply tubes required an increase in diameter from ¾" to 1" in order to reduce the pressure drop associated with a max flow rate of nearly 150SCFM.

The 30kW-1 Test Stand HAZOP was extended to cover RFR fuel gas bypass control and the 30kW-1 P&ID changes (Version 15) reflect those updates in preparation for testing the 40KW SOFC Module. Accordingly, the IO list reflects the most recent updates to the P&ID. The 30kW-1 test stand has begun to reflect those changes including removal and relocation of the Anode Inlet side piping and heaters. Previously the 30kW-1 Facility had 4 inline heaters on the anode inlet side. The four heaters were the Anode Preheater, Vaporizer, Superheater and lastly before the module an Anode Heat Trace Heater. The Anode Heat Trace and the Anode Preheater have been removed ahead of this test allowing a more efficient layout of the piping. This change has been reflected in the present 30kW-1 P&ID, including the addition of a supplemental Anode Superheater to further heat the anode above that of DFC inlet conditions for the SOFC test.

Reformer Fuel Bypass Humidifier has been fabricated and getting ready to be installed in the test stand. The function of the Reformer Fuel Bypass Humidifier is critical for optimal operation as we plan on sending some of the natural gas around the Radiative Fuel Reformer and blend with the Radiative Fuel Reformer Exit just before entering into the SOFC anode inlet. To prevent coke formation from the decomposition of methane in high temperature SOFC module without sufficient steam prior to mixing FCE has made the decision to humidify the Radiative Fuel Reformer

bypassed methane. The planned Steam-to-Carbon Ratio is 1.5 S/C Ratio. The humidifier is a bubbler style humidifier with six parallel tube sections for individually humidifying the bypassed methane to the six stacks within the module in a common humidifier with a single controlled heater.

Another piece of equipment being used in this test stand is an Air Ejector (Figure 4.3-22). The Air Ejector allows a small amount of fresh room air to flow into the module upon loss of power. The Air Ejector is powered by compressed nitrogen. Nitrogen is considered far more reliable as it is stored on site via liquid source compared to compressed air which is subject to maintenance issues and other availability issues. The Air Ejector selected is a standard part from Fox Valve which has a max flow of 6 SCFM Air. Recently this was bench tested to confirm Ejector operation. Proof of expected gas flowrate was confirmed via GC. The GC results showed that the original Flow Switch selected was adding excessive pressure drop to the Air Ejector outlet line, so much so that the air flow rate was much lower than expected.

A second test was run without the plunger style flow switch and the O2% in the resulting stream went from 8→16% O2 balance nitrogen. As a result, a different low pressure drop thermal dispersion style flow switch was selected and should arrive by the end of this month. The stainless-steel air Ejector has redundant ¼" compressed Nitrogen Fail Open Ejector supply valves and the Ejector exit has two larger ½" N2/Air Mixture Fail Open Valves in parallel to ensure reliable supply of room air to the SOFC Module.

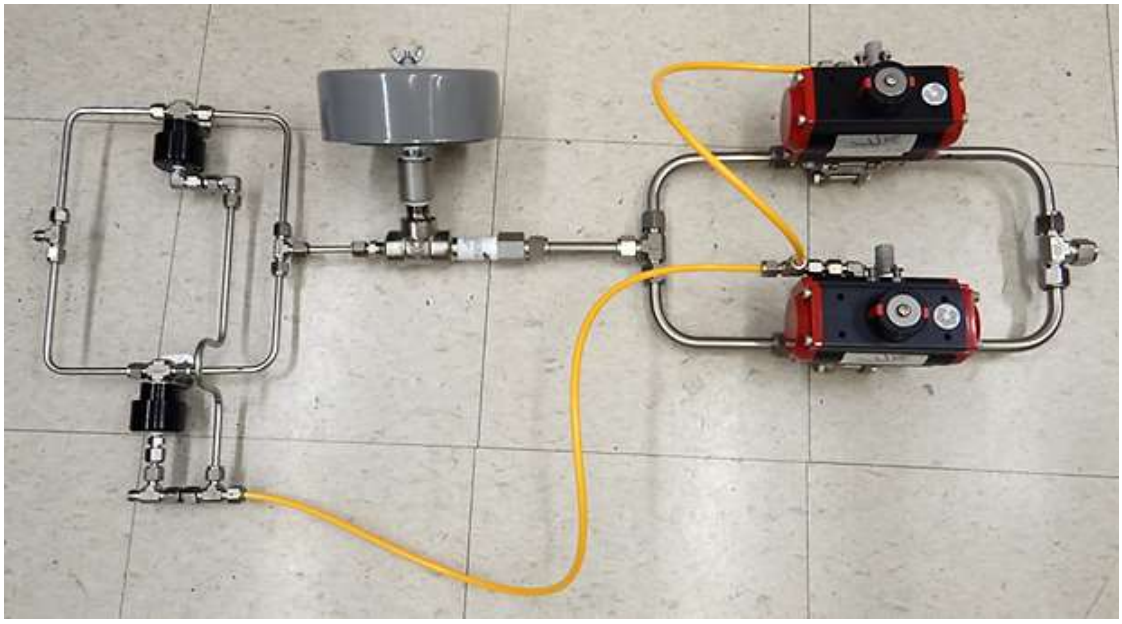

Figure 4.3-22 Air Ejector Hardware and Control Valves

5 40 kW Module Demonstration

Objective:

This objective of this task is to demonstrate long term reliability performance of a modular SOFC system as a building block for ≥100kW and MW-class power plants. The purpose of this task is to fabricate a 40kW stack module and demonstrate long term reliable performance that meets the voltage degradation targets of this project.

5.1 Stack Module Fabrication

Approach:

This task involved the fabrication of a module consisting of six 350-cell stacks with control systems and thermal management design strategies developed as part of Task 4.0, quality control measures developed as part of Task 3.1 and 3.2, and stacks consisting of improved Cr-getter cathodes developed as part of Task 2.1 and 2.3. Mass flow controllers, blowers, data acquisition instrumentation, and valves were utilized where prescribed by the topology determined during Task 4.0. This module was integrated into FCE's test facility providing house gas, proper exhausting, grounding, and stat-up power. A full modular system checkout was completed in the test facility prior to installing the six CSA stacks and commencing module testing, Task 5.2

Results & Discussion:

A facility at FuelCell Energy, Inc office in Danbury, typically used for 30kW molten carbonate fuel cell (MCFC) tests, is being re-worked for use with this SOFC module. Some resizing of mass flow controllers has been required but the bulk of the facility is capable. The main upgrades include additional supply gas heater equipment, individual load banks for individual strings of CSA stacks, separate instrumentation cabinets specific to the SOFC module, and some control software changes. Supply gas heaters were added to make up for the higher operating temperatures required of inlet gas stream as compared to the MCFC equipment currently in place. Individual load banks provide a control strategy being investigated whereby localized control of current can lower on-cell temperatures to extend the lives of the stacks. Each load bank supports a string of two CSA stacks; three load banks total. The currently installed instrumentation cabinet input-to-output hardware (I/O) is not rated for the higher voltage of the CSA stacks. A separate I/O cabinet is required for this purpose along with voltage conditioning hardware to support this I/O cabinet. The instrumentation needs of the SOFC technology stacks is different enough from the MCFC technology stacks that a benefit exists to having a separate cabinet to allow for ease of swapping between future test facility needs. The load banks were purchased and received (Figure 5.1-1a). Facility supplies and exhaust pipe spools were cut back and prepared (Figure 5.1-1b) for reconfigured pipe runs for the module as well as equipment connections.

Figure 5.1-1 Photos of a) Load Banks Received/Installed; b) Test Facility Pipe Prep

30kW-1 stand requires significant P&ID refinements in preparation for 40kW SOFC operation. The most significant change was the addition of a bubbler humidifier (Figure 5.1-2) to provide steam for the radiative fuel reformer (RFR) bypass natural gas. One of the concerns in adding dry methane to a hot system is the possibility of coking. To mitigate coke formation, FCE looked at CO2 addition, hydrogen addition as well as steam addition to the bypass methane line. After careful review it was concluded that the best way to prevent coke formation in a manner that does not significantly alter the operation of the fuel cell was steam addition. Two methods of bypass methane steam addition were considered for this unit operation, those were a bubbler and vaporizer. The key metrics were ease of operation, cost and overall complexity and the bubbler was chosen for the task of humidifying the bypass methane. This is a unique bubbler as it has one methane inlet and six humidified exits.

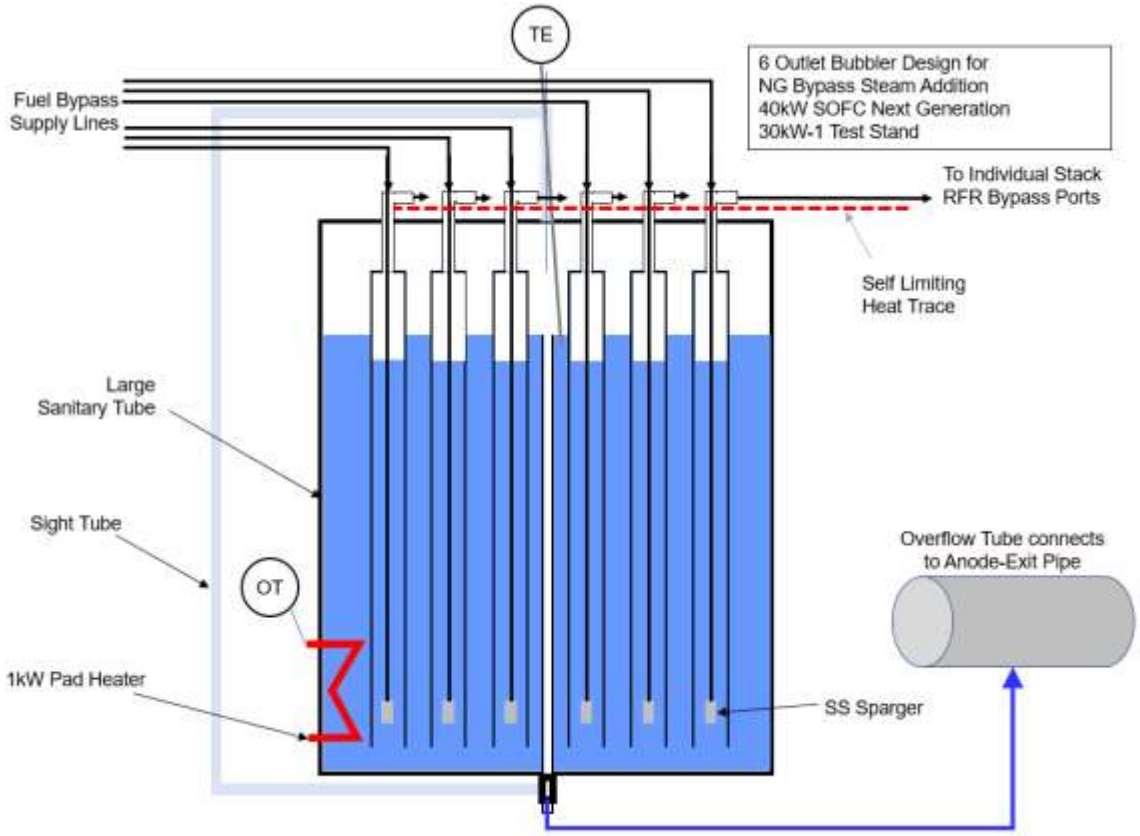

Figure 5.1-2 Water Bubbler Fuel Gas Humidifier

Another decision that was undertaken for the 30kW-1 system was how to provide air to the cathode side when compressed air is not available. It is very important to provide a small amount of air while the SOFC is at operating temperature to provide sufficient O2 partial pressure to maintain electrode stability. It was decided that 1SCFM of air per stack, 6SCFM total would provide suitable cathode electrode protection. During the HAZOP, three likely scenarios emerged that would jeopardize the system air flow: loss of power, loss of compressed air supply or a malfunction of the air mass flow controller. Several back-up air supply options were investigated. Originally a small back-up air compressor appeared to be the simplest most reliable option, other options included a small blower and lastly an air ejector was considered. After careful consideration, the most reliable option was determined to be an air ejector. An off-the-

shelf commercial part was found and is being procured that provides 6 SCFM of backup air to the facility during any one of the three scenarios identified.

The design of the test facility piping has been adjusted to more improved install and fabrication methods. Additionally, adjustments to location of module inlet gas stream heaters allowed for a significant improvement of accessibility. This is critical for tasks such as plumbing, instrumenting and inspections that make it much easier and safer for welders, technicians, and engineers to perform such work. An illustration of the resultant layout of this improvement, with 40kW SOFC module installed, is shown below in Figure 5.1-3. Lastly, before testing the 40kW SOFC system a separate hot test was performed on the two heat exchangers. The first heat exchanger is a relatively straightforward test of a new SOFC anode heat exchanger. The second heat exchanger is more complicated since it includes a catalytic oxidizer to help preheat incoming air to the cathode of the fuel cell. Additional P&ID sheets for these pieces of equipment were made and separately analyzed via HAZOP.

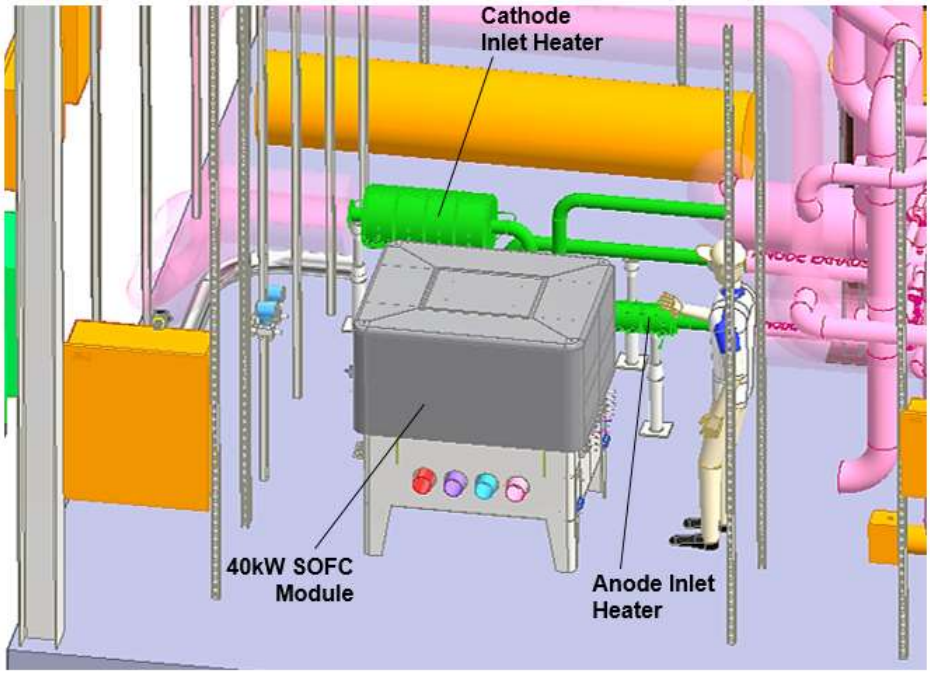

Figure 5.1-3 Accessibility Improvement after Optimizing Heater Locations

The P&ID (Figure 5.1-4, left) provides a basis for HAZOP activities and is revisited at times when any new hazards become identified that pose a potential risk to safe operation of the system. Aluminization is a coating practiced typically used to prevent corrosion of stainless steels that would otherwise result in chromia joining the air supply streams supplying SOFC stacks. Chromia poses a risk to the functional cathode layer of SOFC's by reducing the porosity required to allow the electrochemical action of the cells to take place. While other techniques, such as use of "chrome-getters", are used to minimize the risk of this poisoning, aluminization can provide a level of protection that can limit the need of these other techniques. This also, specifically, increases the lifetime of "chrome-getters" and lifetime of the SOFC cells and stacks. Figure 5.1-4, right shows images of edges of supplemental heater components where masking of weld edges needed to take place prior to aluminizing the bulk of the surfaces in contact with cathode supply air. Aluminization can also be an effective technique to protect thin-walled metal components exposed to dual atmosphere at elevated temperatures. This is being considered for use on some

facility and module components for protection against corrosion risk associated with these types of environments.

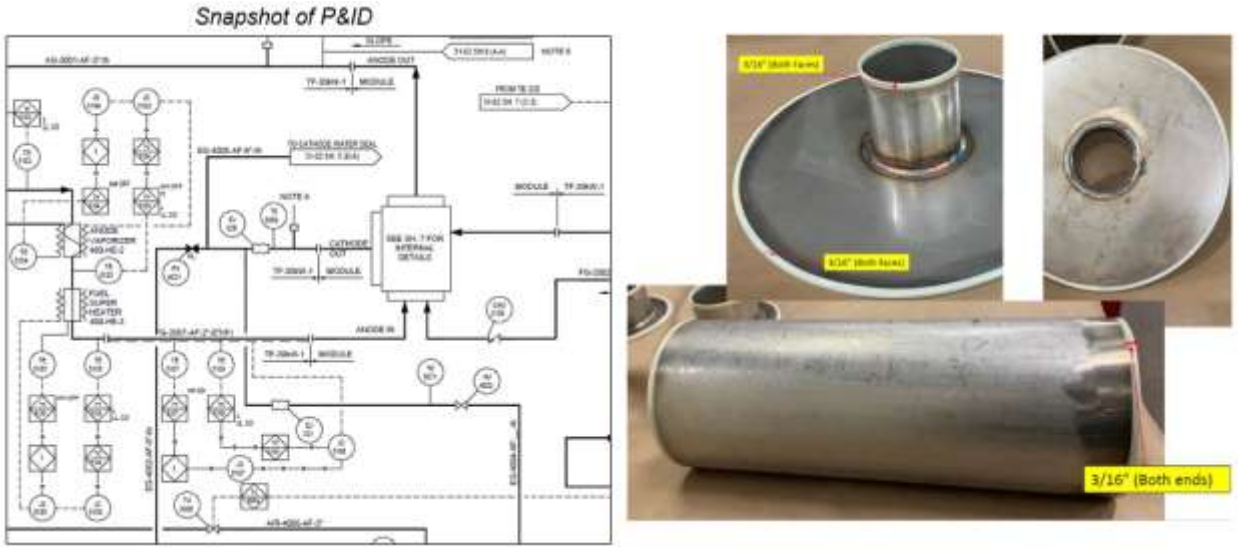

Figure 5.1-4 Images Supporting Controls and Equipment Work Completed

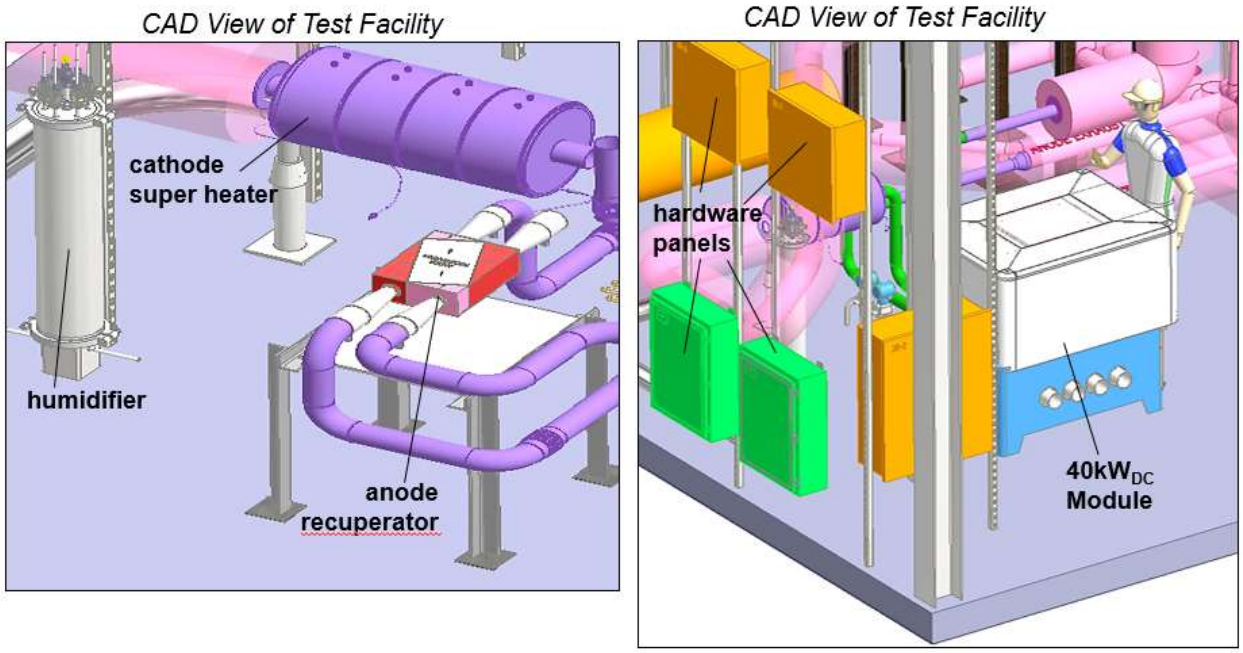

Figure 5.1-5 CAD Images of Designed-In Facility Components

Evaluation of compact heat exchangers are being characterized as part of this SOFC module project. These give some flexibility to future module designs whereby cost improvements are realized. This also allows for close packaging adjacent to the module and to the hot gas stream connections of the module, as in current non-integrated layout. These assessments use a negligible amount of the project timeline but also provide the benefit of use for “hot” checkouts of the test facility (Figure 5.1-5) prior to installing the 40kW SOFC module. For example, the anode

recuperator used for “hot’ checkouts prior to evaluation of this heat exchanger for pressure drops and outlet temperatures. This was then swapped out for the catalytic air-preheater (CAP) for evaluation of pressure drops and outlet temperatures as well as percent of combustibles destroyed.

More than 100 alarms protect the 40kW SOFC Next Generation system allowing safe operation. These alarms ensure that the 40kW SOFC Next Generation system runs within prescribed pressures, temperatures, flow rates, compositions, and voltages. When an alarm is detected and an action is required, the system goes to one of three alarm trip levels.

- Trip to OCV
- Trip to Standby Gas
- Trip to Breach

Each alarm trip level has been thoroughly defined in the control software to prevent further damage to the SOFC test article, facility, and personnel. A significant amount of time has been dedicated to the review and refinement of the alarms list this quarter in an Access Database from which the programmer can program into the control software. Operators are alerted to all alarms via SMS, they can remotely go into the HMI software to monitor the system and adjust the process accordingly. Most system alarms have two levels, the first level is a warning to notify the operator of a process deviation. The second alarm level, the result of a more significant process deviation takes corrective action.

One type of alarm that is different than the rest is the process heater control alarms. There are eight heaters in the system ranging in power output from less than 1kW to 20kW. The 40kW SOFC Next Generation system heater controllers have an independent local over temperature alarm controller that limits the heater temperature and when the setpoint has been exceeded turning off the heater via contact switch.

The safety system consists of several combustible gas sensors in both the gas prep area as well as near the module, push button e-stop, an UV-IR flame detector and a three-tiered alarm shutdown. Inside the 6-stack module a separate port has been incorporated into the enclosure design to continuously sample vessel (cathode inlet) gas detecting any combustible gas leaks, if a combustible gas is detected above 50% LEL the system shut down. FCE has included this safety feature from its extensive kW-Size lab stack testing experience. Area hydrogen detectors are also present to capture any combustible gas leaks from this or other adjacent fuel cell systems in the plant. The SOFC module has three independently controlled DC load banks. The six 350-Cell stacks are arranged in three parallel stack pairs so that each pair can be run independently for optimal fuel cell and module performance. Remaining power control components and power supply were being sourced to complete installation and check outs.

The 40kW Next Generation SOFC HMI screens allow process operators to efficiently monitor the system and make changes to the process to keep the system running smoothly and ensure the program goals are met. Some of the stack parameters being monitored include current, voltage, temperatures. Other screens show the gas preparation for the anode and cathode gasses, heaters, and process exhaust including the oxidizer. A sample image of an HMI screen is shown in Figure 5.1-6 below.

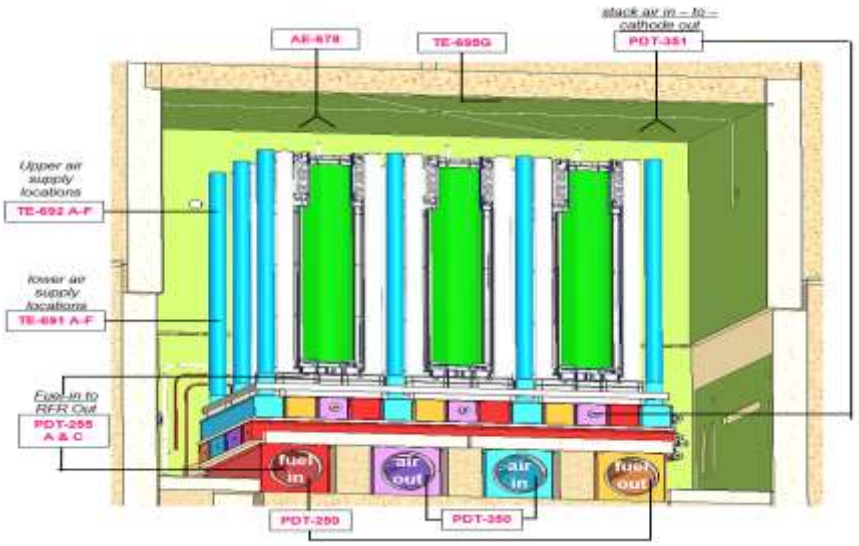

Figure 5.1-6 Sample HMI Screen

Installs of test facility high duty heaters and the anode recuperator were completed (Figure 5.1-7). The heaters need to add enough pre-heat capacity for the fuel gas and air supply streams. The anode recuperator was used for 'hot' check outs of the facility while the 40kW module was procured. In addition, the anode recuperator was evaluated for performance as a critical component to service the module in a complete system. The insulated equipment with associated plumbing is shown in Figure 5.1-8.

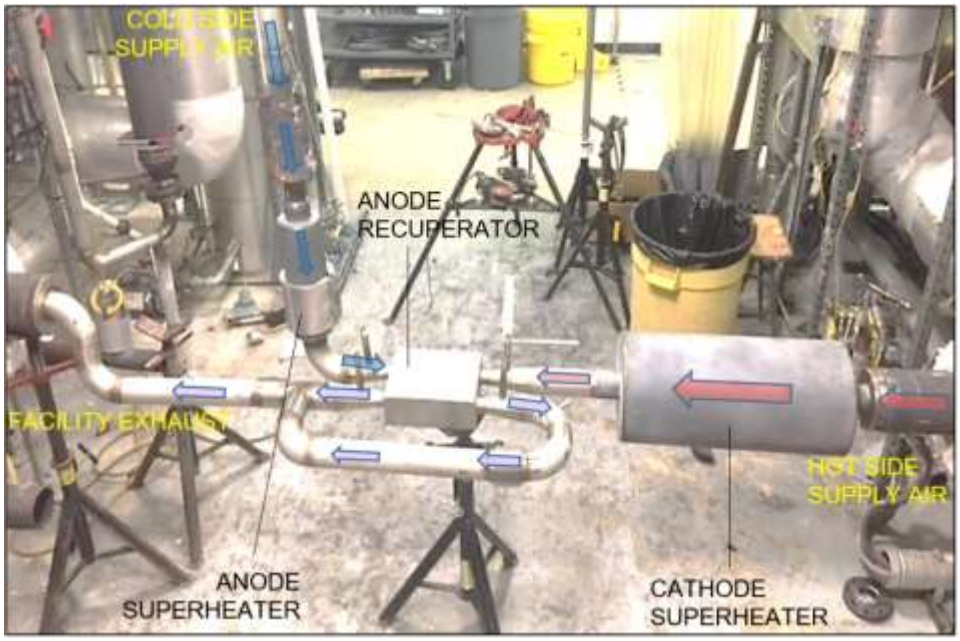

Figure 5.1-7 Installed Plumbing for Facility Check Outs / Recuperator Test

Figure 5.1-8 Insulated Equipment and Plumbing (L), Instrumented Recuperator (R)

The instrumentation and controls elements of the module validation test facility were completed. The final touches included the creation of intuitive user interface screens that help relate monitored data to actual module features, facility equipment and gas conditions (Figure 5.1-9).

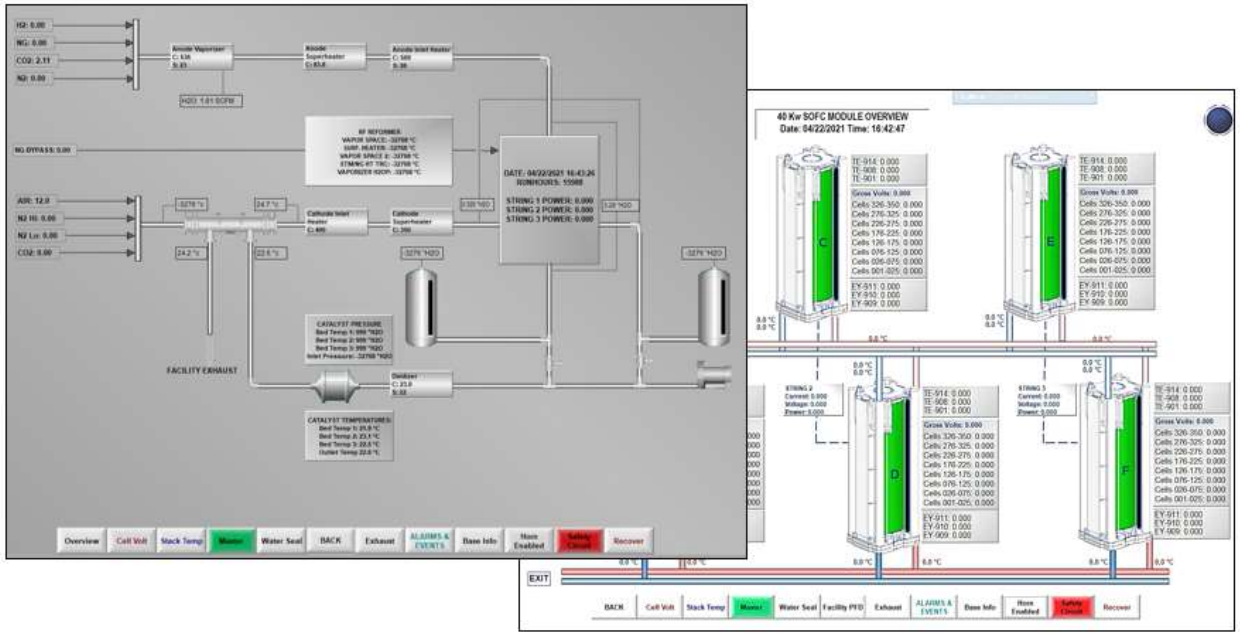

Figure 5.1-9 Test Facility HMI Screens

The anode recuperator exchanges heat from the recycled portion of the hot anode exhaust and the cool anode inlet gas stream. The test was run to ensure that the anode recuperator met both performance specifications of heat transfer efficiency as well as differential pressure. Heat transfer is required to sufficiently cool the anode exit gas going to the recycle blower and sufficiently heat the anode inlet gas to a suitable temperature before reaching the anode. Maintaining low differential pressure across the anode recuperator is critical for overall SOFC system efficiency as excessive pressure drop results in additional parasitic losses from the recycle blower.

For safety and ease of testing process air was used as the gas media on both sides of the anode recuperator. The hot side of the anode recuperator was supplied air from the facility's compressed air system and the cold side air was supplied from the test stand's quench air blower. Several cases involving different flow rates and temperatures were tested representing various operating conditions FCE plans to operate the 40kW SOFC system at. The performance of the heat exchanger was monitored real time via HMI at the 30kW-1 test facility. The anode recuperator test also served as a validation of the custom-made anode and cathode inlet supplemental superheaters. These supplemental heaters (shown below) along with the uninsulated anode recuperator, were designed specifically for the Next Generation SOFC 40kW system by the FCE mechanical design team. It was determined that additional high temperature heaters were required in the 30kW-1 Test Facility. The 40kW SOFC module is designed to run at approximately 100°C higher temperature and higher anode and cathode flow rates compared to the MCFC stacks typically operated in the test stand.

Initial testing with the various cases showed that the hot side of the anode recuperator temperature drop came very close (within 10°C) to the expected value. Following completion of all test cases the data was tabulated and the results analyzed. The pressure drop on the cold side of the anode recuperator was ~75% higher than expected in the Rated Power case and ~15% higher than expected in the hot side. FCE worked with the anode recuperator manufacturer to understand the higher-than-expected pressure drop for improvement in subsequent anode recuperator designs.

Assembly drawings were developed to assist in the build of the 40kW SOFC Module. Sample views to be used in these drawings are illustrated in Figure 5.1-10 below.

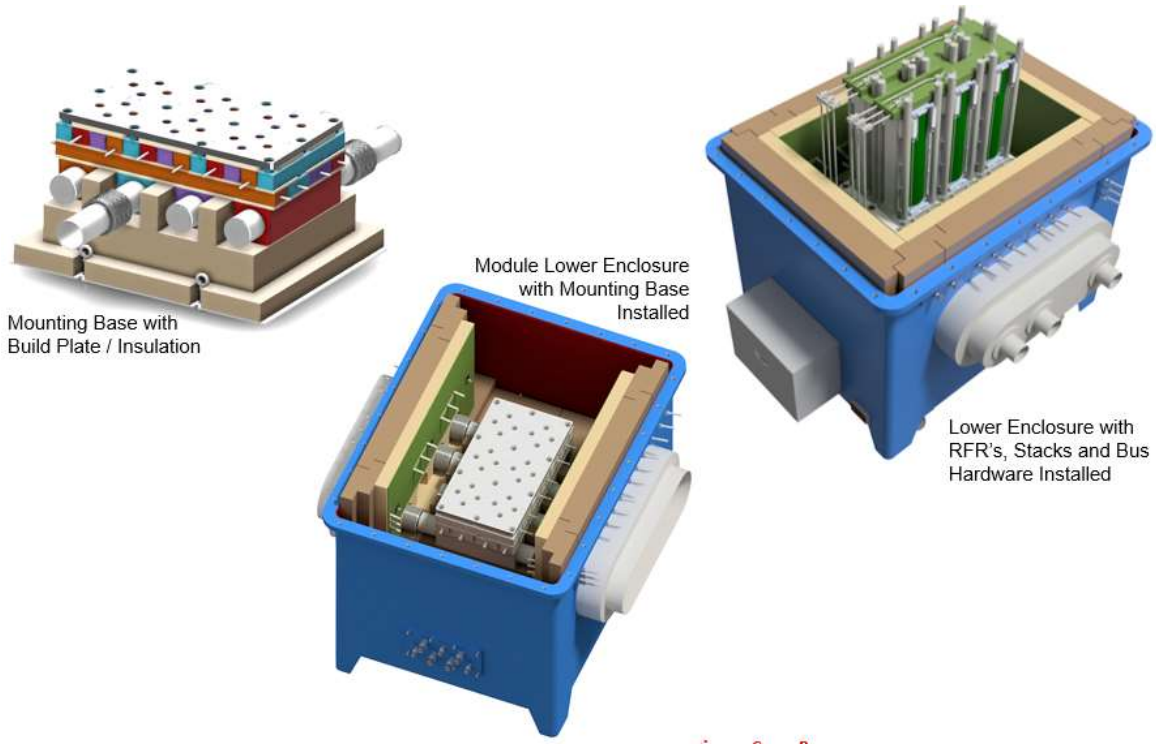

Figure 5.1-10 Assembly Views of 40kW SOFC Module

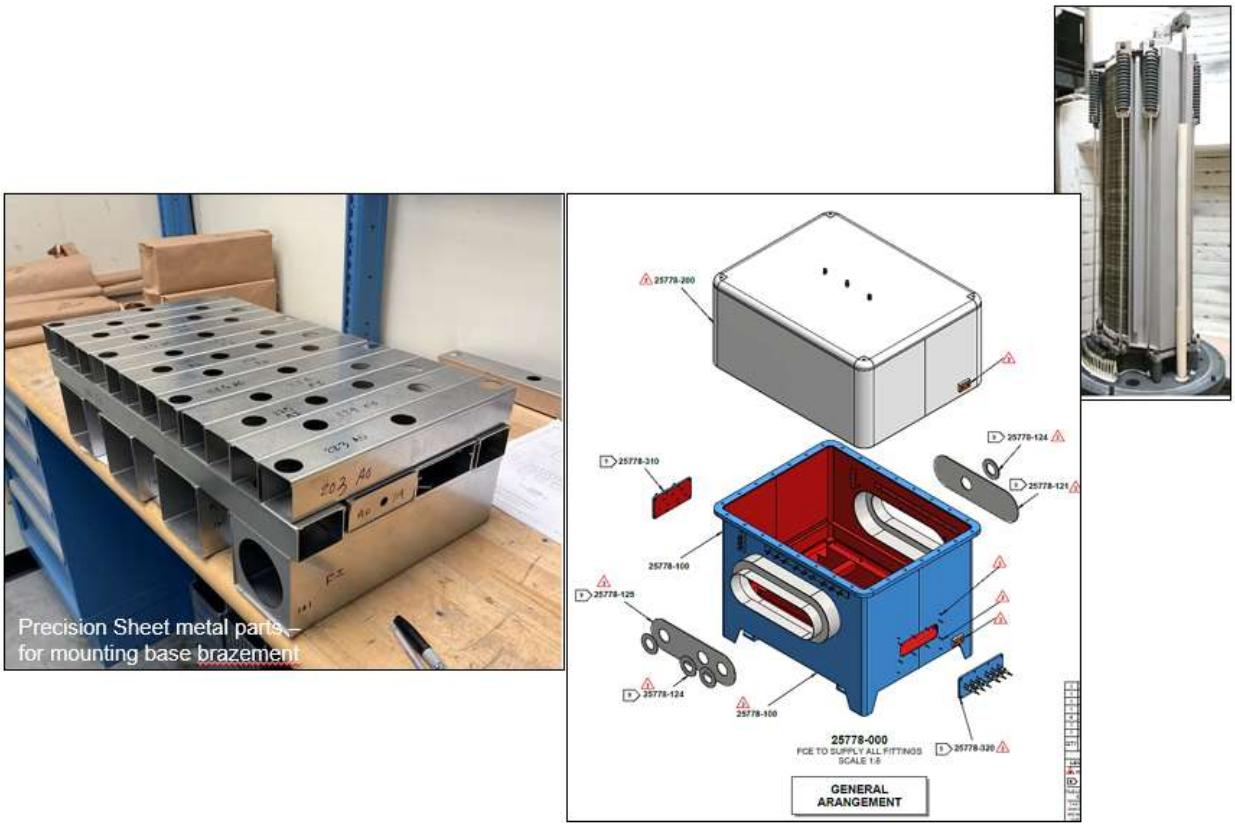

Figure 5.1-11 Sample Fabrication Parts and Drawing View

Figure 5.1-12 Module Enclosure Component Fabrication

Figure 5.1-13 Fabricated Module Enclosure: Lower Enclosure (left); Upper Enclosure (right)

Several module assembly components as received (Figure 5.1-12 and Figure 5.1-13). The distribution base was fabricated as a brazement at the FCE Calgary location. Some photos illustrating component install are show below (Figure 5.1-14)

Figure 5.1-14 2x3 Distribution Base Component Fabrication

Initial testing of the Anode Recuperator revealed that the test article was losing up to 3kW during initial hot testing. After careful review of the test data, FCE decided to add additional insulation to decrease heat loss to the environment and to increase the heat exchanger heat recovery. This insulation upgrade was successful in reducing the amount of heat loss to the surroundings to less than 1kW. A picture of the anode recuperator following testing is shown below in Figure 5.1-15.

Figure 5.1-15 Anode Recuperator Unit

At the Rated Power Flow rate, FCE had expected higher than observed levels of Effectivity based on the design and the performance data from the manufacturer. Discussions with the vendor are continuing to understand and resolve these performance discrepancies for future anode recuperator design orders. An item that was brought to attention from the supplier was how critical it was of the placement of the outlet thermocouple tips and number of thermocouples to get accurate enough measurements. This is being looked at closer for continued heat exchanger evaluation efforts.

The experience gained from testing of this heat exchanger (as well as a catalytic air-preheater – i.e. CAP-HEX) was critical input to full SOFC systems delivered as products. To simplify testing and for safety considerations air was used as the working gas for both sides of the Anode Recuperator. While several cases were tested at different flow rates and temperatures, the cold side air was approximately 160°C and the Hot side was at 715°C for all cases. Another test that was conducted was a Hot Side Flow Sensitivity Test. The results of the test in terms of Effectivity are shown in the plot below in Figure 5.1-16. Heat Exchanger Effectivity of 78% was found at the rated power flow rate.

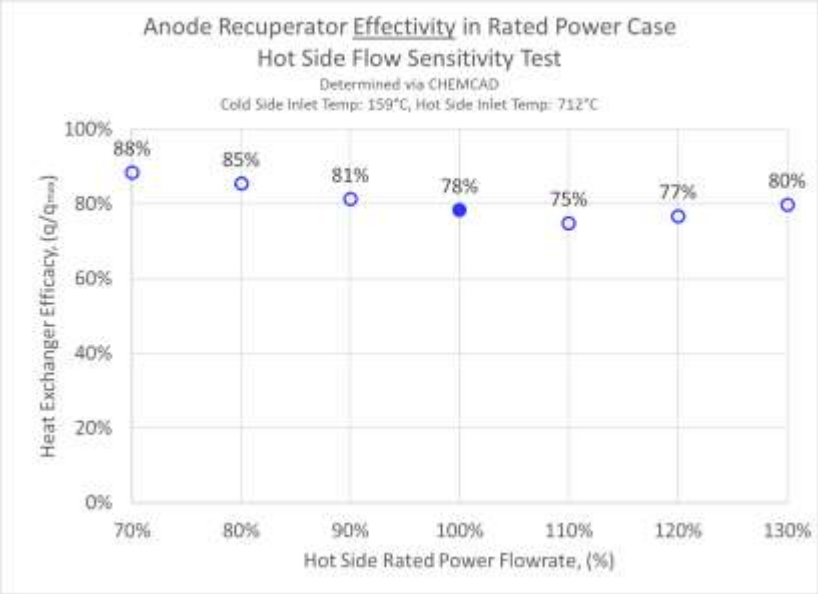

Figure 5.1-16 Hot Side Flow Sensitivity Effectivity Test

The next article to be tested in the 30kW-1 facility, following anode recuperator tests, is the CAP-HEX. The CAPHEX is a heat exchanger oxidizer designed to combine the hot anode and cathode exhaust oxidizing any leftover fuel on the oxidizer side of the catalyzed heat exchanger. The anode and cathode effluent heat as well as heat of oxidation is transferred into the incoming cathode air heating it from near ambient temperature to over 700°C. The CAPHEX utilizes precious metal-based catalyst on the oxidizer side for the destruction of hydrogen, carbon monoxide and methane.

FCE has extensive testing experience with oxidizers which guided the safe and efficient testing of this Next Generation SOFC CAPHEX test. To better understand the performance of the test article, FCE added additional thermocouples in the CAPHEX at the oxidizer entrance and exit to monitor the uniformity of the reaction as well as ensuring that no section within the reactor reaches excessive temperatures. Figure 5.1-17, shown below, is a photo of the installed CAPHEX with the necessary instrumentation prior to getting insulated in the 30kW-1 facility.

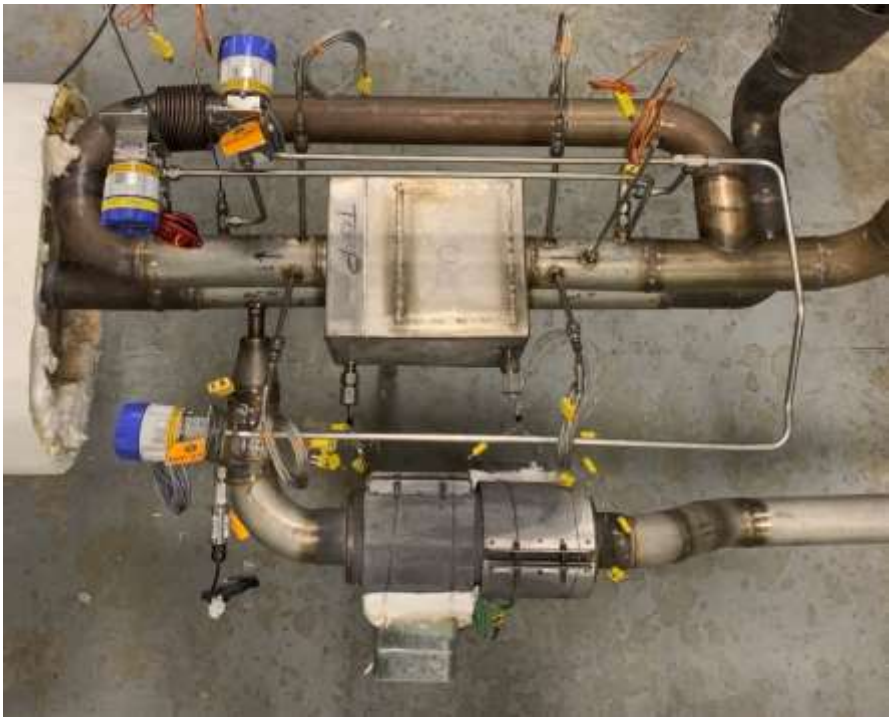

Figure 5.1-17 Instrumented CAPHEX Installed into Test Facility

The test article manufacturer has also recommended adding additional thermocouples at the exit of the oxidizer and cold air sides to ensure that FCE captures any temperature uniformity issues in the exhaust. The effluent of the oxidizer section is periodically analyzed via gas chromatograph looking for trace levels of fuel (H2/CO/CH4).

FCE received two reformer tubes from the reformer catalyst vendor for Radiative Fuel Reformer (RFR) testing. Both reformers ran successfully and demonstrated the viability of the design. A picture of the monolith reformer is shown below in Figure 5.1-18. A key change in both reformers tested this quarter was the inlet tube size in the reactor. The inlet tube brings the anode gas from the base of the reformer to the top of the reformer tube. The reformate then flows back down through the annulus where it gets reformed on SMR catalyst. It was determined that the inlet tube had a higher than desired pressure drop at the rated power flow rate. This tube OD was increased which led to a significant reduction in pressure drop compared to the earlier RFR versions that were fabricated.

Figure 5.1-18 Monolith Test Article

Installation and testing of the first reformer tube monolith (version 2A) commenced in May of this year. The monolith based RFR ran for several weeks successfully with very stable performance

in terms of exit temperature and % methane remaining. A plot of version 2A performance is shown below in Figure 5.1-19 below. After reviewing the temperature and exit gas composition data, it was found that the RFR was reforming more methane than desired and had a lower than desired exit temperature for the 40kW SOFC system design.

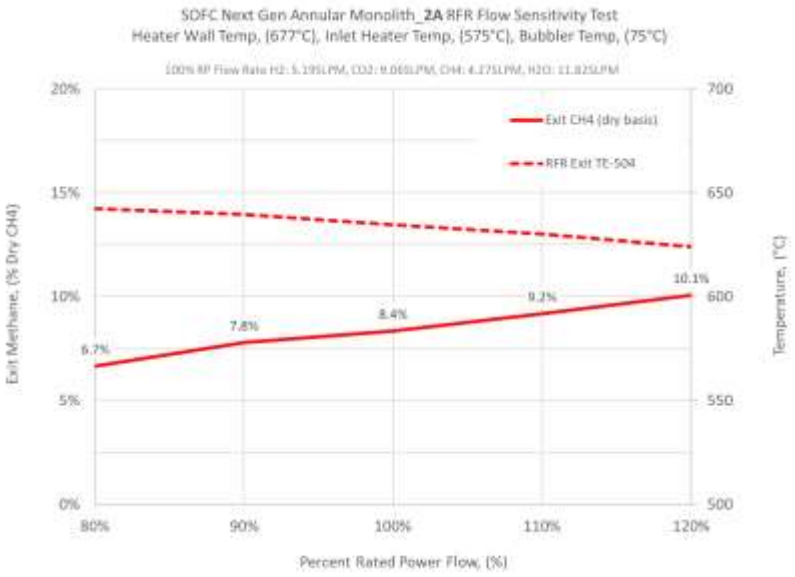

Figure 5.1-19 Monolith 2A Flow Sensitivity Test

A follow-on revision (version 2B) of this initial design was then procured and tested. The version 2B RFR was identical to prior version except the catalyst section was ~20% shorter than version 2A. This important change was made to decrease the amount of reforming while increasing sensible heat. Testing revealed that this simple change was successful in both reducing the amount of reforming while increasing the exit temperature out of the RFR. A plot of the flow sensitivity test for RFR version 2B is shown below in Figure 5.1-20.

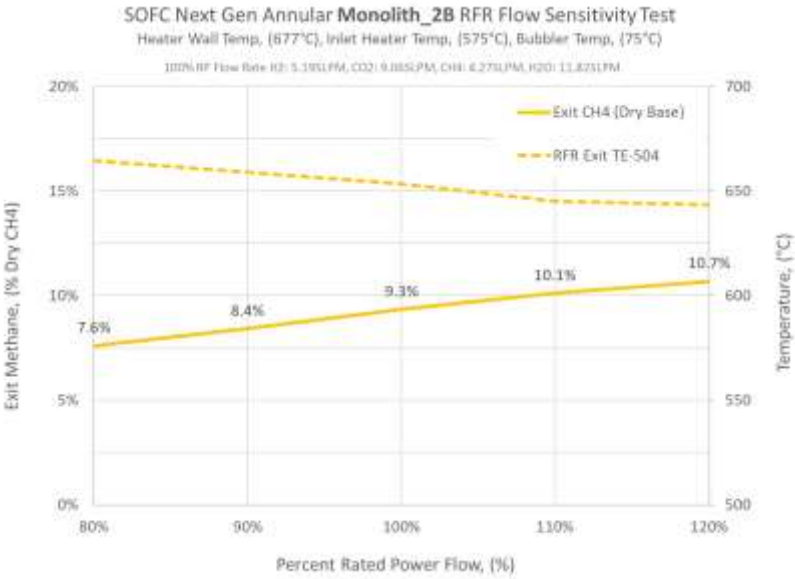

Figure 5.1-20 Monolith 2B Flow Sensitivity Test

The RFR design performance has met and exceeded expectations. Procurement tasks are being completed to incorporate these latest design changes into a larger order of units to be installed into the module enclosure fabrication.

The fabrication base was fully painted and received at FCE. Photos of this are shown below in Figure 5.1-21. In addition to that, the load bearing insulation, used to support the SDB and all six stacks, was found to have been too brittle for this application. The bulk of the inventory material can still be used for vertical wall panel insulations. And replacement insulation, sufficient to withstand loads, was acquired.

Figure 5.1-21 Module Enclosure: Lower, Upper Enclosures (l); Inside Lower Enclosure (r)

One component of fabrication critical to the radiative fuel reforming (RFR) tubes is the brazed plates of the Stack Interface Plate. The Stack Interface Plates serve multiple purposes: 1) distribute fuel gas to and received fuel gas from the four RFR's of one stack; 2) provide a means of mounting the CSA stack to a process gas sealing service prior to mounting to the module; 3) provide a means of mounting a process gas sealing service to the mounting plate of the SDB. Future larger modules incorporate the RFR tubes into the SDB. In the meantime, precision machined plates, brazing foil, and alignment pins were received (Figure 5.1-22**).**

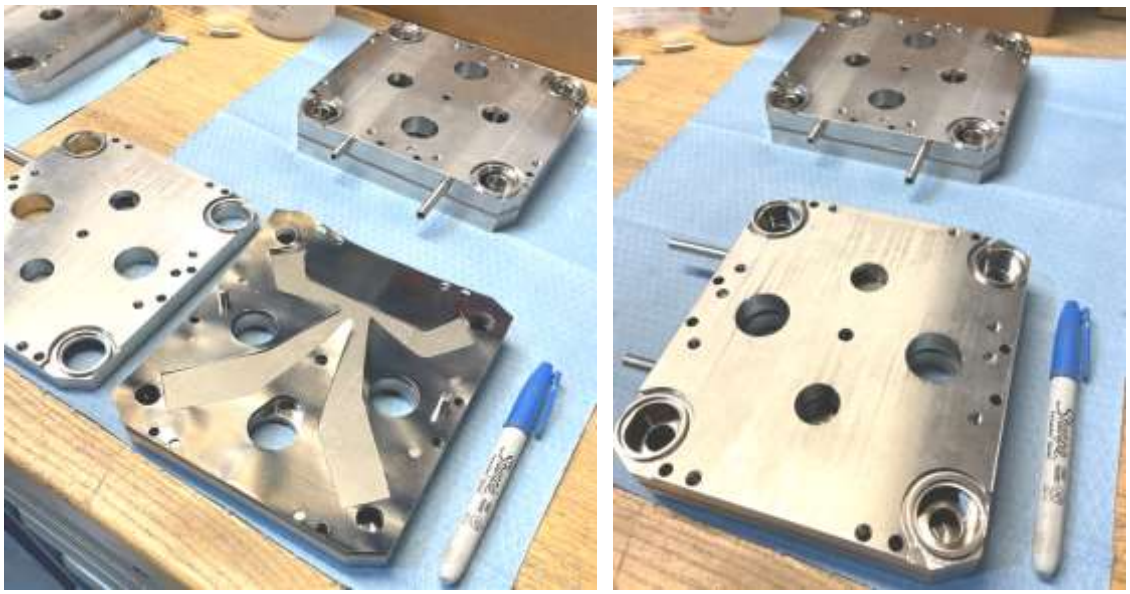

Figure 5.1-22 Stack Interface Plates with Brazing Foil (l) and Precision Mating Surface (r)

The first ‘check-out’ is planned to be a test using the module but without any stacks installed. In order to do this first test, Crossover Plates are required to install onto the SDB at each of the six locations where CSA stacks would be mounted. This enables unobstructed flow of fuel and oxidant gases to the respective stack positions while preventing these gases to mix. Crossover plates are made of precision machined metals used for high temperature applications and require a tubing jumper welded on to route fuel-in gas to fuel-out gas ports. Components have been fabricated in-house (Figure 5.1-23).

Figure 5.1-23 Crossover Plate for Empty Module “Hot” Test

Figure 5.1-24 Blanking Plates for Module 2-Stack Test

2x3 Stack Distribution Base

Fabrication efforts on the 2x3 Stack Distribution Base (DSB) are continuing. This fabrication requires the use of baffle-like inserts to keep the temperature and flow rate of process gases (fuel and oxidant) distributed evenly between stacks. These baffle inserts are designed to be placed within the flow channels of DSB. To support this design and fabrication effort, a full-scale CFD model was developed for the stack distribution base to evaluate the temperatures and flow rates of process gases flowing to the stacks (Figure 5.1-25). The modeling shows the fuel gas delivered to each stack has a mass flow rate within +/-2% of average and a maximum difference in temperature of less than 10°C, which is within our targets. For the oxidant gas flowing into the stacks, the mass flow rate distribution is within +/-10% of average and have a maximum difference in temperature of less than 15°C, which is also within our targeted range. The CFD model was also used to determine the effectiveness of insulation around the flow channels. It was determined that horizontal insulation and vertical insulation between the flow channels are sufficient to meet our temperature distribution requirements.

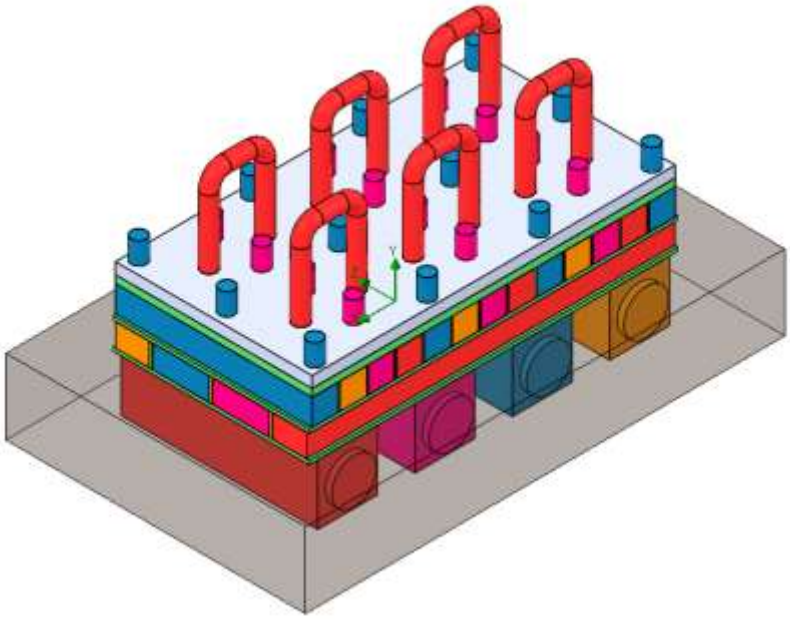

Figure 5.1-25 Stack Distribution Base CFD Model

Fabrication challenges with the stack distribution base led to pivoting to a design that is primarily welded rather than brazed. On the former design, difficulty arose on forming a hermetic seal on the corners of the box tube (Figure 5.1-26). The inaccessibility of certain joints after brazing to repair any leaks also contributed to the decision to pivot the design. The new design for the stack distribution base follows the same general design and shares the same footprint as the former design, but it is modified to allow for the entire assembly to be welded to a single brazement sub-assembly. (Figure 5.1-27) The welded construction gives a high level of confidence in producing a hermetically sealed stack distribution base, which is critical to separate fuel and oxidant gases.

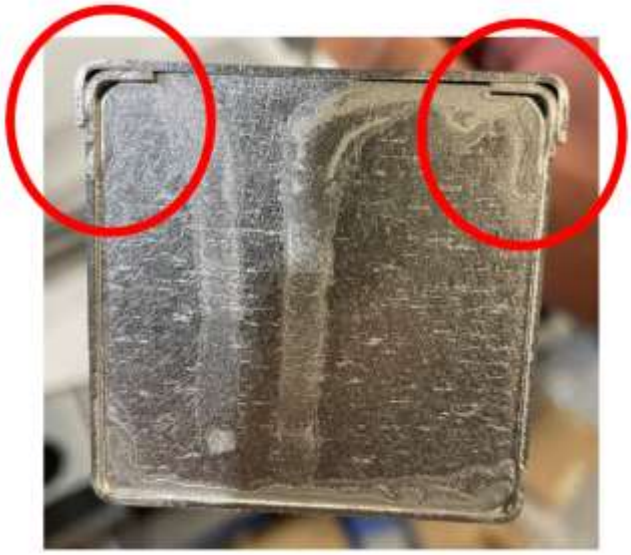

Figure 5.1-26 Stack Distribution Base Sealing Challenges

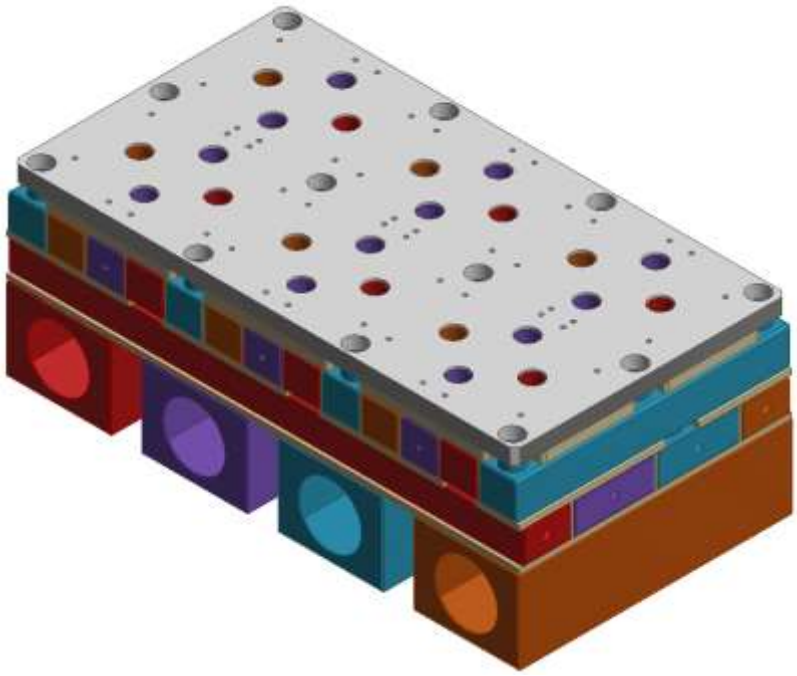

Figure 5.1-27 Welded Stack Distribution Base

Radiative Fuel Reforming Testing

Monolith 2B has successfully reached over 3,000hrs of operation in the RFR Test Stand. The reformer has been running at the Rated Power condition for most of that time. The key performance metrics for the RFR are the exit methane concentration as well as the exit gas temperature. It is important for the radiative fuel reformer to reform some of the methane to increase the hydrogen concentration before the fuel reaches the fuel cell anode for high performance. Secondly the exit temperature of the reformate gas stream following reforming needs to be sufficiently hot as to not over cool the anode inlet of the fuel cell.

During endurance testing it was determined that the exit gas temperature over time was dropping. For reasons previously mentioned it is very important that the reformer exit temperature be relatively close to the stack operating temperature. The reactor was carefully shut down to inspect the insulation. It was discovered that additional insulation could be added specifically to the base of the reactor at the core of the test setup closest to the inlet feed tube. Higher performing insulation known as Temp Mat was added to the hottest sections of the reactor replacing the Cerawool insulation. After resuming operations, the reactor running Rated Power conditions saw a temperature increase of more than 30 Celsius degrees indicating that the reason for the temperature drop was the test system and not the RFR itself.

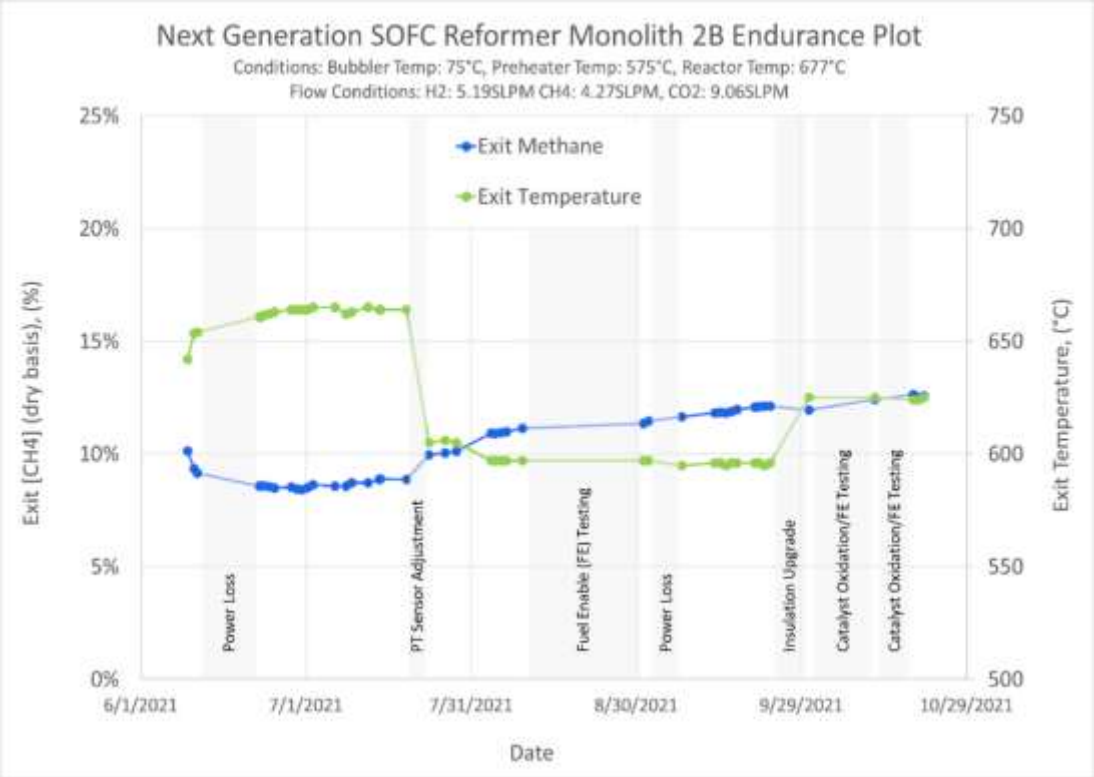

Figure 5.1-28 RFR Monolith 2B Endurance Plot

During the >3,000hrs of operation, the exit methane concentration has risen in the reactor exit. This is expected behavior as the catalyst ages. The exit [CH4] trend can be seen in Figure 5.1-28. When fuel cell power plants are shut down for preventative maintenance, repair and system upgrades it is reasonable to assume that the reforming catalyst may be exposed to oxygen thereby changing the catalyst from a reduced to an oxidized state. While catalyst oxidation is not desired it is important to test its impact on performance to improve catalyst, reformer, and operating procedures to minimize the occurrence of oxidation and its effect.

FCE has extensive experience in carefully oxidizing catalysts from molten carbonate and solid oxide cells and stacks as well as reactors. To simulate real world conditions the catalyst was carefully exposed to oxygen at initially very low levels then gradually increased over several hours starting from less than 1% O2 balance N2 to 20.8% O2 (100% air). This varying oxygen concentration blend was accomplished using two mass flow controllers, one for nitrogen and one for air. The starting low oxygen concentration was verified by GC before adding to the reactor. This test was performed at 25°C and 250°C to understand the effect of temperature during oxidation.

Immediately following each of the two catalyst oxidation tests, the reactor was brought to a fuel enable condition (S/C = 3.0, fuel enable temperature) to observe how easily the oxidized catalyst reforms methane. GC testing confirmed that the reforming catalyst still creates hydrogen from steam and methane thereby self reduces the nickel without using external hydrogen to initiate catalyst reduction in the reactor. A significant amount of testing was dedicated to simulating the fuel enable condition to observe the self-reducing characteristics of the reforming catalyst while at the fuel enable condition.

FCE added recycle capability to the existing test stand, to match the field condition more closely for an accurate demonstration of the self-reducing properties of the reforming catalyst. For ease of installation and instrumentation, and to minimize interferences, a slightly shorter reactor is desired. The two key performance metrics of the shorter reactors are the same as before; exit gas temperature and methane content. Photos of the components for these various lengths are shown in Figure 5.1-29 below.

Figure 5.1-29 RFR Components, Various Lengths

SOFC CAP-HEX (Cathode Air Preheater Heat Exchanger) Testing

CAP-HEX Testing was performed in the 30kW-1 subscale test facility FCE's headquarters in Danbury, CT. After the CAP-HEX was welded into place the test article was instrumented and insulated to handle very high process temperatures. The unit was heated up and several predetermined cases were tested. These cases were called Low Current, Full Power, Rated Power and Low Air Utilization. One of the key metrics was achieving a sufficiently high Cathode Inlet Temperature (CIT). Another criterion being evaluated was the pressure drop of the CAP-HEX. At each case small amounts of methane were added to assess the CH4 destruction capability of the CAP-HEX which is critical for emissions. Figure 5.1-30 below shows the CAP-HEX HMI control screen during operation.

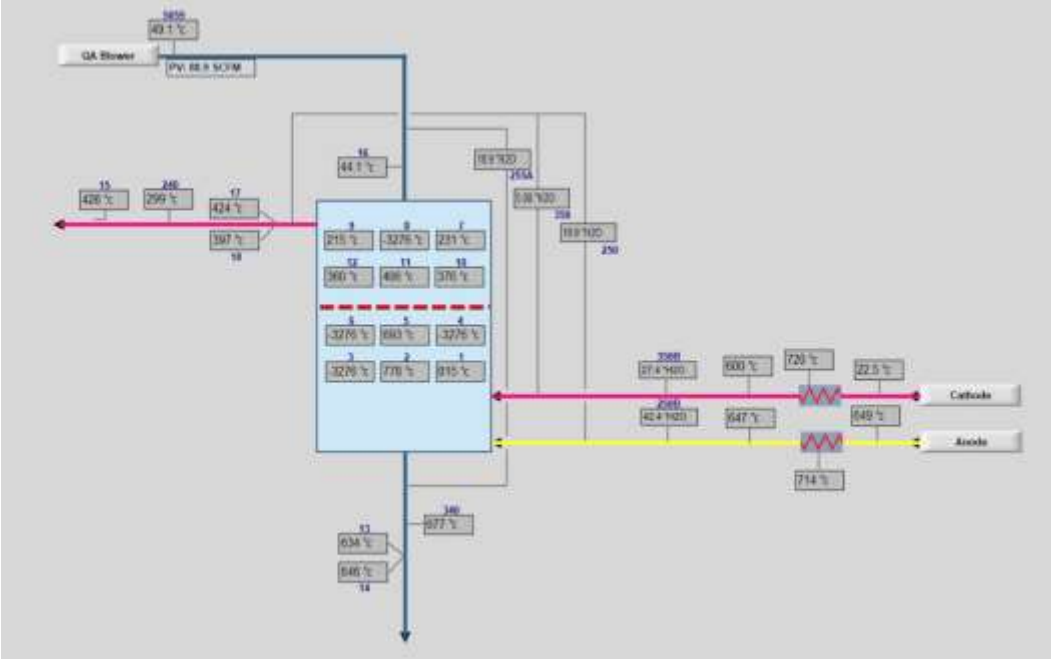

Figure 5.1-30 CAP-HEX Test HMI Screen

One design parameter of the CAP-HEX is the pressure drop through the anode exhaust gas (AEG) sparger, which is used to blend the AEG with the cathode exhaust gas at the hot inlet to the CAP-HEX. Pressure drop through this sparger impacts the anode pressure, increasing it greater than the cathode pressure inside the fuel cell. A low-pressure drop is desired to maintain an anode pressure not too much more than the cathode, with values of 0.75 psi being too high, values ~ 0.5 psi being acceptable, and values ~ 0.2 psi being ideal. This testing found the pressure drop through the sparger, while at the highest AEG flow rates, to be in the range of 0.5 psi. Thus, this baseline design is acceptable.

The mixing effectiveness was evaluated further with the addition of more working thermocouples in the mixing region, with new higher-temperature-rated thermocouple to be added, as detailed below. Design improvements may be considered based on those more detailed results in the future. Pressure drops through the heat exchanger portions of the CAP-HEX were as expected, being within the specifications provided to the vendor.

A key element to control during CAP-HEX operation is the peak temperatures that occur where the fuel and air first mix at the CAP-HEX oxidizer inlet. It is well known that the oxidizer catalyst degrades as the temperatures exceed 800°C, whereas temperatures above 1,000°C can be realized where the air and fuel mix if they are not pre-cooled. To manage the peak temperatures, the test demonstrated the use of quench air to both cool down as well bulk up the cathode exhaust gas going into the CAP-HEX. The test system simulated the addition of quench from an independent air blower by increasing the cathode flow rate while dropping the cathode temperature going into the CAP-HEX.

One of the challenges during oxidizer testing is temperature monitoring within the high temperature zone. Specifically, thermocouples exposed to temperatures more than 800°C are prone to failure unless purpose built. The thermocouples in the oxidizer inlet were 0.032” diameter type K thermocouples rated to <900°C. After several CAP-HEX tests were completed, just two of the original six thermocouples are still working in the oxidizer inlet zone. The CAP-HEX was

cooled down for thermocouple replacement with new thermocouples that are rated to >1,000°C. The new thermocouples have been purchased and installed. These type K thermocouples are larger diameter 0.062" vs 0.032" versions. In addition to their higher temperature rating, it is generally understood that larger diameter thermocouples tend to last longer than smaller ones better withstanding the aggressive conditions of the oxidizer inlet.

Results of the CAP-HEX testing are shown below. For all cases tested using the quench air, the test demonstrated sufficiently high CIT while limiting the maximum temperature at the CAP-HEX inlet to less than 820° (Figure 5.1-31).

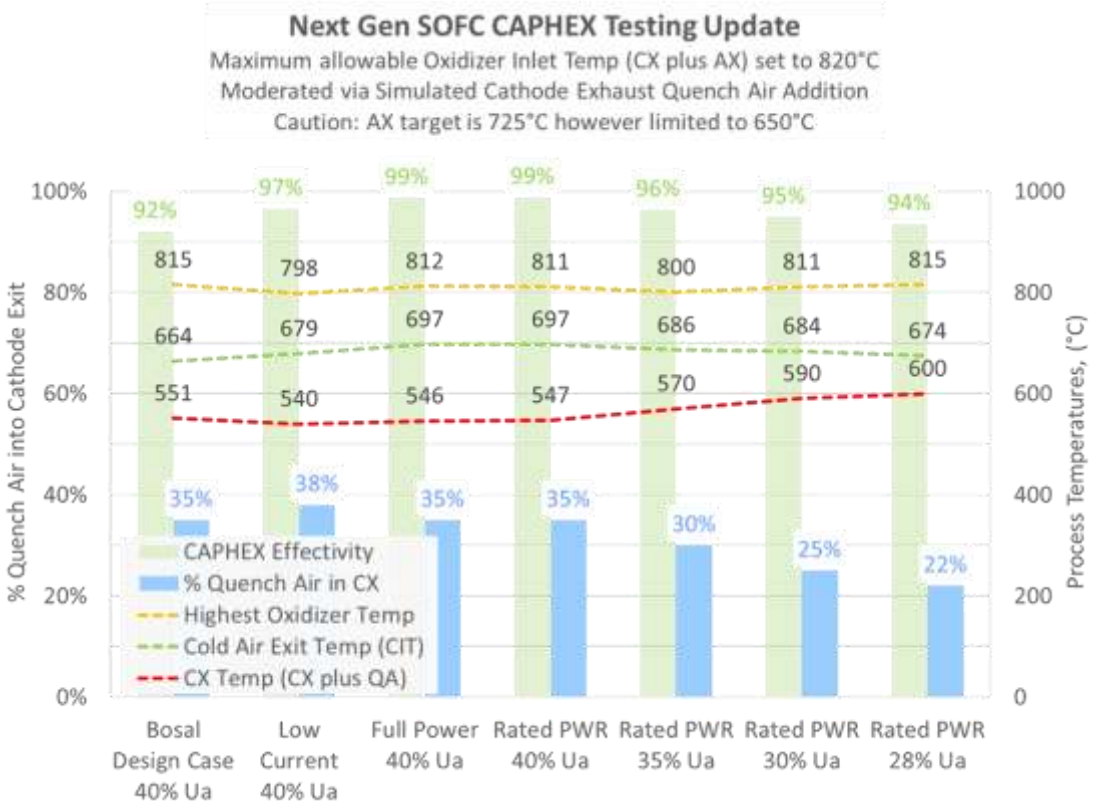

Figure 5.1-31 CAPHEX Individual Case Performance Plot

The CH4 destruction testing, as previously mentioned, was a success in the elimination of methane in the CAP-HEX on the precious metal catalyst.

One component of fabrication critical to the power take off system are the bus bars. These bus bars allow for power to be taken off the top of the stacks inside the hot module environment. From the top of the stacks, the bus bars run down to the purgatory zone where lower temperature rated electrical connectors are used. The bus bar components were machined, assembled, and then brazed (Figure 5.1-22). Final bends were field fit during final assembly.

Figure 5.1-32 Power Take Off Bus Bar Hardware

Another component that has been manufactured are the stack interface plates (Figure 5.1-33). The stack interface plates are sandwiched between the CSA stacks and the stack distribution base. They act as a process gas sealing surface and carry four radiative fuel reforming (RFR) tubes. The internal geometry of the stack interface plate distributes fuel gas to and receives returning fuel gas from the four RFR tubes of each stack. The stack interface plate is made up of precision machined plates that were brazed together using brazing foil.

Figure 5.1-33 Brazed Stack Interface Plates

Radiative Fuel Reforming Testing

In the previous reporting above, the methane-conversion performance of RFR #2B, operated over 3,000 hours, was shown to degrade over time. The performance actually changed rather abruptly during an operational event that occurred in July 2021. Post test analysis of the RFR #2B revealed coke covering the catalyst. Coke is a soot formed by the thermal decomposition of methane, operationally caused when insufficient steam is provided to the methane. The event that caused this episode has been identified. What this means is, the RFR is anticipated to have much better life than as witnessed in RFR #2B.

A significant amount of effort was focused on optimizing RFR performance. On the production RFR units, the top of the reactor was capped, but the test reactor has a ½" tube welded on top to house test instrumentation. The test instrumentation consists of thermocouples to measure feed tube inlet and exit temperatures and gas sensing line for a pressure tap.

Upon analysis of the temperature trends of the reactor, it was determined that the upper reactor instrumentation tube was causing excessive heat loss. This manifested as low temperature at the feed tube exit, far lower than would be expected in the real-world condition where the RFR would be installed inside the fuel cell module hot zone. In this test set up, the upper instrumentation tube exited through the radiant heater vestibules to a non-insulated zone. Once above the insulated zone the tube is connected to a compression tee fitting with the top port connecting to Conax fitting for the two thermocouple sheaths, and a side pressure tap port leading to both differential pressure transducers. The assembly of the upper instrumentation tube is shown in Figure 5.1-34.

Figure 5.1-34 Upper Instrumentation Tube Assembly

In order to reduce the heat loss from the upper instrumentation tube, FCE's reactor design team decided to make two changes to the test configuration. The intent of both changes was to reduce the conduction of heat out of the upper section of the RFR. The first change was to lower the RFR position inside the radiant heater. By lowering the RFR, the radiant heater had more of a dominant effect on the RFR upper temperatures, i.e., at the feed-tube exit, thereby mirroring the real-world in-module condition. The second change was to replace the ½" instrumentation tube with a ¼" tube. To make the ¼" stainless steel tube work, thinner 1/16" thermocouple sheaths were selected, and the ¼" tube was constructed of relatively thin wall. The thermocouples that

pass through to the reactor (TE-305A and TE-305B) now fit tightly in the smaller diameter instrumentation tube while still providing a pressure reference port. Altering the tube was accomplished by cutting off the ½" instrumentation tube and welding a new ¼" tube onto the reactor. Upon testing, both reactors were found to have feed tube exit temperatures about 50°C higher than before. This is a very significant increase – the modification is considered a success, and this shall be the design going forward for a) the position of the reactor within the radiant heater, and b) using the smaller ¼" upper instrumentation tube.

Figure 5.1-35 Upper Section of RFR showing Upper Instrumentation Tubing

In Figure 5.1-35 above two reactors are shown: the lower RFR is the original with the ½" instrumentation tube and the upper RFR is the new design with ¼" tubing.

Upon confirmatory testing with the improved upper instrumentation tube design, the data showed the RFR was overproducing in hydrogen, but underproducing on exit temperature. For this reason, the RFR design has been modified, by reducing the active reforming length. Reducing the active reformer length resulted in less methane conversion to hydrogen, while allowing the temperature at the exit to rise due to less cooling by the endothermic reforming reaction.

SOFC CAP-HEX (Cathode Air Preheater Heat Exchanger) Testing

As reported above, the testing of the CAPHEX provided many insights about operating considerations, especially as related to peak temperatures and mixing of the air stream (or cathode exhaust stream) and fuel stream (or anode exhaust stream). Based on those results, the CAPHEX, as well as the power plant operation and configuration, has been reconsidered specifically to control the peak temperatures that occur as the air and fuel are first mixed. Baseline decisions have been made: The plant design shall include quench air capability. And the CAPHEX shall be designed with inlet air and fuel distribution system, with variable mixing configurations, with the goal of demonstrating Rated Load operations with limited or no need for Quench Air, while maintaining peak temperatures within design targets. With these changes afoot, and due to the fact that future CAPHEX articles with be much larger, the decision has been made to discontinue testing of the current CAPHEX.

While the test stand was idle, the 30kW-1 Cathode Air Mass Flow Controller had an electronic failure. This 5,000SLPM air mass flow controller is needed for the next facility operation, which is the two-stack module test. It has been sent back to the manufacturer for evaluation and repair.

The IO boxes have been installed and are being tested for proper communication between the panels and the PLC/HMI. Electric power and communications (ethernet) to the IO boxes were connected. A key component that recently arrived to enable 40kW SOFC testing were the cannon plug connectors. These connectors were professionally fabricated and tested and connect the

IO box to the 40kW SOFC module. Now that the cannon connector wiring harness have arrived with their cables, FCE can test the IO from the end of the wire harness back to the PLC reading the signal via HMI.

Several of the newly received Cannon Plug connectors with wires for module voltage and temperature measurement are shown in Figure 5.1-36.

Figure 5.1-36 Cannon Connector Wiring Harness

Anode Recycle Capability

In October 2021 FCE realized its need of performing actual Anode Recycle in the RFR test stand, specifically for the fuel enable case. This is because for the fuel enable case the conversion of methane to hydrogen, at relatively low temperatures, is an important performance metric for the RFR. Previously a once-through, or single pass flow, had been used, using only the feed flow rate rather than the flow rate that would be achieved with anode recycle. The hydrogen found exiting the reactor by GC was then added at the inlet, to simulate recycle. However, because this technique appeared to give abnormally high hydrogen concentrations, FCE procured and installed a small, heated diaphragm pump and operated with actual anode recycle at a recycle ratio of 6 to 1. Comparing results, FCE discovered that adding H2 and CO2 via rotameter into the dry gas feed yielded artificially high methane conversion to hydrogen. Therefore, to produce valid data for the fuel enable case the NextGen module test in 30kW-1 should also implement anode recycle. This is especially important during the Fuel Enable phase of heat up, which occurs around 300°C, because the reformers have low activity at this temperature and the inlet fuel and steam flow rates are particularly small. Using the anode recycle at Load Rated operations is less important, because the composition into the RFR is much more predictable, since the AX has come out of the hot fuel cell. Therefore, simulation of anode recycle is relatively straightforward for the Load Rated and other power cases.

Fabrication Activities

Module construction efforts made significant progress on producing a stack distribution base (SDB) that evenly distributes process gases to the 6 stack positions. The brazement subassembly was completed (Figure 5.1-37) and each port was individually leak checked to ensure a proper seal at every braze joint.

Figure 5.1-37 Stack Distribution Base Brazement Subassembly in Progress

After the completion of the SDB brazement sub-assembly, the remaining sheet metal parts were welded to the brazement sub-assembly to produce a completed assembly (Figure 5.1-38).

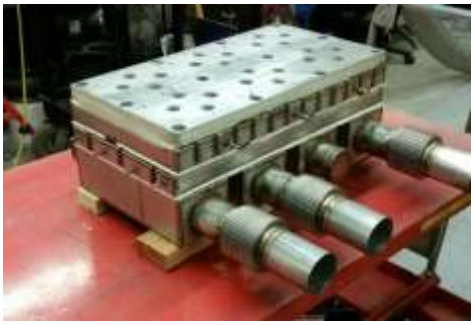

Figure 5.1-38 Stack Distribution Base Brazement Weldment Assembly

Initial inspection after welding revealed a crown in the upper surface of the base plate of the SDB. The base plate needs to be of a certain flatness for the metal c-ring seals to form a proper seal. The local flatness requirement of a stack location is 0.002” with the overall flatness requirement on the base plate at 0.010”. The SDB arrived out of spec due to the welding of the sheet metal channels which caused shrinkage and warpage that bent the base plate. The base plate only bent across the short side of the top plate (Figure 5.1-39) with a measurable 0.06” gap from a reference plane globally and a 0.004” gap in localized stack locations.

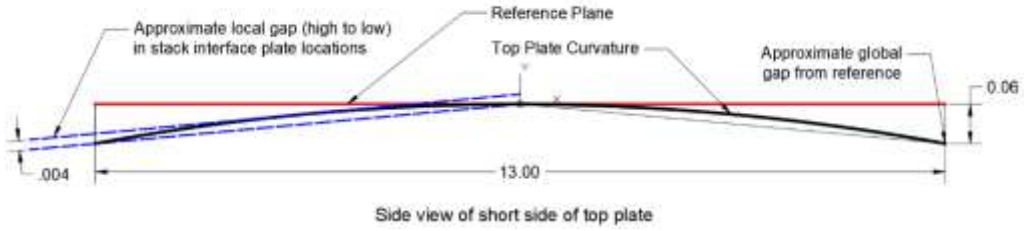

Figure 5.1-39 Diagram of the Top Plate Warpage on the Stack Distribution Base

Fortunately, the base plate has more of a center ridge line, which is not bridged by any individual fuel cell stack. Within the footprint of any stack, the plate flatness is acceptable. As an evaluation, the base plate flatness was evaluated by using blank off plates to seal off the top ports and a pressure bleed-down test was run. Three bleed-down tests were run with c-rings seals installed at two different stack positions for each test (Figure 5.1-40). The remaining four stack positions were sealed off with a thick closed-cell gasket.

Figure 5.1-40 Top Plate C-ring Seal Leak Test

The results of the bleed down test (Figure 5.1-41) demonstrated that the bend in the top plate does not measurably affect the performance of the seals at room temperature with air. The small differences in leak rate are within the measurement error.

The SDB baseline leak rate was first measured with all the stack gas ports blocked off with rubber gasketing, prior to measuring the leak with the C rings. This leak rate is shown in the Figure 5-5 as the “Baseline Leak.” As seen in Figure 5-5, the Baseline Leak is high for the Anode In flow path. The cause has been identified as defective welds. These defects may be patched by corrective welding, or if this is not possible the defects can be patched with a ceramic paste so the SDB can still be used for test operations.

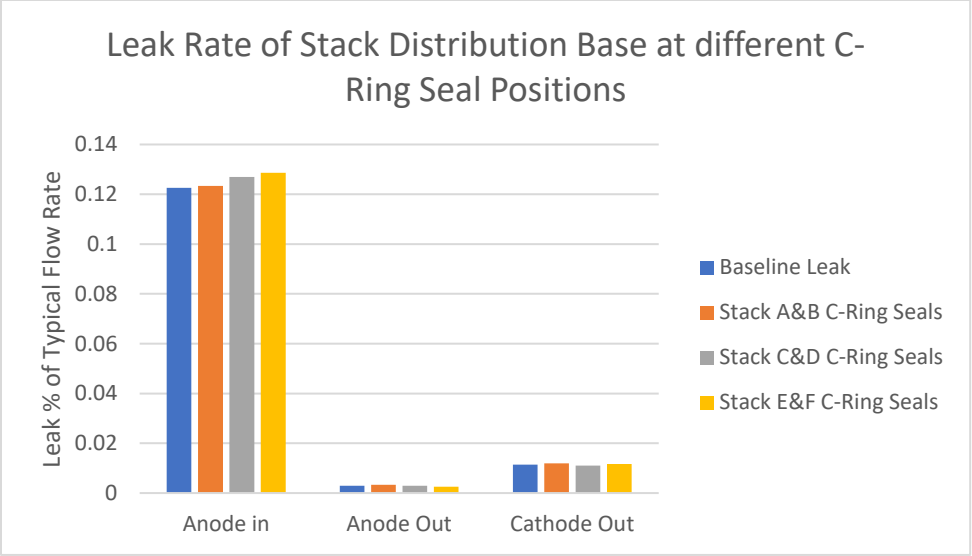

Figure 5.1-41 Top Plate C-ring Seal Leak Test Results

Progress has been made on the other parts of the 40kW module build. The vessel shell has been fully insulated with microporous silica insulation and mica dust covers (Figure 5.1-42).

Figure 5.1-42 Vessel Shell Insulated

The tube-in-tube radiative fuel reformers (RFR) have arrived after being coated in catalyst (Figure 5.1-43) and are ready to be welded onto the stack interface plate. The stack interface plate takes one anode inlet stream and splits it up into four RFR tubes. The plate then takes the four RFR tube output streams and collects it into one to feed the partially reformed fuel into the bottom of the CSA stack.

Figure 5.1-43 Radiative Fuel Reformer Tube

Cold Flow Testing Validation

Having an equal distribution of gas to all stacks in the module is critical to their performance. To meet this goal CFD was performed on the 2x3 Base. It is important to validate the CFD to give more confidence in the distribution, however testing the distribution at temperature with the process gases is not feasible. Therefore, a cold flow test utilizing air was run with scaled flows.

To select the flow rate for each manifold Darcey pressure scaling was used. This method of scaling flows adjusts the flow rate based on the density and viscosity of the test vs. actual gases so that the pressure drop through the system during the test is equivalent to the actual process flows. These flows were then run in the existing CFD model, as described above in Section 4.1. If the results of the laboratory test with air match the CFD with air, we have increased confidence in the process gas CFD. Table 5.1-4 below shows the flow rates and pressure drops that were tested in the lab.

Table 5.1-1 Cold Flow Values

Stream	Calculated Air Volumetric Flow Rate @ 15°C, 1 atm [SLPM]	Calculated Air Volumetric Flow Rate Per Outlet [SLPM]	Actual Manifold Pressure Drop [IWC]	Actual Porous Media/Orifice Pressure Drop [IWC]	Total Pressure Drop [IWC]
Fuel In	950.3	158.4	5.7	12.8	18.5
Fuel Out	1387.5	231.3	1.9	12.8	14.7
Oxidant In	4698.1	391.5	9.3	6.5	15.8
Oxidant Out	4595.8	383.0	10.3	13	23.3

To test the flow distribution some additional equipment was needed: a flow meter to measure flow, a pressure tap to measure backpressure, and an orifice to simulate the stack's backpressure. Based on

previous experience with distribution tests, if the flow resistance for each outlet is different that can have a big impact on the distribution. Each port had to have the exact same setup to minimize this effect.

Sourcing a flowmeter with sufficient range, accuracy, and required low pressure drop was a major challenge. The only meters that existed and met all the criteria were prohibitively expensive. To overcome this challenge, custom venturi flow meters were 3D printed. A cross section of these flow meters can be seen in Figure 5.1-44. They utilize the venturi effect of a reduced static pressure in a constricted section of pipe. The ratio of cross-sectional areas was chosen so that there was ~ 5 IWC pressure difference between the throat pressure tap and the inlet pressure tap at the nominal flow rate. Different flow meters were required for the anode and cathode manifolds due to the difference in the "per outlet" flow rate. These flow meters were serialized and calibrated using a laminar flow element to generate a flow vs differential pressure curve for each flow meter.

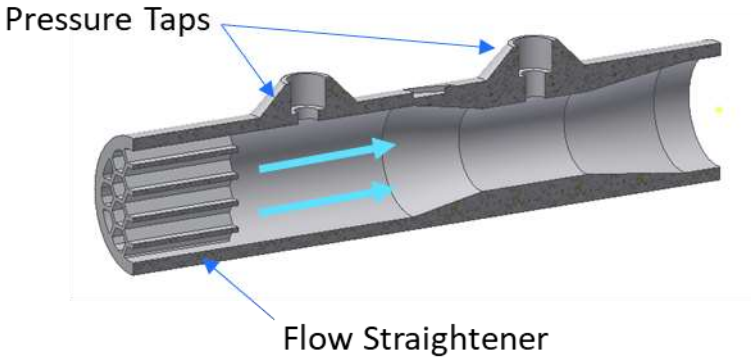

Figure 5.1-44 3D printed venturi flow meter CAD model.

Sourcing an orifice with accurate pressure drop was also a challenge. Based on previous experience a simple hole orifice needed to have extremely precise dimensions in order to have a consistent backpressure. Similar to the flowmeters purchasing these orifices would be prohibitively expensive. To overcome this adjustable 3D printed orifices were used. The 3D printed orifices had a rotating inset that when rotated changed the open area. They were calibrated to have the correct backpressure at the flow rates stated in Table 5-1. A set of orifices were made for each of the 4 distribution tests. A CAD model of the adjustable orifices can be seen in Figure 5.1-45.

Figure 5.1-45 3D printed adjustable orifice.

The complete setup for flow measurement can be seen in Figure 5.1-46 and Figure 5.1-47 below. Each port on the manifold being tested had a pressure tap, flow meter, and adjustable orifice. A 7/8" tube was used to connect them in series. A blower was used for Cathode In and Anode In tests to supply the air to the base. For the Cathode Out and Anode Out tests it was necessary to pull a vacuum and suck the air through the manifold rather than push air through it, so the flow moved in the correct direction. To accomplish this, the manifold was connected to the suction inlet of the blower. The venturi meter and orifices were marked with flow direction arrows to ensure they were installed in the correct direction since the suction test reversed the direction of the flow. An outline of the testing procedure and a summary of the results are listed below.

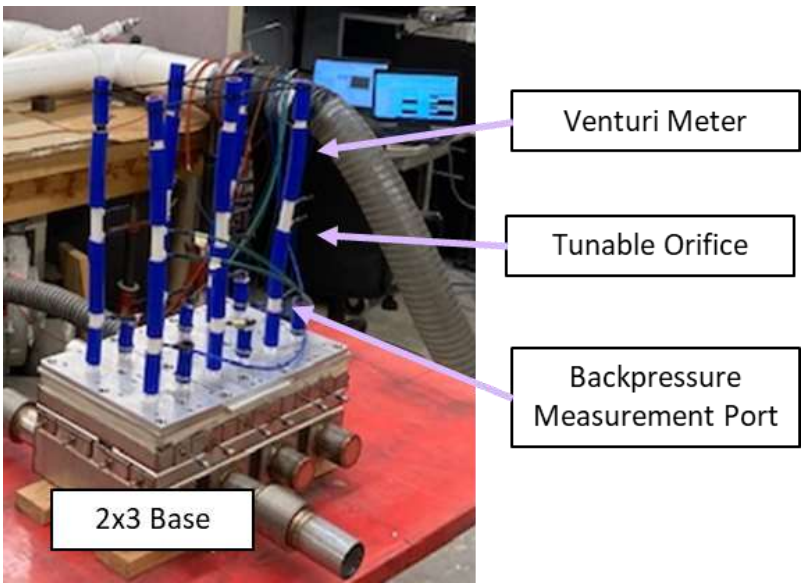

Figure 5.1-46 Test setup for flow distribution test.

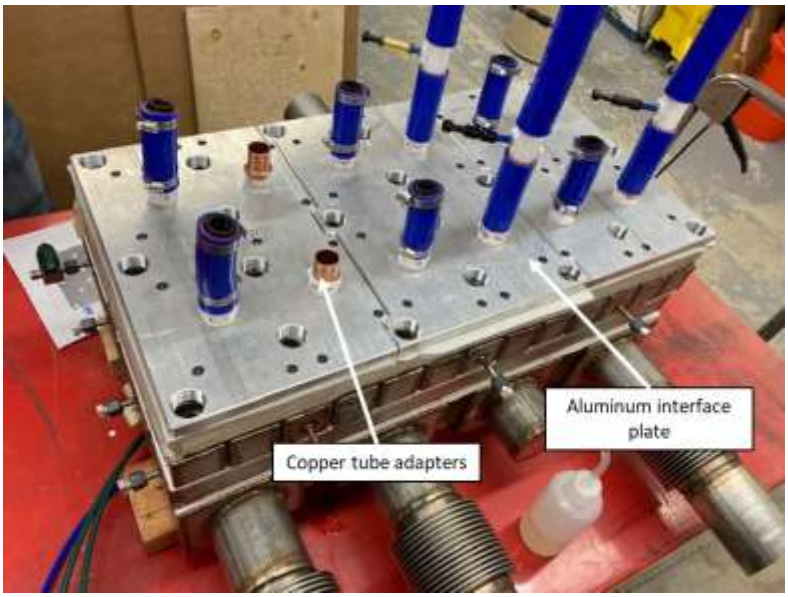

Figure 5.1-47 2x3 base setup.

PROCEDURE

- Setup
  - Mount aluminum interface plate to top of 2x3 base.
  - Install Copper tube adapters onto ports on aluminum plate.
  - Connect silicon tube assemblies (includes pressure tap, flow meter, and orifice) onto copper tube fittings for manifold being tested.
- Distribution test (pushing air)
  - Perform this test for cathode in and anode in ports on 2x3 base.
  - Connect blower outlet to 2x3 base inlet.
  - Adjust speed of blower to supply total air flow rate shown in Table 5-1.
  - Measure differential pressure for each venturi flow meter.
    - Calculate flow rate based on flow meter calibration.
  - Repeat test at 2 alternate flow rates.
- Distribution test (sucking air)
  - Perform this test for cathode out and anode out ports on 2x3 base.
  - Connect blower inlet to 2x3 base outlet.
  - Adjust speed of blower to supply total air flow rate shown in Table 5-1
  - Measure differential pressure for each venturi flow meter.
    - Calculate flow rate based on flow meter calibration.
  - Repeat test at 2 other flow rates.

In addition to the 6 stack CFD distribution being validated the distribution was tested if only 2 stacks were installed on the 2x3 base. No CFD was performed for this configuration, however this is how the base was used in the test facility, so it was important to ensure it has an even distribution. Figure 5.1-48 below shows which ports on the 2x3 base were used in the 2-stack

distribution test. The same procedure as the 6-stack distribution test was used, except the ports not circled in Figure 5.1-48 were capped off. No ports were capped off for the cathode in 2 stack distribution tests. The module is a cathode in flush environment so instead of capping off ports the base was tested with all 12 ports open at 1/3 the total flow rate.

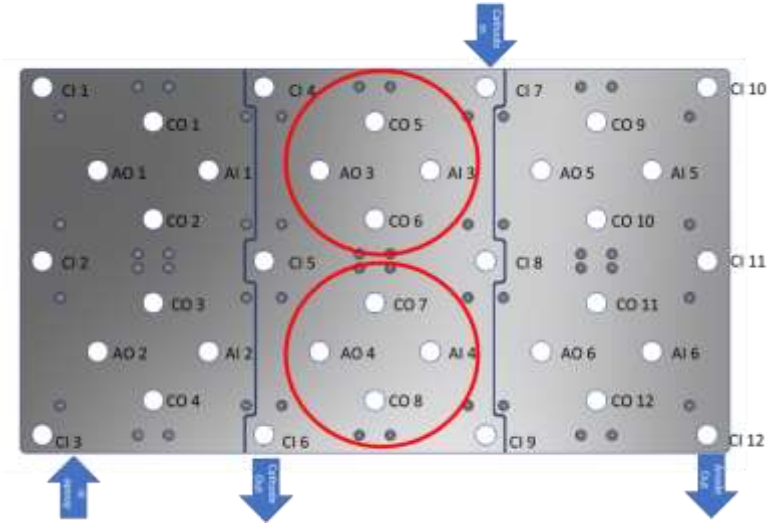

Figure 5.1-48 2-Stack distribution base ports tested.

RESULTS

The distributions met or exceeded the expectations based on the CFD analysis. The bar charts below (Figure 5.1-49-Figure 5.1-52) show the percent deviation from the average flow measures compared with the CFD results. Additionally, the distribution of the 2-stack configuration was even better than the 6-stack configuration. Those results are shown below in Figure 5.1-53, Figure 5.1-54, and Figure 5.1-55.

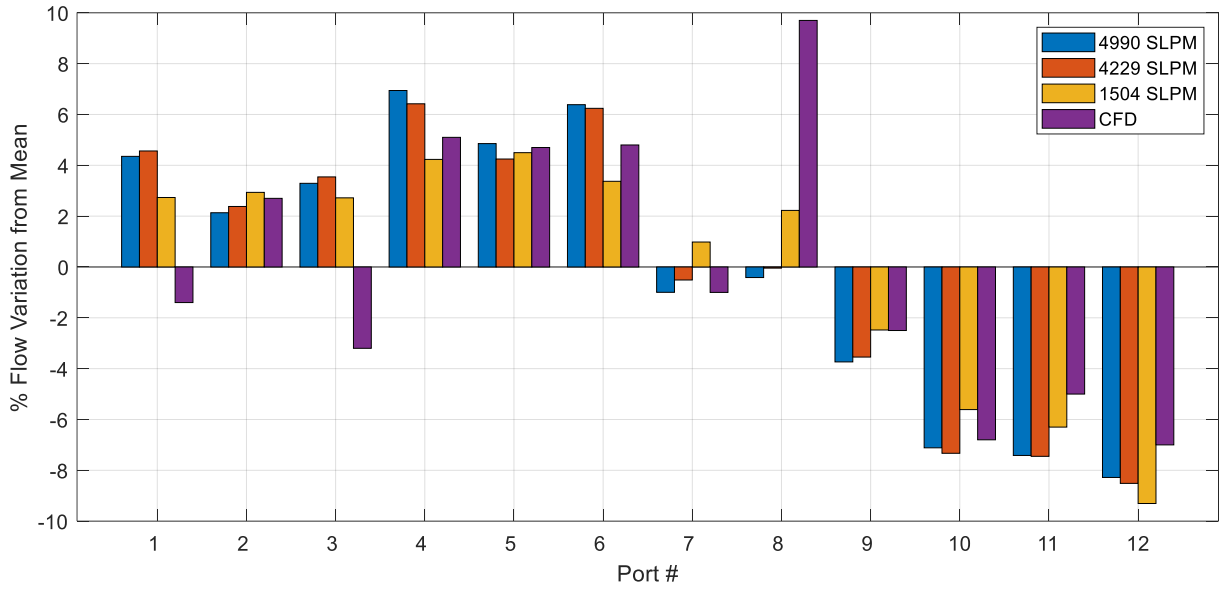

Figure 5.1-49 Cathode In flow distribution.

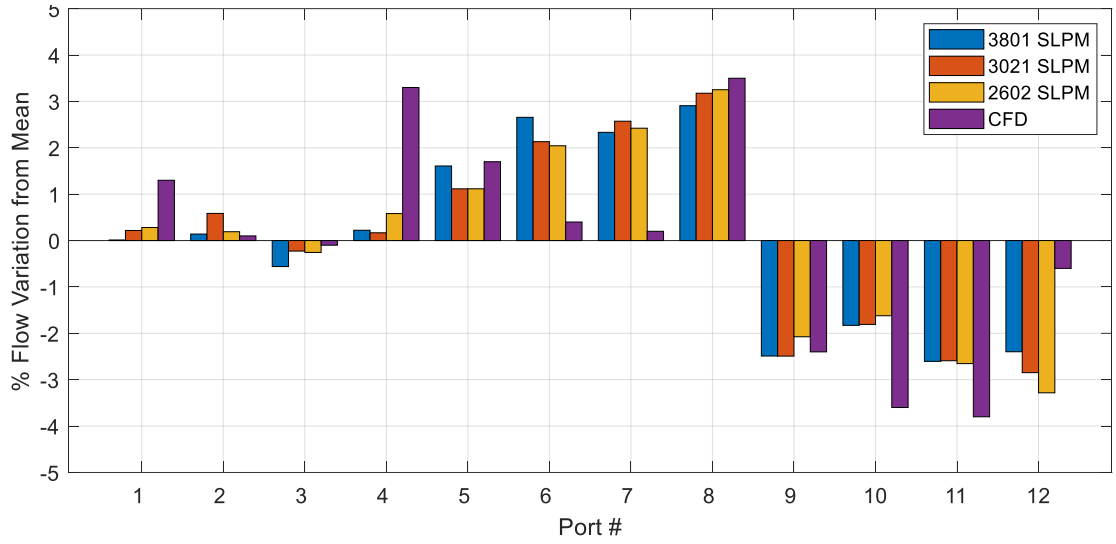

Figure 5.1-50 Cathode Out 6-stack flow distribution.

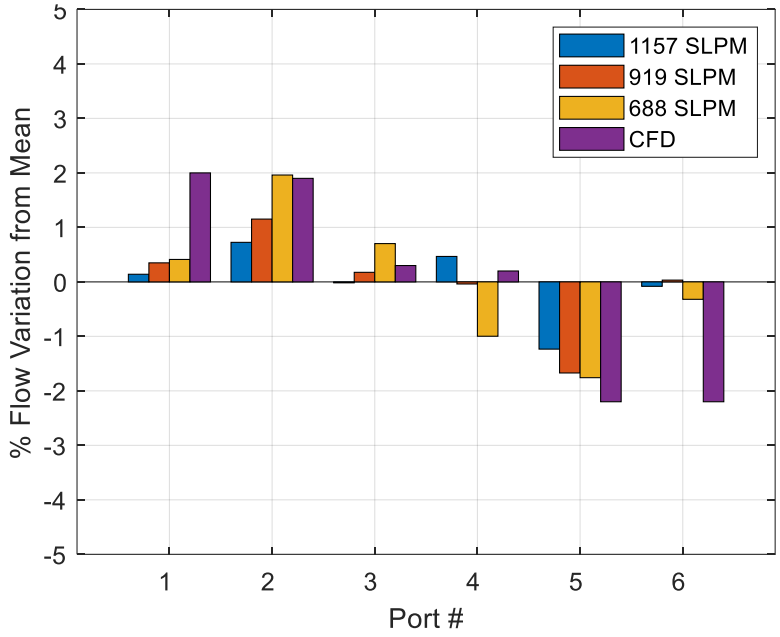

Figure 5.1-51 Anode In 6-stack flow distribution.

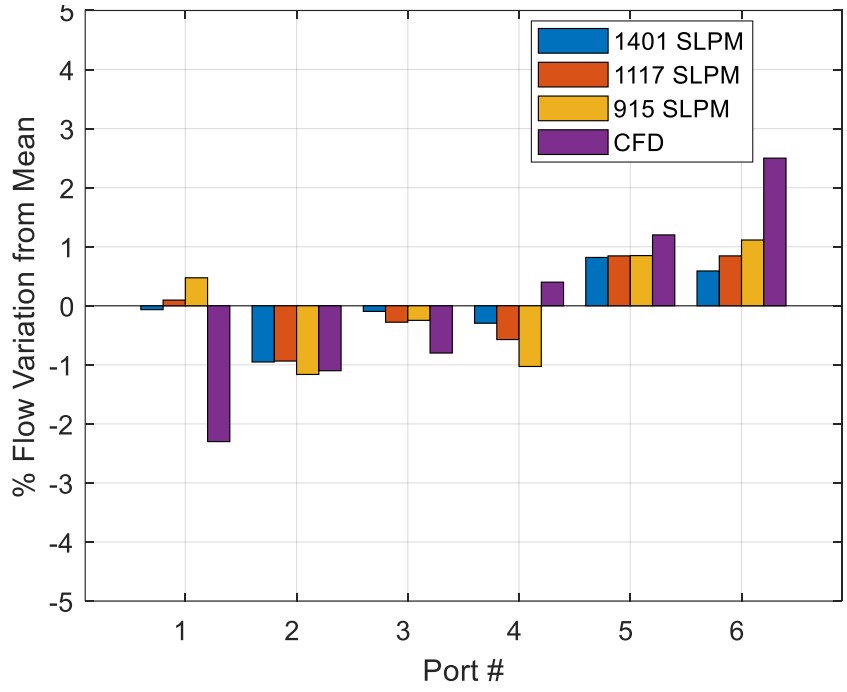

Figure 5.1-52 Anode Out 6-stack flow distribution.

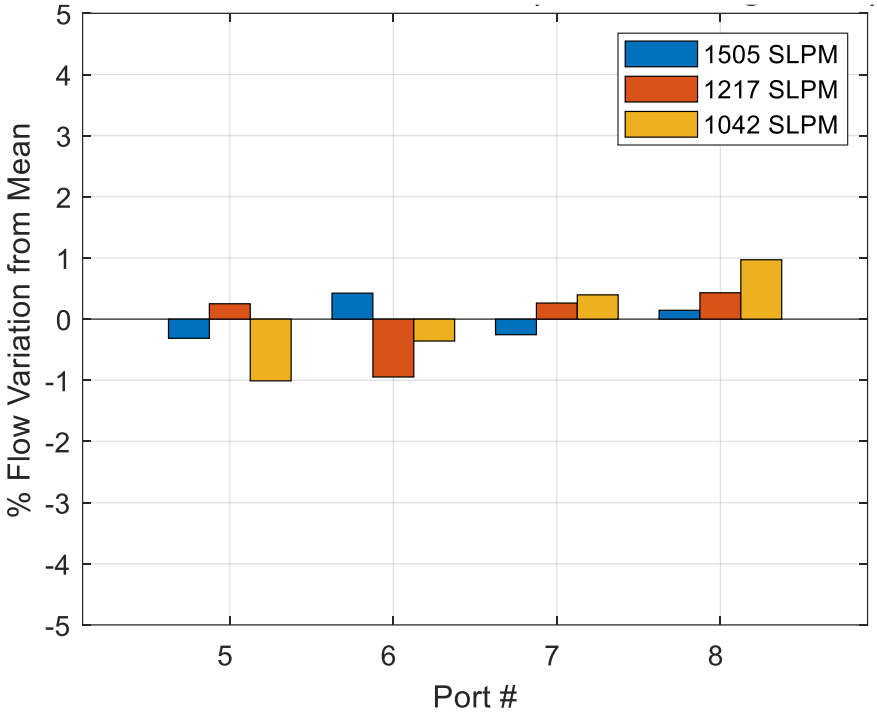

Figure 5.1-53 Cathode Out 2-stack flow distribution.

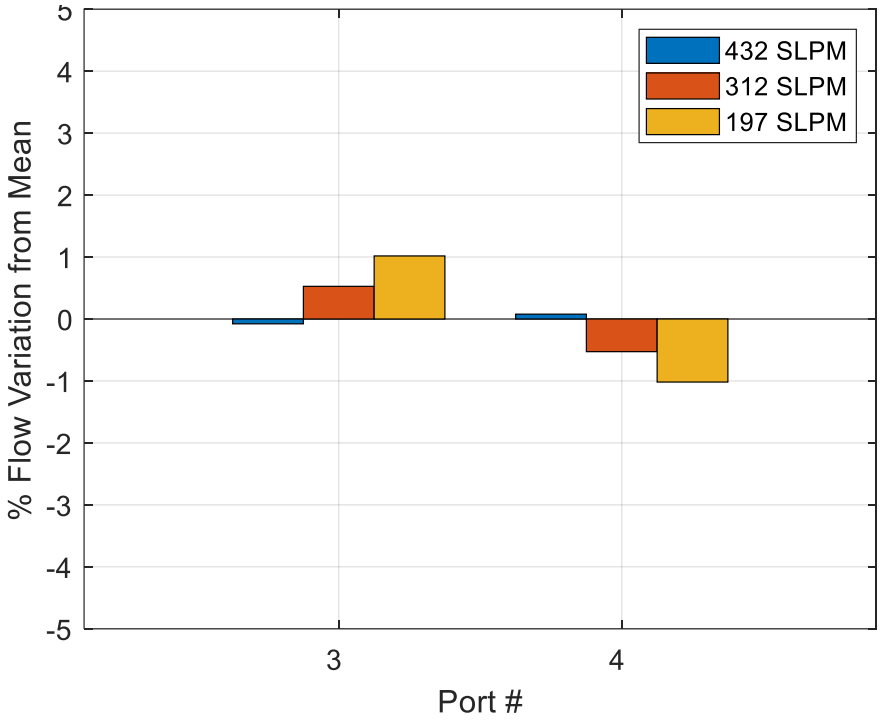

Figure 5.1-54 Anode In 2-stack flow distribution.

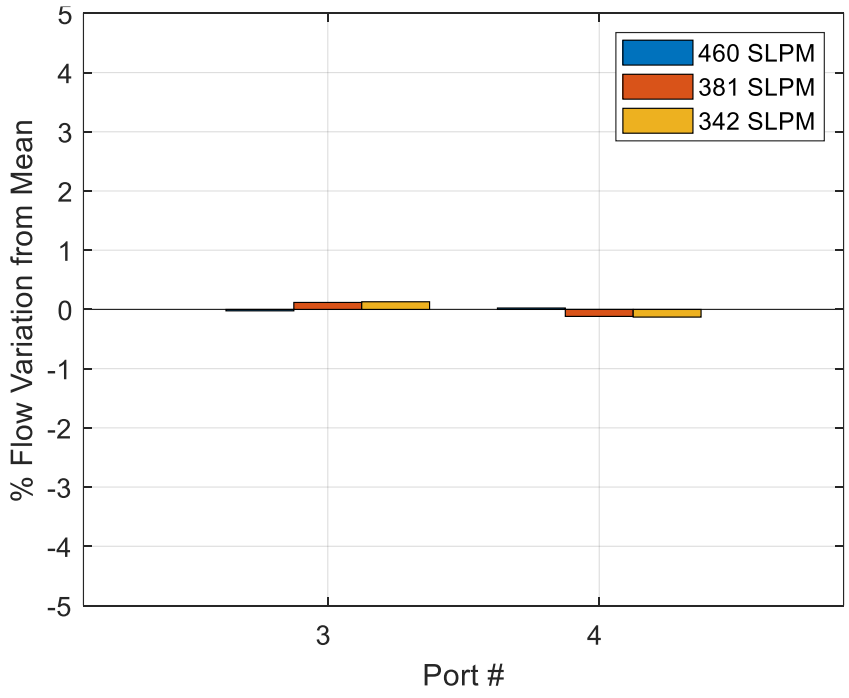

Figure 5.1-55 Anode Out 2-stack flow distribution.

Radiative Fuel Reforming Testing

FCE tested five new Radiative Fuel Reformers with the goal of raising the RFR exit temperature as well as decreasing the amount of methane reformed. Previous RFR designs reformed more

methane than desired, so the 4 Series reactors tested this were made with less catalyst. As expected, the 4 Series RFR's with reduced catalyst resulted in lower methane conversion, increasing the exit methane concentration into the desired range.

To raise the RFR exit temperature, several baffle designs were considered for use in the bottom section of the RFR to increase the heat transfer. Inspired by FCE's successful use of similarly shaped baffles in other process equipment, FCE found commercially available stainless steel clipped washers. After receiving those washers FCE welded them to the bottom section of the RFR tube in 1" intervals at 180° to one another along the feed tube, as shown in Figure 5-20 below.

Figure 5.1-56 RFR with Half-Moon Baffles Welded to RFR Lower Portion

Half-moon shaped stainless steel washers should increase heat transfer between the wall of the RFR and the reformate gas with little pressure drop increase. Ambient temperature flow testing revealed that the total pressure drop of the reformer would increase by less than 1.0 iwc at rated power flow rates with six half-moon washers spaced at 1" intervals.

The performance of the 4 Series RFR's tested is shown in Table 5-2 below. While the exit methane content moved into the desired range of ~ 11%, the baffles did not appear to have an impact on the exit temperature. FCE desires to see the RFR gas exit temperature in the neighborhood of 650°C to match the stack temperature at the anode inlet region.

Table 5.1-2 4-Series RFR Performance at Rated Power condition

RFR ID	RP Exit [CH4] (% Dry Basis)	RP Exit Temp (°C)	RP Total DP (iwc)	SS Baffle Washers
4C	10.6	636	7.3	None
4B	11.2	615	7.8	None
4B-2	11.4	630	7.9	None
4C-2	10.4	623	8.4	Yes
4B-3	12.1	630	9.0	Yes

Another area of RFR refinement explored was adding reforming catalyst along the RFR feed tube inner wall. Successful coating was verified by taking a GC of the feed tube exit at the top of the reformer tube with the addition of a GC port. The decision has been made to proceed with a coated feed tube for the initial module installation.

NextGen SOFC 30kW-1 Test Station Modifications and Preparations
The Cathode Inlet heater was relocated in the 30kW-1 facility such that it would be immediately upstream of the module entrance. This was done to limit the amount of heat loss to ambient from the hot cathode air (~700°C) prior to going into the 40kW module. The SOFC cathode Inlet heater is one of the largest heaters in the 30kW-1 facility being approximately 30kW and is responsible for bringing the cathode air up to SOFC operating temperature.

The SOFC Cathode Air Mass Flow Controller arrived following warranty related repair and was installed. This mass flow controller is the largest unit available from the manufacturer (5,000SLPM unit). The MFC was selected due to the high Cathode Air flow rate requirement of the 40kW SOFC when operating at Rated Power and low air utilization. Due to extended delays in the global supply chain as well as staffing challenges from the manufacturer the unit took longer than usual to diagnose and repair.

The 30kW-1 Next Gen IO cabinet was successfully tested after discovering a wiring issue which led to communication problems with the PLC. The team quickly identified and resolved the issue.

FCE is planning on testing the 40kW module initially with two out of the six SOFC stacks, including four reformers per stack, in order to put the minimum number of stacks at risk while this new module design is validated.

Anode Recycle Capability
An Anode Recycle blower was taken from a previous SOFC system for use in the Next Gen SOFC Module Test. This hot anode recycle blower (MAWT = 850°C) allowed the characterization of the self-reducing properties of the reforming catalyst used in the RFR's, and the ability of the RFR's to produce hydrogen at low temperatures, during system Heat Up, to protect the fuel cells. If the RFR produces hydrogen as expected, it would allow FCE to Heat Up the NextGen module from ambient temperature without using external hydrogen. The Anode Recycle loop was used during the Fuel Enable step to operating temperature. After the module Heat Up is completed, the spectacle flanges going to and from the anode recycle blower were changed from Open to Closed to prevent bypass flow for the subsequent power operations.

The welded version of the stack distribution base (Figure 5.1-57) was found to have leaks in the fuel-in manifolding. This was discussed above and after further investigation, the leak is not accessible to repair. Instead of attempting to repair or rebuild the welded version of the stack distribution base, a new design was pursued using a machined stack distribution base.

Figure 5.1-57 Stack Distribution Base Assembly (Welded Version)

The new stack distribution base design features machined plates that are brazed together **(**Figure 5.1-58**)** with lower ducts that have a sheet metal box tube construction. This machined design has flow channels very similar to the welded version of the stack distribution base. This similarity limits the amount of computation fluid dynamics (CFD) simulations that need to be run to ensure good flow and temperature distribution to the stacks.

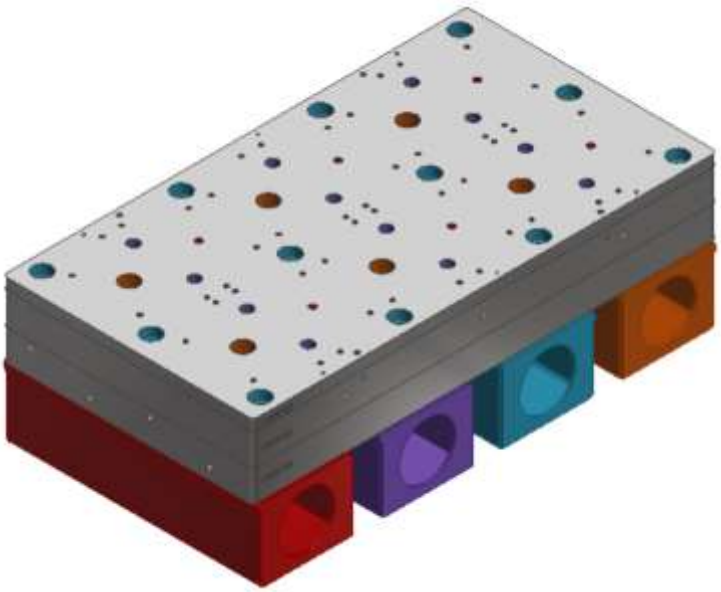

Figure 5.1-58 Stack Distribution Base Assembly (Machined Version)

The CFD simulation results for the machined version of the stack distribution base were found to be similar to the welded version (Table 5.1-3). The temperature range for the anode in flow was only 7.1°C and the mass flow distribution from average to the CSA stacks was -1.6% to 2.3%. Both are within the acceptable targets for the fuel flow. The cathode in and out flow were within the acceptable targets and were closely matched to the welded version results.

Table 5.1-3 Stack Distribution Base Machined Version CFD Results

Flow Stream	Maximum Temperature Deviation	Mass Flow Rate Deviation Range
Anode In	7.1°C	-1.6% to 2.3%
Anode Out	1.1°C	-0.4% to 1.7%
Oxidant In	12.7°C	-5.5% to 6.2%
Oxidant Out	N/A	-3.4% to 2.9%

Progress has been made on completing the stack distribution base brazement. The three distribution base plates were sent to be heat treated and ground down to within a 0.002" flatness. The plates have a strict flatness requirement because each braze foil layer is only 0.002" thick. The braze foil was cut by waterjet to match the distribution base plate geometry. Figure 5.1-59 shows the exploded assembly of the 2x3 stack distribution base brazement.

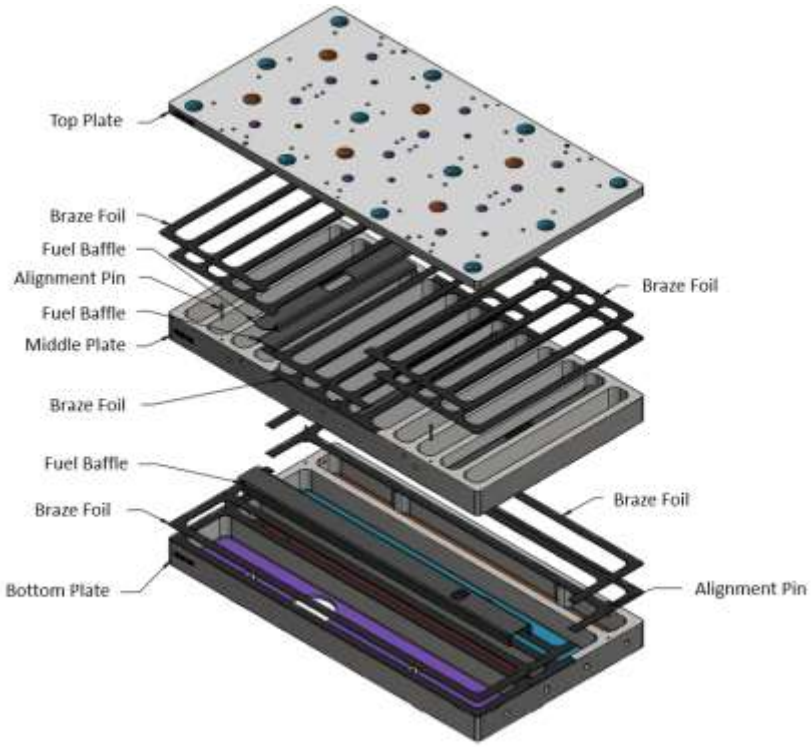

Figure 5.1-59 Exploded Assembly View of 2x3 Stack Distribution Base Brazement

The first step for the assembly was to attach by stitch weld all the sheet metal baffles (Figure 5.1-60). The baffles are designed to improve flow and temperature distribution of the fuel to the 6 stack positions. A single fuel inlet baffle is placed inside the bottom plate. A double layer baffle is placed inside each of the three fuel inlet channels in the middle plate.

Additional steps were taken to ensure a successful braze with no leaks. Cyanoacrylate glue dots were placed periodically along the channel walls to secure the braze foil in place. A 0.002" thick stainless-steel shim was placed periodically along the channel walls. The shim controls the

distance between the plates to prevent the braze material from getting pushed out as it melts at brazing temperatures. After the next plate was placed on top, by using the openings on the plates it was verified that none of the foil shifted during assembly.

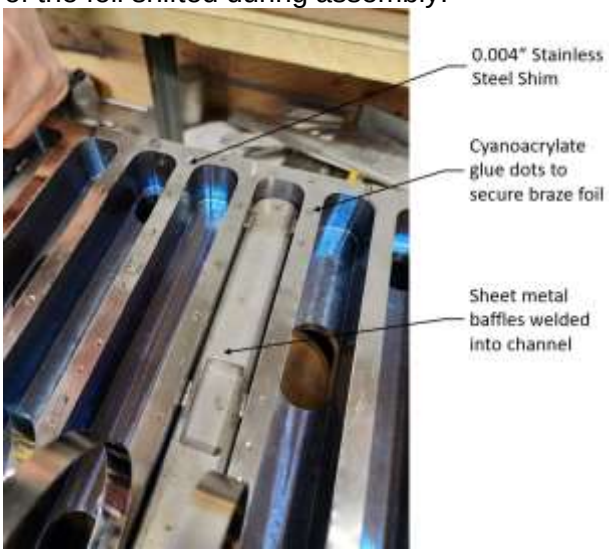

Figure 5.1-60 Assembly Details of Stack Distribution Base

The process was repeated for the additional layers of braze foil and plates. Figure 5.1-61 shows the completed stack distribution base brazement sub-assembly. This sub-assembly forms the primarily flow channels which distributes the fuel and oxidant gases to each of the 6 CSA stacks.

Figure 5.1-61 Completed Distribution Base Assembly, Ready for Brazing

Radiative Fuel Reforming Testing

Testing consisted of endurance testing the Radiative Fuel Reformer RFR 4C-3 and running that RFR in a variety of conditions in support of various fuel side operating conditions.

Table 5.1-4 below lists the Series 4 RFR's tested to date.

Table 5.1-4 RFR Series 4 Performance at Rated Power Condition

RFR ID	Rated Power Runtime, (Hours)	Exit [CH4] % Dry Basis	Exit Temp TE-504 °C	RFR Main Tube Length
4C	240	10.6	636	Short
4B	456	11.2	615	Mid
4B-2	624	11.4	630	Mid
4C-2	288	10.4	623	Short
4B-3 (BOL)	168	10.7	635	Mid
4B-4	576	11.4	640	Mid
4C-3	2016	11.6	642	Short

RFR 4C-3 has run for over 2,000 hours at rated power condition. As shown in Figure 5.1-62 below, a modest performance change has been observed during the endurance operation, resulting in less methane getting reformed and a lower temperature at the exit. Diagnostic tests performed while operating have not indicated the cause of the performance drop.

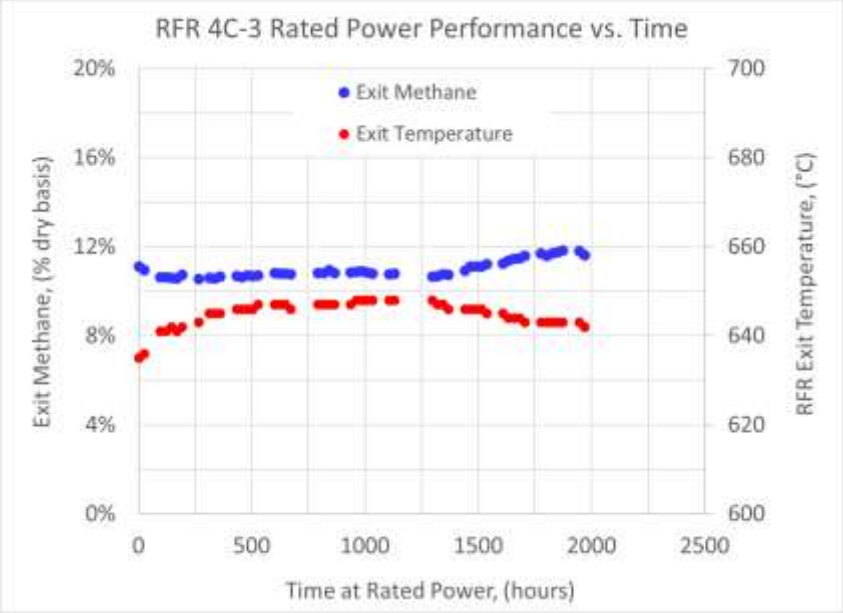

Figure 5.1-62 RFR 4C-3 Performance Change Plot

The RFR bypass humidifier was upgraded in preparation of operating in the facility was installed in the 30kW-1 test stand (See Figure 5.1-63 below).

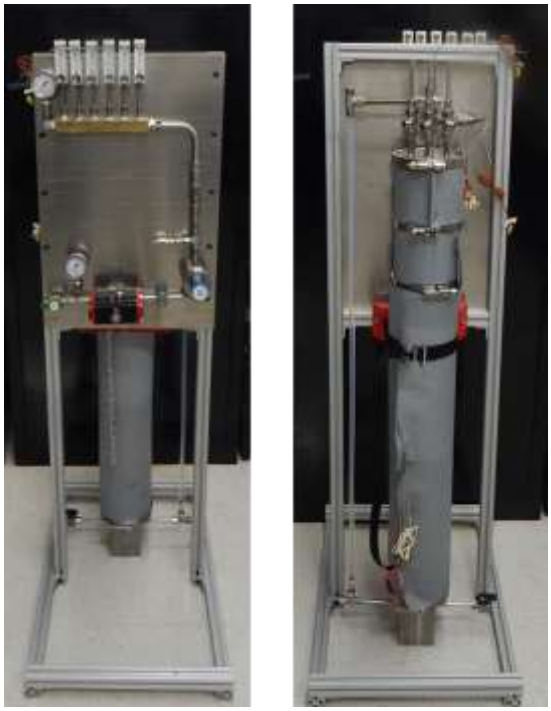

Figure 5.1-63 Upgraded RFR Bypass Humidifier

The bypass humidifier has undergone several upgrades to meet the expected range of operating conditions. The most significant change that has been made is adding height to the bypass humidifier. Originally it had a height to allow a differential pressure capacity of 20iwc from anode inlet to anode exit. However, a performance test revealed that water would be entrained in the exiting gas. In order to eliminate the possibility of water entrainment, the maximum water level in the humidifier was reduced by 8", to bringing the maximum allowable differential pressure from 20 to 12iwc. This was deemed to be insufficient based on the expected anode-side pressure drop of 16iwc. For this reason, the height of the bypass humidifier, including the internal tube length, was increased by 12", to allow the bubbler to operate with an anode pressure drop of up to 24iwc.

It was determined that the selected heater power of the bypass humidifier would be insufficient at 1.5 kW. It was therefore increased to 2.2 kW by adding higher watt density heaters, to assure that it has the capacity to vaporize sufficient steam at the maximum fuel flow rate.

NextGen SOFC Stack Leak Test Results

Two 350-Cell SOFC Stacks have arrived in Danbury from Calgary and were leak tested. These two SOFC stacks had, prior to shipping, successfully passed the leak test in Calgary. It is important that the stacks pass the leak test following transport from Canada to ensure that the stacks were not damaged in transit. The Danbury leak test results were passing, and consistent with those performed in Calgary. The leak test consists of pressurizing the anode side of the SOFC stack with air to a modest pressure level and measuring the leak rate several times to ensure repeatability and accuracy.

The brazing of the stack distribution base was completed. Because the distribution base separates fuel gas from oxidant gas, there are strict requirements for allowable leak rates. The distribution base did not meet the required leak rates for safe operation. A pressure decay leak test was setup (Figure 5.1-64) to quantify the leak rate in the distribution base. The base was pressurized to 2 psig with air at room temperature and lost pressure rapidly when the air source was shut off. There were severe leaks in the distribution base that are too high to measure with a pressure decay leak test.

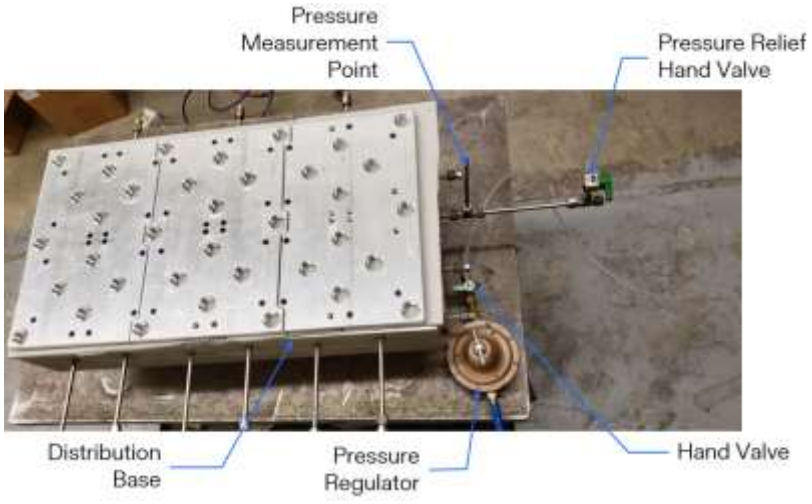

Figure 5.1-64 Leak Test Setup for Brazed Distribution Base

A qualitative leak test was done with liquid leak detector. The fuel-in channel was pressurized to 2 psig and the leak detector was used across the brazed seams of the distribution base (Figure 5.1-65). The leak was present along the majority of the seams and shows a significant amount of cross-leak between the channels and to the ambient environment.

Figure 5.1-65 Assembly Details of Stack Distribution Base

The severe leakage in the brazed distribution base was deemed irreparable and the distribution base was redesigned to be a single plate casting (Figure 5.1-66). By redesigning the base to be primarily a single plate casting, all leak paths can be qualified, and repaired if necessary, during assembly. The cast plate design is with FCE vendor who is currently in process of producing the casting.

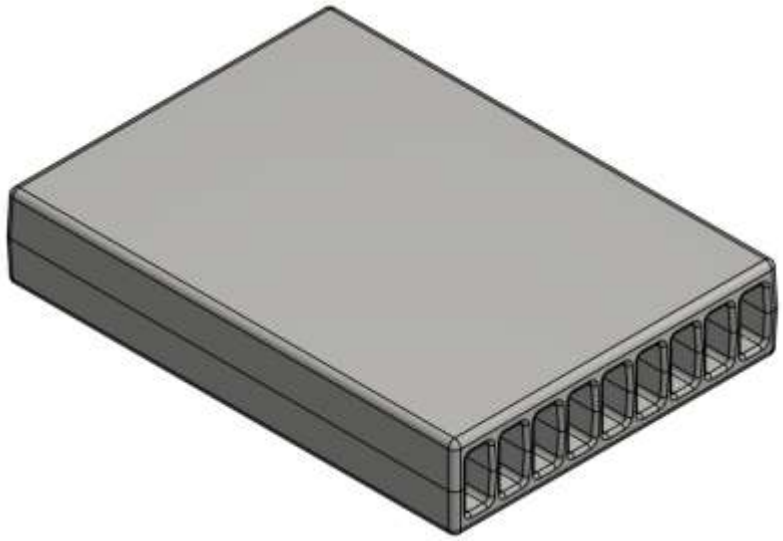

Figure 5.1-66 Completed Distribution Base Assembly, Cast version

The cast single-piece plate was machined and the welded sheet metal components to construct the distribution base unit (Figure 5.1-67) were recieved. The design allows for leak testing between weld steps so that any potential leak can be found while still accessible and repaired. The design of the cast distribution base has a larger footprint and rotates the CSA stacks 90 degrees compared to the brazed version. These changes drive some rework on other components in the 40kW module.

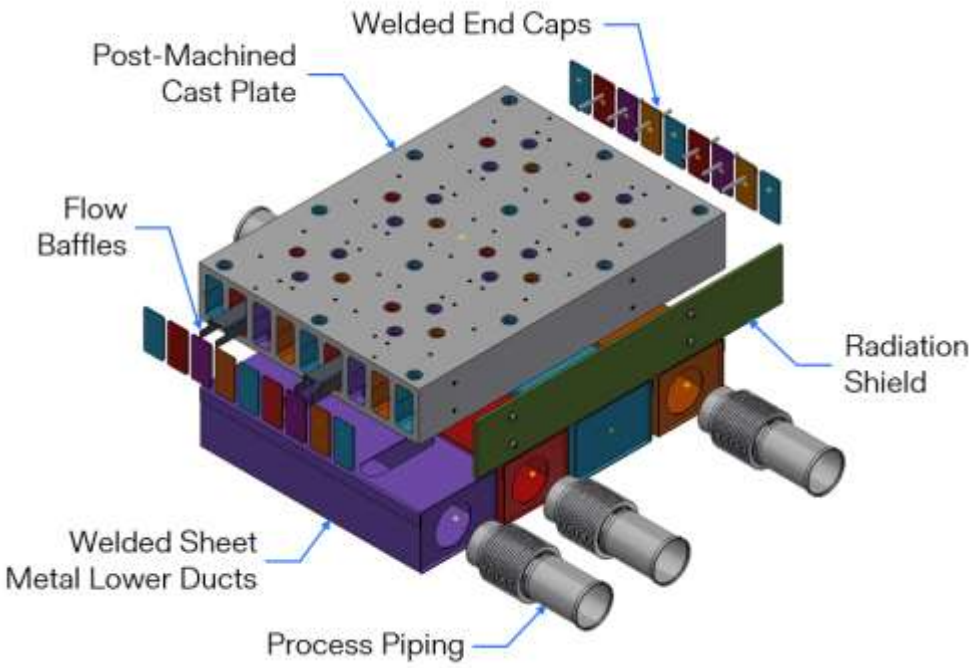

Figure 5.1-67 Distribution Base Weldment Assembly (Cast Version)

Radiative Fuel Reforming Testing

To review, this RFR began operation in mid-July and ran for nearly 2,300 hours of Rated Power operation. This reformer design incorporates all the lessons learned up to this point in SOFC RFR development. The RFR performed well and was shut down in mid-October due to an unrelated CO2 supply issue.

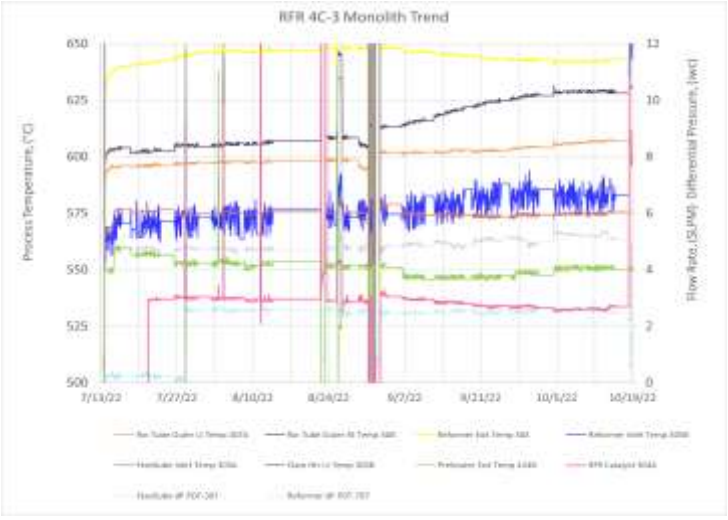

Figure 5-5 RFR Test Stand Performance Trend

The performance change that started to occur in early September (shown in Figure 5.1-68) was determined to be from a series of high flowrate and high pressure drop tests exploring the operational envelope of system configurations and fuel compositions with respect to RFR performance. After carefully investigating the data and operations throughout this time period, FCE has determined that the RFR experienced a test-stand related degradation event at that time, and therefore this type of degradation is not anticipated in a field-installed RFR.

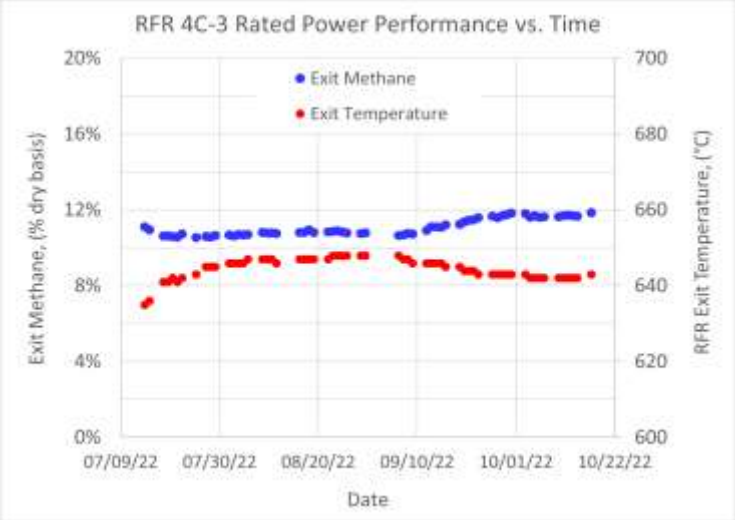

Figure 5.1-68 RFR 4C-3 Performance Trend

The performance change that occurred in early September was noted. In order to mitigate the performance changes observed with respect to time, the steam content was increased to move reforming equilibrium towards additional methane reforming. After the steam content was increased performance stabilized and was running well at the time of RFR shutdown.

Figure 5.1-69 Picture of RFR 4C-3.

After cooling down and inspecting the internals of the reformer (shown above in Figure 5.1-69) FCE found small amounts of coke formation on the inside of the RFR. FCE believes this issue to be an artifact related to the test stand.

High Temperature C-Ring Seal Testing

FCE performed leak tests on its high temperature seals at the stack base to ensure long life and high performance. High temperature seals are employed in the CSA stack to seal the anode inlet

and exit as well as the cathode exit of the CSA stack, to channel the gases to the intended destination and prevent harmful gas crossover. A C-Ring Seal design has been selected to achieve the seal.

A purpose-built leak test stand was created using a muffle furnace to safely test the C-Ring seal using hydrogen as the internal gas. While the seal test could be accomplished using an inert gas such as helium, nitrogen, or argon, using hydrogen gives three benefits. First, using hydrogen has the benefit of directly measuring the leak rate without the need for normalization based on the gas density, molecular geometry, and viscosity. Second, using hydrogen reveals the seal's resistance to dual atmosphere corrosion. And finally, any hydrogen leaks oxidize, leaving witness marks to show the precise location of the leak. From the precise location, the leak mechanism is more determined.

Endurance testing, and cyclical testing, of these C-Ring seals is important to make sure that the material can handle high temperatures and temperature fluctuations without degrading. The test plan involves operating the seals up to 750°C for extended periods of time, interspersed with temperature cycling down to 250°C per various schedules. FCE tested these seals at moderate differential pressures (up to 2psid).

Figure 5.1-70 High Temperature SOFC Seal Test Stand

Several steps were taken to ensure that the system would handle hydrogen safely. A picture of the C-Ring seal test stand can be seen in Figure 5.1-70. Some of the engineering design features to guarantee safe testing include area hydrogen sensors, a test stand hood, fixed and limited

hydrogen volume, flowrate limiting orifice, air flow rate to hydrogen flow rate ratio, nitrogen backup to hydrogen flow, constant furnace sweep gas and hydrogen supply interlocks.

The first cast single-piece plate was produced from a 3D printed sand mold at our casting vendor (**Figure** 5.1-71). The casting met the dimensional specifications but had issues with leaks due to cracks on the internal ribs.

Figure 5.1-71 Cast Plate Prior to Clean Up Work

It is critical that the casting does not have any channel-to-channel leakage as each channel alternates between air and fuel gases. Each channel was pressure tested and the adjacent channel's pressure was measured to determine if there was a cross-channel leak (Figure 5.1-72). The channels were also pressurized individually with liquid leak detector used on adjacent channels, top of the plate, and bottom of the plates to identify the source of any leaks.

Figure 5.1-72 Two Channel Leak Test Setup

It was found that two out of the eight internal channel-to-channel walls had a severe leak which was difficult to quantify (Figure 5.1-73). The channels were pressurized to 2 psig with room temperature air and it immediately lost pressure when the air source was shut off. This amount of leakage was far above our allowable leak rates between fuel and air. The location of the leak is not accessible for weld repair and the casting was not used. The casting vendor is currently revising the casting process to eliminate the cracking that occurs on the internal ribs.

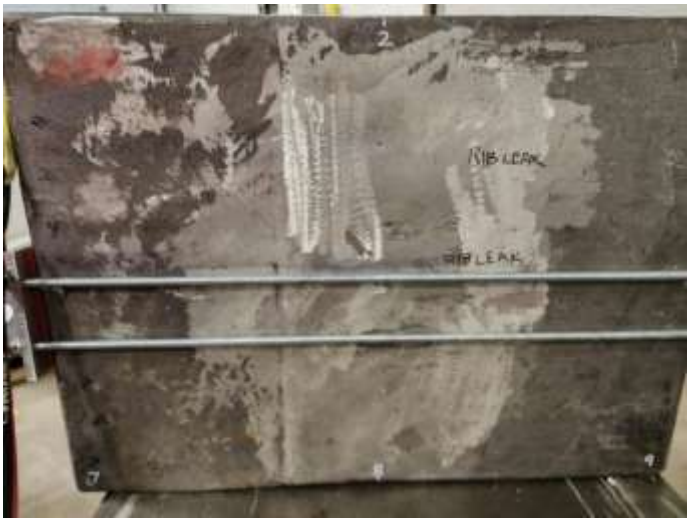

Figure 5.1-73 Channel-to-Channel (Rib) Leak Locations

Radiative Fuel Reforming (RFR) and Adapter Plate Update

RFR Testing this quarter involved developing a test fixture for testing different methods of attaching the feed tube to the adapter plate. Presently FCE is welding the feed tube to the bottom of the adapter plate. FCE plans to test different means of joining the feed tube to the CSA adapter plate. While a small leak is tolerable FCE plans to determine the leak rate of alternate joining methods for design flexibility.

A leak test apparatus having temperature and pressure control capability as well as using different gases to test the leak rate of nitrogen and hydrogen through a test joint. The apparatus is designed to be very safe intrinsically. The outer tube contains any hydrogen leak in the case of small leaks or total test joint failure. A Process Flow Diagram (PFD) of the leak test apparatus is shown below in Figure 5.1-74.

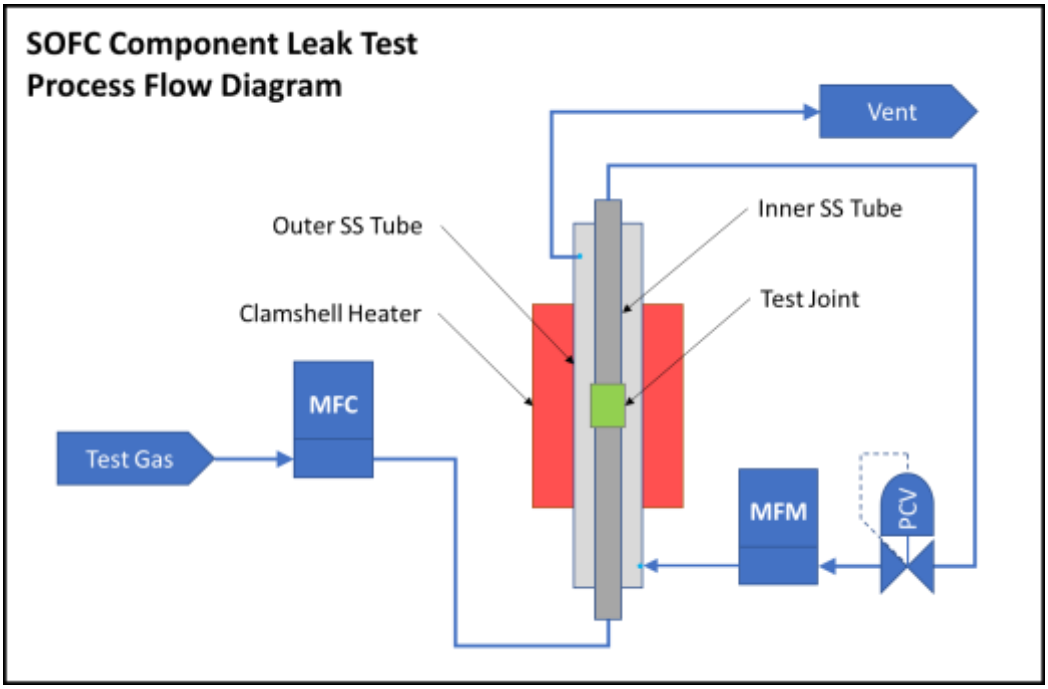

Figure 5.1-74 PFD Component Leak Test Apparatus

CSA Adapter Plate leak testing

The adapter Plate leak test stand (shown in Figure 5.1-75) was created to test each adapter plate ensuring leak free parts post brazing. The test stand can use a variety of gases to test for leaks such as nitrogen, helium, or hydrogen up to 2psig. The test stand is designed with several safety features including a nitrogen sweep, flow orifices to limit maximum hydrogen flow and test gas ventilation via explosion proof exhaust. All six adapter plates being used in the 40kW SOFC module were tested and found to be leak free.

Figure 5.1-75 CSA Adapter Plate Leak Test Stand

Box Tube Base Version Updates

A box tube 2x3 distribution base was developed as a parallel path to the cast version. The box tube version is constructed with off-the-shelf 2” x 4” and 1.5” x 4” box tubes (Figure 5.1-76). The advantage over the cast design is that each component is relatively small and lightweight which allowed most fabrication work to be rapidly done in-house.

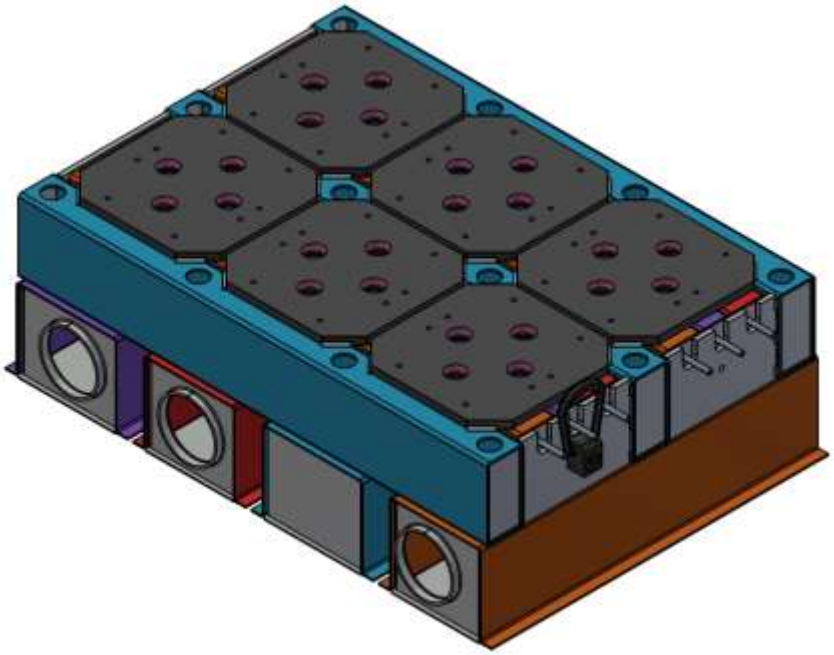

Figure 5.1-76 2x3 Distribution Base Box Tube Version CAD Model

Two individual 1x3 stack mounting sections consisting of a fuel in, oxidant out, and fuel out box tube are fabricated. The oxidant in sub-assembly, which is made from 3 box tubes connected with plate, is also completed. Figure 5.1-77 shows the 1x3 stack mounting sections inside of the oxidant in sub-assembly with 4 blanking plates and 2 adaptor plates on top. This configuration

was used to run the 2-stack setup. The blanking plates can be replaced with adaptor plates for the 6-stack configuration.

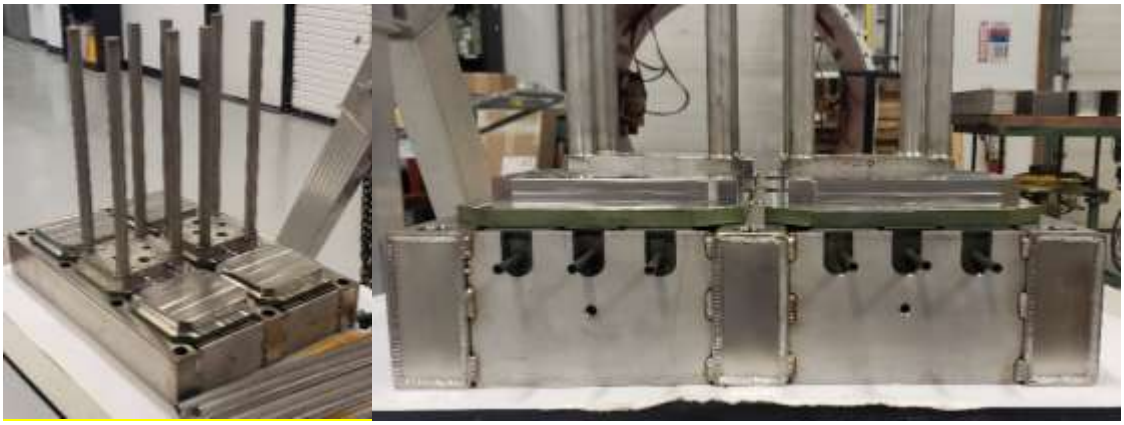

Figure 5.1-77 2x3 Box Tube Base Construction Progress

Casting Base Version Updates

The failed first casting was identified to have two issues: the 3D printed mold uses a lower quality sand which results in a rougher finish and cold cracking occurred at the ribs due to uneven cooling. Our vendor produced a second casting using a wood pattern mold with higher quality sand and slowly control cooled the casting in a furnace. This resulted in a much higher quality casting (Figure 5.1-78) that passed our leak tests. The casting is then machined for all the gas port and mounting holes.

Figure 5.1-78 Internal Cast Channel Surface Finishes

Each channel of the casting was leak tested at either 5 or 10 psig over 5 minutes and the pressure decay was measured. The only leak evident was at the gasket to casting interface across all channels. There was no evidence of cross-leak between the channels using a second pressure gauge in the adjacent channels (Table 5.1-5). The cast version of the distribution base is the preferred option for future builds, but the module test was done with the Box Tube version.

Table 5.1-5 2x3 Casting Leak Test Results

Channel	Test Pressure [psig]	Pressure Drop [psi]
1	5	0.09
2	5	0.05
3	5	0.07
4	5	0.00
5	5	0.00
6	10	0.04
7	10	0.01
8	5	0.09
9	5	0.05

5.2 Module Test

Approach:

A test plan was thoroughly vetted out along with input from a HAZOP (Hazard and Operability) review. The test plan was provided to the DOE prior to initiating testing.

Results & Discussion:

NextGen SOFC Module Installation and Test

The NextGen SOFC module was installed into the 30kW-1 facility. The anode inlet and exit as well as the cathode inlet and exit piping were welded into the facility. Following welding high temperature insulation was added to the piping to mitigate heat loss.

Two stacks were installed in the module along with their RFR's (Figure 5.2-1). Following piping connections, the in-stack thermocouples, voltage leads, and the current power take-offs were added. Insulation was added to the inside of the module base to reduce heat loss. Pressure transducers and differential pressure transducers were also added to monitor the pressures on the anode and cathode sides. Lastly an IO check was performed to ensure that the HMI is reading all the instrumentation. Then the lid was lowered and sealed.

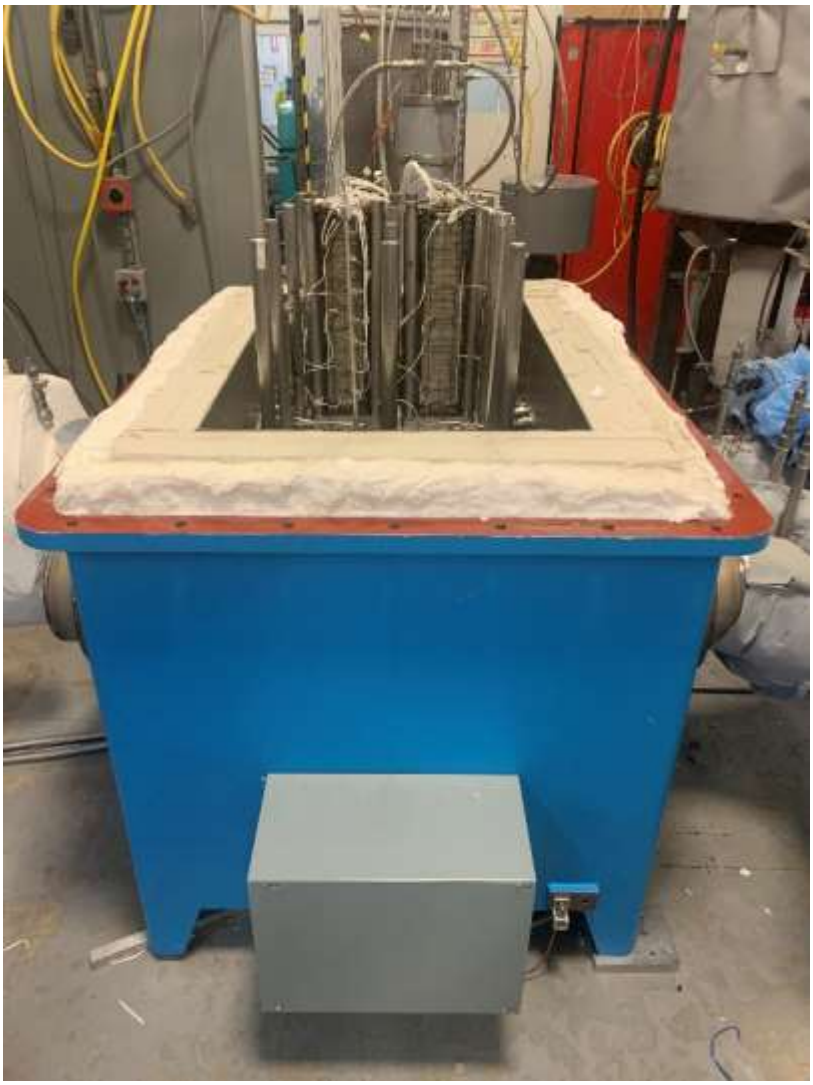

Figure 5.2-1 NextGen SOFC Module with Two CSA Stacks Installed

RFR Self Reduction Test

The module was heated up using inlet gas heating on both the anode and cathode sides. From ambient temperature air and nitrogen was sent to the SOFC cathode and anode respectively. The module was slowly heated to 250°C over the course of several hours.

At 250°C methane and steam were added to the anode side and were recirculated using a small SOFC anode recycle blower. Air was constantly fed to the cathode side during this time. The goal of this test is to use the Radiative Fuel Reformers at relatively low temperatures to create small amounts of hydrogen and recirculate that hydrogen on the anode side to reduce the anodes as outlined in Figure 5.2-2).

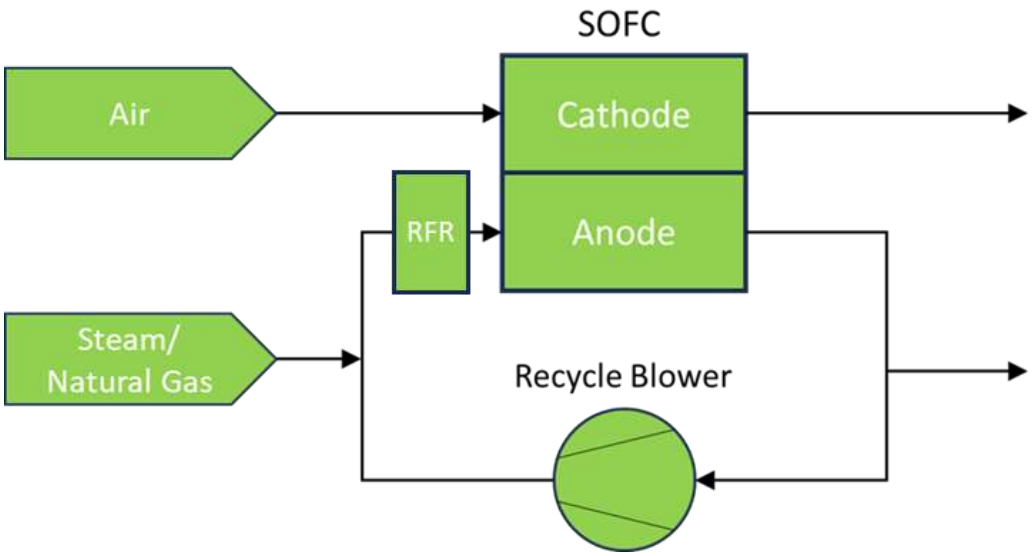

Figure 5.2-2 Self Reduction PFD with Anode Recycle Blower

The system benefit of generating a reducing gas for the fuel sides is elimination of the need for hydrogen storage on site for SOFC startup. This was successfully demonstrated. A GC was utilized to confirm the presence of hydrogen on the anode side being recycled via Anode Recycle Blower (Figure 5.2-3).

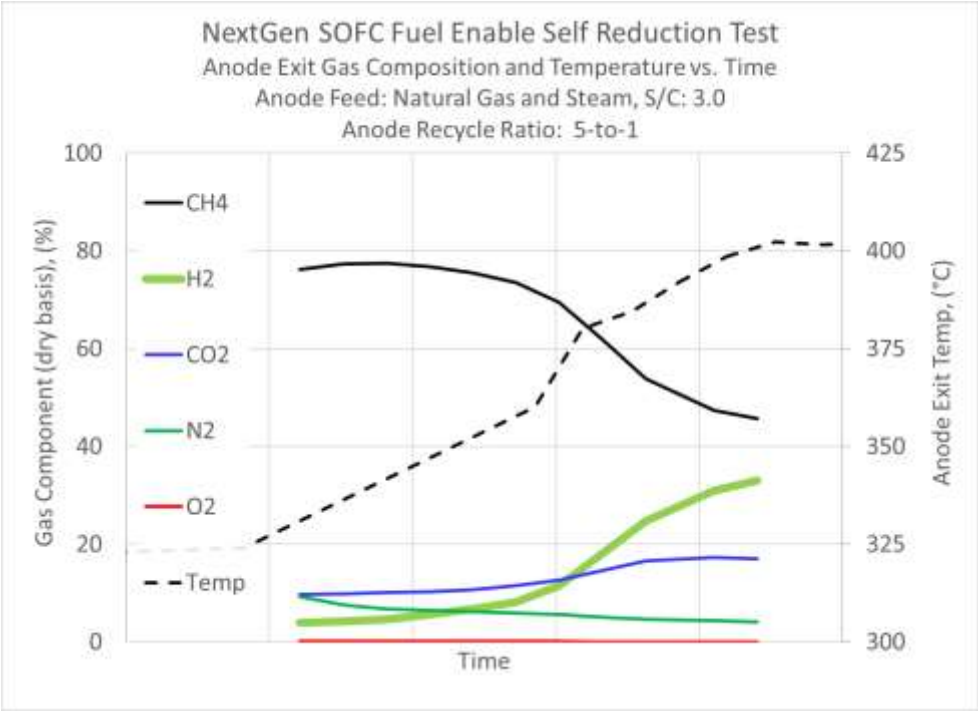

Figure 5.2-3 GC Results During Self Reduction Test

At 250°C the anode flow was transitioned from pure nitrogen to a mixture of steam and methane to begin the self-reduction test. No hydrogen was detected in the anode recycle at 250°C. However, as the module was heated up past 300°C the presence of hydrogen was confirmed. As

the module heated up from 300 to 400°C the hydrogen concentration increased from <5% to >30%! FCE was excited to see that the method of self-reduction using only methane and steam was successful.

Module Heat Up

Our initial heat up revealed some unforeseen issues related to module temperature and voltage stability. The module was prematurely cooled down for lid removal and inspection. It was found that thermocouples in the hot zone had low temperature wire insulation which led to faulty signals. These thermocouples were replaced. Also, in stack thermocouples proved to be troublesome so the thermocouples were removed for system reliability.

On the second heat up as the stacks heated up the voltage stability issue presented itself in the second stack. In an abundance of caution the module was cooled down for inspection. Testing revealed that cells midway up both stacks were in electrical continuity with the baseplate. It is believed that both stacks suffered an internal short.

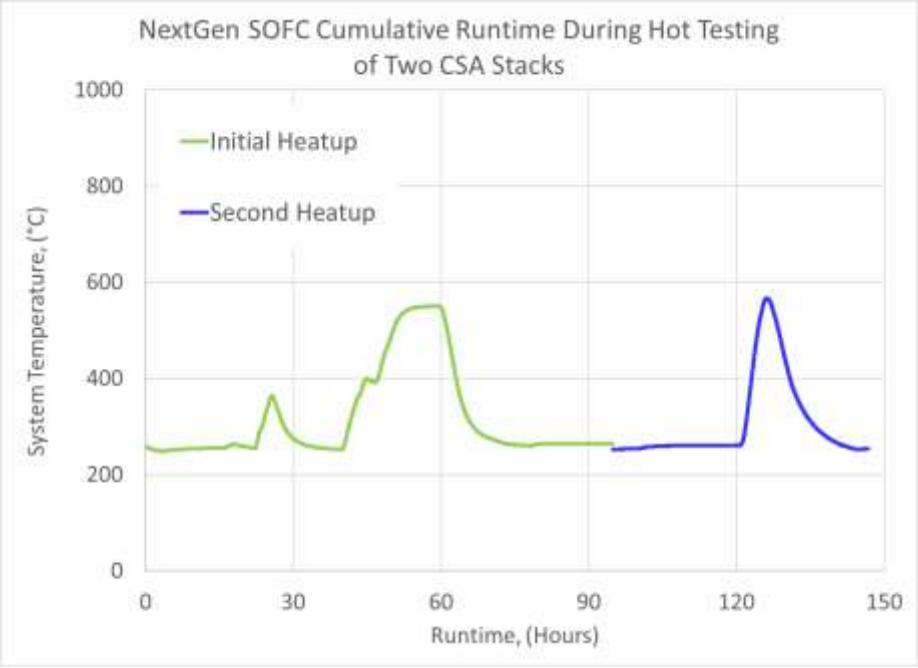

Figure 5.2-4 Cumulative Run Time of Next Gen Module

While we were unable to operate the stacks on load, FCE was able to perform nearly 150 hours of hot testing as shown in Figure 5.2-4. The team cooled down the module for inspection and removal of both stacks. Post-test examination of the stacks confirmed internal shorting between the stack and the center post. Analysis of the stacks and the test facility indicated that a few factors likely contributed to the shorting. They include debris in the test facility that got conveyed into the stack, impact of module temperature distribution and shipping on the internal electrical isolation within the stack. Steps were taken to filter debris and make the internal electrical isolation more robust to withstand shipping and module internal temperatures which were different than the test chambers in FCE Calgary. Extensive testing at FCE verified robustness of the electrical isolation with the improvements. SOFC module testing is planned in 2025 as part of FCE's internal

research and development effort. With the electrical isolation concerns resolved, we expect the stacks to operate at the designed output.